Operation of Cool Thermal Energy Storage to Enable Renewable Electricity Generation

By

Amy Van Asselt

A dissertation submitted in partial fulfillment of

the requirements for the degree of

Doctor of Philosophy

(Mechanical Engineering)

at the

UNIVERSITY OF WISCONSIN-MADISON

2018

Date of final oral examination: April 23, 2018

This dissertation is approved by the following members of the Final Oral Committee:

Gregory F. Nellis, Professor, Mechanical Engineering
Douglas T. Reindl, Professor, Engineering Professional Development
Sanford A. Klein, Professor Emeritus, Mechanical Engineering
Franklin K. Miller, Associate Professor, Mechanical Engineering
Krishnan Suresh, Professor, Mechanical Engineering

(This page intentionally left blank)

ABSTRACT

With an eye toward decreasing reliance on fossil fuels, electric utilities are increasingly deploying directly or supporting others to deploy more and more renewable generation assets. Although there are cases where renewable electricity is being generated by solar thermal systems, the dominant renewable energy generation technologies being used today include both photovoltaic (PV) and wind energy. Although the generation of electricity from renewable energy sources displaces the consumption of fossil fuels, it creates a number of significant challenges for utilities. By its very nature, the production of electricity from renewable energy generation sources is intermittent and often not directly correlated with the demand for electricity. Because utilities need to dynamically produce electricity to meet coincident demands as they occur, utilities have not experienced benefits of reducing their traditional generation assets as their renewable energy portfolios have grown.

Most larger buildings rely on one or more electric chillers operating on-demand providing chilled water to meet space cooling loads instantaneously as they occur. As a building mechanical subsystem, chillers are, collectively, one of the higher consumers of electricity for buildings. Unfortunately, the cost of electricity is highest during daytime, on-peak periods when building thermal loads are highest which translates into higher space conditioning operating costs for the building owner. Furthermore, the aggregate of high electricity demands for building chilling systems directly impacts electric utilities. The additive effects of building chilling systems operating coincidently to meet space cooling loads results in the need for electric utilities to build and operate larger generation and transmission infrastructure to meet the peak electric loads of their customers as they occur. Recognizing that space conditioning systems drive the peak electricity demand for most utilities and the periods of peak demand persist for a very limited

number of hours in a year, approaches that can reduce or shift electricity demands can provide significant benefit for both building owners and utilities.

Cool Thermal Energy Storage (CTES) is a proven technology that enables decoupling of the production of cooling from the coincident demand for cooling within a building or a group of buildings served by a district cooling system. CTES systems utilize either sensible (chilled water) or latent (ice) energy change media as a means of storing thermal energy. For decades, building owners have benefited from the ability of CTES to reduce electricity costs by shifting energy-intensive chiller operation from high cost on-peak periods to low cost off-peak periods. Looking toward the future, CTES is a technology that offers the potential for utilities to increase their deployment of renewable energy production. Specifically, CTES is a technology that can bridge mismatches between intermittent renewable generation and the aggregate demand for electricity.

This dissertation describes parametric studies of CTES control strategies that aim to more effectively utilize the generation of electricity from renewable energy resources. Specifically, the control strategies function to operate electricity-intensive chillers to charge thermal storage systems during periods when electricity from renewable generation sources is available followed by idling the chillers and discharging storage to meet building cooling loads during periods when renewable energy is not available. The strategies aim to maximize the fraction of the chiller energy consumption met by electricity generated from wind or solar. Additional CTES control strategies aim to maximize the net economic benefit of owning and operating a CTES system. Lastly, dynamic control strategies which utilize optimization algorithms are employed with increasingly variable simulation inputs.

The analysis considers four geographic locations across the continental United States for both a prototypical secondary school and a large commercial office building. The building cooling

loads are based on the U.S. Department of Energy Commercial Reference Building Models. To meet the building's primary thermal loads, the secondary school employs air-cooled chillers and a CTES system while the large office building employs water-cooled chillers and a CTES system. Both stratified chilled water and internal-melt ice CTES systems are considered.

The parametric studies with constant parameter control strategies show a trade-off between maximizing the use of renewable power and minimizing life-cycle cost, but a storage system designed to optimize the fraction of chiller energy consumption met by renewable resources will always be more cost effective and better at utilizing electricity from renewable energy resources than a building without storage. Buildings equipped with CTES and appropriate chilling system control strategies, enabled an increase in renewable energy utilization that ranged from 10% to more than 50% compared to non-storage cases. The conditions leading to these improvements are generally consistent across geographic region and building type. Aggregating individual building results over a region and plotting the impact on the utility system load results in an enhanced utilization of the renewable resource with a reduction of the peak system load. Results from dynamic control strategies show a 24% electricity cost reduction from the constant parameter control strategy when using a highly variable electricity rate input. With a less variable rate, the electricity cost reduction for the dynamic strategy over that with constant control parameters is 11%. These results show that implementing dynamic control results in significantly improved attainment of control strategy objectives (between 11% and 24% better in this case). These improvements are greater when the control strategy inputs are more variable as would be the case with intermittent renewable generation. These results suggest that widespread implementation of CTES systems, whether by retrofitting existing chilled water cooling systems or by incorporating CTES into new systems, will assist utilities in reaching their renewable penetration targets.

ACKNOWLEDGEMENTS

This work would not have been possible without the help and support of numerous family members, friends, and colleagues. Doug, Greg, and Sandy, you have taught me so much over these past four years both technically and professionally. Each of you brought a different background and advising qualities that added up to a very supportive environment for this research.

Bess, what a wild idea to pursue these graduate degrees together. I never could have done any of this without your unwavering support. We were both pushing hard to do our best and then along came our biggest project, sweet Berlin. The love I have felt from both of you has greatly motivated me and I cannot thank you enough. Berlin, we will read this together before bed in a few years.

My family, both immediate and extended, provided me with the environment and tools I needed to pursue this path. Thank you for always being there for me and for providing sets of outside eyes to review various pieces of technical writing. I have been inspired by your life stories and especially by the inordinate number of educators among you.

I also want to thank all of my colleagues in and outside of the Solar Energy Laboratory. Ana, Uzo, Rachel, Wenjie, Arganthäel, Mike, Kris, and all of the others who engaged in fruitful and frivolous conversations with me, I appreciate your friendship. Lastly, I want to thank the many undergraduate students I had in my classes. I started teaching early on in this program and my interactions with you assured me that I was on a good career path. You all provided me with extra confidence that helped me to carry out this research. I wish you all the best in your careers and thank you for your contribution to mine.

TABLE OF CONTENTS

LIST OF FIGURES

LIST OF TABLES

NOMENCLATURE

c	specific heat capacity [Btu/lb-°F (kJ/kg-K)]
c	cooling tower mass transfer coefficient [-]
Cap	chiller capacity at current conditions [tons(kWt)]
Δt	time step [hours]
I	current [amperes]
$\dot{m}$	mass flow rate [lbm/hr (kg/s)]
n	cooling tower mass transfer coefficient [-]
N	number of time steps in the control horizon
P	power [hp (kWe)]
$\dot{Q}$	heat transfer rate [tons (kWt)]
T	temperature [°F (°C)]
UA	overall heat transfer coefficient area product [Btu/hr-°F (W/K)]
V	voltage [V]
$\dot{V}$	volumetric flow rate [GPM (m^3/s)]

Subscripts

a	air
AC	alternating current
c	cooling, chiller
ch	charging
chws	chilled water set point
db	dry-bulb
DC	direct current
dis	discharging
ecw	entering condenser water
f	fan
fr	freezing point of water

full	full-load operation
gly	glycol
h	heat rejection
i	in
ice	ice CTES tank inlet
load	to cooling load
M	maximum
o	out
OC	open circuit
out	tank outlet
p	pump
rated	at standard rating conditions
ref	reference
return	return from cooling load
s	saturation
SC	short circuit
storage	ice CTES tank outlet; relating to the storage system
w	water
wb	wet-bulb

GLOSSARY

CAES	compressed air energy storage
CAISO	California Independent System Operator
CEC	California Energy Commission
COP	coefficient of performance
CPUC	California Public Utilities Commission
CTES	cool thermal energy storage
EEG	Energy Economics Group
EIA	Energy Information Administration
EPRI	Electric Power Research Institute
ERCOT	Electric Reliability Council of Texas
FERC	Federal Energy Regulatory Commission
ISO	Independent System Operator
kWe	kilowatt electric
kWt	kilowatt thermal
LP	linear programming
MISO	Midcontinent Independent System Operator
MPC	model predictive control
MPP(T)	maximum power point (tracking)
NLP	nonlinear programming
NREL	National Renewable Energy Laboratory
NTU	number of transfer units [-]
NYISO	New York Independent System Operator
PLR	part-load ratio of the chiller system [-]
PV	photovoltaic
SCE	Southern California Edison
SRC	standard rating conditions

TMY	typical meteorological year
TRNSYS	Transient System Simulation Tool
USDOE	United States Department of Energy
IEAD	insulation entirely above deck
VFD	variable frequency drive

1 MOTIVATION AND OBJECTIVES

1.1 Background Motivation

The utility demand for electricity varies significantly on both a seasonal and diurnal basis. For example, Figure 1-1 shows the normalized aggregate utility system electric load for the Midcontinent Independent System Operator (MISO) region in 2015 (MISO 2016). Examination of the aggregate electric load shows that the system operates near its peak load (a normalized load of one) for only a few hours of the year and the minimum electric load never decreases below approximately 45% of the peak load. The aggregate electric demand experienced by most electric utilities ranges between 80-100% of the peak for a period of less than 8% of the annual hours of operation. The culprit end-use electric load that drives peak electric demands for many utilities is building air-conditioning systems.

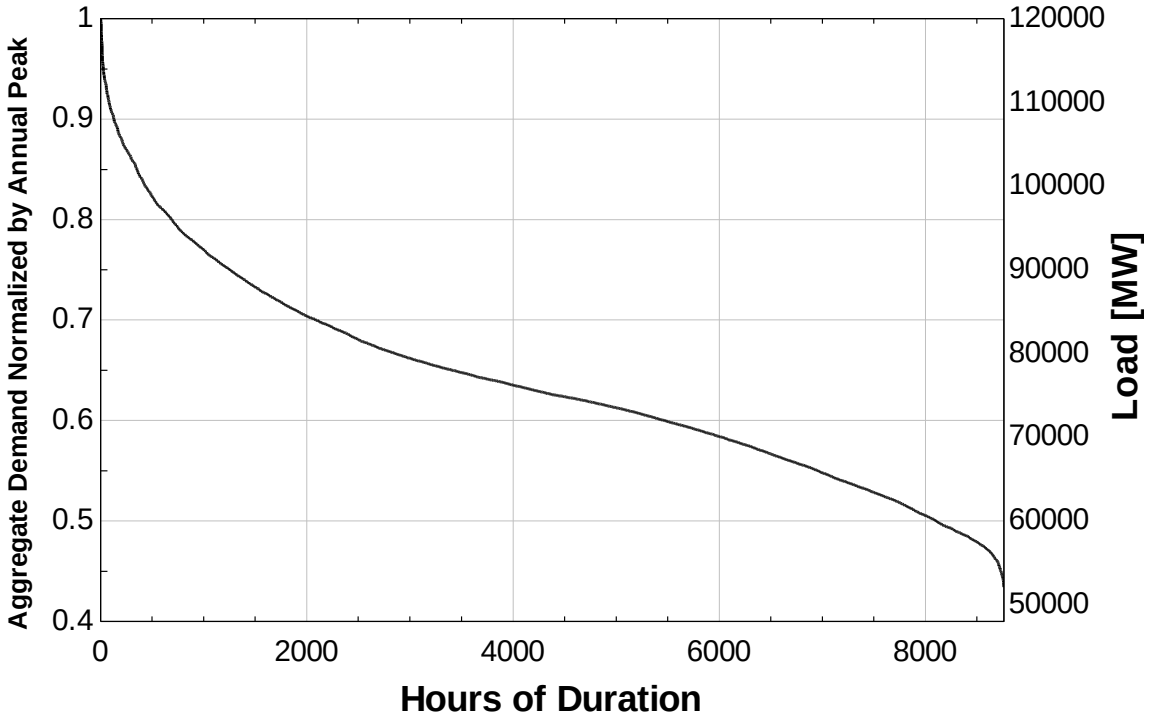

Figure 1-1. Aggregate load duration curve for MISO in 2015 (data from MISO 2016)

Myers, et al. (2010) evaluated the impact of the level of solar energy technology penetration on the aggregate load curve. For example, Figure 1-2 illustrates the aggregate electric utility load (demand) experienced on a typical day in Wisconsin in the spring, summer, and winter normalized to the all-time peak demand. Also shown is the power produced by a substantial penetration of PV (nominal capacity equal to 50% of the peak load) and the impact of that power on reducing aggregate load. In 2002, the aggregate peak utility demand in Wisconsin was 13,200 MW. The analysis prepared by Myers, et al. showed that the deployment of 6,600 MW of nominal photovoltaic capacity (50% of the utility aggregate peak) only reduced the required peak electric demand from traditional generation sources by 4.3%. Figure 1-2 shows the utility aggregate load along with the electricity produced by 6,600 MW of photovoltaics during the peak demand day for the winter, spring, and summer seasons. The minimal reduction in peak electrical demand with such a large renewable energy deployment is due to the mismatch between the peak electricity production by solar (PV) that occurs at noon and the aggregate utility peak demand for electricity that occurs hours later at approximately 4 p.m. The authors of this work noted that the future success of large-scale penetration of photovoltaic renewables hinges on the deployment of some form of energy storage that can bridge the time mismatch between renewable energy generation supply and end-use demand. Another option that could help better manage the supply of electricity from renewable means would be other forms of demand-side management (e.g. load-shedding), but these strategies have broader economic impacts on the businesses that do take steps to reduce their electric demand.

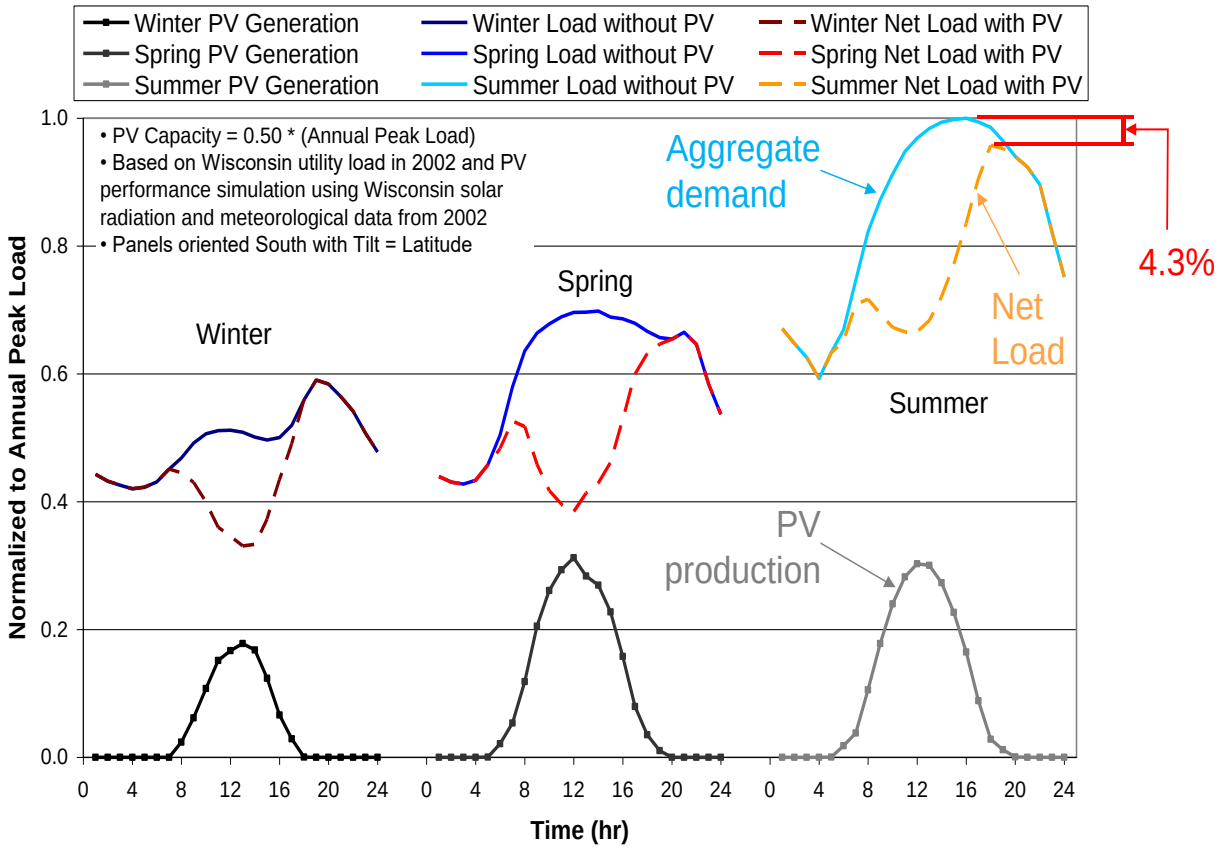

Figure 1-2. Load curves for winter, spring, and summer for Wisconsin utilities in 2002 (adapted from Myers et al. 2010)

Achieving a significant penetration of electricity production from not only photovoltaics, but all renewable energy resources, including wind, continues to be a high priority both on utility and individual building scales. From a utility perspective, ambitious legislation is driving increased deployment of renewable energy generation such as in California where there is a codified target of achieving 50% of electricity procured by retail sellers and publicly-owned utilities originating from renewable sources by 2030 (CEC 2016). At the building scale, sustainability-minded owners are deploying increasing amounts of renewable energy generation with the intent of reducing their carbon footprint and reliance on energy derived from fossil fuel sources.

In addition to renewable penetration targets, there is growing interest in approaches that are able to support net-zero energy performance for individual buildings. Although definitions vary, "net-zero buildings" aim to generate enough electric energy using renewable means to meet the building's energy needs on an annual basis. Essentially every current effort toward achieving net-zero energy buildings relies on the building being connected to the electric utility grid. Furthermore, it is assumed that the utility grid will reliably bridge any mismatches between the available production of electricity from renewables and the building's simultaneous energy demands by absorbing and utilizing any excess electricity generated by renewable means at the site and providing electricity when renewables are not available. This current approach to designing buildings with renewable generation that relies on the electric utility infrastructure as an infinite "sink" and "source" for electricity has a number of unintended and undesirable consequences when viewed on a scale broader than the building itself, e.g. at the utility level.

The intermittent nature of renewable energy production, coupled with the electric utility industry's obligation to provide a firm supply of electricity with a high degree of reliability, has created both operational and capital challenges. From an operations perspective, utilities have been challenged by the difficulty in coping with the significant grid dynamics that are created when the rapidly changing electricity production from renewable energy sources have to be met coincidently with traditional electricity generation sources. The time rate change of electricity demand and supply far exceed the normal variations in electric demands traditionally experienced from their end-use customers. Evidence of such dynamics includes utilities experiencing very high electricity production ramp rates and base load generation encroachment (over-generation). The California Independent System Operator (CAISO) region has been observing these two specific issues due to increased solar electricity production as illustrated by the popular "duck curve" shown in Figure

1-3 (CAISO 2013). From a capital perspective, utilities have not appreciably benefited from any reductions in their traditional fixed asset generation or transmission/distribution infrastructure that might be expected as increasing amounts of renewable energy generation sources are deployed. On the contrary, utilities have had to increase investments in transmission, distribution, and grid controls in order to accommodate the increased renewable energy generation. Furthermore, utilities have not been able to forego investments in traditional generation assets due to the renewables' inability to provide firm generation capacity.

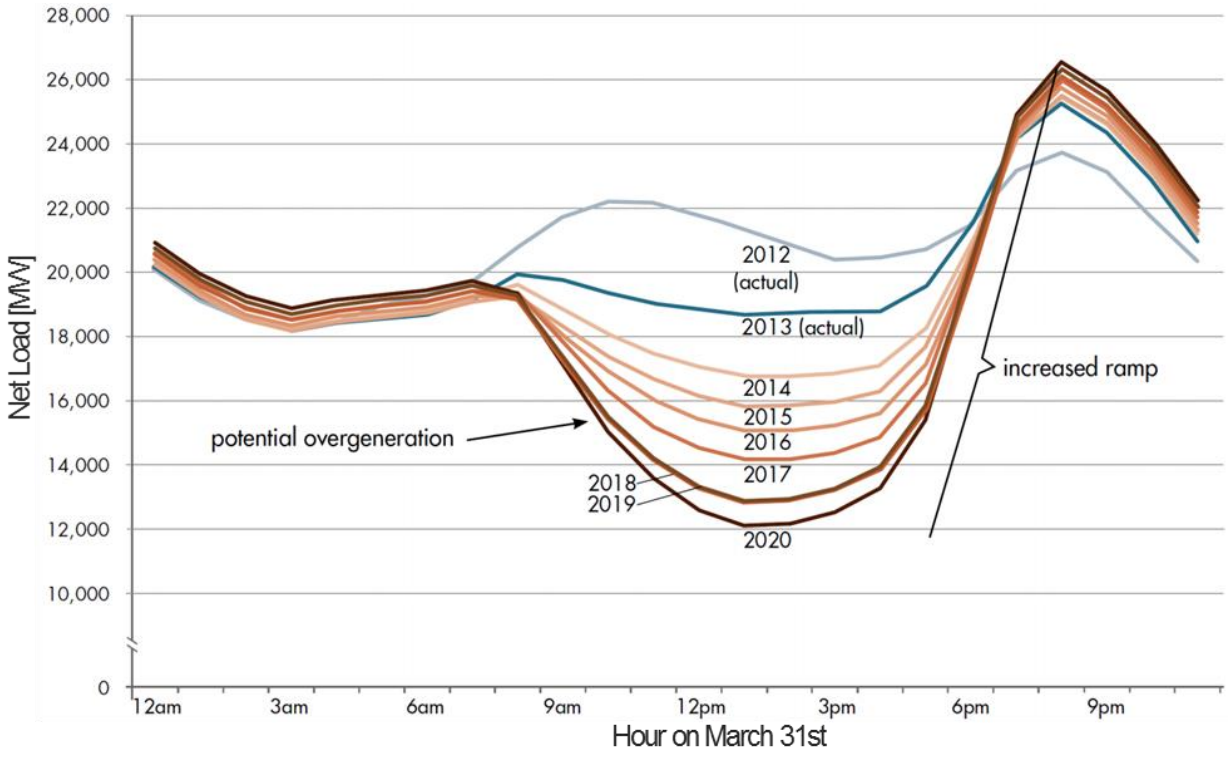

Figure 1-3. CAISO net load duck curve showing the over-generation risk and ramp rate for several years on March 31st (CAISO 2013)

Energy storage is a crucial technology needed to effectively bridge mismatches between the renewable energy production and utility aggregate demand. The storage must be functional over a timescale of several hours to enable arbitrage or peak-shifting. Although not all are practical or cost-effective, various forms of electric energy storage for this timescale could be considered

including lithium-ion batteries, hydrogen fuel cells, compressed air energy storage, and pumped hydroelectric storage. Of these, pumped hydroelectric storage is the most mature and, by far, most widely implemented. Figure 1-4 shows that, of all existing electrical energy storage installations, pumped hydro accounts for more than 96% of installed energy storage (Sandia National Laboratories 2016). In this figure, “electro-chemical systems” include battery and hydrogen fuel cell systems while “electro-mechanical systems” include compressed air energy storage systems and flywheels. It is also noteworthy that the thermal storage shown in the figure includes only utility-scale, high temperature fluid storage systems used as support to power plant systems which store energy in a fluid for later electricity production. It does not account for distributed thermal storage systems. A thorough comparison of these competing storage technologies is provided in Section 5.6.

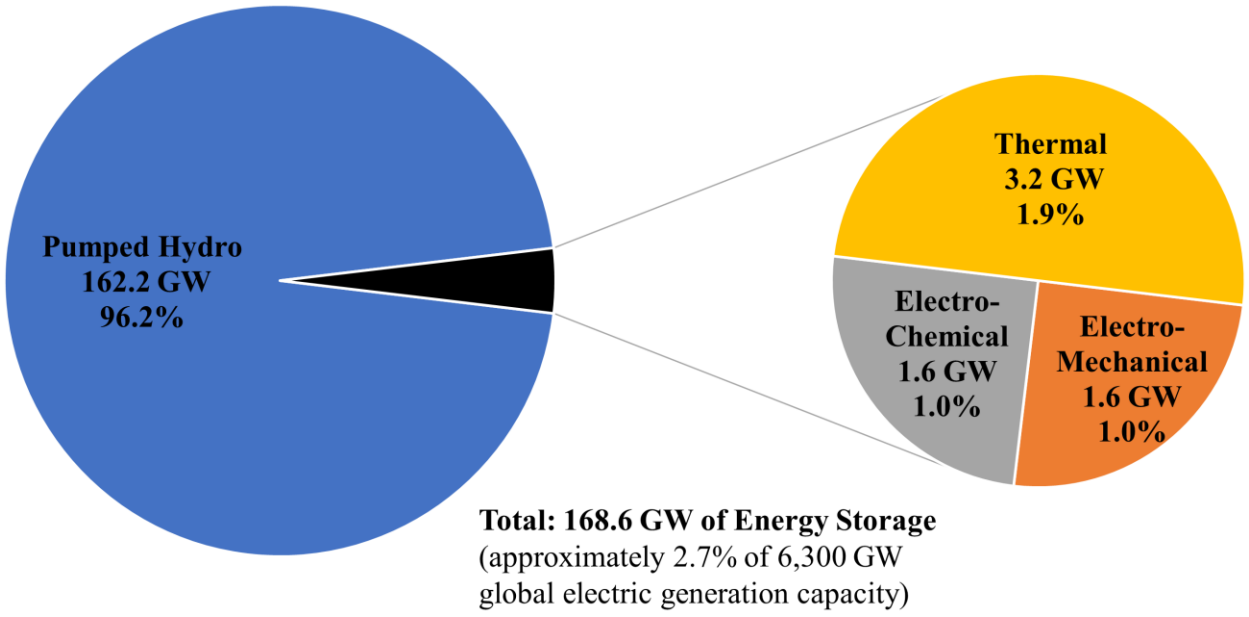

Figure 1-4. Global operational energy storage by type (thermal includes only power plant systems) (data from Sandia National Laboratories 2016)

Because the utility peak electric demands in many areas of the U.S. are driven by building air-conditioning loads, storage in the form of thermal energy becomes an alternative that offers the potential of bridging mismatches in the renewable energy production and end-use demand. In this strategy, chillers are operated during periods of excess renewable energy production to charge a cool thermal energy storage (CTES) system. This stored thermal energy can then be utilized to meet space cooling loads, in whole or part, during periods of lower renewable energy production. By operating chillers to charge CTES systems during periods when renewable energy resources are available and then discharging to meet building air-conditioning loads during periods of resource unavailability, CTES offers the potential to enable a more effective utilization of electricity produced from renewable energy resources. My hypothesis is that, beyond electricity cost savings, CTES can cost-effectively enable a significantly greater penetration of renewable energy than currently exists today. CTES is not only a proven energy storage technology but it is

considerably more cost-effective compared to alternative electric energy storage technologies that are being considered to mitigate issues related to renewable energy deployment (see Section 5.6 for the cost comparison).

1.2 Objectives

The overall objective of this work is to evaluate the potential of cool thermal energy storage as an enabling technology that will allow for an increased penetration of renewable energy generation – including understanding its benefits and limitations. In addition, the proposed research provides guidance on designing CTES systems, including control strategies and sizing, considering their impact in both a renewable energy and financial context. It also provides policy recommendations relating to the benefits of the CTES systems designed. The following summarizes the objectives set forth in this project:

1. Identify the specific value propositions CTES provides for end-users (at an individual building-level and campus-level), utilities, sustainability advocates, and equipment manufacturers.

2. Develop a methodology to quantify those value propositions.

3. Quantify the magnitude of these value propositions for selected case study buildings and utility systems using utility data, weather data (wind and irradiance), and building load profile data.

4. Relate the value propositions to the design of CTES systems (technology selection, sizing, and operating strategies) in order to develop a better understanding of the CTES design principles.

5. Formulate a design procedure that optimizes the operational capabilities of the technology to enable increased penetration of PV and wind.

1.3 Geographic Locations for Analysis

In order to account for the variation in building construction practices and external cooling loads as well as the variability of renewable energy resources, this research considers four geographic/climate regions. The criteria used for the selection of these regions include:

- Diversity of weather and cooling loads
- Diversity of wind and solar as energy resources
- Population density (as a surrogate measure of impact potential)
- Availability of publicly-accessible data

Figure 1-5 illustrates the solar resource (PV) for the contiguous states (NREL 2011). The scale shows average daily total solar insolation (kWh/m^2/day) incident on a PV panel oriented due south and tilted at an angle equal to the latitude of the location. It is clear that the country's solar resource is heavily concentrated in the Southwest followed by the Southeast. The far Pacific Northwest, Upper Midwest, and Northeast have limited resource in comparison.

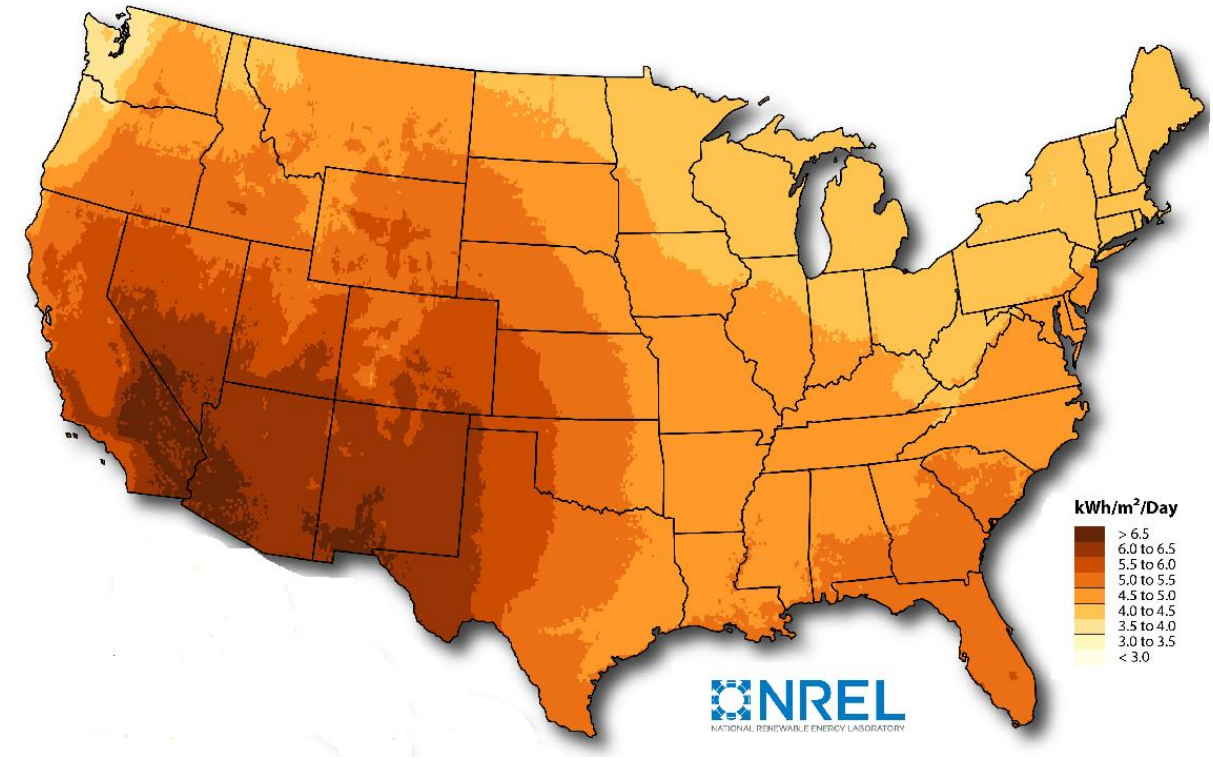

Figure 1-5. Photovoltaic solar resource map, 1998-2005 (NREL 2011)

Figure 1-6 shows the annual average wind resource for the contiguous states at a height of 260 ft (80 m) (NREL 2011). This height is consistent with the hub height of wind turbines typically installed (due to the effects of wind shear, other sources such as wind data collected from airports cannot reliably predict availability of wind resources because the measurements are made at a typical height of 33 ft (10 m) height). The scale in Figure 1-6 shows the wind speed and it ignores data below 9 mph (4 m/s) because this wind velocity threshold is below the cut-in speed for most wind turbines. It is important to note that wind power production increases as the cube of the wind speed, so small increases in velocity equate to large increases in power output. Looking at the solar and wind resource maps together, the Southwest and Southeast have limited wind resource compared to solar. The Great Plains region in the U.S. has very high wind speeds with a variety of solar resource. The Upper Midwest region has moderate wind resource while the Northeast has

limited wind and solar resource. Taking these maps into account, selecting regions which have significant renewable resource of solar only, wind only, both types and neither type will give the most variety.

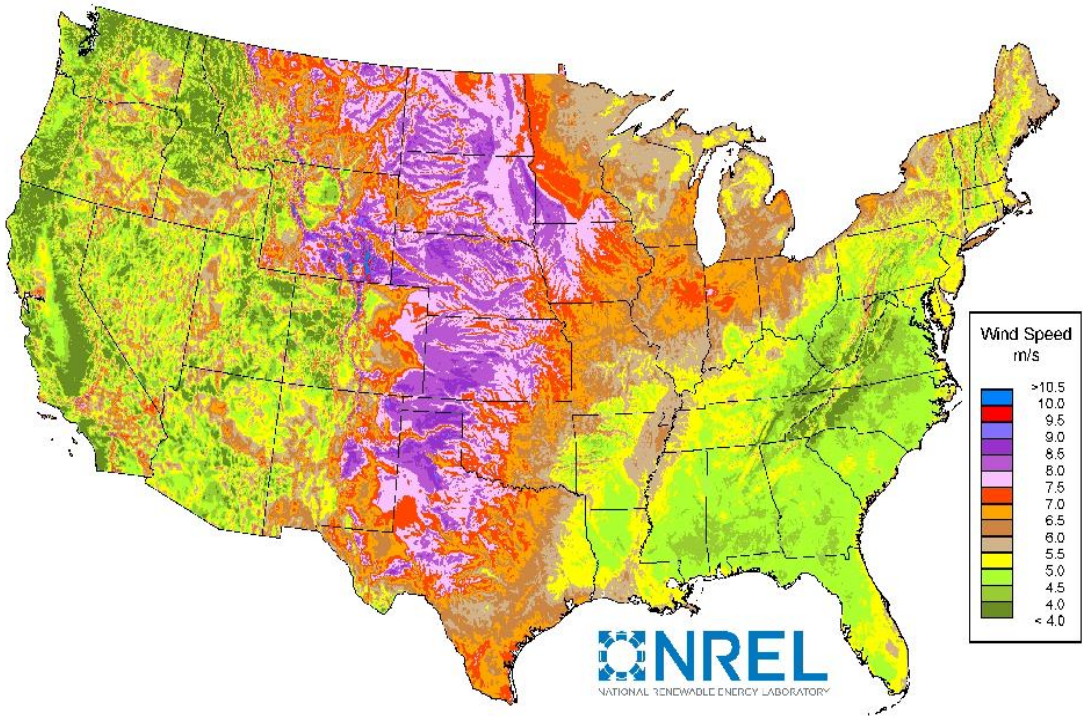

Figure 1-6. Wind resource map at 260 ft (80 m) (NREL 2011)

Availability of utility data that are time-resolved on an hourly scale or smaller is essential for performing a utility grid-scale analysis. In 1999, the Federal Energy Regulatory Commission (FERC) suggested the voluntary creation of Independent System Operators (ISO) to "satisfy the requirement of providing non-discriminatory access to transmission" (FERC 2015). Along with maintaining grid reliability with various interconnected power supply companies, many of the ISOs maintain a wealth of information including: detailed generator dispatch, operating reserves, emissions, and other utility data. For this reason, the selection of geographic regions encompassed by ISOs is desirable. In addition, the majority of the US population is covered by an ISO (or a

similar Regional Transmission Organization), so selection of these regions also fits the criteria of significant population coverage.

Figure 1-7 shows the geographic regions selected for this research, the state of Wisconsin (part of the Midcontinent ISO), the region covered by the California Independent System Operator (CAISO), the region in Texas covered by the Electric Reliability Council of Texas (ERCOT), and the state of New York (covered entirely by the New York Independent System Operator, NYISO). These four regions cover approximately one quarter of the US population and have good data availability. Each region also has typical weather that requires large cooling loads through at least the summer season. In terms of renewable resource, ERCOT has significant solar and wind resource, CAISO generally has significant solar and little wind, Wisconsin has little solar and moderate wind, and NYISO has little of both resources. These regions provide enough variety to be assured that control system strategies developed are effective with various levels of renewable resource.

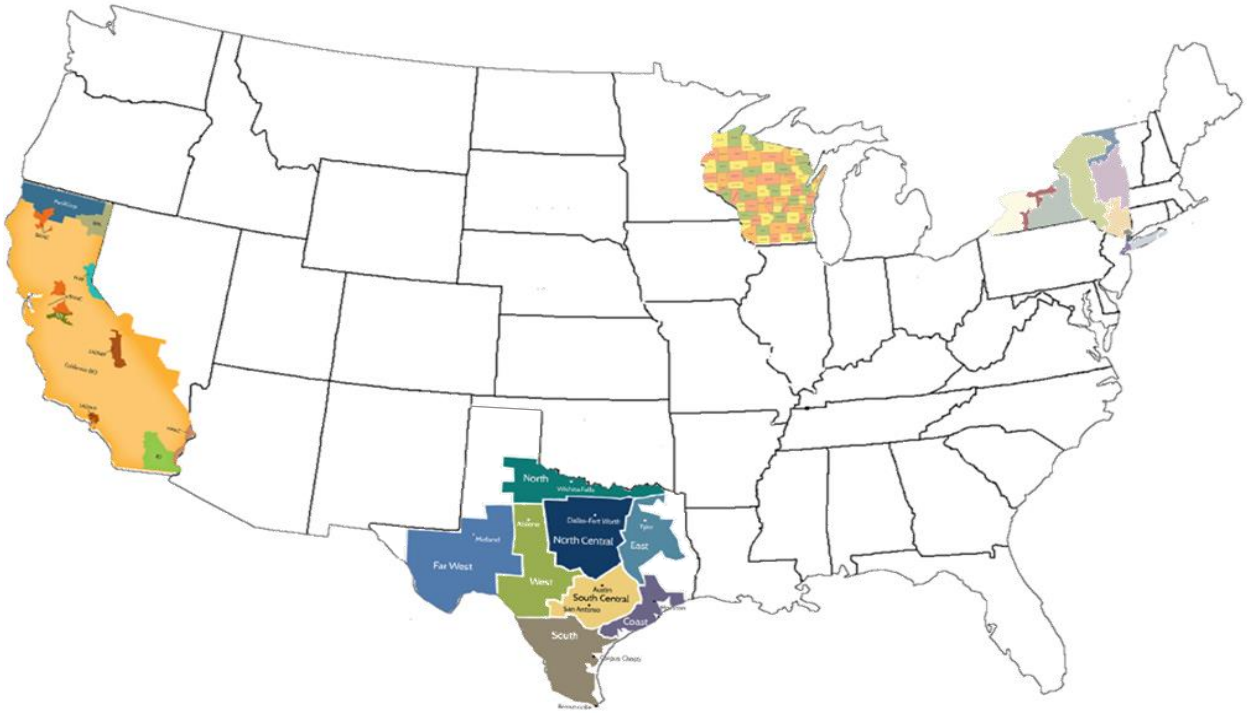

Figure 1-7. Geographic regions selected for this research

1.4 Building Types for Analysis

The United States Department of Energy (USDOE) has released a set of commercial reference buildings intended to represent approximately two-thirds of the commercial building stock in the U.S. on a floor area basis. The purpose for creating these reference buildings was to provide baseline models for use in the ongoing development of building energy standards and codes. In addition, the reference building models provide a platform to assess potential impacts of new building-related energy technologies. The model set includes sixteen building types, each with envelope parameters applicable to 16 different U.S. climate zones, and each representing practices over a range of time periods from pre-1980, post-1980, and new construction. The weather data for each of the climate zones comes from Typical Meteorological Year (TMY) data for representative cities within those zones. Collectively, the 768 models represent hypothetical buildings that meet minimum requirements for energy standards and building

construction/operation practices applicable during the aforementioned time periods. Differences across the time periods are represented in the building envelope insulation, lighting levels, HVAC equipment types, and the HVAC equipment efficiencies. The corresponding energy standards met for each time period include: ASHRAE 90.1-2004 for new construction, ASHRAE 90.1-1989 for post-1980 construction, and a "set of requirements developed from previous standards and other studies of construction practices" for pre-1980 models (USDOE 2011). The 16 building types were chosen using data from the 2003 Commercial Buildings Energy Consumption Survey (CBECS) and can be found in Table 1-1 (EIA 2005).

Since this project aims to understand the role of CTES in an energy market with the growing deployment of renewables, the decision was made to focus on those building types that utilize chilled water-based space conditioning systems. Winiarski et. al. (2006) analyzed the CBECS to determine the most common HVAC equipment types in use and their recommendations were adopted in the development of the reference buildings. Table 1-1 shows the cooling equipment types used for each of the sixteen buildings.

Table 1-1. Post-1980 and New Construction Cooling HVAC Types in the Commercial Reference Buildings (adapted from USDOE 2011)

Building Type	Cooling	Air Distribution
Small Office	PACU (packaged air-conditioning unit)	SZ CAV (single-zone constant air volume)
Medium Office	PACU	MZ VAV (multi-zone variable air volume)
Large Office	Chiller (2) – water cooled	MZ VAV
Primary School	PACU	CAV
Secondary School	Chiller – air cooled	MZ VAV
Stand-Alone Retail	PACU	SZ CAV
Strip Mall	PACU	SZ CAV
Supermarket	PACU	CAV
Quick Service Restaurant	PACU	SZ CAV
Full Service Restaurant	PACU	SZ CAV
Small Hotel	IRAC (individual room air conditioner), PACU	SZ CAV
Large Hotel	Chiller (2) – air cooled	FCU (fan coil unit) and VAV
Hospital	Chiller – water cooled	CAV and VAV
Outpatient Healthcare	PACU	CAV and VAV
Warehouse	PACU	SZ CAV
Midrise Apartment	PACU-SS (split system)	SZ CAV

The four building models utilizing chillers include: Large Office, Secondary School, Large Hotel, and Hospital. Beyond the recommendations shown in Table 1-1, the Large Office and Hotel are modeled with two chillers in a primary-only system, the office using water-cooled chillers and the hotel using air-cooled chillers. Interestingly, the model for the hospital has a single water-cooled chiller and the Secondary School has one air-cooled chiller. This added detail for these systems was determined through information from the ASHRAE Standard 90.1 mechanical subcommittee (USDOE 2011). The USDOE document states, "[t]he number of chillers and

condenser type (air or water) were determined by discussions with the ASHRAE Standard 90.1 mechanical subcommittee."

In selecting the specific building types to be used for this research, the design day load profile and the magnitude of the peak cooling load were primary considerations. Figure 1-8 depicts design day cooling load profiles for the four building types with chiller systems. The profiles are shown for each of the four geographic regions considered. The internal loads impacting these profiles are caused partially by human occupancy with the design day occupancy profile for each building type shown in Figure 1-9. The occupancy for each building is normalized by the maximum occupancy for that particular building type. These maximum values as well as the schedules were developed using the ASHRAE Advanced Energy Design Guides for the Large Hotel and Secondary School, the ASHRAE 90.1-2004 standard for the Large Office building, and the Green Guide for Health Care for the Hospital (USDOE 2011). The Secondary School peak cooling load ranges between 185 to 410 tons (650 to 1,440 kWt) and occurs on a date which lands during the period of the year where school is in session. This means that although the cooling load would normally be higher in the July and August summer months (due to the elevated temperatures and humidity), the reduced occupancy and internal loads lead to reduced overall building cooling loads.

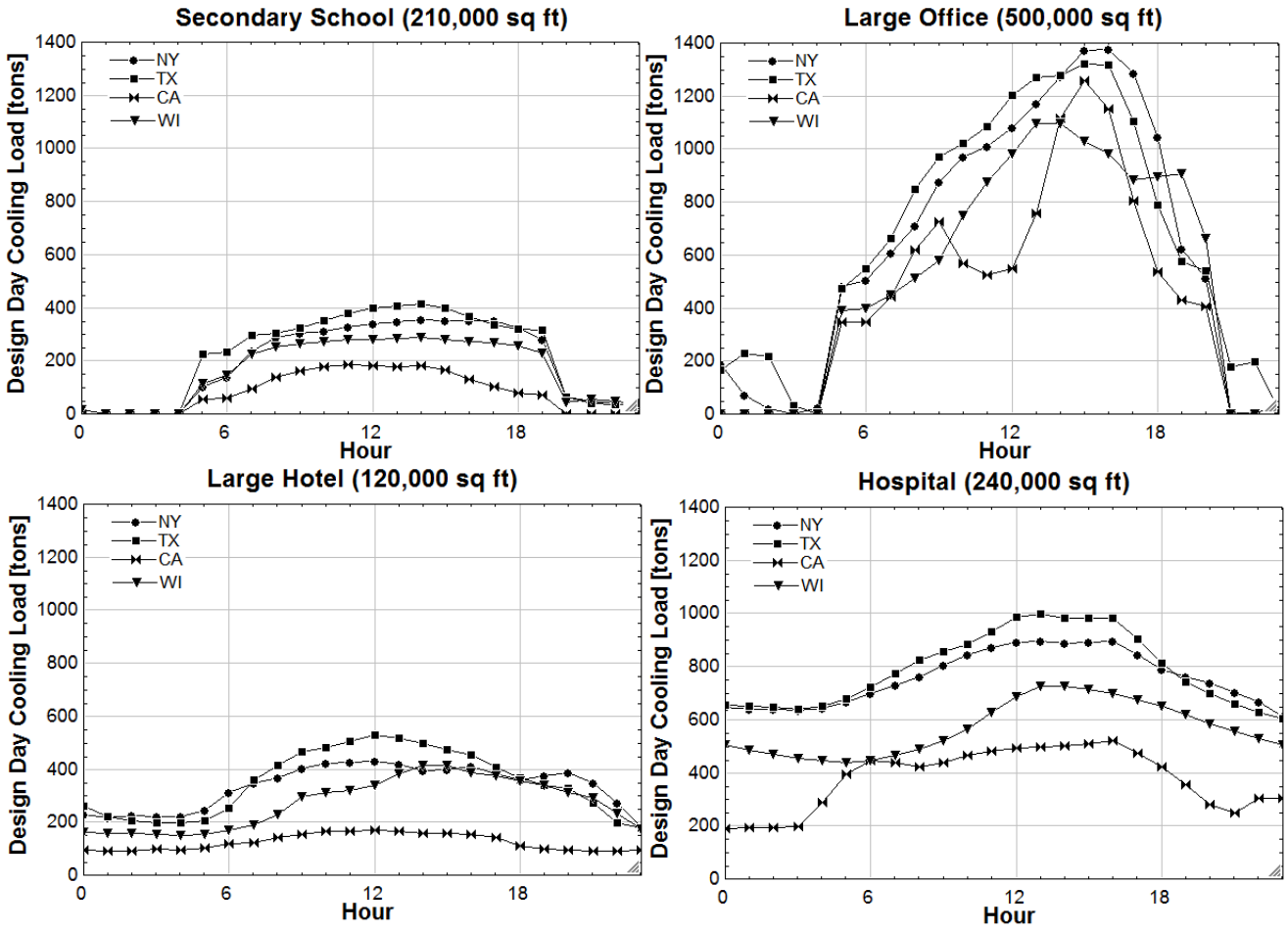

Figure 1-8. Commercial reference building design day cooling load profiles (data from USDOE 2012)

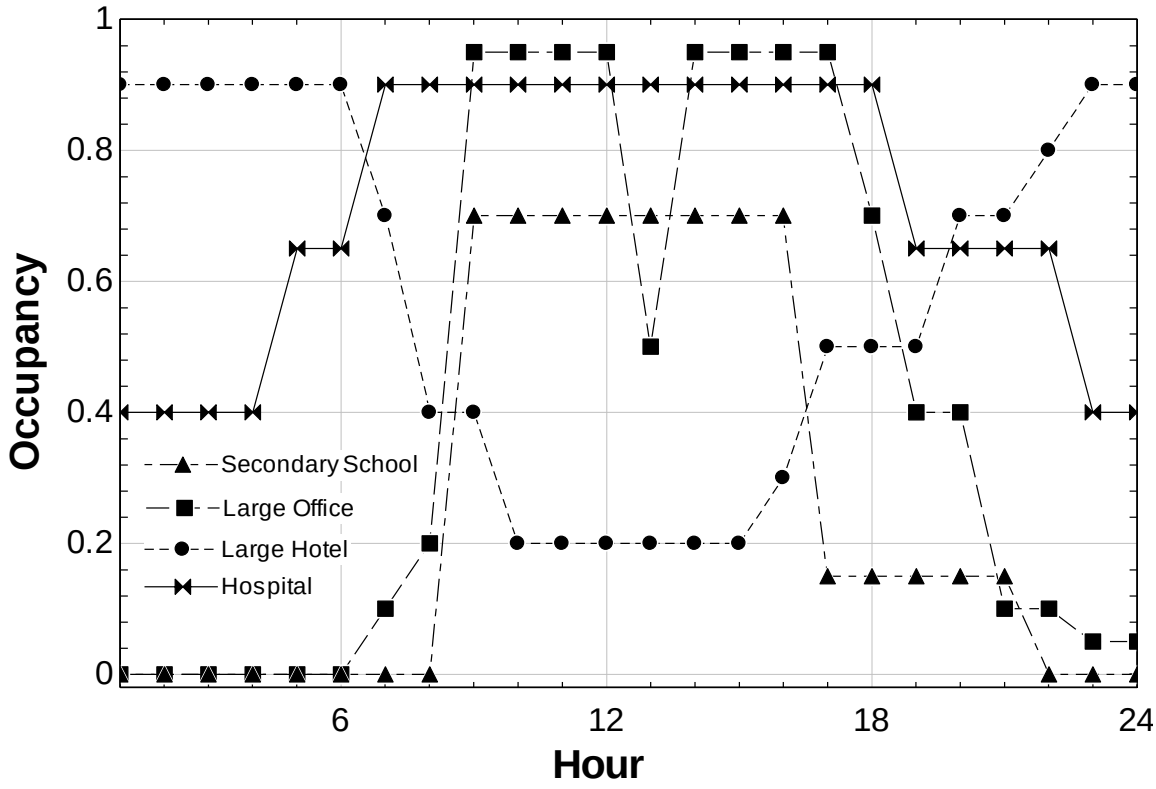

Figure 1-9. Commercial reference building design day occupancy schedules (data from USDOE 2012).

Based on the chiller technology employed, the design day cooling load profile, and the potential aggregate impact, the Large Office and Secondary School buildings were selected for analysis as part of the current research effort. The Large Office has the largest cooling load which increases the economy of scale for a CTES system. It also has a more diverse load profile when compared to the other buildings that utilize chilled water for cooling. This varied cooling load profile provides greater opportunity for shaping the electric demand associated with the building by shifting cool loads; thereby, making better use of variable renewable resource profiles. Even though they have differing occupancy schedules, the Secondary School and Large Hotel have similar cooling load profiles and peak cooling load magnitudes as shown in Figure 1-8. The decision was made to use the Secondary School due to its potential aggregate impact by application of the results. As of 2012, there are 43,000 secondary schools totaling 3.1 billion square feet

(280 million m^2) and 30,000 large hotels totaling 2.7 billion square feet (250 million m^2) (EIA 2012). Because there are a greater number of secondary schools covering a greater amount of floor space, a final decision was made to use the Secondary School model.

2 MODELING

Annual cooling system simulations provide the basis for analysis of CTES systems. Models are required for renewable electricity generation, building cooling loads, CTES systems, chiller plants, and system life-cycle costs. In order to facilitate computationally efficient CTES system analysis and optimization, simulation models are used that are not iterative in their calculations. In order to achieve this goal, some of the systems were modeled separately using relatively complex and computationally intensive models (e.g. solar panels, cooling towers). Reduced order models of these systems were developed from these results and subsequently used in the annual simulations for computational expediency.

2.1 Wind Resource Data and Model

2.1.1 Wind Resource Data

Accurate and time-resolved wind speed data are essential for the determination of wind power generation potential in a particular region. Typical Meteorological Year (TMY) weather data have been compiled by examining many years of data and selecting the one month for each of the twelve calendar months which is judged to be the most typical (NREL 2008). For example, for the TMY3 weather data set for Los Angeles, CA, the year 2000 was judged to have the most typical July, so all weather data for that particular month are used in the data set. Each of the twelve typical months are concatenated to form a complete “typical year” weather data set. There are five criteria used for judging the months: global horizontal radiation, direct normal radiation, dry bulb

temperature, dew point temperature, and wind speed. Even though wind speed is included in the selection process, it is given the lowest weighting factor of the five criteria and therefore the wind data included in the TMY sets are not well suited for predicting the performance of wind energy conversion systems. Additionally, most of the wind data in the TMY data sets come from anemometers positioned approximately 33 ft (10 m) above the ground. Although it is possible to estimate the equivalent wind speed at other heights using a wind shear exponent that is a function of terrain, data that are gathered at the relevant heights of 164 ft (50 m) or higher are more accurate for determining potential wind power generation. Additionally, the TMY data set reports wind speed only at hourly intervals while intra-hour fluctuations can be significant. Data which are collected on intervals of between five to fifteen minutes would be preferable.

Regions that have significant wind resource are likely to have tall anemometers installed to characterize the wind resource. Some of the data collected with these devices are made publicly available; for example, data from White Deer, TX, which is a town forty miles outside of Amarillo, TX. Wind speed data from White Deer, TX are collected at a height of 164 ft (50 m) and the data are time-resolved at ten minute intervals (AEI 2012).

Figure 2-1 shows the monthly averaged wind speed for each month in 2012, separated into the cooling season from April to September and the off season from October to March. Because wind turbines typically have a cut-in wind speed of between 7 and 9 mph (3 to 4 m/s), all wind speeds below 7 mph (3 m/s) have been set to zero. The data for this particular location show that the wind speeds are slightly elevated overnight and this behavior is more prominent in the summer months. This behavior is also seen in the tabulated statistics shown in Table 2-1. The wind speeds are generally higher between the hours of 6 p.m. and 6 a.m. (when daily cooling

loads are lower) and the full day average column shows that the wind speeds are generally higher in the winter months (again, when cooling loads are lowest). The plotted mean wind speeds in Figure 2-1 do not show the variation in the recorded wind speeds throughout the month. The standard deviation column shows values ranging between 2.8 and 4.4 m/s and, since the power output increases as approximately the cube of the wind speed, this variation leads to changes in generation throughout the day that are on the same order as the monthly mean.

Table 2-1. White Deer, TX wind speed statistics with extremes in italics

Mean Wind Speed (m/s)	Full Day	0:00-6:00	6:00-12:00	12:00-18:00	18:00-24:00	Std. Dev
Jan	8.68	***9.44***	8.18	8.73	8.37	4.33
Feb	8.76	8.61	8.65	9.24	8.53	4.40
Mar	8.97	***10.29***	8.49	8.21	8.89	3.85
Apr	8.49	8.93	8.30	7.98	8.77	3.29
May	8.13	9.08	7.92	7.14	8.36	3.77
Jun	8.86	9.60	8.28	8.21	9.33	3.37
Jul	7.51	8.32	7.29	6.46	7.99	2.79
Aug	6.67	7.68	***5.93***	***5.71***	7.37	3.10
Sept	6.79	7.83	6.19	***5.73***	7.40	3.75
Oct	7.93	8.73	7.73	7.33	7.92	3.65
Nov	8.01	8.89	7.86	7.11	8.18	3.71
Dec	8.96	***9.66***	8.58	8.25	9.35	4.04

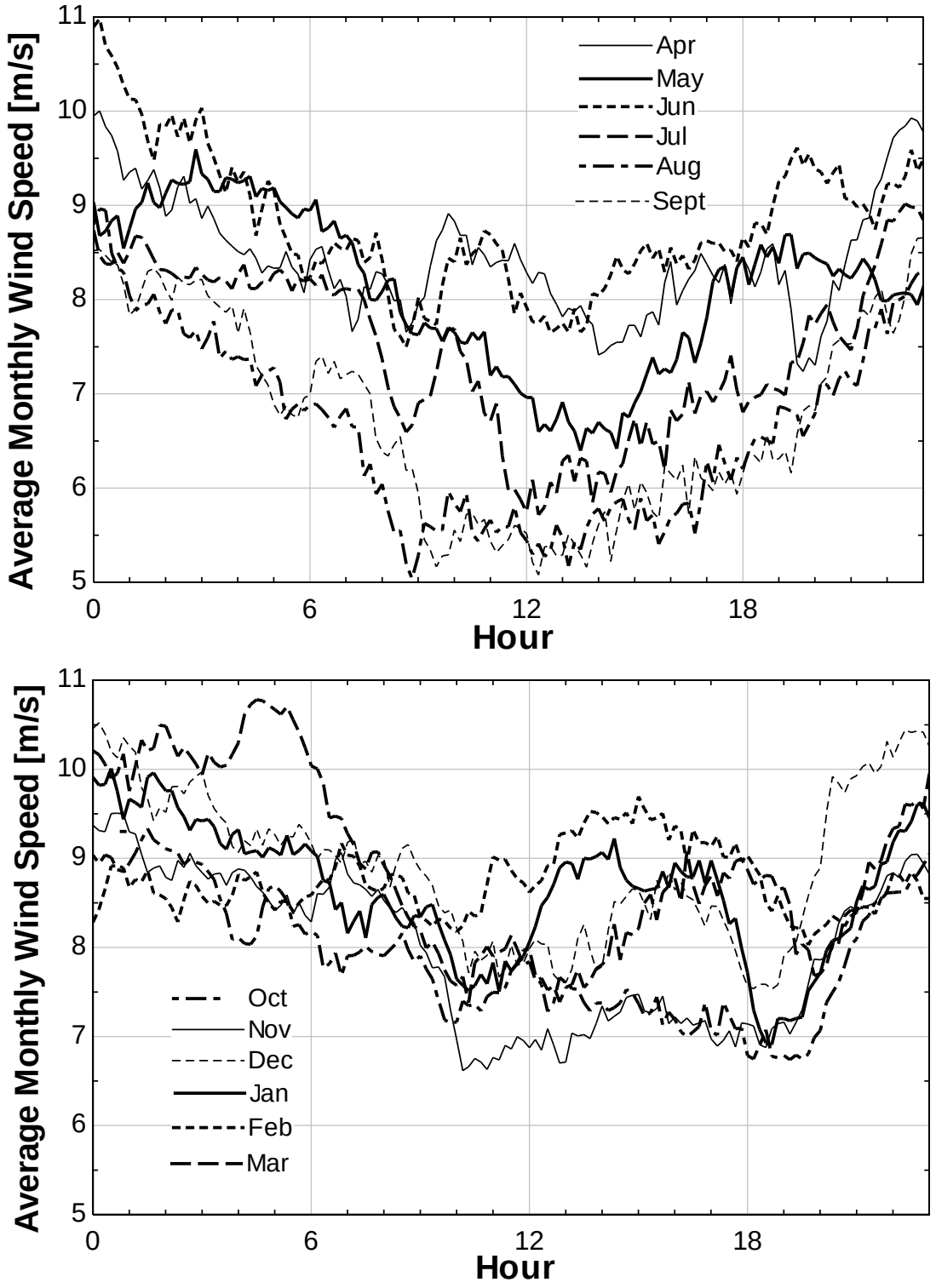

Figure 2-1. Ten-minute averaged monthly wind speed data for White Deer, TX during the cooling season Apr-Sep (top) and the off season Oct-March (bottom) in 2012 (AEI 2012)

In addition to publicly-available data, such as that for White Deer, TX, the National Renewable Energy Laboratory has compiled data sets for the purpose of wind power integration studies and estimating wind power production (NREL 2010). The data sets are entitled the "Eastern and Western Wind Integration Data Sets" and cover 2004, 2005, and 2006 with wind data being provided at five-minute intervals. The 2006 data are used for the California, Wisconsin and New York regions.

2.1.2 Wind Power Generation Model

The wind speed data are used to model wind power generation. In the range between the cut-in speed and the rated wind speed, the wind turbine power output increases approximately with the cube of the wind speed. A piecewise function is fitted to the wind power output curve (as shown in Figure 2-2) to predict the generated wind power as a function of wind speed. The piecewise function consists of the following segments:

- From zero wind speed to the cut-in speed of just under 7 mph (3 m/s), there is no power output from the turbine
- From the cut-in speed to the rated speed of 25 mph (11 m/s), a fitted third order polynomial is used to predict the wind power output
- From the rated speed to the cut-out speed of 56 mph (25 m/s), the power output is constant at the rated power
- Beyond the cut-out speed the power output is zero since the wind turbine must be stopped to avoid damage

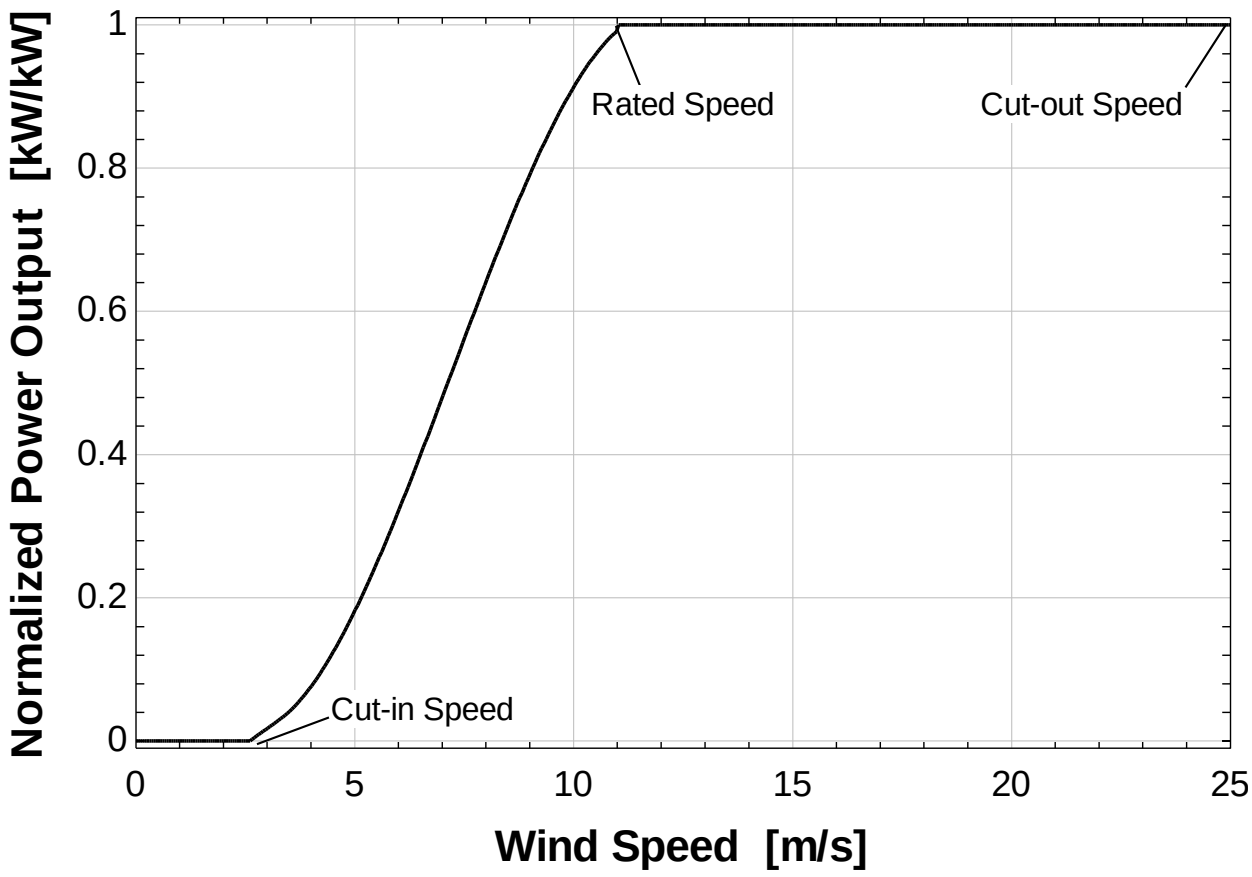

Figure 2-2. Wind turbine power curve (data from NREL 2015)

2.2 Solar Resource Data and Model

2.2.1 Solar Resource Data

The selection process for the TMY weather data heavily weights both global horizontal radiation and direct normal radiation in the selection process. This makes these data sets suitable for solar resource data as compared to the wind resource data. The precise locations for both the solar and wind resource data are displayed for each of the four geographic locations in Figure 2-3. The weather data used for both the solar resource and the cooling load simulations is TMY data and the wind speed data sources are detailed in Section 2.1.1.

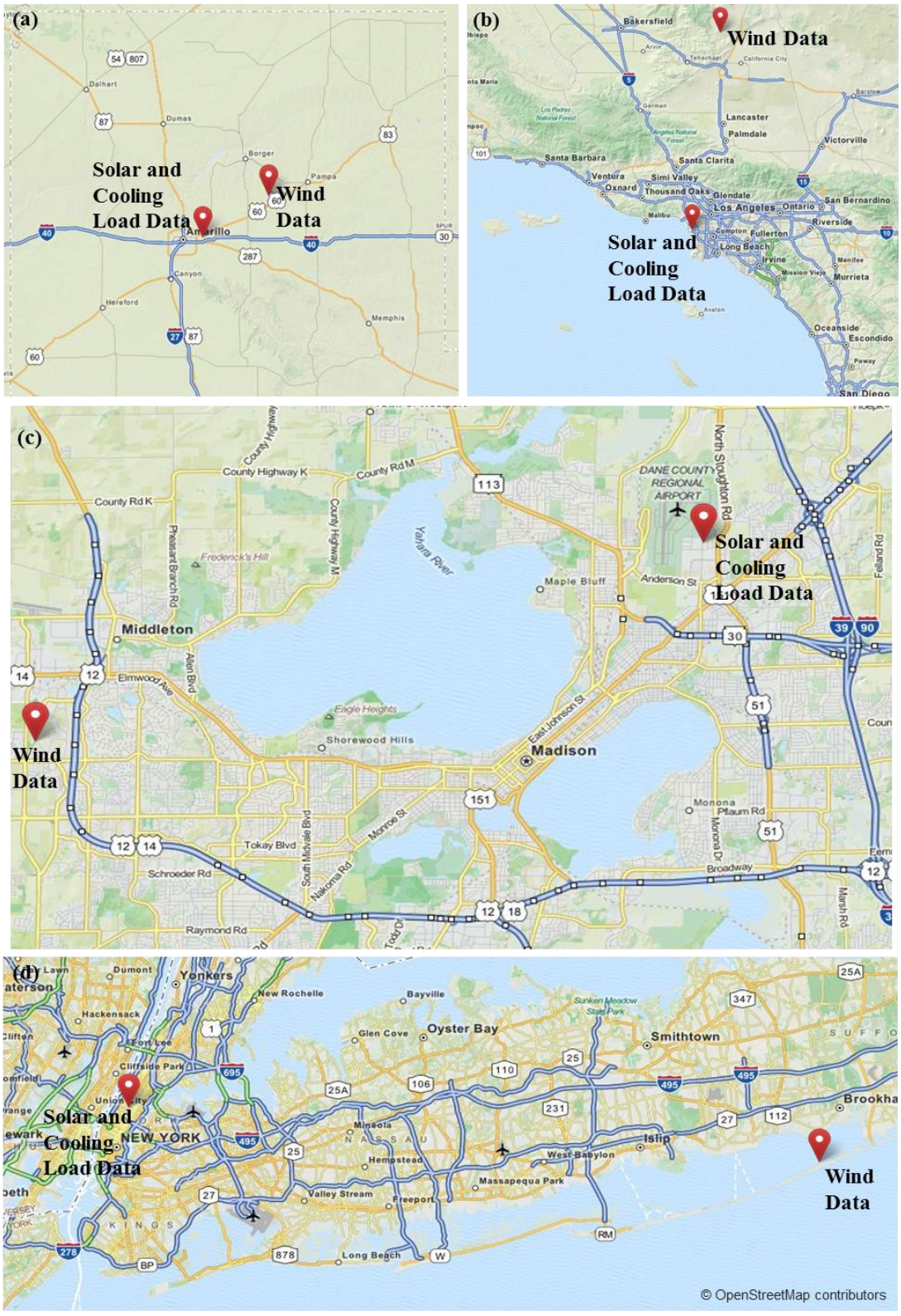

Figure 2-3. Cooling load, solar, and wind data locations for (a) Amarillo, TX, (b) Los Angeles, CA, (c) Madison, WI, and (d) New York, NY

The TMY solar resource data does not account for any intra-hour variation in the solar resource. As with the wind data, it would be preferable to have solar data at five to fifteen-minute intervals for analyzing the CTES control systems. In order to simulate solar generation, both interpolation of the TMY hourly solar data to shorter time intervals and calculation of the total radiation on a tilted PV panel surface are required. Simple linear interpolation of solar radiation data can lead to positive values before sunrise and after sunset if those time periods do not fall on the whole hour (Duffie & Beckman 2013). As an example, if the sun rises at 6:45 a.m. and the hourly data shows 0 W/m^2 at 6:00 and 40 W/m^2 at 7:00, linear interpolation will give 10 W/m^2 at 6:15 a.m. and 20 W/m^2 at 6:30 a.m. As a result, calculations for the ratio of total beam radiation incident on a tilted surface close to sunrise and sunset lead to asymptotically large values at these times due to division by the cosine of the zenith angle of ninety degrees, zero. If linear interpolation were not providing positive radiation values before sunrise and after sunset, this large term would be multiplied by zero when calculating the total radiation incident on the surface. To correct for these related issues, the curve for extraterrestrial radiation is used as a basis for interpolation rather than linearly interpolating the ground measured data (TESS 2015).

Figure 2-4 shows five distinct components that can be included in the total radiation calculation. In isotropic models, only beam, isotropic diffuse from sky dome, and ground reflected sources are considered. More advanced, anisotropic models were developed to also take into account the circumsolar diffuse and diffuse from horizon (horizon brightening) radiation. The model used by Transient System Simulation Tool (TRNSYS) in this work is referred to as the HDKR model (Hay, Davies, Klucher and Reindl) and it accounts for all five radiation components shown in Figure 2-4 (Reindl et al. 1990). The tilted surface used in this work is fixed and oriented to face due south and is tilted from the horizontal at an angle equal to the latitude of the location.

Average monthly data for Amarillo, TX in the cooling season and off season are interpolated to ten-minute intervals and displayed in Figure 2-5. The resulting values for total radiation on a tilted surface are used to simulate intra-hour power generation for an array of PV panels.

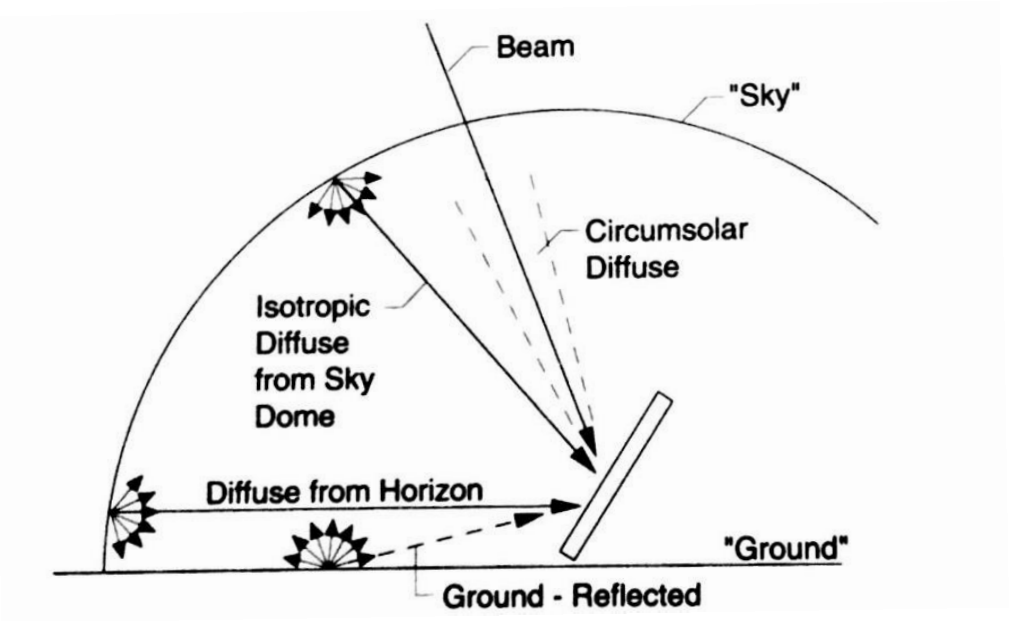

Figure 2-4. Components of total radiation on a tilted surface with an anisotropic sky (Duffie & Beckman 2013)

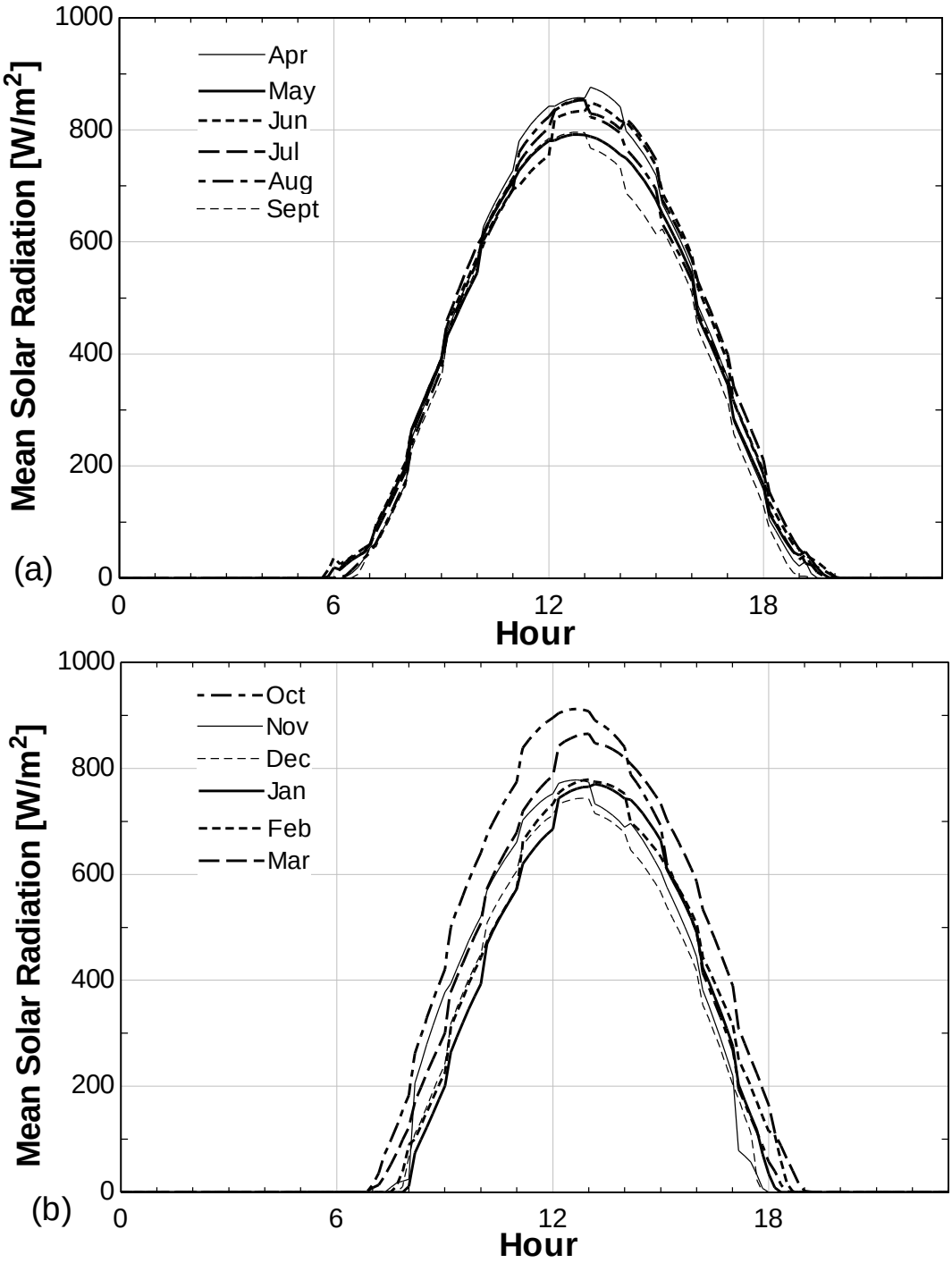

Figure 2-5. TMY3 ten-minute averaged monthly total radiation for a tilted surface data for Amarillo, TX during the (a) cooling season and (b) off season

2.2.2 Solar Power Generation Model

The solar PV panel power output is modeled using only the incident solar radiation on the tilted panel (as described in Section 2.2.1), the modeled cell temperature, and manufacturer-provided temperature coefficients that specify the change in performance with increasing cell temperature. The power output is simulated using TRNSYS Type 94a, photovoltaic array (TESS 2016). The solar output at each time-step is used as an input to the CTES system model.

The PV operating voltage, *V*, can either be set as a characteristic of the load or it is ideally varied to maximize the power output of the module. In this research, maximum power point tracking (MPPT) is used such that, for a given irradiance, the operating voltage is varied to maximize the power output. In the example shown in Figure 2-6, the red curve is the characteristic current-voltage relationship for a particular PV panel at the standard rating conditions (SRC). The SRC correspond to a solar irradiance of 1,000 W/m^2 and a cell temperature of 77°F (25°C). Without MPPT, the operating voltage would be determined by the load and the module would operate at the power corresponding to this voltage, which may be significantly below its maximum power at these conditions. Utilizing a maximum power point tracker to operate at V_M and I_M gives the best overall array performance and maximum power trackers would certainly be installed in the large-scale installations studied in this work.

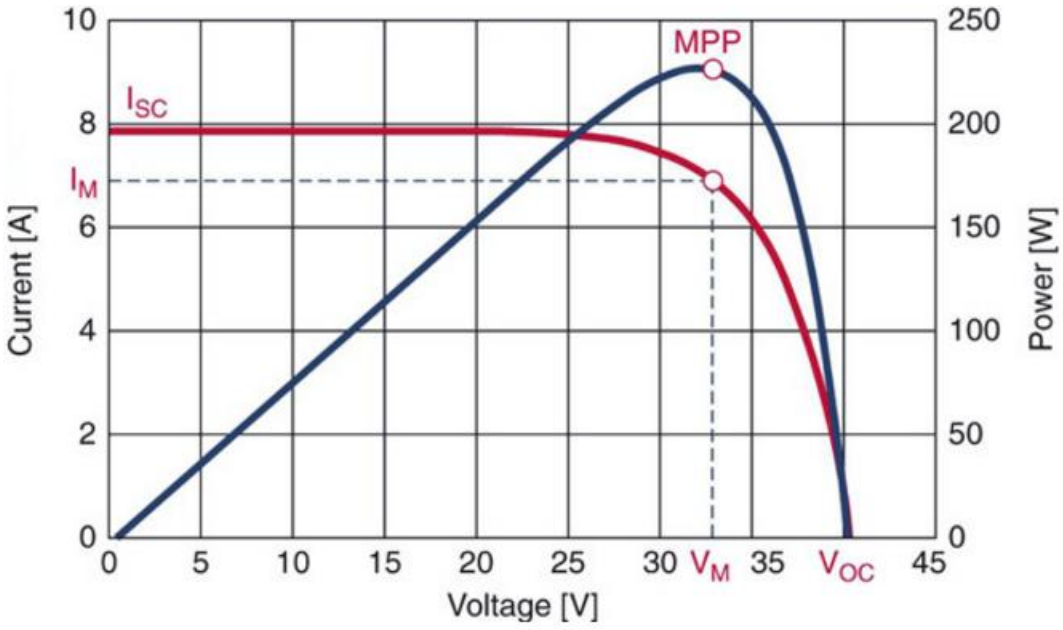

Figure 2-6. One panel current vs. voltage curve and the associated power vs. voltage curve showing the operation point for MPPT at one solar irradiance level

2.3 Building and Cooling Load Models

The Commercial Reference Building details are defined through simulation input files to EnergyPlus, a USDOE-sponsored building energy simulation program. The building envelope and internal loads are fully defined within the input file with exterior wall R-values and window U-factors that vary according to location. The two-story Secondary School building considered in this project is depicted in Figure 2-7 and the twelve-story Large Office building is depicted in Figure 2-8. Both buildings have a roof with the insulation entirely above deck (IEAD), but the Secondary School uses steel frame construction while the Large Office building uses 8 in (0.2 m) concrete wall construction.

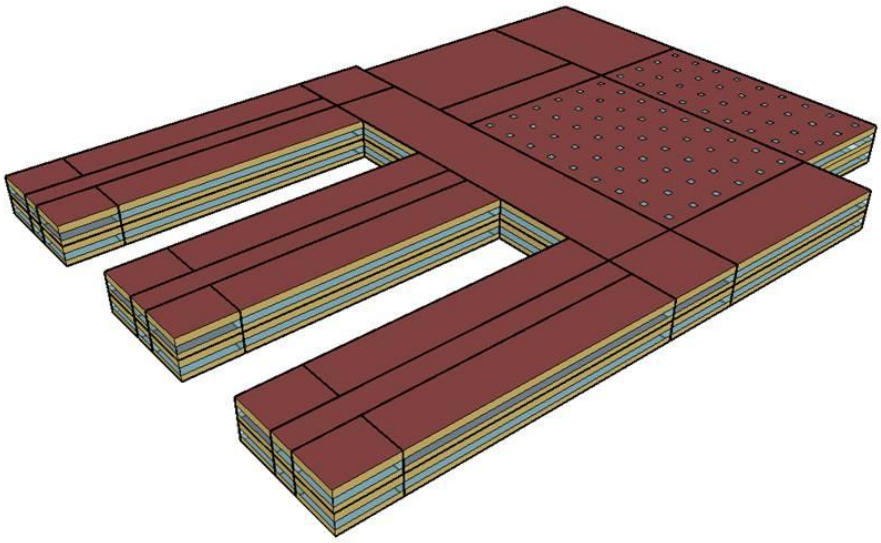

Figure 2-7. Secondary School Commercial Reference Building depiction (USDOE 2012)

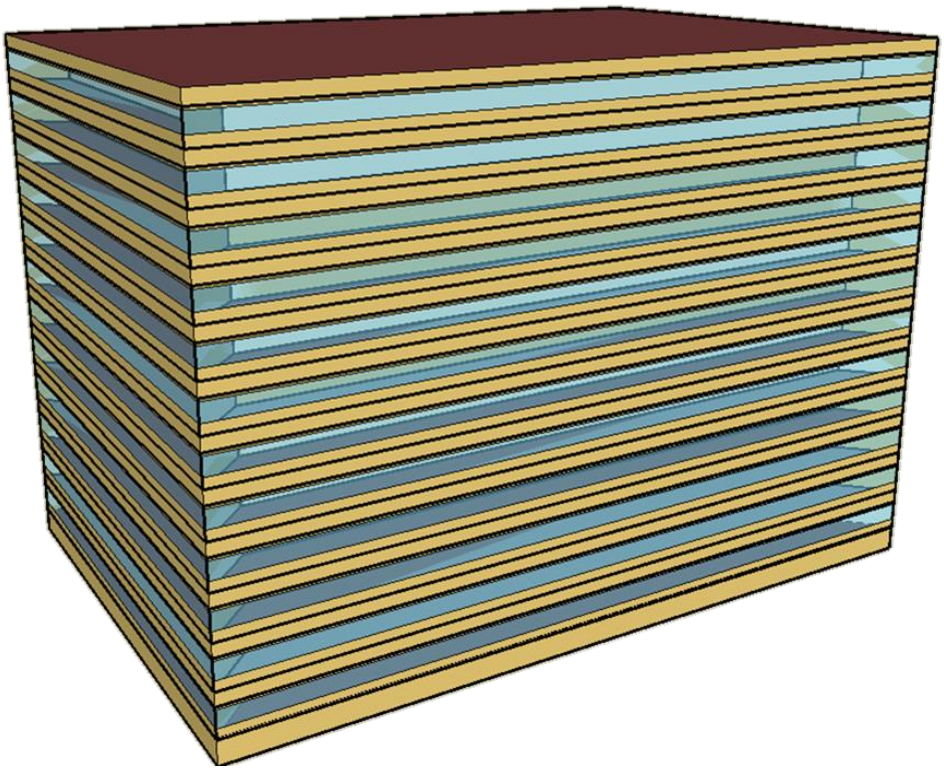

Figure 2-8. Large Office Commercial Reference Building depiction (USDOE 2012)

In addition to the input file, a weather data file for the particular location is required. These weather data are used to calculate the building loads which must be met by the building's mechanical systems that are the subject of this project. For typical year simulations, the weather data is TMY data, but for simulations covering a particular year, historical weather data is required to determine cooling loads. There are many sources for this historical weather data and some provide it in the EnergyPlus weather file format (White Box Technologies 2017). The necessity of aligning weather data with a typical or historical simulation is discussed in Section 5.4. In this project, the EnergyPlus software is used only to obtain building cooling load profiles. The nature of the optimization work being pursued necessitated simulation of the building's mechanical systems in a MATLAB program.

2.4 Cool Thermal Energy Storage System Models

Although the term "thermal energy storage" potentially encompasses many types of storage technologies operating over various time scales, this project considers only a specific technology subset pertinent to building space conditioning systems that has the potential to support increased deployment of renewable energy resources through the shifting of electrical energy demands associated with meeting building cooling loads. Specifically considered in this project will be actively controlled, cool thermal energy storage systems utilizing either water (sensible) or ice (latent) technologies operating on a daily cycle. Thermal storage technologies such as aquifer, borehole, building mass, and other approaches intended to function in support of heating and/or cooling loads on daily, weekly, or seasonal timescales are not considered. In limiting the present analysis to building-applied CTES, the primary focus is on shifting the electricity-intensive CTES charge cycle to periods where solar or wind generated electricity is in excess of the building's electric demand. The stored thermal energy is then subsequently utilized during periods when the

building's cooling loads persist but the electricity available from solar or wind resources has diminished.

A chiller plant that directly meets the facility load without storage serves as the baseline for comparison with the CTES system options. This system is referred to as the "no-storage" case throughout this work and corresponds to the simple direct-chilling system as shown schematically in Figure 2-9. The chiller for the non-storage system operates anytime the building has a cooling load. The fluid flow rate to the building's air-handlers is variable and adjusted to maintain a chilled water temperature differential of 10°F (5.5°C). This differential applies to the no-storage case only. The installed chiller capacity is sized to meet the annual peak cooling load. The simulation model for the central plant consists of two equally sized chillers for both redundancy and improved efficiency at part-load operation.

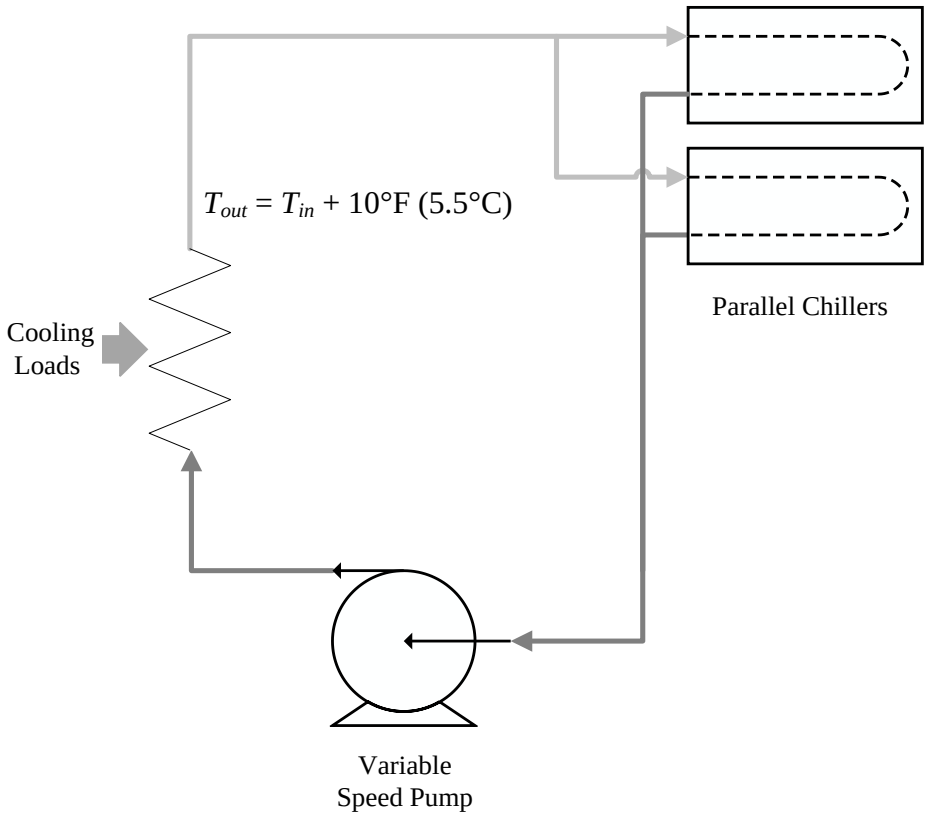

Figure 2-9. No-storage system schematic

2.4.1 Chilled Water CTES Model

In a stratified chilled water CTES system, a single tank stores thermal energy by utilizing water's natural tendency to stratify – warmer, less dense fluid at the top and cooler, more dense fluid at the bottom. The energy density for a stratified chilled water tank is approximately 0.1 ton-hr/ft^3 (12 kWh/m^3) (EPRI 2008). During a charge cycle, warm water is drawn from the top of the tank and circulated through the chiller where it is cooled to the supply water temperature set point and supplied back to the bottom of the storage tank where it is made available to subsequently meet building loads during its discharge cycle. During a discharge cycle, the cool water is drawn off the bottom of the storage tank and circulated to cooling coils in the building's air-handling units where the temperature increases due to heat exchange with the air being cooled before being

returned back to the top of the storage tank. The discharge cycle can proceed with or without chiller operation.

The schematic in Figure 2-10 shows the stratified chilled water CTES system layout simulated in this work. The EnergyPlus building model provides the water-side cooling load to be met by the chiller plant and storage system, when equipped. The system is designed to operate with a 20°F (11°C) water-side temperature differential. This larger temperature differential is typical of stratified chilled water CTES systems in building applications. Compared to a no-storage case, it offers benefits that include reduced chilled water pumping power (on the load side), increased storage density, and improved stratification due to the greater differential fluid density.

The power consumed by the building's air handling system and circulating pumps are not considered as part of this work because both storage and non-storage system options are presumed to utilize similar inter-building cooling infrastructure. The one exception is that the fan and pump power for cooling tower operation are included. The variation in pumping power between no-storage systems and CTES systems have been assumed to be negligibly small. This assumption is based on the EnergyPlus simulation for the Secondary School which shows that annual pumping energy is less than 3% of the annual chiller energy consumption. On the air-handling side, the decision to neglect the circulating pumping power is a conservative one since the load-side temperature differential is larger for CTES systems than no-storage systems. The larger differential allows for reduced pumping power to meet the same cooling load. On the primary side, overall pumping energy consumption may be higher for CTES systems than no-storage systems since pumps run more frequently to charge storage without cooling loads. Thermal losses from the water tank and piping have been neglected and the tank is modeled as a two-zone isothermal tank. This means that the typical thermocline width of a few feet or less is assumed to have zero height. The

consequence of this assumption is a slight underestimate of the required tank volume for the capital cost calculations.

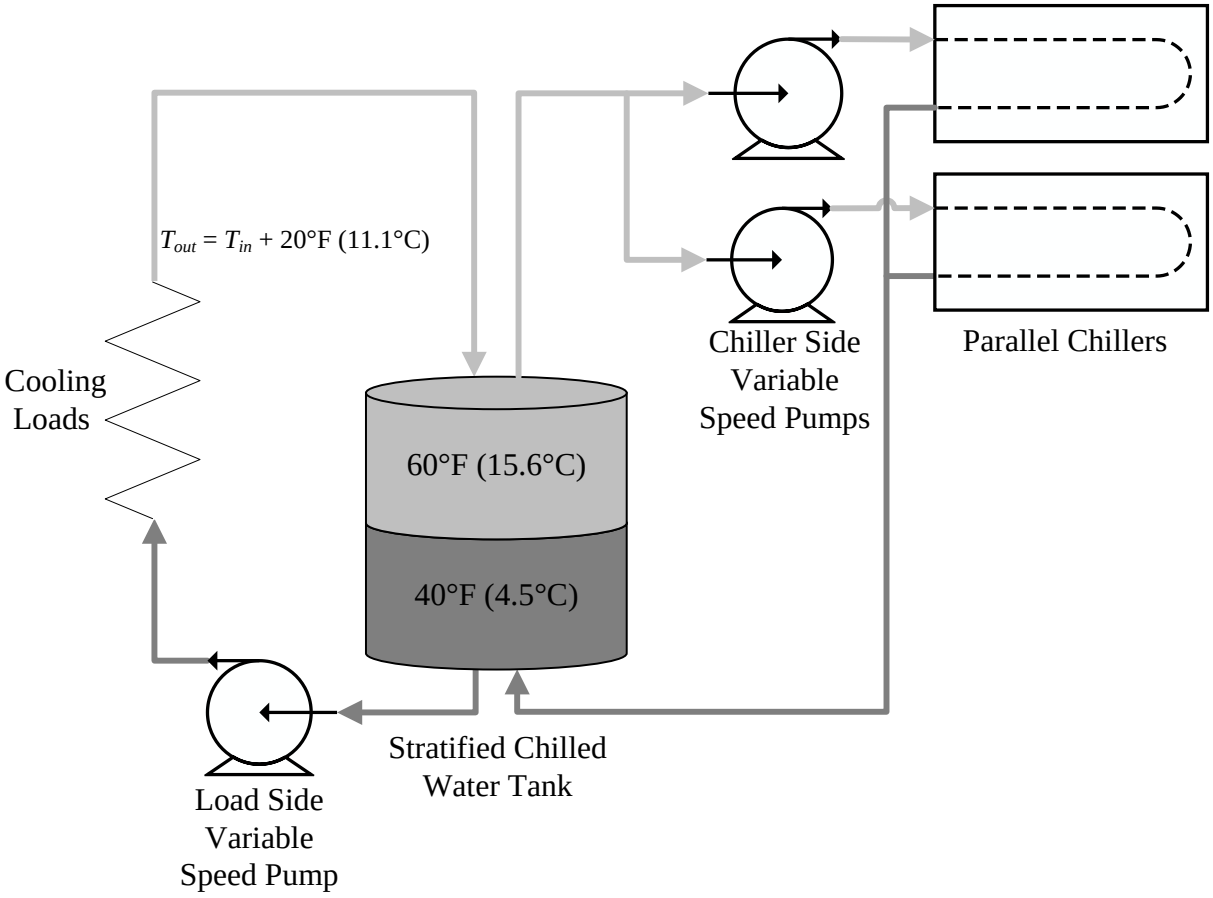

Figure 2-10. Stratified chilled water CTES with parallel chillers schematic

The chilled water CTES tank decouples the chillers from the building cooling loads. The primary loop circulating pumps connecting the chillers to the stratified chilled water tank operate at variable speed. Warm water drawn from the top of the water tank returns to the bottom with the same mass flow rate. The secondary loop pump connecting the water tank to the building cooling loads (air handling equipment) also operates at varying speeds so that a constant temperature rise can be maintained with varying cooling loads.

2.4.2 Ice CTES Model

Latent CTES systems take advantage of the energy absorbed and released during the solidification and melting of water at a constant temperature during its phase change. Generally, this latent heat of solidification/melting allows ice CTES systems to yield a higher energy storage density compared to the sensible energy change in chilled water systems. Although other types of phase change materials have been used, ice is the most widely applied medium for latent CTES systems. Ice CTES systems have a density in the range of 0.29-0.45 ton-hr/ft^3 (36-56 kWh/m^3) compared to 0.1 ton-hr/ft^3 (12 kWh/m^3) for chilled water (EPRI 2008). Due to the increased energy storage density, ice CTES systems have a distinct advantage in building applications where space for siting a storage system is limited.

The ice CTES technology employed in this work is a static ice-on-coil internal-melt system. A single ice CTES tank, as well as a representation of the charging and discharging processes, is shown in Figure 2-11. These modular ice CTES tanks are piped in parallel as needed to obtain the necessary integrated storage capacity for a given building mechanical system. During a charge cycle, low temperature glycol leaving the chillers flows through a coiled heat exchanger immersed in each cylindrical water-filled storage tank. Water within the tank freezes on the outside of the heat exchanger which will then be available to absorb heat during a subsequent discharge cycle. During the discharge cycle, warm glycol returning from the load circulates through the spiral-coiled heat exchanger and is cooled as it melts the ice stored within the tanks.

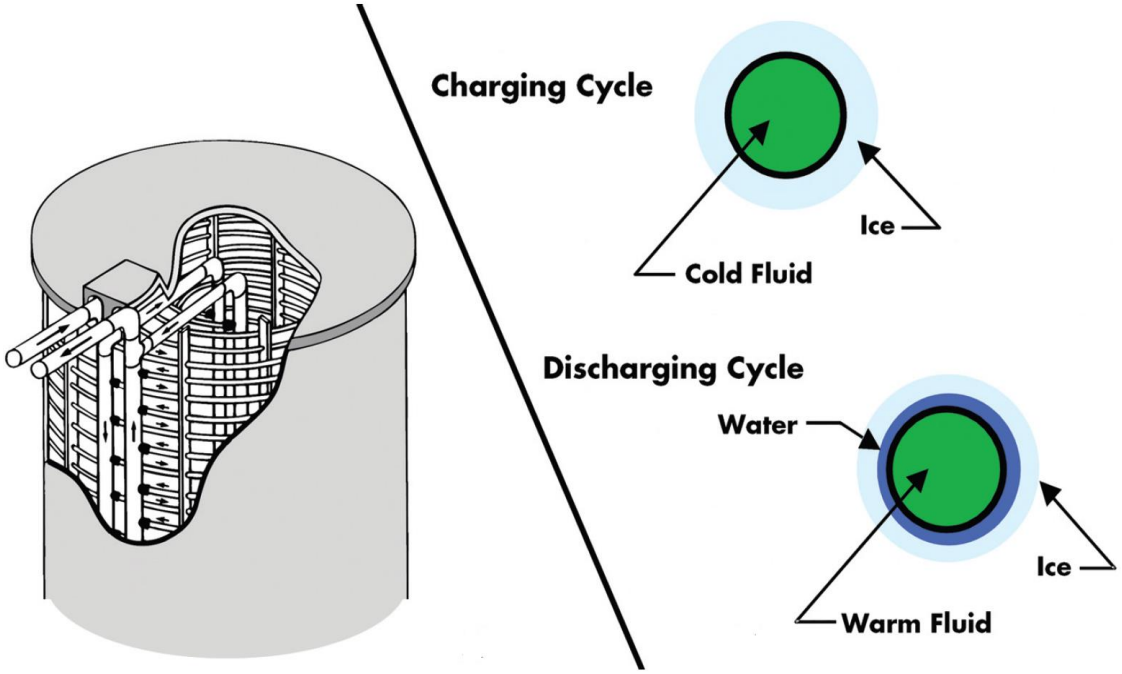

Figure 2-11. Ice CTES tank cutaway with charging and discharging cycle detail (EPRI 2008)

A schematic of the ice CTES system modeled for this work is shown in Figure 2-12. The working fluid is a solution of 25% (by mass) ethylene glycol and water referred to simply as "glycol" throughout this work. The parameters defining the ice CTES system are summarized in Table 2-2. Two chillers in parallel provide chilled glycol at a variable mass flow rate and fixed set point temperature, T_{chws}. The maximum glycol mass flow rate, $\dot{m}$, is a constant and multiplied by the number of tanks piped in parallel (Trane 1990). When charging storage, the glycol supply temperature is set to T_{ice} and when discharging and/or meeting the cooling loads directly, the supply temperature is set to T_{load}. Depending on the discharge mode of operation and current cooling

loads, the chiller system may not always be able to achieve the desired set point temperature of T_{load} and the glycol supplied to the tanks will be warmer than this temperature.

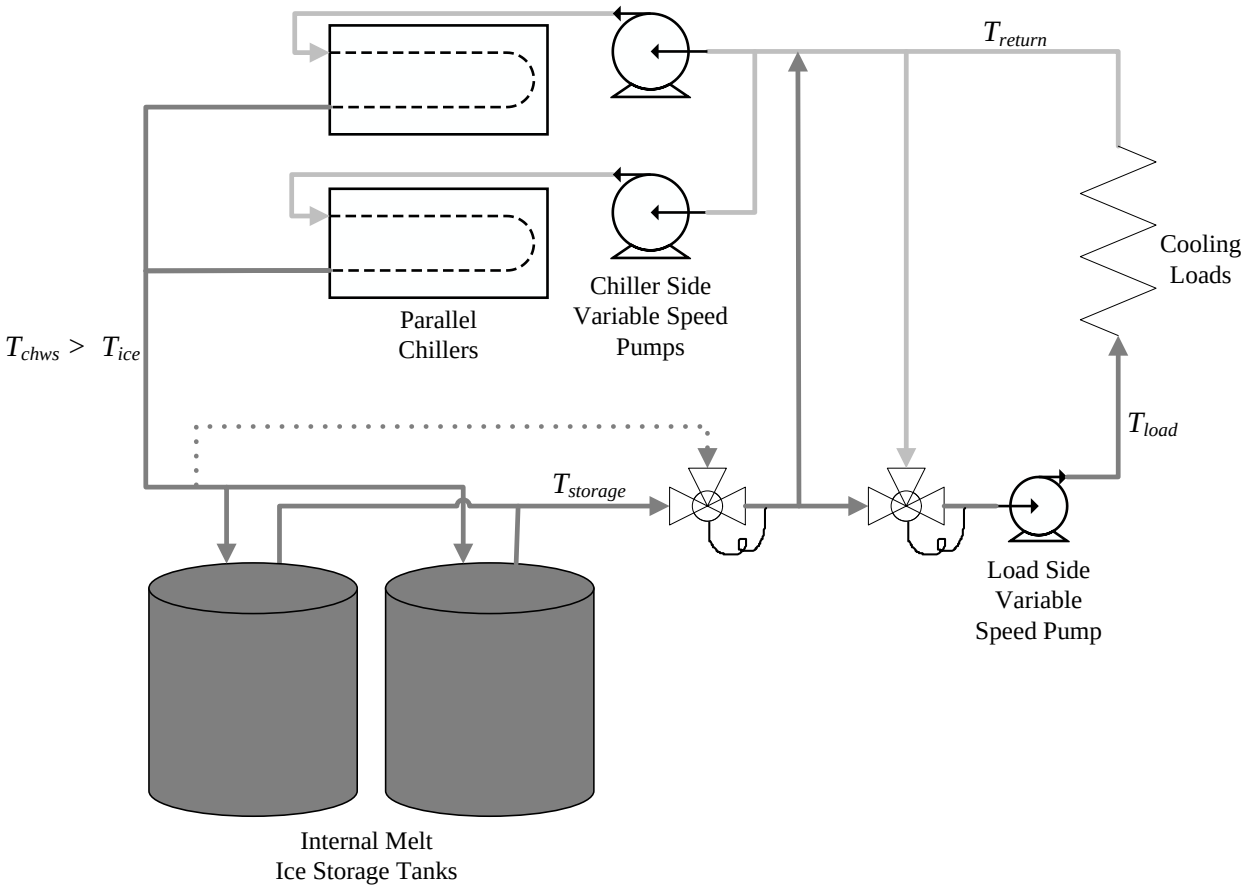

Figure 2-12. Ice CTES system schematic while in the "Make Ice and Cool" charging operation mode

Table 2-2. Ice CTES model parameters

Parameter	Definition	Value
T_{ice}	Ice-making temperature	20°F (-6.7°C)
T_{load}	Secondary loop temperature to meet load	44°F (6.7°C)
T_{chws}	Chilled water set point temperature	Set to either T_{ice} or T_{load}
T_{return}	Cooling load return temperature	56°F (13.3°C)
$T_{storage}$	Ice tank glycol outlet temperature	Output of model
T_{fr}	Freezing point of water	32°F (0°C)
$\dot{m}_{ice}$	Primary loop design mass flow rate	60 GPM per 162 ton-hr tanks (3.9 kg/s per 570 kWh tank)
c_{gly}	Specific heat capacity of the glycol solution	0.90 Btu/lb-°F (3.76 kJ/kg-K)

Downstream of the ice CTES tanks is the first temperature-modulating valve which controls the bypass of glycol around the storage tanks. Immediately following is a second temperature-modulating valve which controls the flow rate of the return glycol being blended to meet the desired secondary loop temperature, T_{load}, of 44°F (6.7°C). This valve is only open when there is a cooling load (as is the situation in Figure 2-12), otherwise the glycol returns directly to the chillers. When there is a demand for cooling by the building, the load-side variable speed pump responds to increase or decrease the glycol flow rate in order to maintain a glycol temperature differential of 12°F (6.7°C), equivalent to a return temperature, T_{return}, of 56°F (13.3°C). Finally, the return glycol stream is either directed fully back to the chillers or a portion of the stream is blended with the storage tank output to achieve the secondary loop supply temperature with the remainder of the return glycol supplied to the chillers.

The thermal performance of the ice CTES tank will depend on its state of charge. The total heat transfer rate is determined using the overall heat transfer coefficient and the log mean temperature difference for the tank as shown in the following equation for the charging case.

$$\dot{Q}_{ice,ch} = UA_{charging} \frac{(T_{storage} - T_{ice})}{\ln\left(\frac{T_{fr} - T_{ice}}{T_{fr} - T_{storage}}\right)} \quad (1)$$

where $UA_{charging}$ is a function of the current state of charge. Looking at the second term in Equation (1), the log mean temperature difference, it is clear that reducing the ice-making glycol temperature, T_{ice}, results in an increase in the charging rate due to the increased in log mean temperature difference.

The performance characteristic of the ice CTES tank used for this work is plotted in Figure 2-13 for two different flow rates. While a constant T_{ice} of 20°F (-6.7°C) is used in this study, ice CTES systems commonly use a varying ice-making temperature which ranges from approximately 26°F (-3.3°C) early in the charge cycle down to 20°F (-6.7°C) toward the end of the charge cycle. In the present analysis, a constant ice-making temperature at the lower end of this range is used and results in a conservative estimate of the chiller energy consumed since the chiller system performance is reduced at this low set point temperature. Furthermore, a charge cycle is terminated when the storage tank's state-of-charge reaches 90% due to the diminishing heat transfer rate capability of the storage tank with the high state-of-charge. This diminishing heat transfer rate is attributable to the model for one ice CTES type and may not be an intrinsic feature of all ice CTES types.

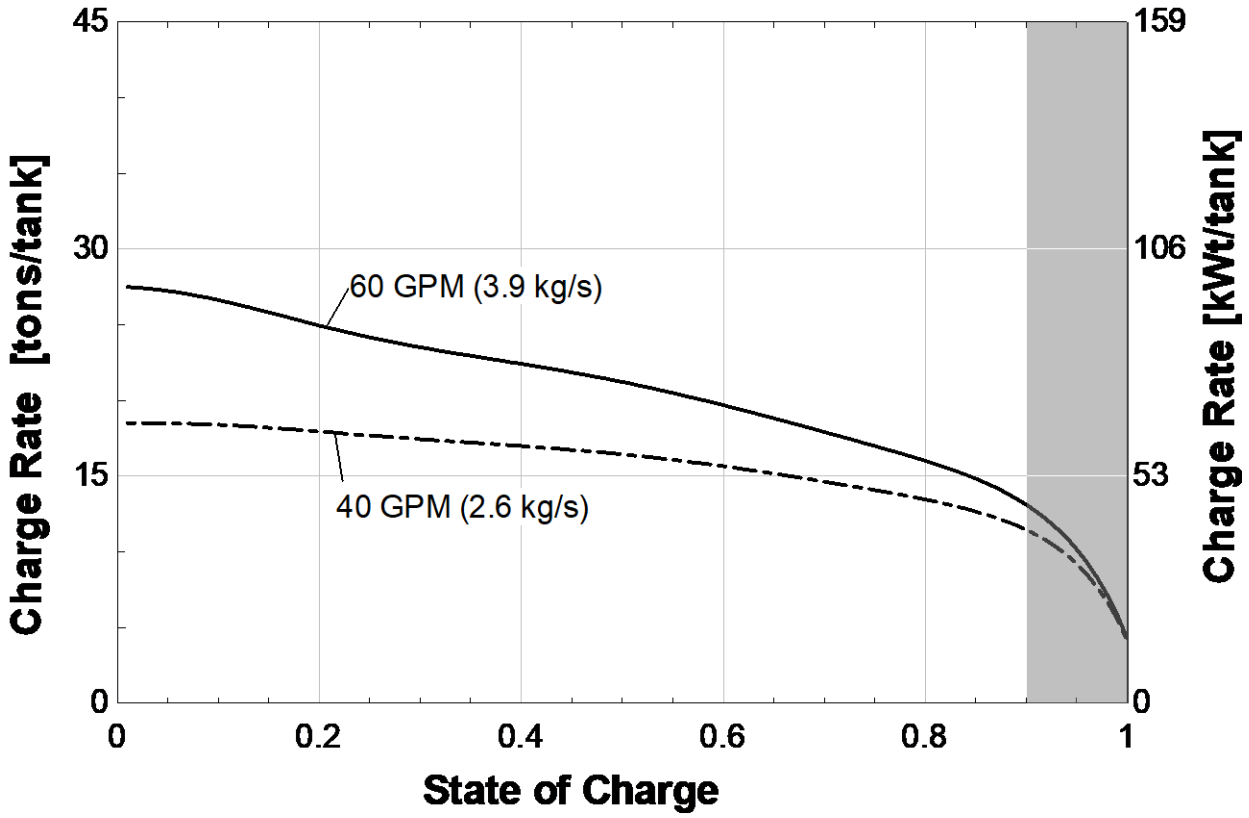

Figure 2-13. CTES charging rate for a constant ice-making glycol temperature of 20°F (-6.7°C) with a shaded region over the unused portion of the curves (data adapted from USDOE 2010)

For the discharging process, the heat transfer rate is calculated using the equation below.

$$\dot{Q}_{ice,dis} = UA_{discharging} \frac{(T_{load} - T_{storage})}{\ln\left(\frac{T_{load} - T_{fr}}{T_{storage} - T_{fr}}\right)} \tag{2}$$

In this equation, the maximum inlet glycol temperature to the storage tank is T_{return}, 56°F (13.3°C) with the actual temperature ranging between 44 and 56°F (6.7 and 13.3°C) depending on the building load. As the building load decreases, the secondary loop flow decreases and a portion of the primary loop flow is used to blend down the return temperature to the chillers. Discharge rates as a function of the tank state of charge are shown in Figure 2-14 for a constant glycol return

temperature of 50°F (10°C). As the tanks discharge to approximately 10% of their capacity, there is a significant drop-off in discharge rate. Again, the magnitude of this drop-off may not necessarily represent all ice CTES types.

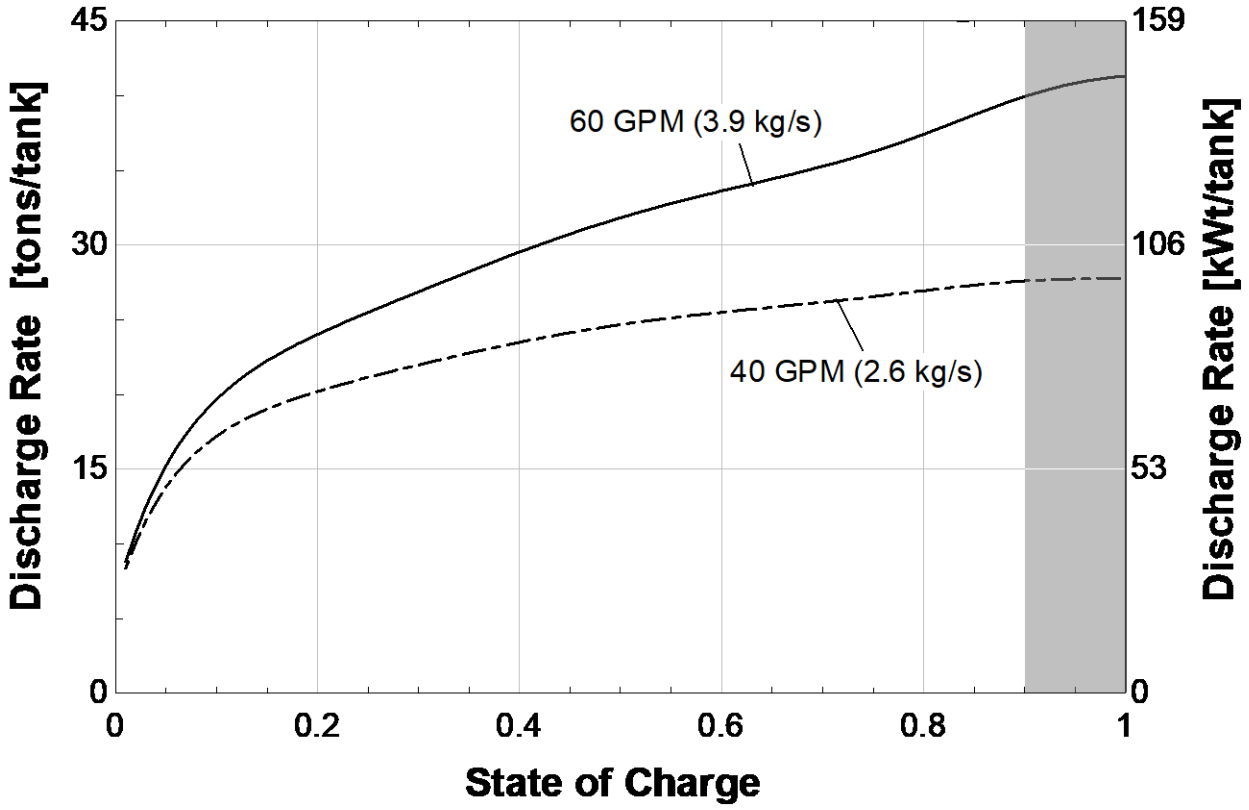

Figure 2-14. CTES discharging rate for a constant glycol return temperature of 50°F (10°C) with a shaded region over the unused portion of the curves (data adapted from USDOE 2010)

Neglecting thermal losses and equating energy balances on the charging storage tank and the glycol stream, a calculation of the storage tank outlet temperature, $T_{storage}$, is possible. For the charging case, the energy balance is shown below.

$$\dot{Q}_{ice,ch} = UA_{charging} \frac{(T_{storage} - T_{ice})}{\ln\left(\frac{T_{fr} - T_{ice}}{T_{fr} - T_{storage}}\right)} = \dot{m}_{ice} c_{gly} (T_{storage} - T_{ice}) \quad (3)$$

Rearranging and setting T_{fr} to 0°C, gives the final expression used for $T_{storage}$.

$$T_{storage} = T_{ice} \exp\left(\frac{-UA_{charging}}{\dot{m}_{ice} c_{gly}} \right) \quad (4)$$

Similarly, for a discharging ice CTES tank, $T_{storage}$ is given by the following equation with the tank inlet temperature being T_{load} rather than T_{ice}.

$$T_{storage} = T_{load} \exp\left(\frac{-UA_{discharging}}{\dot{m}_{ice} c_{gly}} \right) \quad (5)$$

2.4.3 Ice CTES System Operation Modes

The ice CTES system is capable of operating in six distinct modes. The first and simplest mode is "Off" with the chiller system off and the ice storage tanks neither charging nor discharging. The operating modes that include charging are "Make Ice and Cool" and "Make Ice." The discharging modes are "Chiller and Ice" and "Ice Only." The sixth mode, "Chiller Only," neither charges nor discharges the storage tanks, but uses the chillers to directly meet building cooling loads while completely bypassing the storage tanks.

"Make Ice and Cool" is displayed in Figure 2-12 where the chillers are set to T_{ice} and all of the supply glycol leaving the chillers is routed first through the storage tanks. The actual glycol temperature leaving the chillers is based on the currently available chiller capacity (which depends on the chiller's entering glycol temperature, ambient temperature conditions, and whether or not the chiller is operating at part load) and may be equal to or greater than $T_{ice,}$ but will be less than the freezing point of water. The tank outlet glycol temperature, $T_{storage}$, is calculated using Equation (4). Because $T_{storage}$ is colder than T_{load}, 44°F (6.7°C), the temperature required to meet the cooling loads, the second temperature modulating valve blends the return glycol so that the temperature of the glycol supplied to meet the building cooling loads is at T_{load}.

The system schematic for operation in “Make Ice” mode is shown in Figure 2-15. During this operating mode, all of the supply glycol leaving the chillers is routed to the storage tanks by the first valve and the fluid leaving the tanks is all returned to the chillers. No building cooling loads are met during this mode.

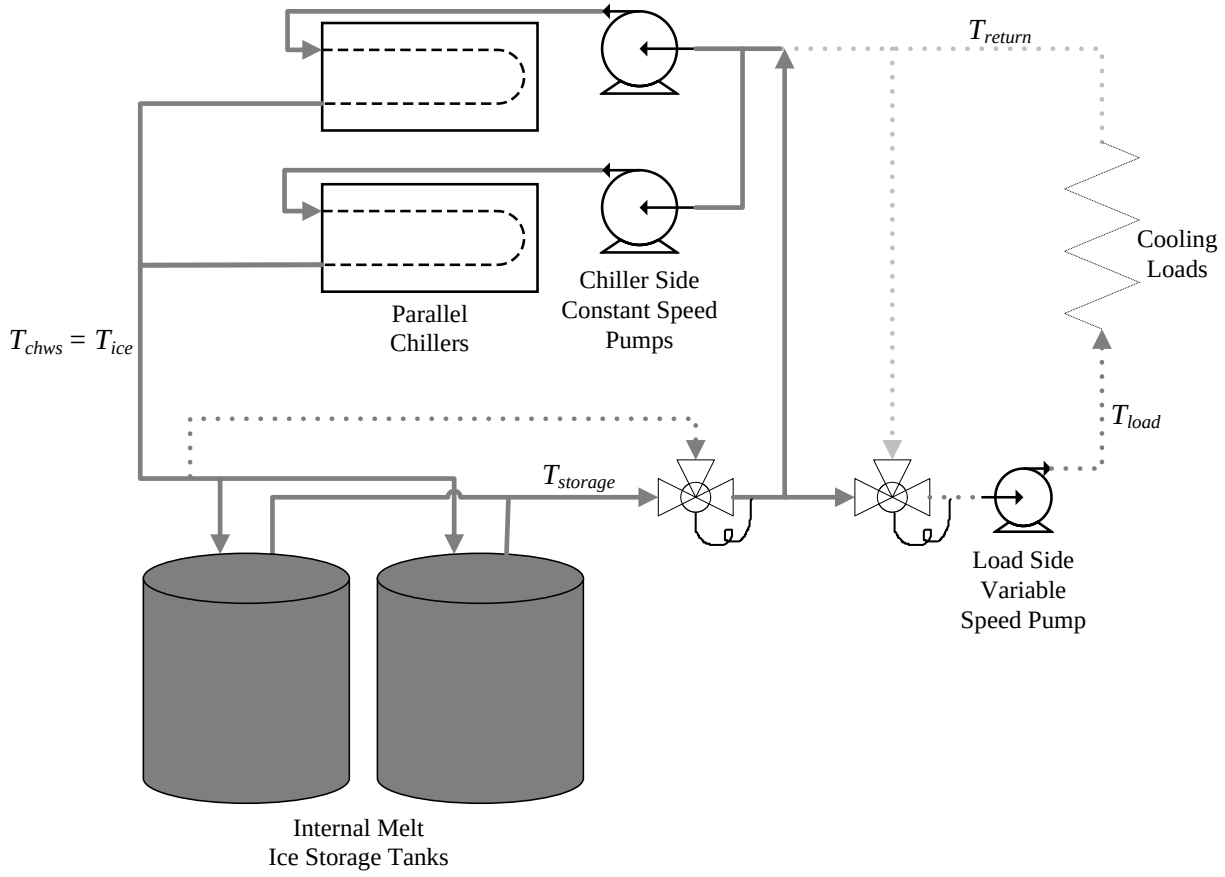

Figure 2-15. Ice CTES system schematic while in the “Make Ice” charging operation mode

The “Chiller and Ice” discharging mode is shown in Figure 2-16. This mode is employed when both the chillers and the storage discharge are required to meet the cooling loads. The chiller leaving glycol set point temperature is T_{load}, 44°F (6.7°C), but the actual leaving glycol temperature is based on the current chiller capacity and entering glycol temperature. If the set point is achieved, the operation mode changes to “Chiller Only.” Based on achieving a temperature of T_{load} at the

outlet of the first valve, some of the flow bypasses the tanks and some is routed through the storage tanks.

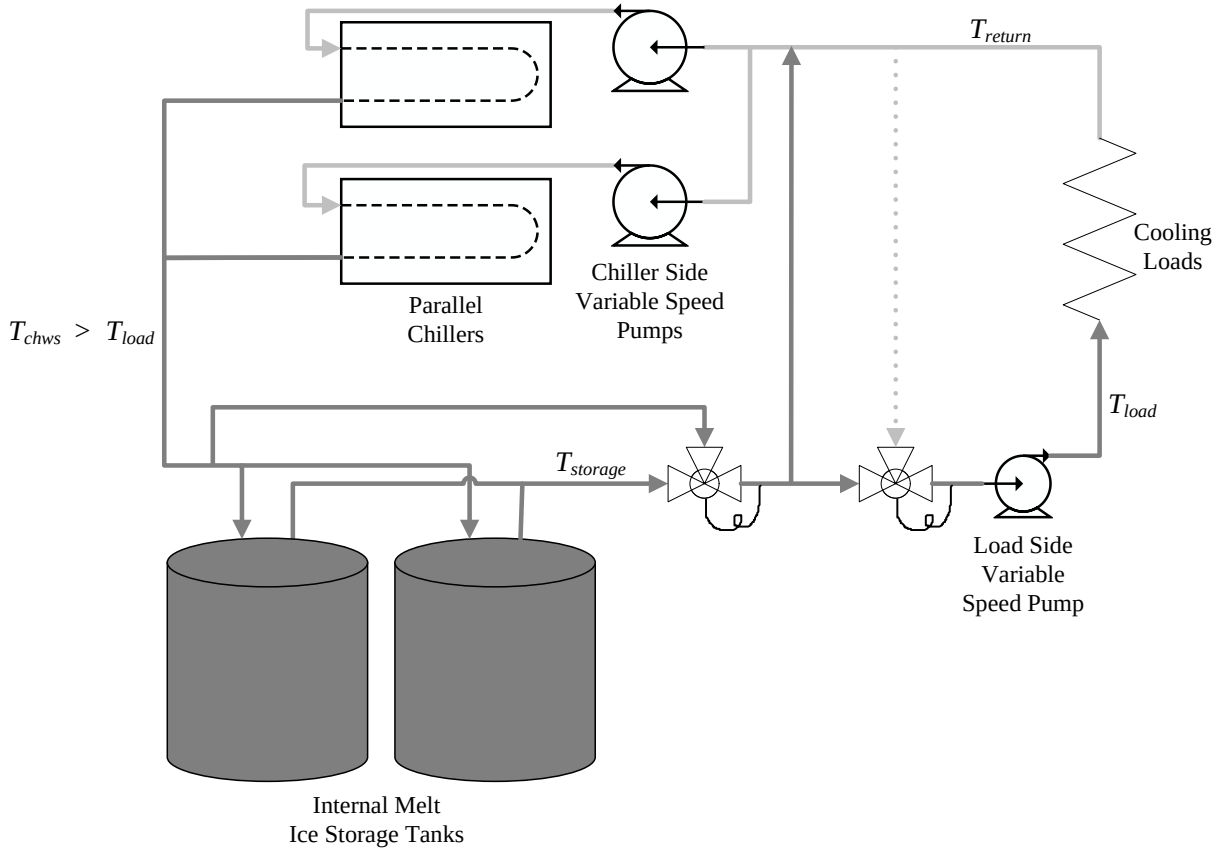

Figure 2-16. Ice CTES system schematic while in the "Chiller and Ice" discharging operation mode

The schematic in Figure 2-17 shows the "Ice Only" discharging operation mode. When the storage discharge rate is sufficient to meet the cooling load and the control strategy dictates that the chillers should be idle, the load is met with storage only. The glycol leaving the storage tanks, at the modeled value for $T_{storage}$, is blended with glycol bypassing the storage tanks to reach the desired load-meeting temperature, T_{load}. The glycol required to meet the cooling loads goes through the secondary loop and the remainder bypasses the loop and mixes with the return glycol to go back to the storage tanks.

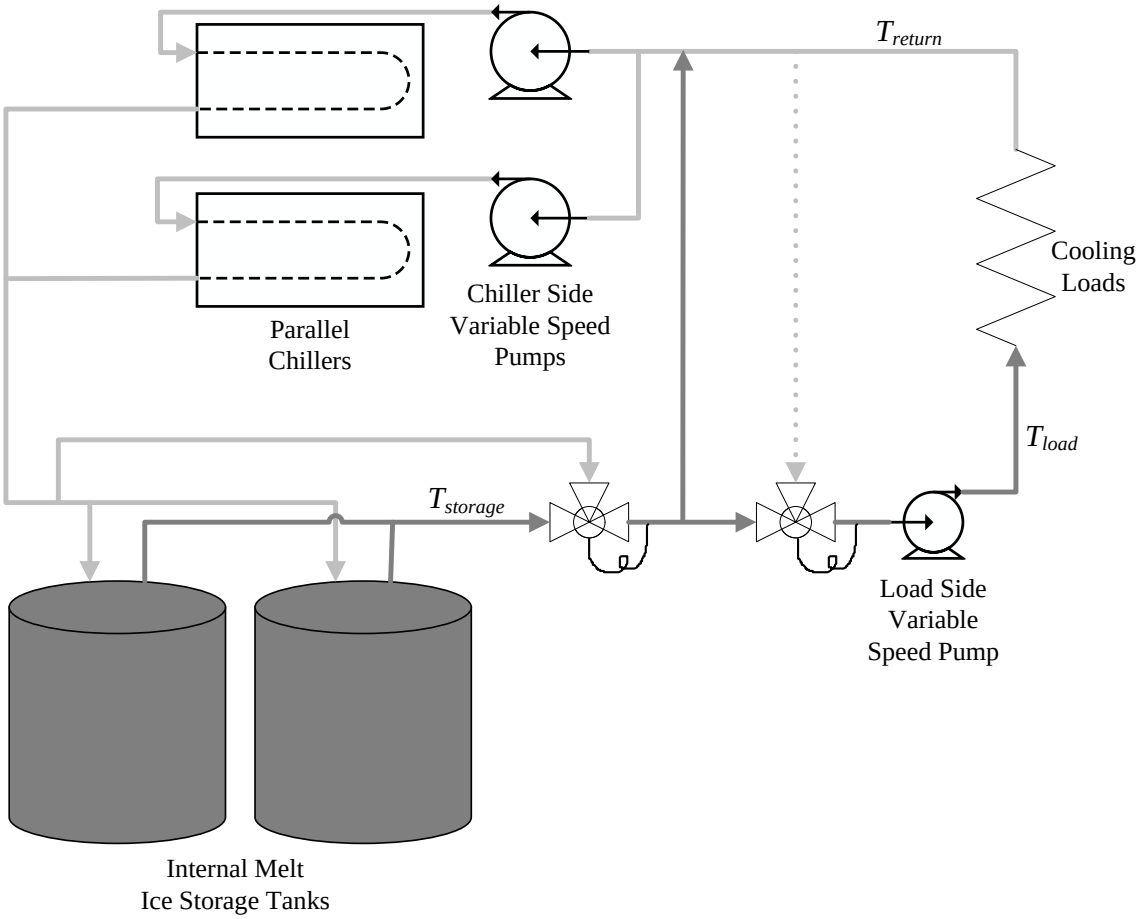

Figure 2-17. Ice CTES system schematic while in the "Ice Only" discharging operation mode

The sixth operation mode is depicted in Figure 2-18 and involves neither charging nor discharging of the storage tanks. The cooling loads are met directly by the chillers in the "Chiller Only" operation mode. The first temperature modulating valve causes the glycol to bypass the storage tanks and the glycol required to meet the cooling loads goes through the secondary loop. The system then operates in a manner similar to the no-storage system shown in Figure 2-9.

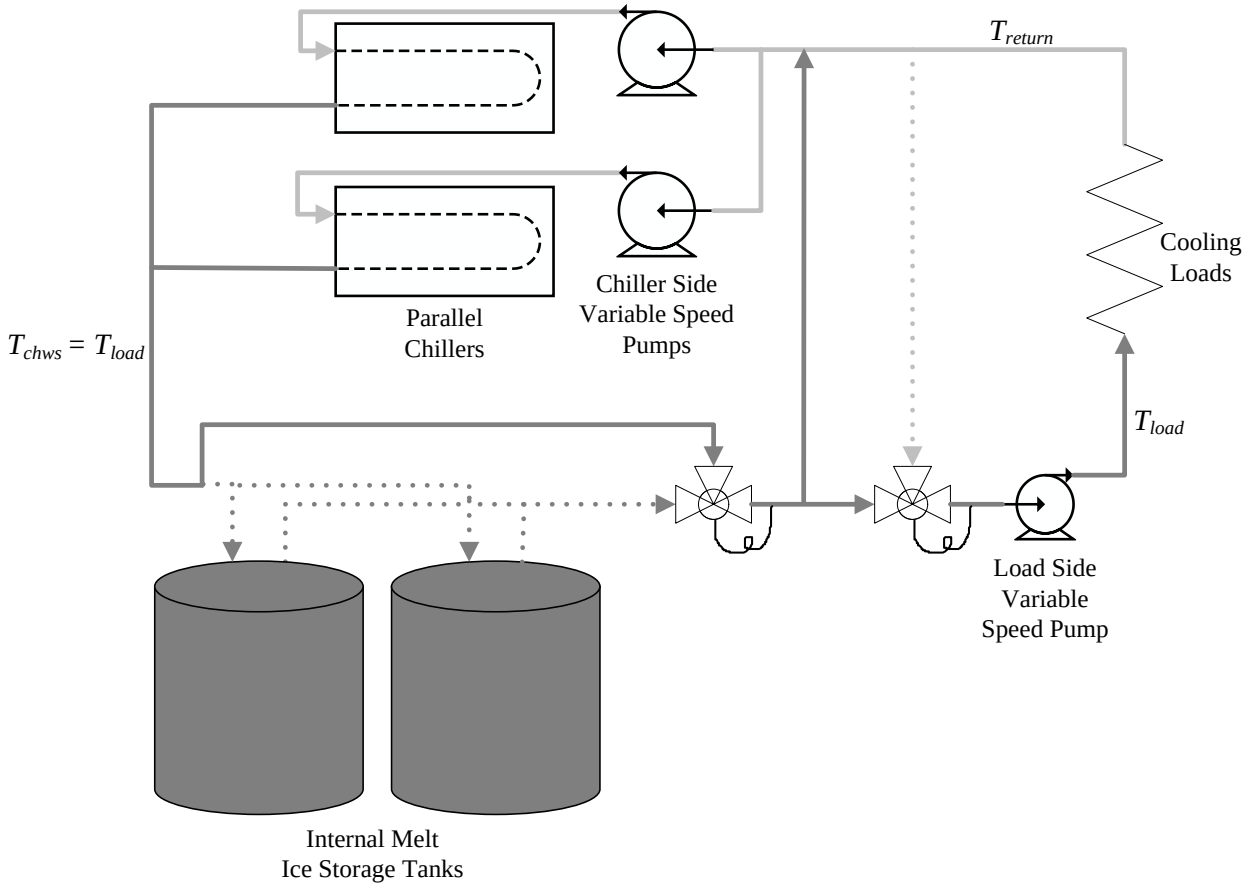

Figure 2-18. Ice CTES system schematic while in the "Chiller Only" operation mode

2.5 Chiller and Cooling Tower Models

The two building types were selected based on the differences in their peak cooling loads. This difference in cooling load justifies a difference in the chiller technology employed. The Secondary School model utilizes air-cooled chillers with screw compressors, an example of which is depicted in Figure 2-19. An example of the water-cooled chiller with a centrifugal compressor used in the Large Office building is shown in Figure 2-20. For this research, neither chiller type uses a variable frequency drive (VFD) for the compressors to unload the chiller. The air-cooled screw chillers use a slide valve for capacity control and the water-cooled chillers use inlet guide vanes to vary the chiller's capacity. Although improved part-load performance is possible with the

use of VFDs, decoupling of the cooling loads from chiller operation with storage allows for reduced operating time at low part-load ratios which results in better performance. Also, this research is intended to assess the impact that is possible in the near term and much of the chilling technology currently deployed in the field is sans VFDs on the chiller's compressor.

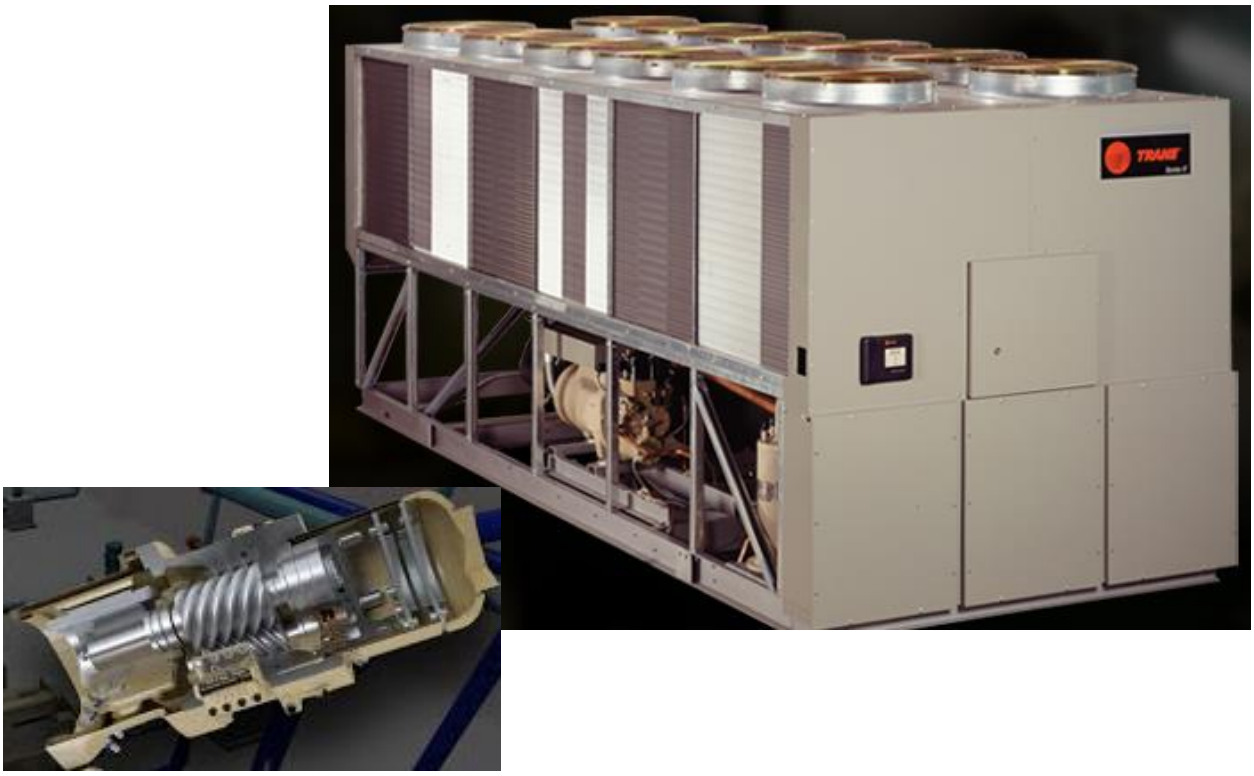

Figure 2-19. Screw compressor and air-cooled rotary screw chiller (photos from Trane 2016)

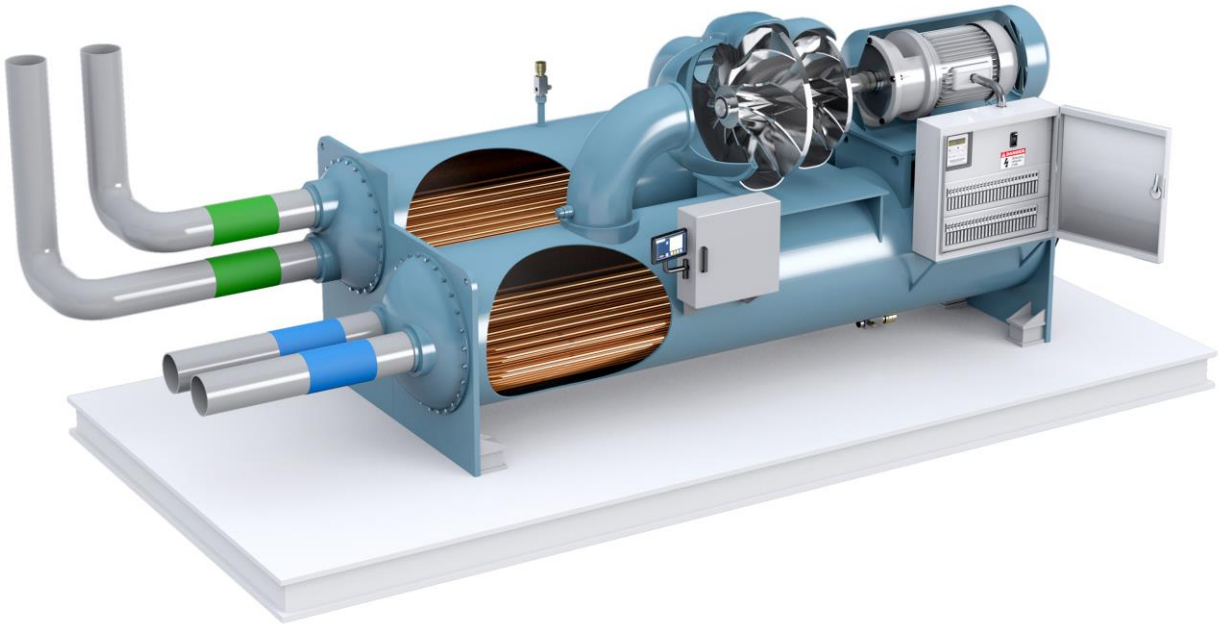

Figure 2-20. Centrifugal water-cooled chiller cutaway view (figure from Bowker 2016)

For the water-cooled chillers, the terminal means of chiller heat rejection takes place in induced-draft cooling towers equipped with axial fans. The cooling tower circulating pumps are constant speed while the tower fans are variable speed. An example of the type of cooling tower modeled in this work is shown in Figure 2-21.

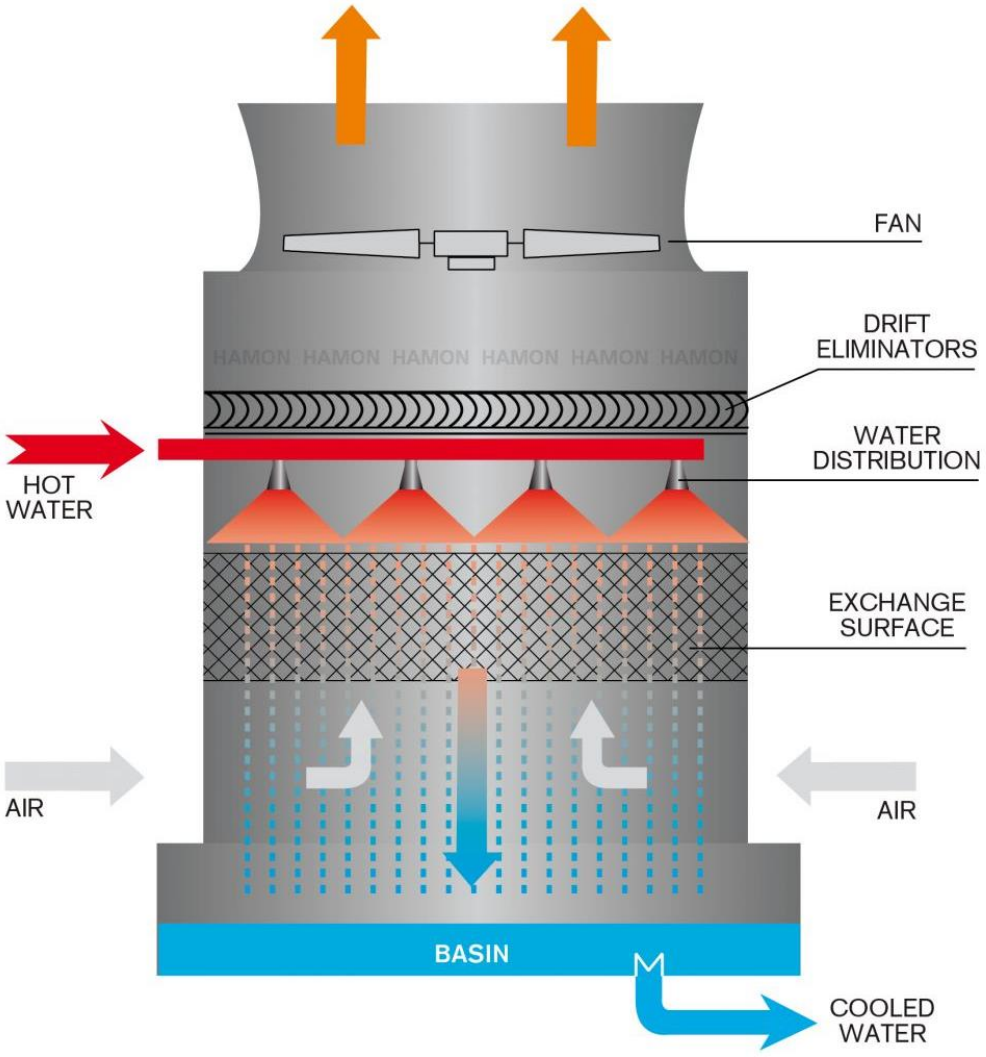

Figure 2-21. Induced-draft cooling tower with an axial fan (figure from Hamon Group 2016)

2.5.1 Air-Cooled Chiller Model

The air-cooled chiller performance is a function of three variables. The first variable is the chiller's part-load ratio. The part-load ratio is defined as the instantaneous chiller load divided by its available full-load capacity at the present ambient conditions and set point. The second variable is the ambient dry-bulb temperature, T_{db}, which impacts the chiller's condensing pressure to achieve the required heat rejection. Higher ambient dry-bulb temperatures will result in greater condensing pressure (and temperature) and decreased chiller efficiency and capacity. The third

variable is the chilled water set point temperature, T_{chws}. A lower T_{chws} increases the chiller lift which, in turn, increases the compressor work and decreases the chiller efficiency and available capacity.

The California Energy Commission (CEC) has performed an analysis of several manufacturers' equipment performance curves (CEC 2012). These curves were developed for use in energy simulations carried out to demonstrate compliance with California energy efficiency standards. The only user-defined variable for these curves is the chiller performance at the rated condition for a chilled water set point of 44°F (6.7°C), an ambient dry-bulb temperature of 95°F (35°C), and full-load chiller operation (AHRI 2011). The performance is defined by the chiller's coefficient of performance (*COP*) given in the equation below.

$$COP = \frac{Cooling\ Power\ Output}{Electric\ Power\ Input} \tag{6}$$

The rated *COP* of 3.0 chosen for the air-cooled chiller in this research meets the ASHRAE 90.1-2013 standard which went into effect on January 1, 2015 (ASHRAE 2013). The chiller performance curves for a chilled water set point of 44°F (6.7°C) are shown in Figure 2-22. The COP is negatively correlated with increasing dry-bulb temperature and positively correlated with increasing part-load ratio. Chiller performance at part-load ratios approaching the lower technical limit of 0.15 is poor. In order to operate less frequently at these poor operating efficiency conditions, two equally sized chillers can be run in parallel. An additional benefit and motivation for meeting the cooling load with two chillers is the redundancy provided. The redundancy is especially valuable in the case of a system which also utilizes a CTES system because the storage can be fully charged and used to meet load in parallel with one of the chillers if the other chiller needs to be brought down for maintenance.

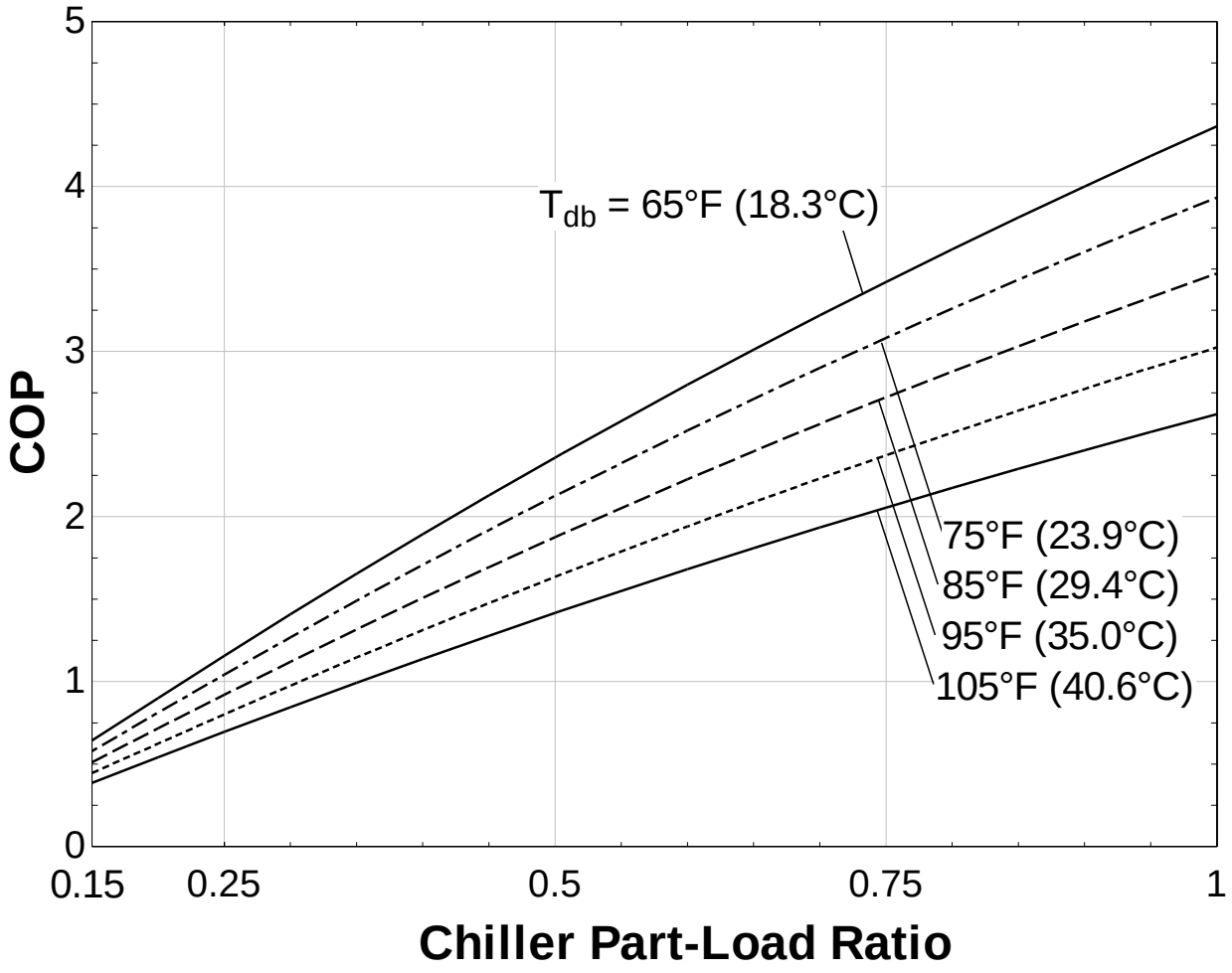

Figure 2-22. Air-cooled chiller performance curves with a chilled water set point of 44°F (6.7°C) (data from CEC 2012)

With two equally-sized chillers in parallel, each chiller is run at equal part-load ratios down to half of the overall building part-load condition. Once the building's part-load decreases below 0.5, only one chiller is needed to meet the overall building load and the system performance will then follow the performance curve of that single chiller. The performance curves for two chillers in parallel are shown in Figure 2-23. In this case, the part-load ratio on the x-axis is the load relative to the installed capacity required for the entire building. With the chillers run in parallel and a dry-bulb temperature of 95°F (35°C), the *COP* stays above 1.6 until the building part-load ratio

drops below 0.25. With a single chiller, the COP would drop below 1.6 at a part-load ratio of just under 0.5.

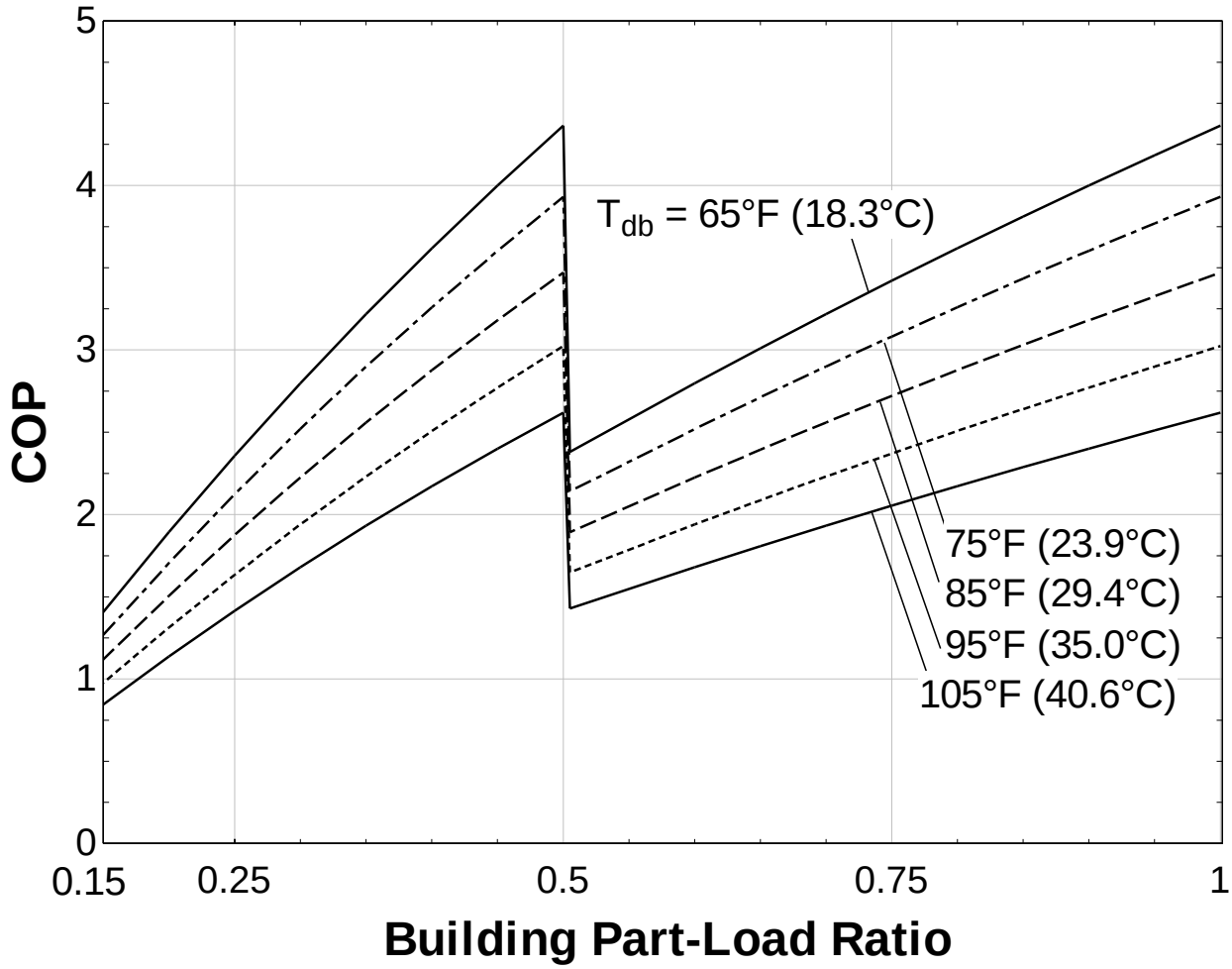

Figure 2-23. Performance curves for parallel air-cooled chillers with a chilled water set point of 44°F (6.7°C) (data from CEC 2012)

The chillers operate at different chilled water set points depending on the storage technology and on whether or not the chillers are meeting building cooling loads directly. As shown in Figure 2-24, decreasing the chilled water set point reduces the chiller capacity; the full-load capacity at a set point of 20°F (-6.7°C) is less than 60% of the capacity at the rated set point of 44°F (6.7°C). This reduced capacity is relevant when sizing equipment for ice CTES systems since the chillers will be frequently operating at low chilled water set points.

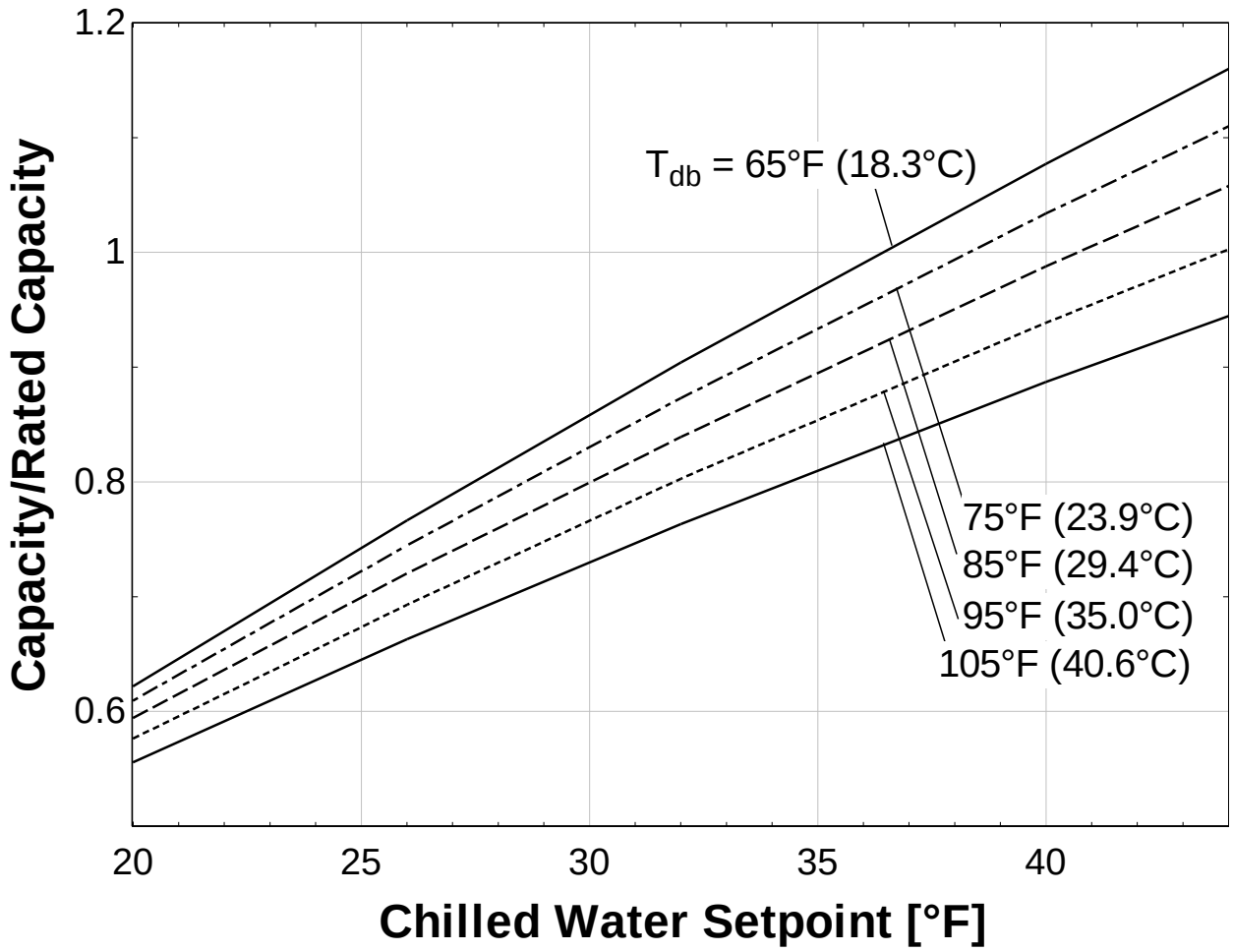

Figure 2-24. Normalized full-load capacity curves (data from CEC 2012)

Figure 2-23 displays the performance curves for chillers operating at a set point of 44°F (6.7°C). In addition to the chiller capacity, the *COP* is a function of the set point. Figure 2-25 shows the set of performance curves for chillers operating at a set point of 20°F (-6.7°C). The curves presented for set points of 20 and 44°F (-6.7 and 6.7°C) represent the two extremes for chiller operation in this research and other set points lie between these two sets of curves. Additional performance curves are used for the intermediate set points.

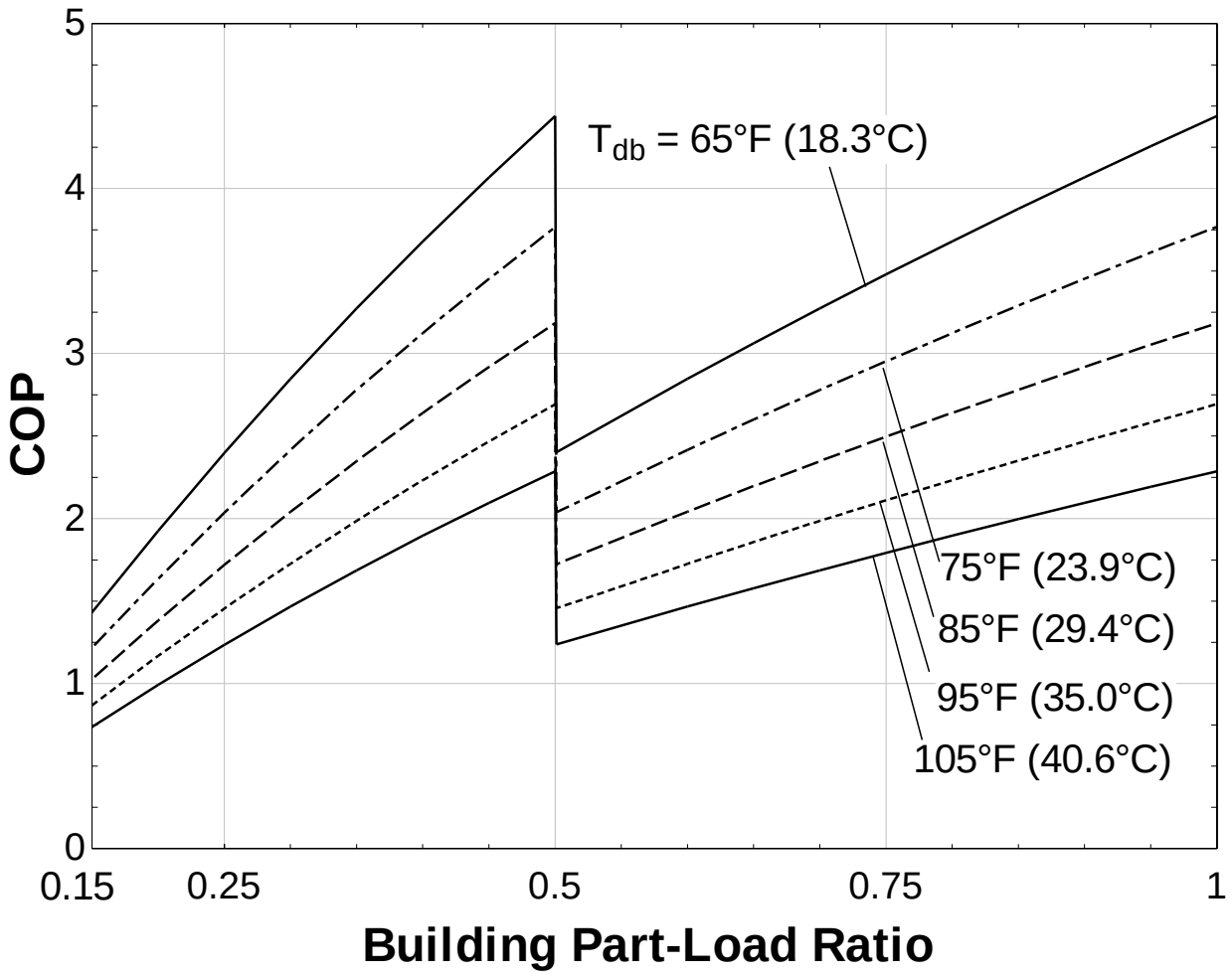

Figure 2-25. Performance curves for parallel air-cooled chillers with a chilled water set point of 20°F (-6.7°C) (data from CEC 2012)

2.5.2 Water-Cooled Chiller Model

Similar to the air-cooled chillers, the water-cooled chillers used for the systems in this work are arranged in parallel. The chilling system performance is a function of the chiller system part-load ratio, the temperature of the water entering the condenser, T_{ecw}, and the chilled water set point temperature, T_{chws}. The entering condenser water temperature is an input rather than the ambient dry-bulb temperature because this chiller model does not take into account the power required to reject heat in the condenser. Therefore, a separate cooling tower model is required to account for this power consumption.

The one user-defined variable in the water-cooled chiller model is the *COP* at the standard rating condition (CEC 2012). The rating condition is defined as a chilled water set point of 44°F (6.7°C), an entering condenser water temperature of 85°F (35°C), and full-load chiller operation (AHRI 2011). In order to meet the standards that went into effect on January 1, 2015 from ASHRAE 90.1-2013, the rated *COP* is 6.3 (ASHRAE 2013). Figure 2-26 displays the parallel chiller system performance curves for a T_{chws} of 44°F (6.7°C).

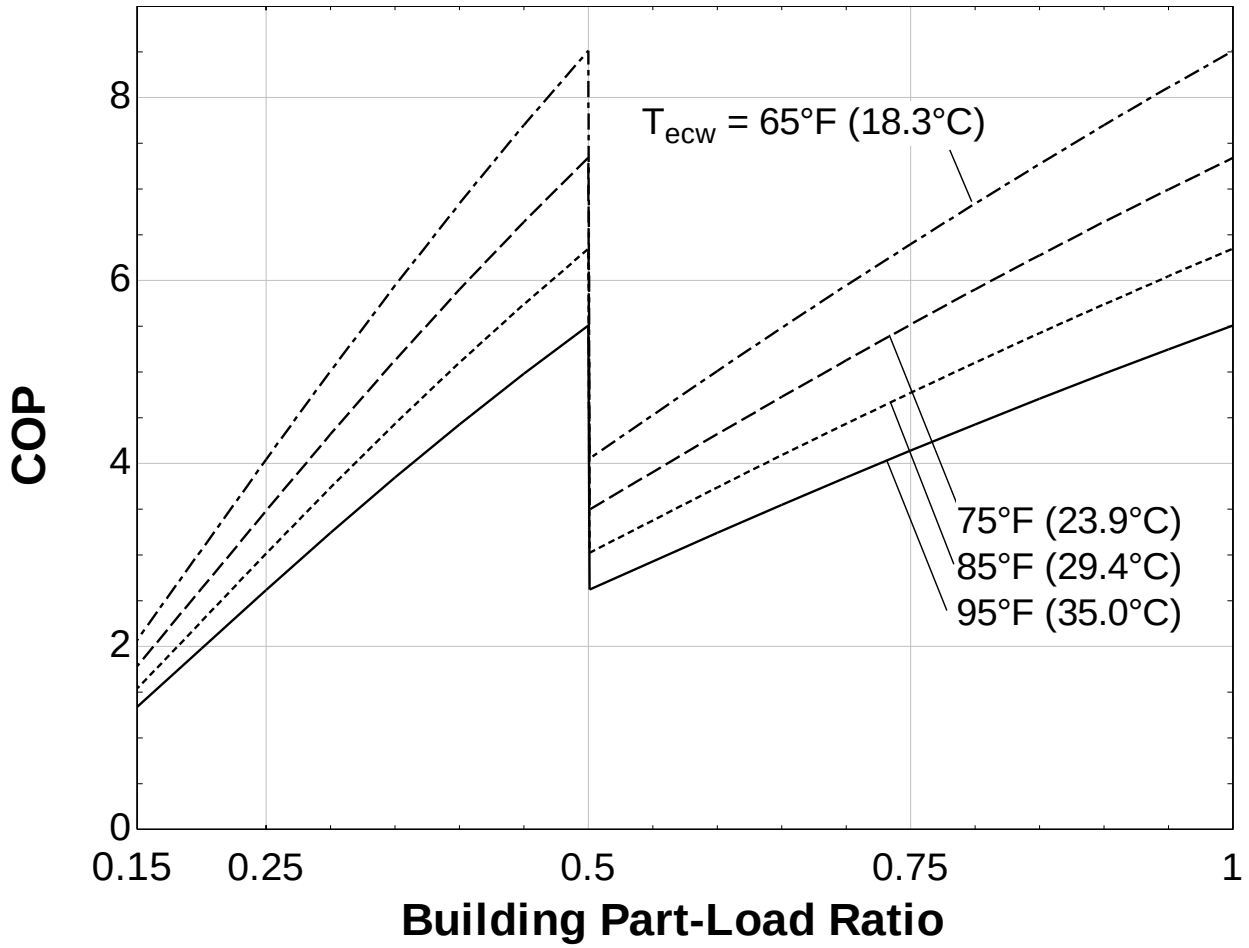

Figure 2-26. Performance curves for parallel water-cooled chillers with a chilled water set point of 44°F (6.7°C) (data from CEC 2012)

Reducing the chilled water set point temperature has a significant impact on performance, as shown by the difference between the curves in Figure 2-26 and those in Figure 2-27. The T_{chws}

difference of 24°F (13.3°C) produces a more drastic difference in chiller performance for the centrifugal water-cooled chillers than for the screw air-cooled chillers.

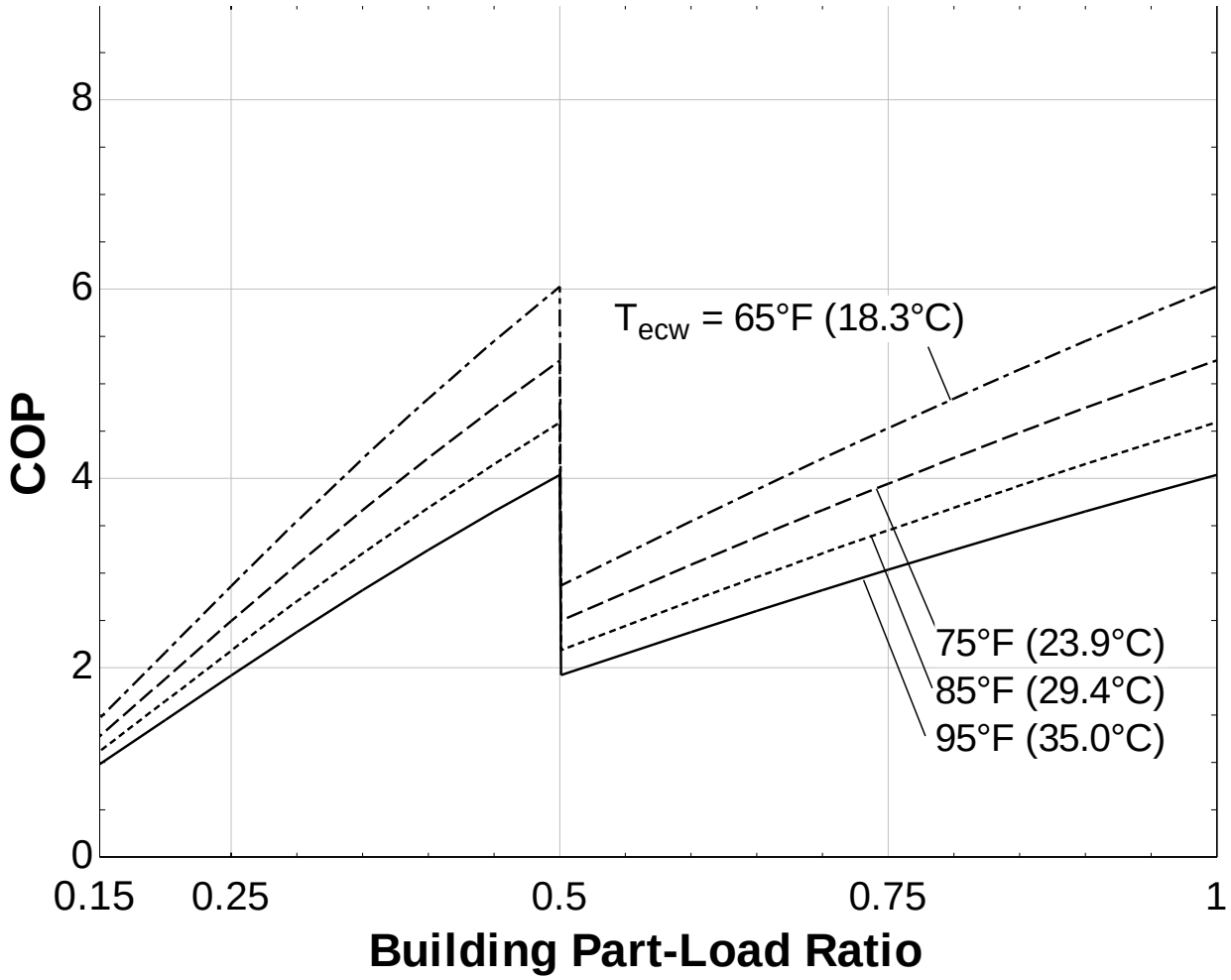

Figure 2-27. Performance curves for parallel water-cooled chillers with a chilled water set point of 20°F (-6.7°C) (data from CEC 2012)

2.5.3 Cooling Tower Model

Cooling towers provide the heat rejection means for the water-cooled chillers. The warm water stream coming from the chiller system comes into direct contact with an air stream and is cooled through both sensible and latent heat transfer. The tower modeled in this research is an induced-draft, counterflow design similar to that in the diagram in Figure 2-21. The ambient air is

pulled upward by axial fans at the top and the warm water stream is sprayed downward. There is a fill material in the interior of the tower which is meant to increase the water surface area that is in contact with the air stream. At the bottom of the tower is a sump which collects the cooled water to be sent back to the condensers. The model used for the cooling towers in this research is an effectiveness model that uses two empirical mass transfer coefficients, *c* and *n* (Braun et al. 1989).

The cooling water flow rate per unit of refrigeration at the chiller rated conditions, $\dot{V}_{ref}$, is 3 GPM/ton (5.4 x 10^{-5} m^3/s-kWt). Calculation of the pumping power requirement requires the pressure drop for the cooling tower system in the Large Office Commercial Reference Building, 60 ftH_2O (179 kPa) (USDOE 2011). The assumed combined motor and pump efficiency, η, is 60%. The following equation gives the pumping power as a function of the volumetric flow rate, $\dot{V}$.

$$P_p \text{ (kWe)} = \frac{\dot{V}h}{\eta} = \frac{\dot{V} \text{ (m}^3\text{/s)(179 kPa)}}{0.6} \tag{7}$$

P_p is the pump electric power consumption and h is the pump head differential. The reference value for the cooling water flow rate per unit of refrigeration is related to the rated chiller capacity, $\dot{Q}_{c,rated}$, through the following relationship.

$$\dot{Q}_{c,rated} \text{ (kWt)} = \frac{\dot{V} \text{ (m}^3\text{/s)}}{\dot{V}_{ref} \text{ (m}^3\text{/s-kWt)}} \tag{8}$$

Solving for $\dot{V}$ and plugging equation (8) into equation (7), gives the pumping power as a function of only known constants and the rated chiller capacity.

$$P_p = \frac{\dot{Q}_{c,rated}\dot{V}_{ref}h}{\eta} \tag{9}$$

In order to use similar performance curves to those used for the air-cooled chillers, the pumping power is incorporated into the chiller system *COP* to develop a new value, COP_{c+p}, which accounts for both the chiller and cooling tower pumping power.

$$COP_{c+p} = \frac{\dot{Q}_c}{P_c + P_p} = \frac{\dot{Q}_c}{\frac{\dot{Q}_c}{COP_c} + \frac{\dot{Q}_{c,rated}\dot{V}_{ref}h}{\eta}} = \frac{\dot{Q}_{c,rated}(PLR)}{\frac{\dot{Q}_{c,rated}(PLR)}{COP_c} + \frac{\dot{Q}_{c,rated}\dot{V}_{ref}h}{\eta}} = \frac{PLR}{\frac{PLR}{COP_c} + \frac{\dot{V}_{ref}h}{\eta}} \quad (10)$$

where COP_c is the *COP* for the chillers only (shown in Figure 2-26), *PLR* is the chiller part-load ratio (current load over current capacity), and $\dot{Q}_c$ is the current chiller load. COP_{c+p} is a function of only known values.

The cooling tower fan power is variable based on the heat being rejected. The assumed temperature difference between the water entering and leaving the tower is 10°F (5.6°C) and the approach temperature, the difference between the water leaving the tower and the ambient wet-bulb temperature, is 7°F (3.9°C). The fan motor rating per unit of refrigeration is assumed to be 0.078 hp/ton (0.016 kWe/kWt) and the full-power air flow rate is 2,000 cfm/hp (1.25 m^3/s-kWe) (Oak Ridge National Laboratory 1997, Iterson 2009). To calculate the electric fan power consumed, P_f, the third fan affinity law is employed in the equation below.

$$P_f = P_{f,full}\left(\frac{\dot{m}_a}{\dot{m}_{a,full}}\right)^3 \quad (11)$$

where $\dot{m}_{a,full}$ and $P_{f,full}$ are the fan rated mass flow rate and power, respectively. The rated mass flow rate is obtained by multiplying the volumetric flow rate by the density of air at 70°F (21°C). The mass flow rate of air required to reject the heat from the chillers, $\dot{m}_a$, is calculated using the effectiveness model. Since the cooling tower is a counter-flow heat exchanger, the heat rejection, $\dot{Q}_h$, is calculated using the following equation.

$$\dot{Q}_h = \varepsilon_a \dot{m}_a (h_{w,i} - h_{a,i}) \tag{12}$$

where $h_{w,i}$ and $h_{a,i}$ are the cooling tower inlet enthalpies of the water and air streams, respectively. The air-side effectiveness, ε_a, is determined using the assumption that the Lewis number is equal to one (thermal and mass transfer are approximately equal). The effectiveness relationships for sensible heat exchangers are utilized with modifications to the definitions of the number of transfer units (NTU) and the capacitance rate ratio, m^*.

$$\varepsilon_a = \frac{1 - \exp(-NTU(1 - m^*))}{1 - m^* \exp(-NTU(1 - m^*))} \tag{13}$$

$$NTU = c\left(\frac{\dot{m}_w}{\dot{m}_a}\right)^{1+n} \tag{14}$$

$$m^* = \frac{\dot{m}_a C_s}{\dot{m}_w c_w} \tag{15}$$

$$C_s = \frac{h_{s,w,i} - h_{s,w,o}}{T_{w,i} - T_{w,o}} \tag{16}$$

where c and n are empirical mass transfer coefficients, 1.130 and -0.617 respectively for this research (Simpson & Sherwood 1946). The variable, C_s, is the saturation specific heat and is defined as the average slope of the saturation enthalpy with respect to temperature and is based on the water stream inlet and outlet conditions.

Using the assumed value for $\dot{V}_{ref}$ of 5.4 x 10^{-5} m^3/s-kWt and an approximate density of water of 1,000 kg/m^3, an $\dot{m}_{w,ref}$ of 5.4 x 10^{-2} kg/s-kWt is used to modify equation (8).

$$\dot{Q}_{c,rated}\ (\text{kWt}) = \frac{\dot{m}_w\ (\text{kg/s})}{\dot{m}_{w,ref}\ (\text{kg/s-kWt})} \tag{17}$$

An energy balance on the chiller relates the heat rejection to the rated chiller capacity through the chiller *COP*, COP_c.

$$\dot{Q}_h = \dot{Q}_c \left(1 + \frac{1}{COP_c}\right) \tag{18}$$

Combining equations (18) and (17) with equation (12) and using the definition of the part-load ratio, *PLR*, gives an equation with the air mass flow rate, $\dot{m}_a$, as the only unknown.

$$\dot{Q}_c \left(1 + \frac{1}{COP_c}\right) = PLR(\dot{Q}_{c,rated})\left(1 + \frac{1}{COP_c}\right) = PLR\frac{\dot{m}_w}{\dot{m}_{w,ref}}\left(1 + \frac{1}{COP_c}\right) = \varepsilon_a \dot{m}_a (h_{w,i} - h_{a,i}) \tag{19}$$

The cooling tower air mass flow rate, $\dot{m}_a$, is required to incorporate cooling tower fan power into the water-cooled chiller system performance. This value comes from equation (19) and can be used in equation (11) to calculate the fan power, P_f, required to modify the coefficient of performance to include the chiller, cooling tower pumping power, and cooling tower fan power.

$$COP_{c+p+f} = \frac{\dot{Q}_c}{P_c + P_p + P_f} = \frac{\dot{Q}_c}{\frac{\dot{Q}_c}{COP_{c+p}} + P_f} = \frac{1}{\frac{1}{COP_{c+p}} + \frac{P_f}{\dot{Q}_c}} = \frac{1}{\frac{1}{COP_{c+p}} + \frac{P_f}{\dot{Q}_{c,rated}(PLR)}} \tag{20}$$

Equation (20) gives the modified *COP* for a single chiller and cooling tower cell.

In the situation where two chillers are operating in parallel and the overall building part-load ratio is below 0.5, only one chiller is running. In this case, the condenser heat rejection can be split between the two cooling tower cells to reduce the total fan power. This strategy improves performance for the lower part-load ratios. The performance curves for the combined performance of the chillers, cooling tower pumps, and fans are shown in Figure 2-28 and Figure 2-29 as a function of the ambient wet-bulb temperature for chilled water set point temperatures of 44°F (6.7°C) and 20°F (-6.7°C), respectively. The overall performance is reduced compared to the

equivalent chiller performance curves in Figure 2-26 and Figure 2-27 because the pumping and fan power add to the system electric consumption while the cooling capacity remains constant.

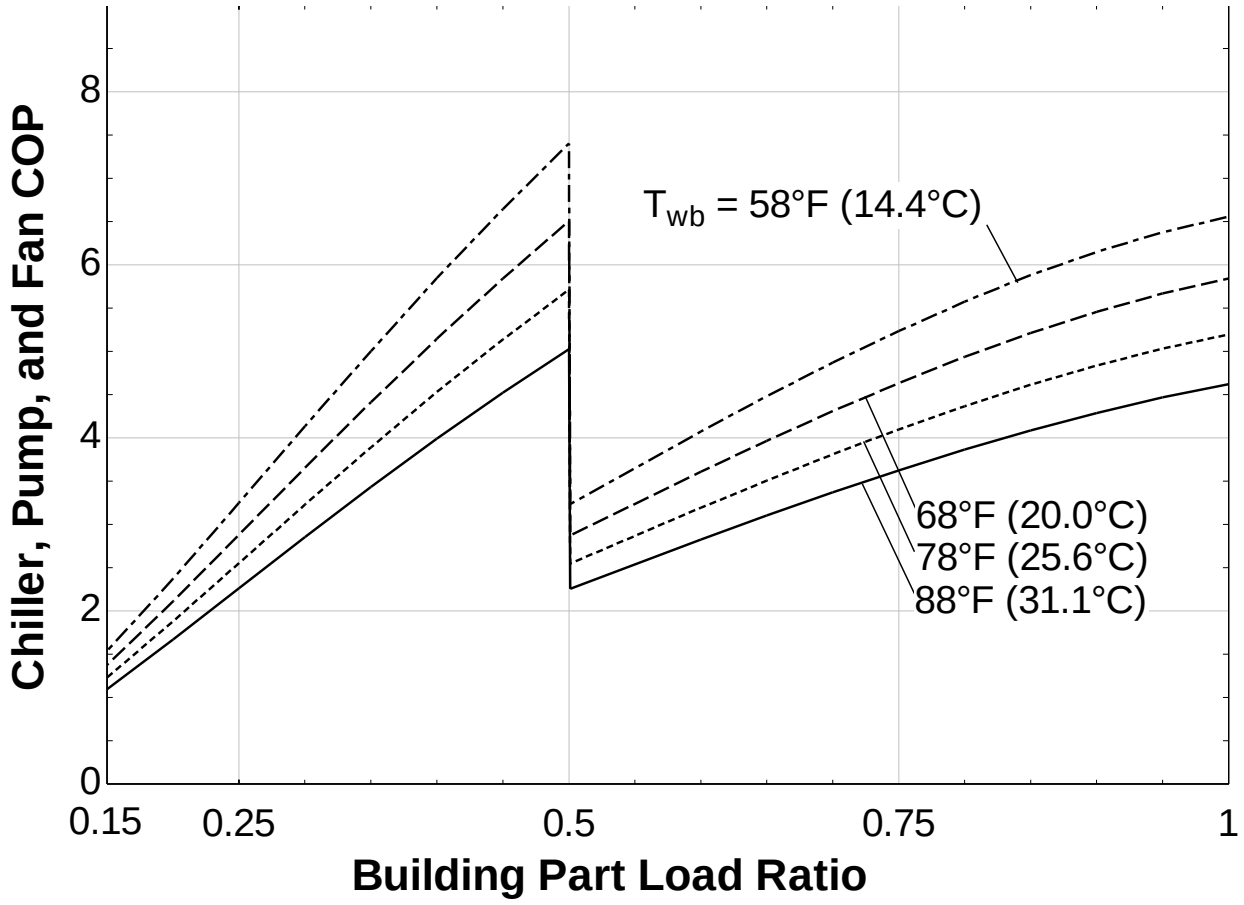

Figure 2-28. Performance curves for parallel water-cooled chiller system with a chilled water set point of 44°F (6.7°C)

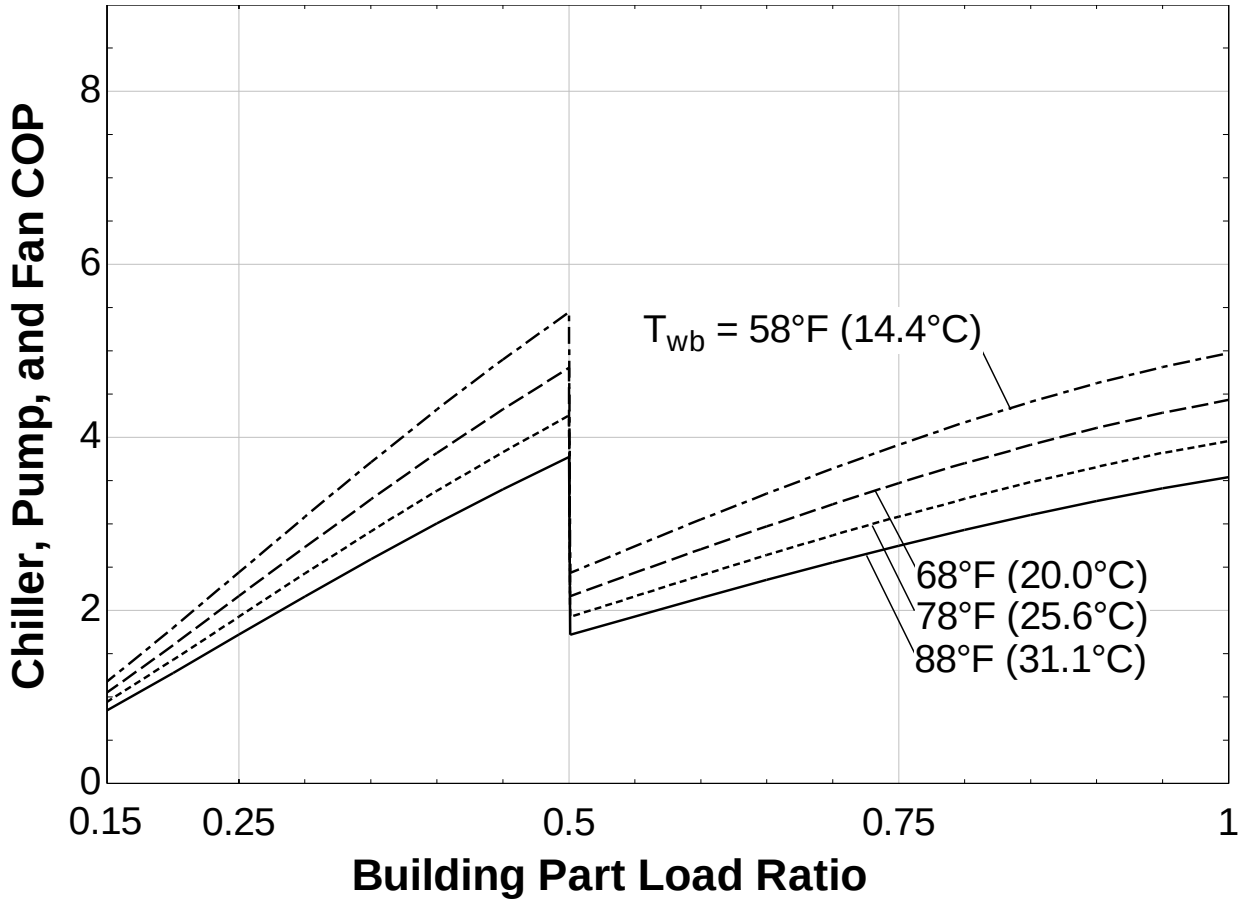

Figure 2-29. Performance curves for parallel water-cooled chiller system with a chilled water set point of 20°F (-6.7°C)

2.5.4 Water-Cooled Chiller System Performance in Parallel versus Series

Because greater energy storage density is possible with larger differences between chilled water supply and return temperatures, chillers used in stratified chilled water CTES systems commonly operate under high lift conditions. A building chiller system without storage typically maintains a temperature difference of around 10°F (5.6°C) while a system with stratified chilled water storage operates around twice that temperature difference. When two or more chillers are available, they can be arranged to operate in parallel (as discussed above and in the preceding sections), series, or series-parallel combinations. For a stratified chilled water CTES system, the parallel arrangement is shown in Figure 2-10 and the series arrangement is shown in Figure 2-30.

The upstream series chiller is labeled the “lag” chiller and the downstream is the “lead.” When the overall building part-load ratio is below 0.5, only the lead chiller operates and chills the entire return water to the supply water temperature set point on its own. In this region of operation, the lead chiller operates in the same manner as a single chiller. Once the building part-load ratio surpasses 0.5, the lag chiller starts and the chilling load is divided evenly between the two chillers. While both chillers are operating at reduced part-load ratios as in the parallel case, they each operate more efficiently due to reduced lift across each chiller. More importantly, the lag chiller is capable of running at a higher COP since its leaving water temperature will, necessarily, be higher than the supply water set point temperature the downstream chiller needs to achieve. The light blue water stream connecting the lag chiller to the lead chiller in Figure 2-30 indicates an intermediate temperature such that each chiller is only maintaining half of the final temperature difference.

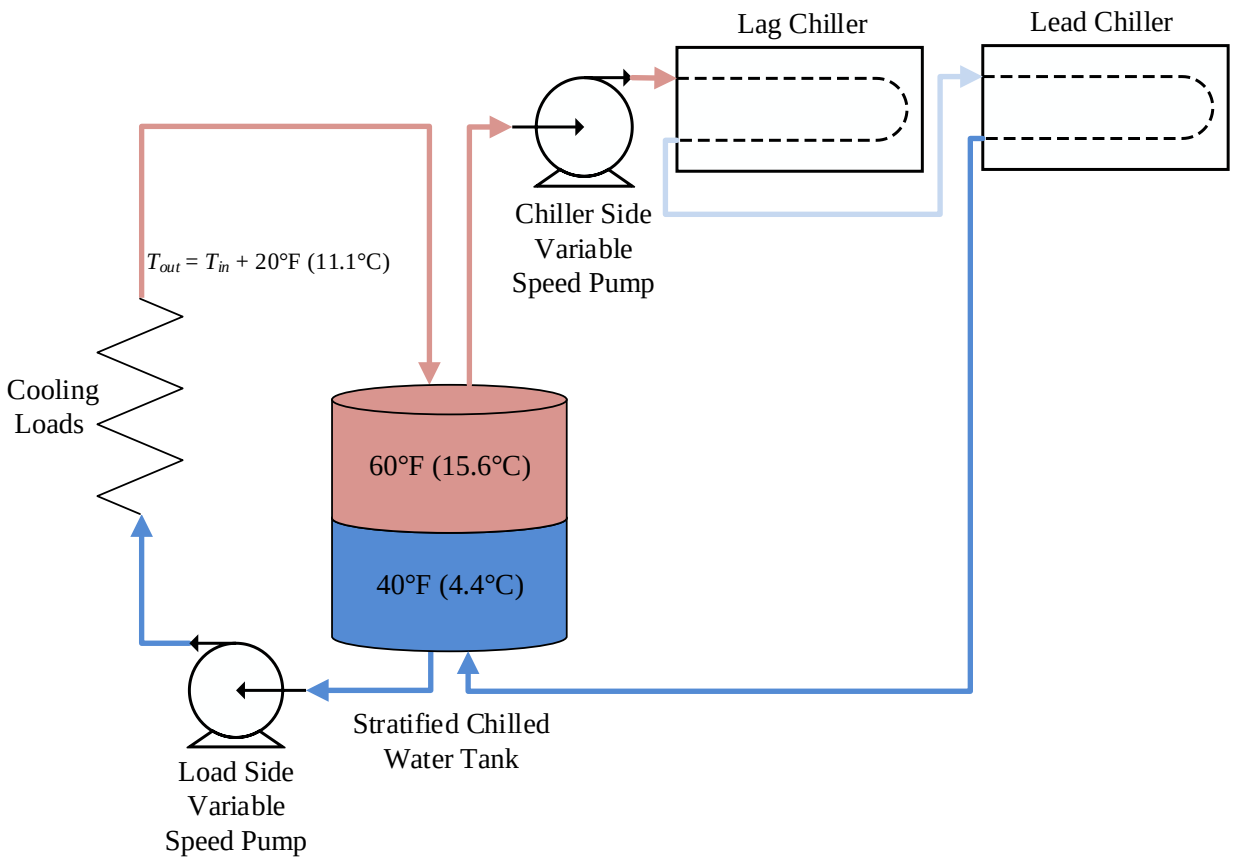

Figure 2-30. Stratified chilled water CTES with series chillers schematic

The increase in efficiency at higher building part load ratios is shown by comparing the right side of Figure 2-31 with Figure 2-32. These plots show the overall chiller system performance including chiller compressor power, and cooling tower pump and fan power for both parallel and series arrangements at a chilled water set point temperature of 40°F (4.4°C) and return temperature of 60°F (15.6°C). The resulting improvement over parallel chiller system performance when both chillers are operating is between ten and fifteen percent depending on the ambient conditions and the part-load ratio.

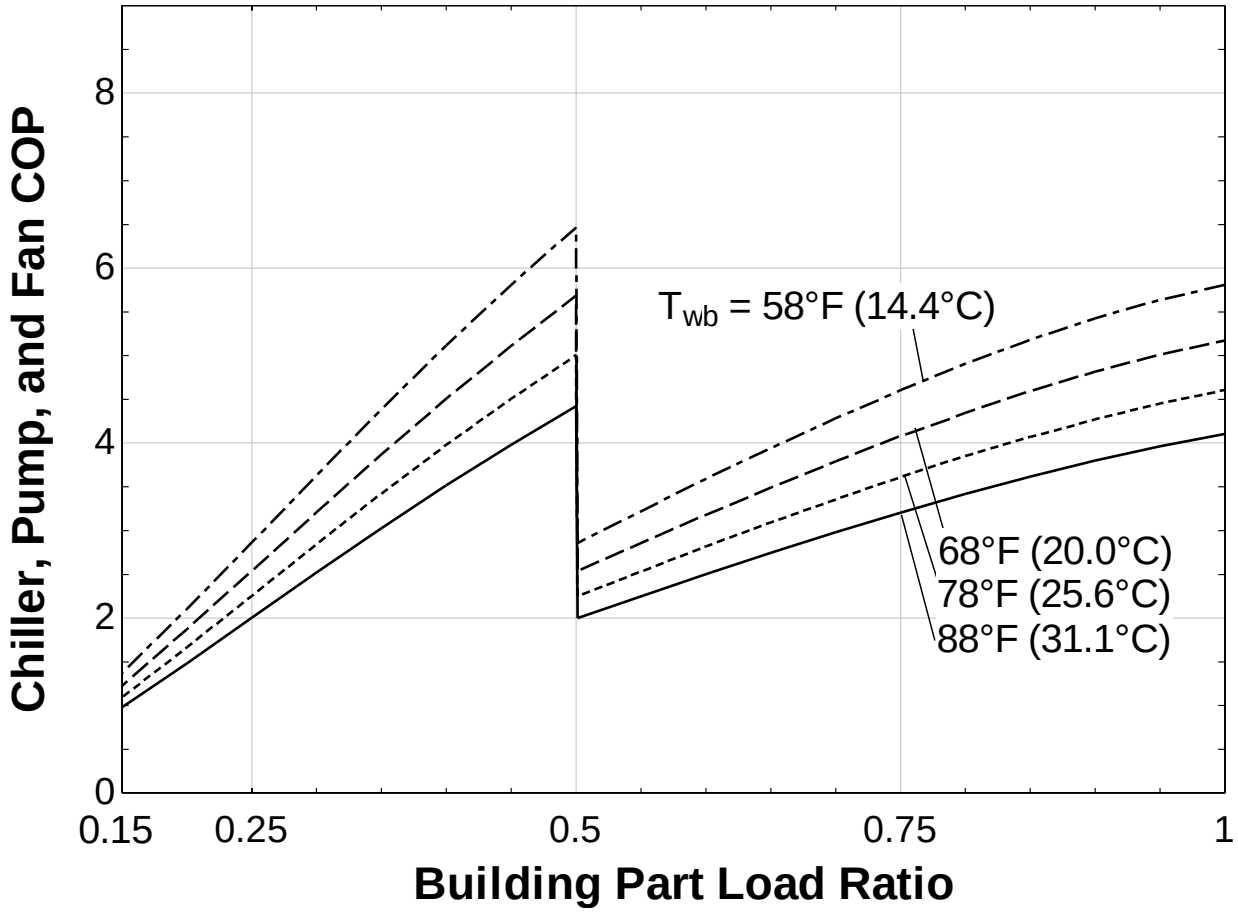

Figure 2-31. Performance curves for parallel water-cooled chiller system with a chilled water set point of 40°F (4.4°C)

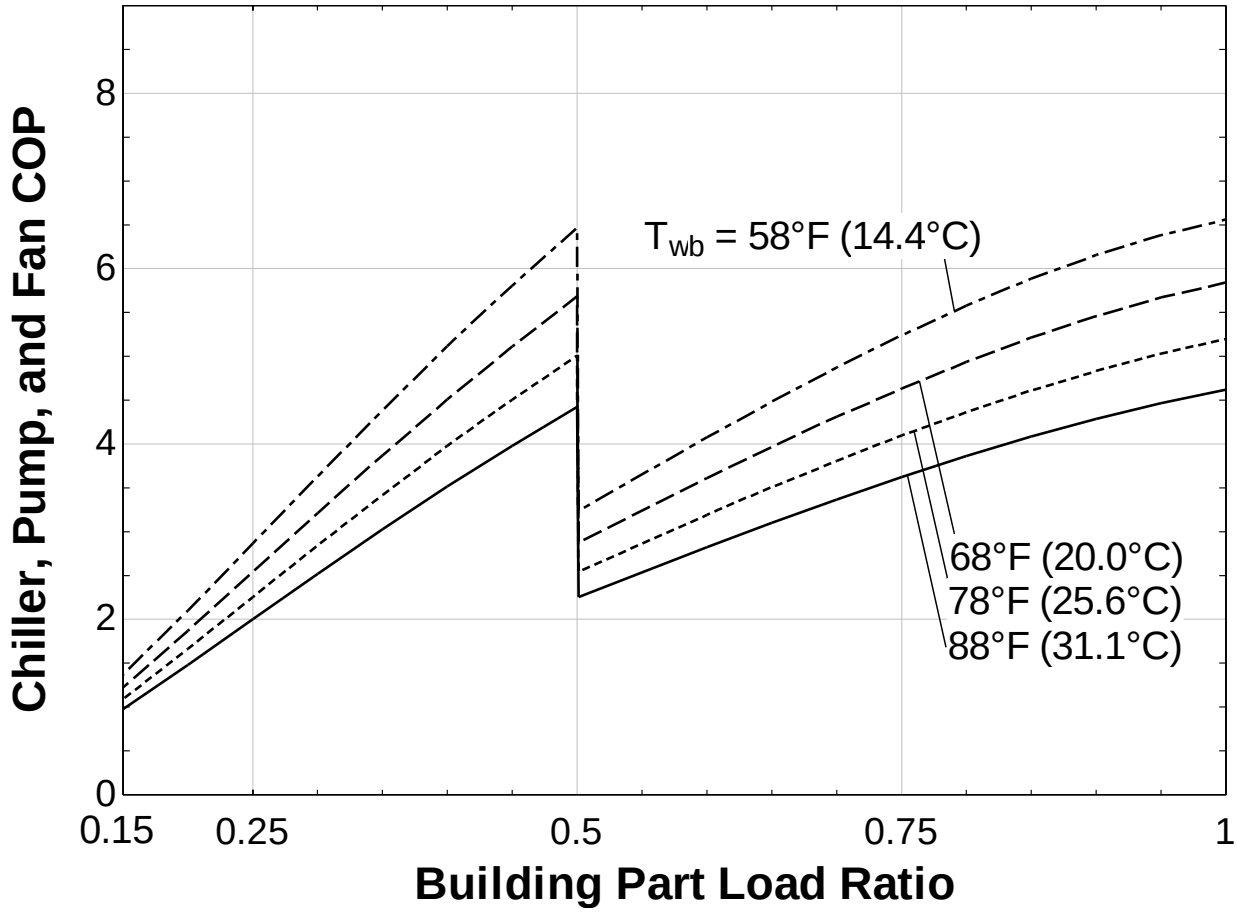

Figure 2-32. Performance curves for series water-cooled chiller system with a chilled water set point of 40°F (4.4°C)

While the series chiller arrangement clearly shows improved performance for high lift applications, the simulation results in the following sections are presented for the parallel chiller arrangement. Parallel chilling is used for the stratified chilled water case to allow it to be compared to the ice storage system options which utilize parallel chillers. Further improvements in operating efficiency can be achieved in series chilling arrangements when used in chilled water storage system applications.

2.5.5 Linearized Water-Cooled Chiller Model

While the chiller performance models presented in Sections 2.5.1 through 2.5.3 are well-suited for explicit parametric studies, they are not ideal for a simulation framework necessary for multi-variate optimization. There are two challenges presented by the using the distilled performance curves for the chilling system. One of the advantages of the two-chiller system is improved system performance at low building part-load ratios, but a chilling system with two (or more) chillers leads to a large discontinuity when operation switches from one chiller to two. This discontinuity creates problems because, as an optimization algorithm searches for a global minimum, it may get stuck in a local minimum as a consequence of the chiller performance curve discontinuity. To address this challenge, a single chiller is used in the simulations which take advantage of optimization algorithms. The chiller system could also be made up of multiple chillers which are all running at the same part load ratio if the required capacity exceeds that provided by a single chiller or if redundancy is required. Performance curves for a chiller system with a single water-cooled chiller with a set point of 40°F (4.4°C) are presented in Figure 2-33. The chiller performance curves, which dominate the behavior of the system performance curves shown, are a mix of bi-quadratic and quadratic curves. The slightly nonlinear behavior is apparent in the curvature of the four lines in Figure 2-33.

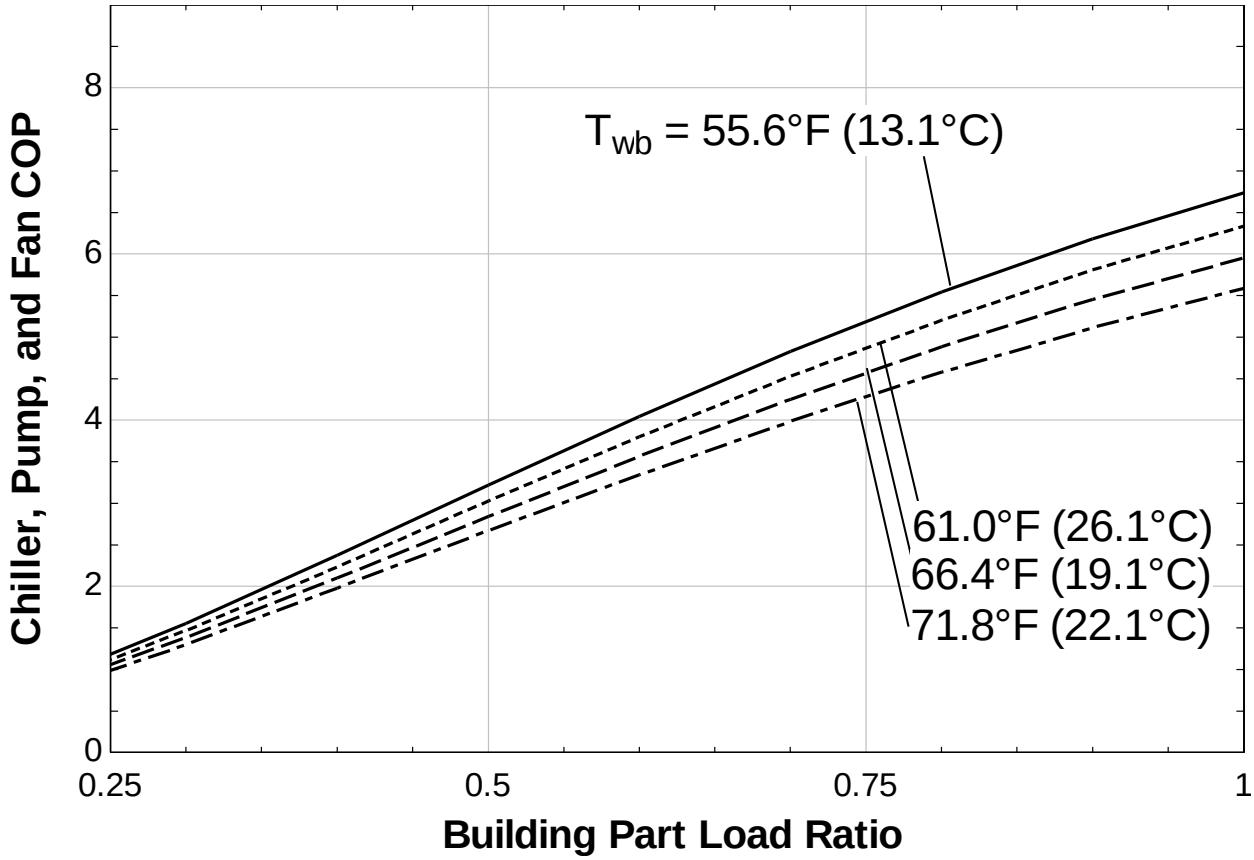

Figure 2-33. Performance curves for water-cooled chiller system with a single chiller and a chilled water set point of 40°F (4.4°C)

Nonlinear chiller performance curves are the second challenge presented to optimized simulations. While many nonlinear programming (NLP) algorithms have been written for and implemented in commercial software, they are not ideal for solving CTES simulation optimizations. Because these algorithms must be able to accommodate a wide range of potentially highly nonlinear inputs, the algorithms are less efficient than those developed for linear programming (LP). Utilization of optimization algorithms in HVAC control systems has become achievable through advances in computational power. This ability was previously afforded only to processes with long time constants such as chemical processing and oil refining. Along with the

increased computational power, the algorithms must be able to reach a global minimum within the sub-hour timesteps required for HVAC system control.

When setting out to solve a nonlinear optimization, one of the first recommended steps is to verify that the problem can't be approximated by a problem with purely linear constraints and a linear objective function (Chinneck 2015). The objective function is the equation to be optimized (typically formulated to be minimized). Because the single-chiller performance curves in Figure 2-33 are nearly linear, they have been approximated as the linear curves shown in Figure 2-34 for use in simulations utilizing optimization algorithms. While these curves introduce small inaccuracies in chiller system performance, they allow the use of linear programming algorithms which can reach the optimum operating points efficiently, accurately, and repeatably.

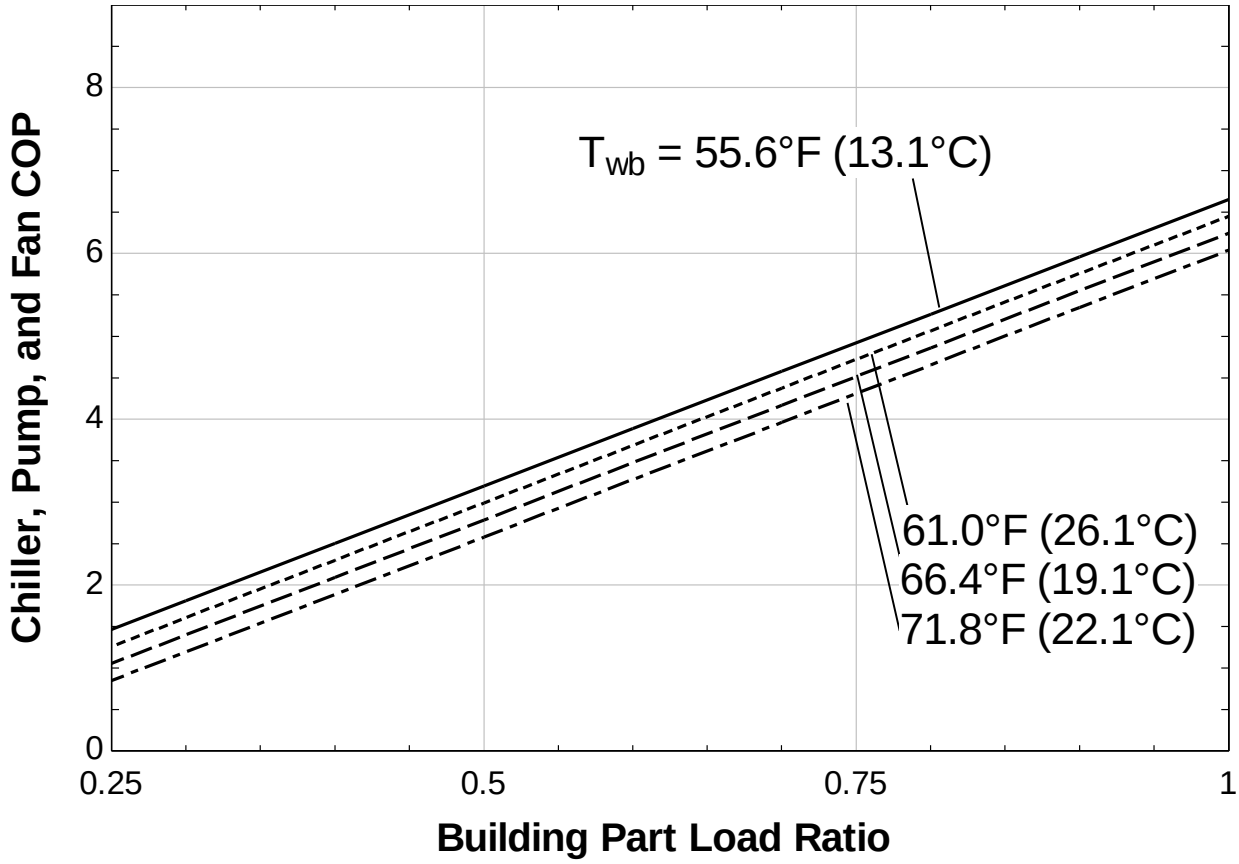

Figure 2-34. Linearized performance curves for water-cooled chiller system with a single chiller and a chilled water set point of 40°F (4.4°C)

2.6 Cost Data and Model

Life-cycle cost calculations are performed for a twenty-year period and include both capital and operating costs. The capital costs include installed wind turbines, PV panels, chiller systems, CTES systems, and their related equipment. The operating costs include the electricity costs and the details for the calculation of the operating costs are presented in Section 5.2. A present value is calculated for the twenty-year period of operating costs. Not considered in the cost calculations are maintenance costs associated with the major capital components.

2.6.1 Time-of-Use Electricity Cost Data

For comparison purposes, the same time-of-use electricity rate structure is used for each of the geographic locations. The rate structure originates from the North Texas CoServ utility tariff in effect in mid-2015 (CoServ 2015). Although most commercial building utility rates include a separate on-peak demand charge, the CoServ rate structure is based solely on energy charges with no separate demand component. The on-peak rate is 16.5 ¢/kWh and the off-peak rate is 7.2 ¢/kWh. The on-peak rate is more than double the off-peak rate which encourages end-use customers to avoid electricity consumption during the on-peak window. As illustrated in Figure 2-35, the on-peak period extends from 3 p.m. to 8 p.m. during the summer months and there is an additional on-peak period added from 6 a.m. to 8 a.m. during the winter months.

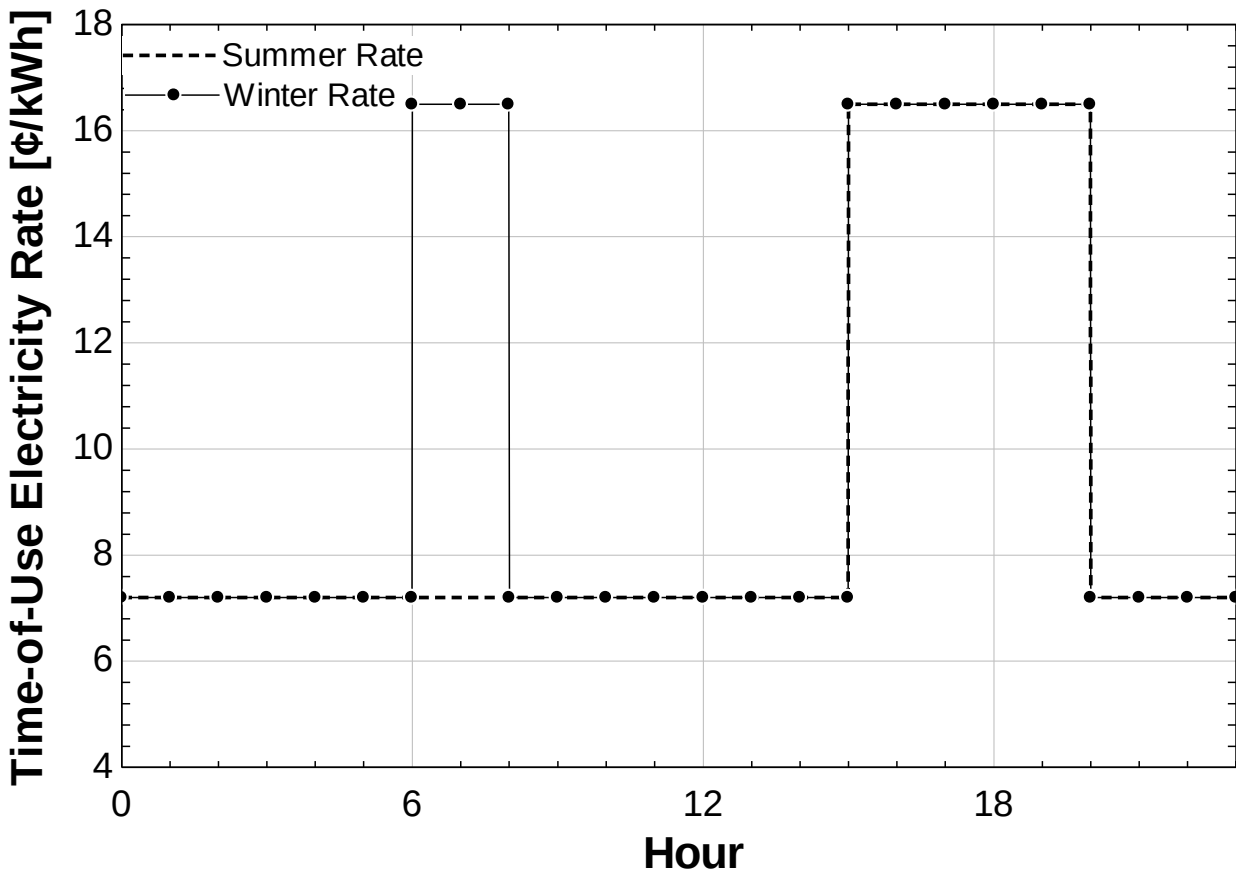

Figure 2-35. Time-of-use energy charges used for all locations (CoServ 2015)

2.6.2 Time-of-Use with Demand Charges Electricity Cost Data

In order to evaluate the impact of the inclusion of demand charges, a second rate structure, in addition to the one in Figure 2-35, is used in the simulation of the Large Office building equipped with ice CTES and located in New York City. This particular case was selected because it has become a popular combination in New York City where both space constraints limit the installation of a large stratified chilled water CTES tank and commercial buildings are subject to utility rate structures that have a significant electricity demand charge component. The rate structure for this comparative example is the Consolidated Edison (Con Edison) General Large Time-of-Day rate applicable to buildings with a minimum peak aggregate demand of 1,500 kWe

(Con Edison 2017b). The rate is comprised of four separate components, two energy charges and two demand charges. The energy charge for delivery is 0.79 ¢/kWh year-round and is levied by Con Edison. The energy charge for supply can be charged by one of many energy services companies chosen by the consumer, but this research uses the Con Edison rate. This rate is 5.06 ¢/kWh during the on-peak hours of 8 a.m. to 10 p.m. Monday through Friday and 4.35 ¢/kWh at all other times (Con Edison 2017a). Figure 2-36 shows the sum of the two energy charges as a function of the time of day using the same scale as Figure 2-35, which shows the rate which considers energy charges only. Notice that the energy charges are significantly lower since the majority of the monthly charge comes from demand charges.

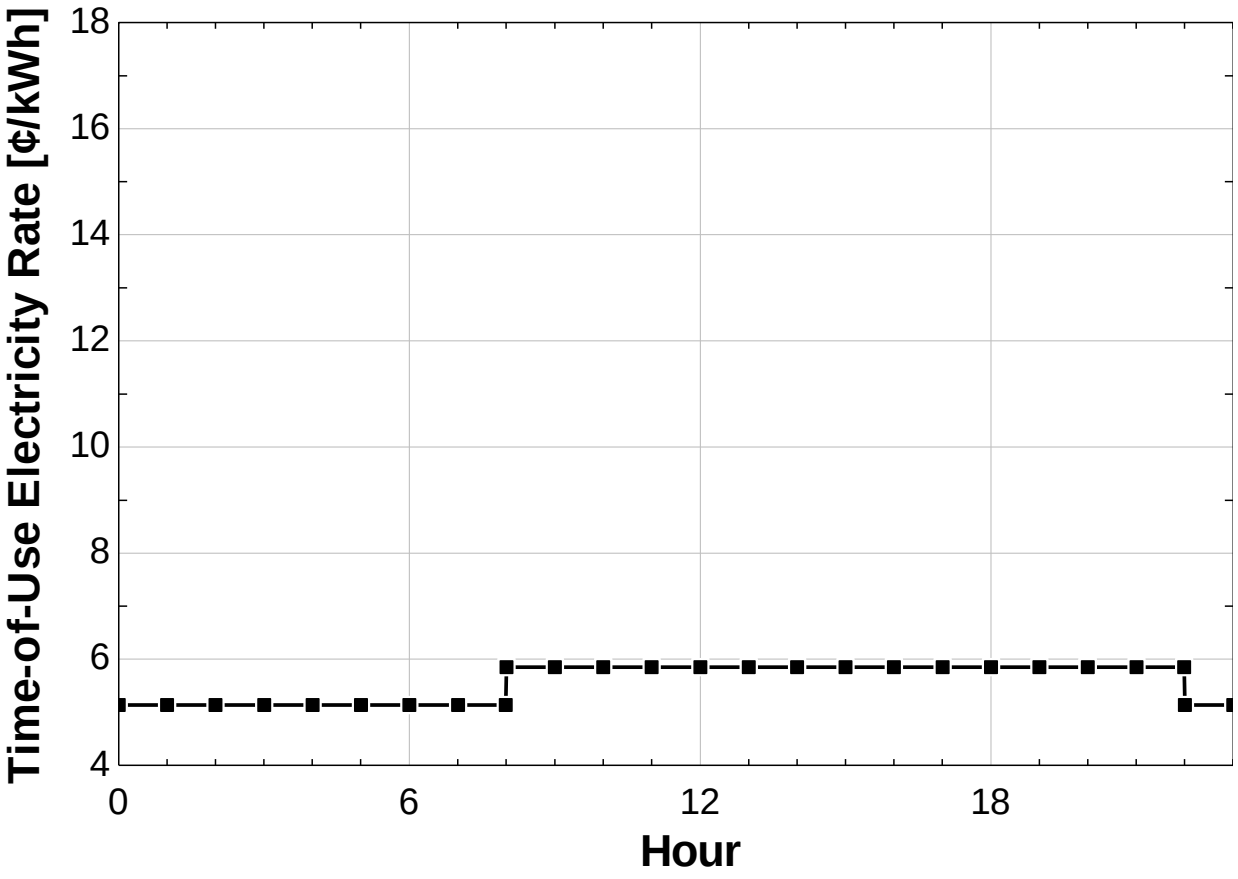

Figure 2-36. Time-of-use energy charges used with demand charges for New York City

Demand charges are based on the facility's peak electric demand. The rate used in this research has a delivery component charged by Con Edison and a capacity component charged by the New York Independent System Operator (NYISO). The Con Edison rate is based on the peak electric demand in each month and amounts to $39.64/kW for June through September and $16.44/kW for all other months (Con Edison 2017b). The NYISO component uses the same peak demand value for a one-year period that comes from the facility demand coinciding with the peak hour for the entire NYISO system. This peak demand is charged at a rate of $10.99/kW for May through October and $3.50/kW for all other months (NYSIO 2017). The total demand charge is shown as a function of the month of the year in Figure 2-37. Each portion of the demand charge is

applied to a different peak demand value except for the month in which the NYISO system experiences peak demand.

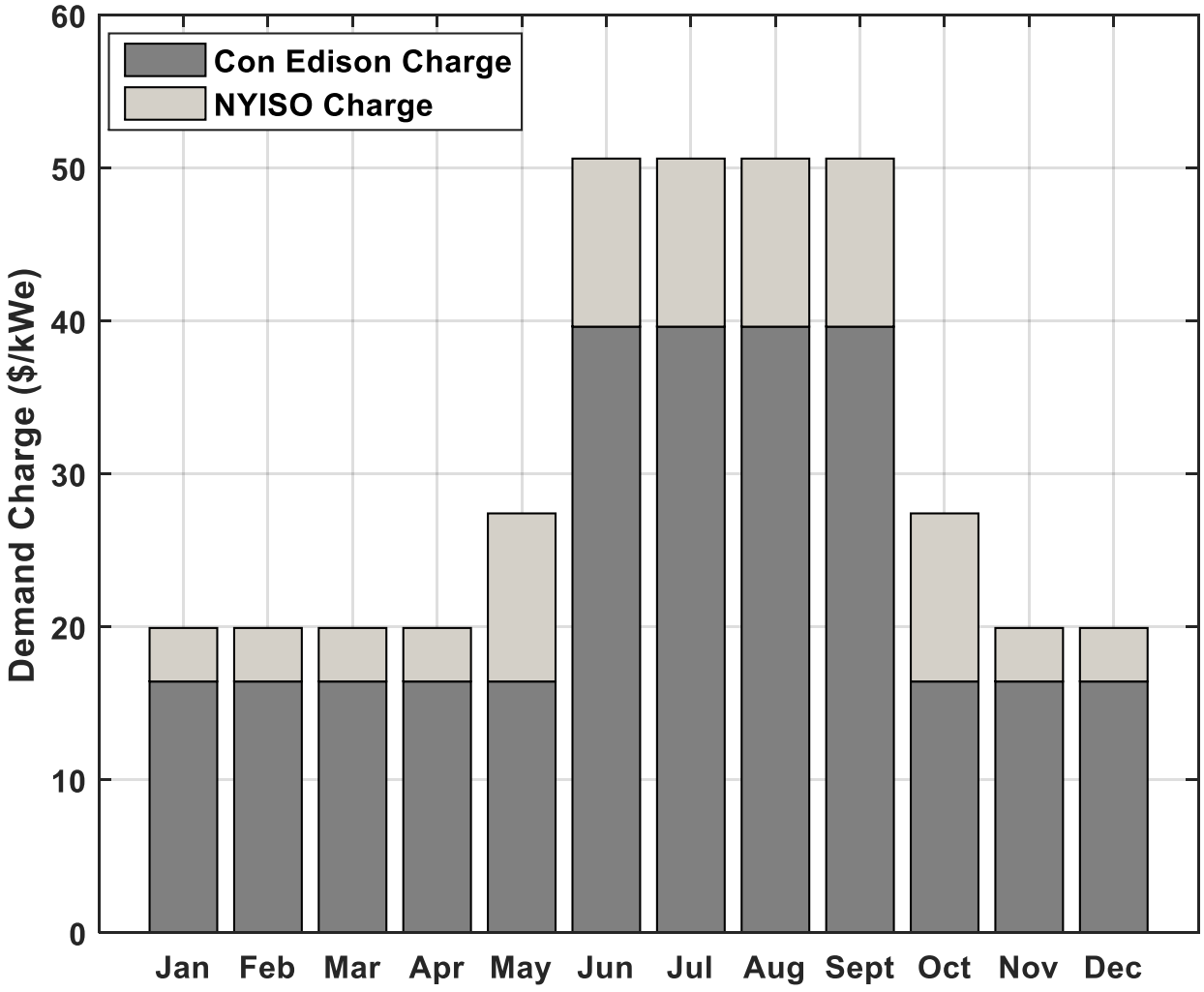

Figure 2-37. Both demand charge components for New York City

2.6.3 Day-Ahead and Real-Time Electricity Cost Data

The electricity rates provided in the previous sections are fully specified throughout the year and formulating a control strategy to reduce electricity costs around these rates is straightforward. The chiller system is idled during on-peak rate periods as much as possible. These rate structures encourage end-customers to reduce electricity consumption when the utilities

typically experience their peak demand. Because the definition of the peak time period set by the rate structure is very coarse, there are occasions during the on-peak rate periods when overall demand is low and vice versa.

There are other dynamic rate structures in use which vary hourly in response to events affecting both demand and supply. The simple graphic in Figure 2-38 shows various dynamic pricing rate structures and their response to a critical event like a heat wave that causes an extreme peak in demand. The plots also show how these various rate structures vary in comparison to a flat-rate structure. The first structure shown is real-time pricing and this encompasses both the day-ahead and real-time electricity prices used in this research. Day-ahead pricing is actually used to bill end customers in some areas, but real-time prices are not known ahead of when they occur and are not used for billing end customers. Real-time pricing fluctuates hourly based on the cost of generation under the current conditions while day-ahead pricing is a prediction of this hourly price fluctuation as the name implies. During the off-peak periods, the real-time rates are lower than a flat rate, but they respond to a peak event in the early evening by raising rates accordingly. The second structure displayed is a time-of-use structure which was presented in the previous sections. This structure is dynamic in that it has different rates for different times of the day, but it has no mechanism for responding to the critical event. The last two rate structures, critical peak pricing and critical peak rebate, are similar in that they occasionally adjust prices when a critical event occurs. Unlike the hourly response to grid conditions for real-time and day-ahead pricing, these structures respond to critical events only on certain days of the year. For critical peak pricing, the standard rate is lower than it would be for a typical flat-rate structure, but the price increases significantly during a critical peak pricing event. The critical peak rebate approach is similar except that it is more customer-friendly in that a rebate is given during the peak event depending on the

level of load reduction compared to what was expected from the end-customer. The two critical peak structures are similar to the day-ahead structure in that they provide end-customers with information about the peak event well before it actually occurs.

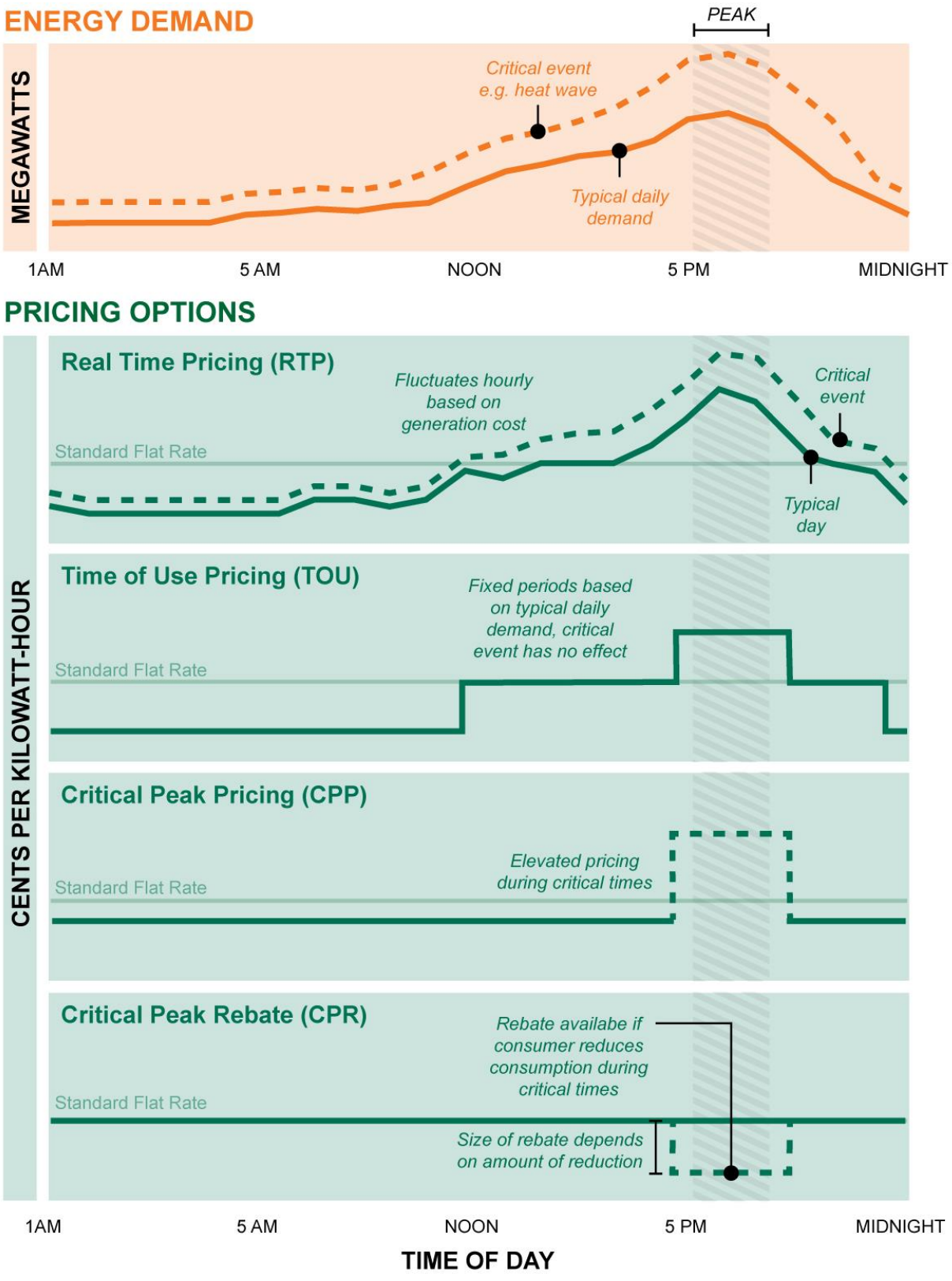

Figure 2-38. Dynamic pricing rate structures (Spiller 2015)

The day-ahead and real-time rates used in this research are for Con Edison in New York for the full year of 2016. The day-ahead rates are defined under Rider M – Day-Ahead Hourly Rates and according to General Rule 25.1, the Market Supply Charge applicable to the hourly energy usage is the NYISO price multiplied by a factor of 1.063 to account for losses of 5.9% (Con Edison 2018; Con Edison 2017c). The NYISO price used is the day-ahead Locational Based Marginal Price (LBMP) for Zone J which covers New York City. These energy charges make up only a portion of the overall electricity bill, but because these rates are used in a comparison between CTES systems subject to day-ahead and real-time rate structures, the remaining portions of the overall bill are assumed to be consistent.

NYISO publishes current and historical rates for day-ahead and real-time rates (NYISO 2017b). The NYISO real-time rates are not used to charge end customers, but the same loss factor is used here to account for loses. An example of these rates for a week in early September is plotted in Figure 2-39. The day-ahead rates exhibit smaller variations throughout the week and there are several periods when the real-time rate far exceeds the day-ahead rate. There are also periods when the day-ahead rate is higher than the real-time rate and the annual mean is actually even for both rates at 3.14 ¢/kWh for 2016. Even though it is clear that the real-time rate data fluctuates significantly, there are also notable fluctuations in the day-ahead rate. For instance, the peak rate on the fifth day is nearly 10 ¢/kWh while on the seventh day it peaks at about 4 ¢/kWh.

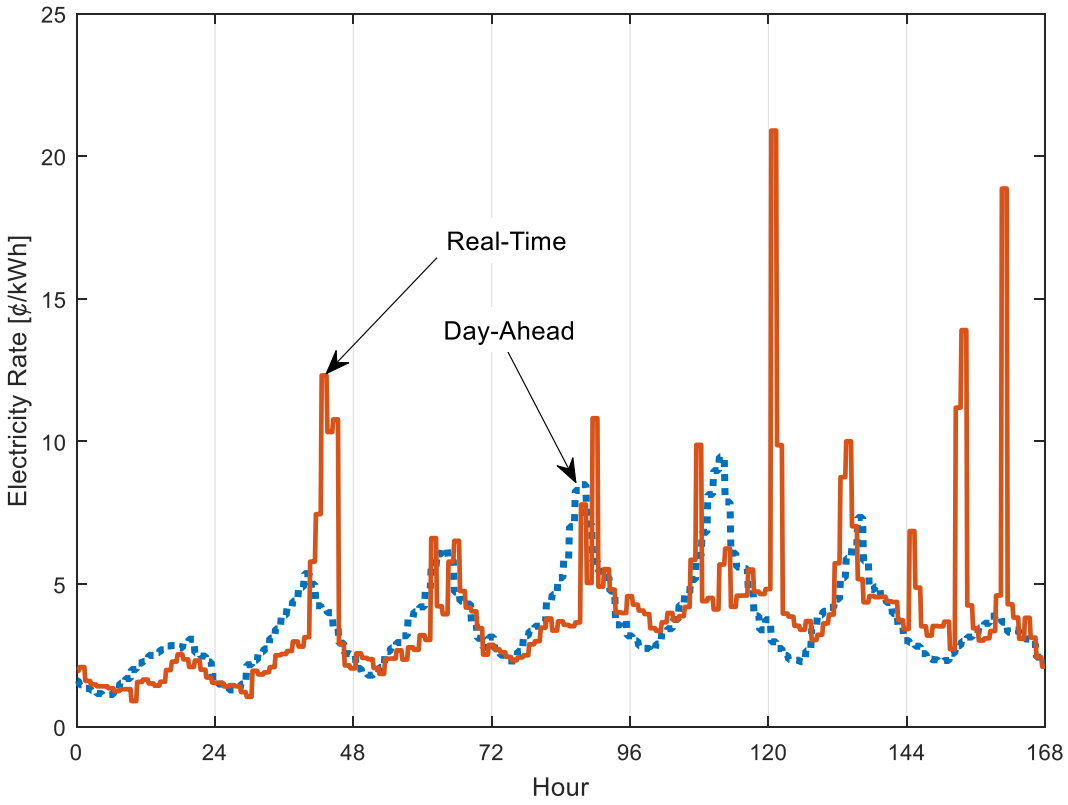

Figure 2-39. Early September day-ahead and real-time Con Edison electricity rates (data from NYISO 2017b)

While the real-time rate is not actually charged to end-customers, it is included in this research to show the benefits of particular control strategies when used in conjunction with increasingly uncertain variable inputs. The prevalence of day-ahead and other dynamic pricing structures is important to the research presented here. Installation of smart electricity metering devices is required for any of the structures presented here since they allow for determination of the time-of-day the electricity was consumed. Beginning in 2013, the Energy Information Administration (EIA) includes information about customers enrolled in dynamic pricing programs in their annual survey of utilities (EIA 2017a). Looking at this data for the years 2013 and 2016, 620 utilities reported some customers enrolled in dynamic pricing in 2013 and 646 in 2016. In both

years, this amounts to approximately 20% of the utilities which responded. The number of end-customers enrolled in these programs increased by 33% from 6 million to 8 million. A significant portion of this increase was in the residential sector, but the number of utilities offering day-ahead rates to commercial and industrial customers increased by 29% from 55 to 71. While this is not a large number of utilities compared to the thousands of respondents, the general trends are encouraging.

2.6.4 Chiller and Cooling Tower Cost Data

RSMeans Mechanical Cost Data provide the basis for estimating the installed chiller cost including profit and overhead (RSMeans 2015). The air-cooled chillers modeled in this work use screw compressors and the *RSMeans* chiller cost includes the integrated condenser. The costs are tabulated as a function of chiller capacity and linear regression is used to calculate costs between these values. The costs range linearly from $85,000 for a 100-ton (350 kWt) chiller to $180,000 for a 250-ton (880 kWt) chiller. Because all of the air-cooled chiller systems modeled use two chillers in parallel, the individual installed chiller cost is multiplied by two to get the total chiller capital cost.

The water-cooled chillers modeled use centrifugal compressors. The condensers are induced-draft cooling towers with axial fans and their costs are accounted for separately. The *RSMeans* linear regression for the water-cooled chiller data gives costs that range linearly from $160,000 for a 300-ton (1,050 kWt) chiller to $490,000 for a 1,000-ton (3,500 kWt) chiller. These costs are in addition to the cooling tower costs. Because the cooling towers are rated according to the rated heat rejected rather than the heat absorbed, the rated chiller *COP* is used to determine the required cooling tower capacity based on the rated chiller capacity. The cooling tower costs range linearly from $45,000 for a 300-ton (1,050 kWt) chiller to $145,000 for a 1,000-ton (3,500 kWt)

chiller. The water-cooled systems modeled in this research all have two parallel chillers with one cooling tower for each chiller, so the chiller and cooling tower cost are each multiplied by two to get the total installed chiller plant cost.

2.6.5 CTES Equipment Cost Data

General cost data for thermal storage systems is not available through *RSMeans* or similar databases. For the stratified chilled water systems, cost data were obtained from a consulting firm that specializes in CTES systems as well as a manufacturer of CTES tanks (J. Andrepont, personal communication, May 3, 2016 and G. Frankenfield, personal communication, January 25, 2017). For ice CTES systems, cost data were obtained from a manufacturer of internal melt systems (M. MacCracken, personal communication, July 8, 2016). A summary of the costs of each of these types of systems is shown in Figure 2-40. For stratified chilled water systems, the modeled cost is shown as a solid line within a shaded cost range. Because these tanks are erected in the field, several location-specific factors affect a particular tank's cost so that it might fall anywhere within this range. These factors include site soil conditions, local labor rates, the tank height-to-diameter ratio, and aesthetic enhancements. In addition to these factors, system parameters such as the chilled water temperature difference and the required charge and discharge rates have a significant cost impact. While Figure 2-40 extends to a storage capacity of 20,000 ton-hr (70,300 kWh), installations are commonly larger than this size and the cost per unit capacity continues to decline for these larger sizes. At a storage capacity of approximately 6,500 ton-hr (23,000 kWh), the modeled costs are equivalent. This capacity is equivalent to approximately forty ice CTES tanks (at 162 ton-hr (570 kWh) each) or a stratified chilled water tank with a volume of 0.5 Mgal (1,900 m^3). Beyond this intersection point, stratified chilled water systems benefit from the increasing economy of scale. The hatched regions in Figure 2-40 represent the approximate minimum storage

capacity range for the Secondary School and the Large Office building. The Secondary School is well within the range in which ice CTES is less expensive, but the Large Office building range includes the intersection of the two cost curves. The least expensive storage technology varies by geographic location for the Large Office building.

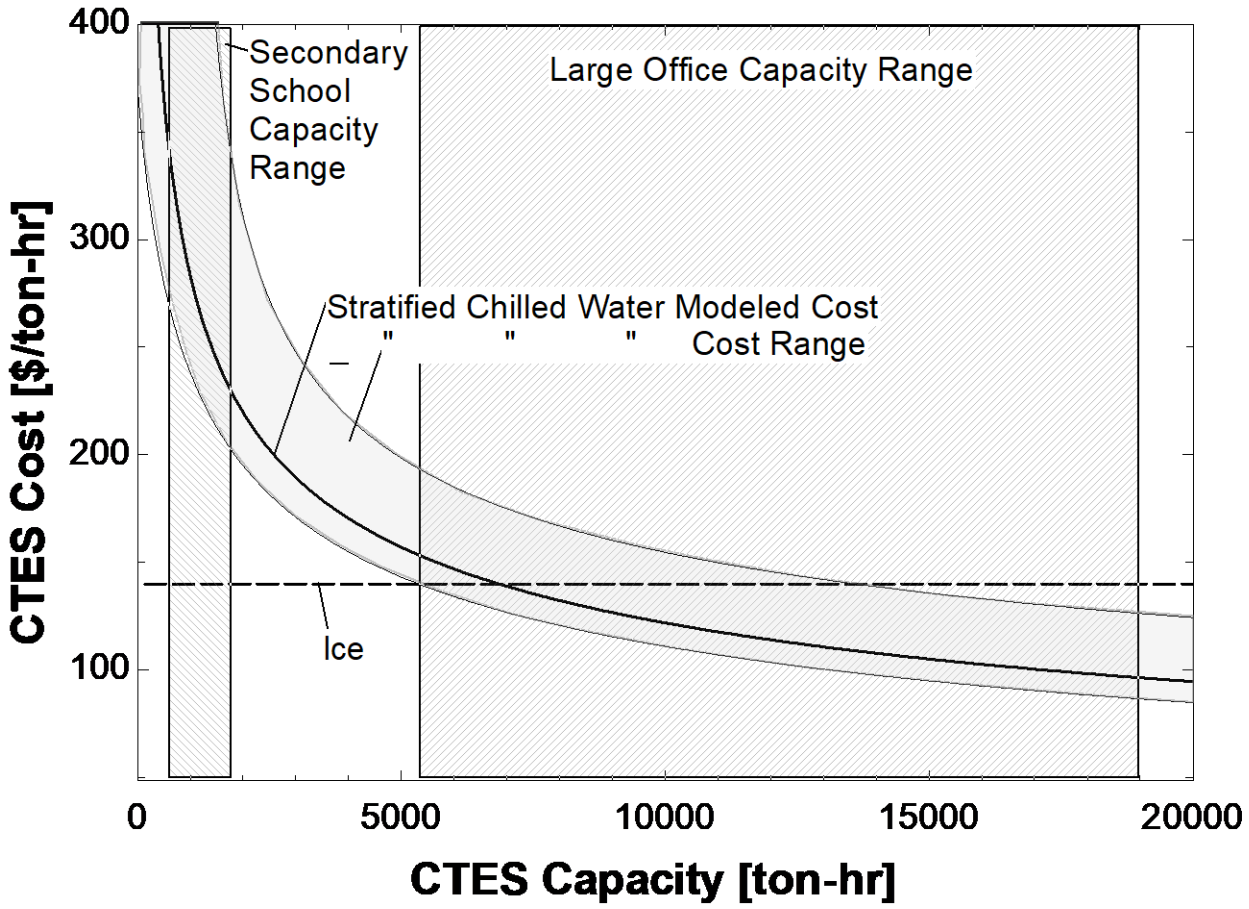

Figure 2-40. CTES cost data and storage capacity ranges

2.6.6 Photovoltaic and Wind Turbine Cost Data

The installed costs for photovoltaic systems have been rapidly declining over the past two decades. The United States Department of Energy publishes an annual overview of the pricing trends which tracks the most current pricing (USDOE 2015). The pricing includes materials, labor,

overhead, profit, and regulatory costs up to the point of grid tie-in. A breakdown that separates the cost of the module itself from the inverter and from the other costs is given. This breakdown is important for this research because the life cycle considered here is twenty years and the approximate lifetime of a PV inverter is ten years. Included in the capital cost for the photovoltaic systems is one inverter replacement. The prices are stated in units of $\$/W_{DC}$ with piecewise economies of scale provided through the use of different sectors. The residential sector pricing uses a system size of 5 kWe, the commercial sector uses a system size of around 200 kWe, and the utility sector uses a system size of 100 MW. For this research, the commercial sector pricing best fits the scale of the PV systems considered and the first quarter 2015 pricing is $\$2.17/W_{DC}$. This price includes $\$0.14/W_{DC}$ for the inverter, so after consideration of one inverter replacement, the final cost is $\$2.31/W_{DC}$. This cost is a conservative estimate with respect to the inverter replacement because the cost will be incurred years into the future and the inverter cost may continue to decline.

The USDOE also publishes an annual *Wind Technologies Market Report* which gives an overview of wind power installations, technologies, and costs (USDOE 2016). The wind turbine costs have also been declining in the last several years, but at a slower rate than the PV costs. The approximate average installed wind turbine cost reported for 2015 is $1.57/W. The same assumption regarding one inverter replacement is made for the wind energy generation option, adding a one-time cost of $0.14/W. The total cost considered for the wind turbine farm is then $1.71/W.

2.6.7 Present Value Cost Model

A present worth factor is used to calculate the present worth of the annual electricity costs (Duffie & Beckman 2013). Using an assumed inflation rate, *i*, an assumed market discount rate, *d*, and a number of years, *N*, the present worth factor is given by the following equation.

$$PWF(N,i,d) = \sum_{j=1}^{N} \frac{(1+i)^{j-1}}{(1+d)^{j}} = \frac{1}{d-i}\left[1-\left(\frac{1+i}{1+d}\right)^{N}\right] \tag{21}$$

This equation assumes that the inflation rate and the discount rate are not the same. For this research, the assumed inflation rate, *i*, is 5% and the discount rate, *d*, is 8%. These inflation and discount rates are based on the rounded averages of the Consumer Price Index inflation rate and the 10-Year Treasury Constant Maturity Rate between 1975 and 2007 (Coin News 2015, Federal Reserve Bank of St. Louis 2017). Using *N* of twenty years, the present worth factor is 14.4. This factor is multiplied by the electricity cost for one year to give the present value to be added to the capital costs. The sum is the twenty-year life-cycle cost.

3 INITIAL CONTROL STRATEGIES

The initial control strategies employed in this research are separated into two categories. The first is explicitly designed to meet the project objectives and utilize renewable power to meet the chiller electric load. These control strategies are termed “Renewable Control” strategies throughout this dissertation. The second category aims to reduce the electricity cost associated with the chiller electricity consumption. These control strategies are called “Cost Control” strategies in this dissertation.

3.1 Variable Parameters

Decision points in each of the initial control strategies depend on the values of several system parameters. Several of these parameters are allowed to vary in order to approach optimum operating conditions with respect to the project objectives. These variable parameters are tabulated in Table 3-1.

Table 3-1. Initial control strategy variable system parameters

Parameter	Values
Control strategy	*Renewable Control* or *Cost Control*
CTES technology	Stratified chilled water or ice
Renewable resource	Wind or solar
Installed renewable capacity	Multiples of the no-storage full-load chiller power
Storage daily recharge hour	Midnight to 11 p.m.
Minimum chiller plant part-load ratio	0.15 to 1
CTES capacity	Multiples of the minimum storage capacity
Chiller capacity	Multiples of the minimum chiller capacity

3.1.1 Baseline Parameter Sizing

The baseline or minimum-sized renewable generation, chiller, and CTES equipment vary by geographic location. To ensure that simulation results are comparable from region-to-region, the equipment sizes are normalized by appropriate values specific to the location. The rated capacity of the wind turbines and/or solar PV system is a multiple of the full-load chiller power for the no-storage system. This value is the peak cooling load for the building (in the particular geographic location) divided by the coefficient of performance at the ambient conditions during

the peak period. For the Secondary School, these values range from 380 kWe in California to 580 kWe in New York. For the Large Office building, the values range from 1,000 kWe in California to 1,300 kWe in New York.

The baseline capacity for the chillers and the thermal storage system assume a partial storage strategy. This strategy is designed to level the chiller load on the design day and represents the minimum possible equipment size while still meeting the cooling loads. The Texas Secondary School cooling load and chiller output for the partial storage strategy are shown in Figure 3-1 for stratified chilled water CTES. The storage tank is charged when the facility's cooling load is less than the chiller capacity and when the building cooling load exceeds the chiller capacity, the tank discharges to meet the load in parallel with the chiller. Because every day of the year other than the design day has a lower integrated cooling load, the chiller can be cycled off during all or a portion of the peak period on most days. When larger chillers are selected, they can be cycled off even during the design day. The chiller capacity shown in blue in Figure 3-1 is calculated by dividing the design day integrated cooling load by 24 hours. The storage tank capacity is the integrated area of the portion of the cooling load which lies above the chiller output.

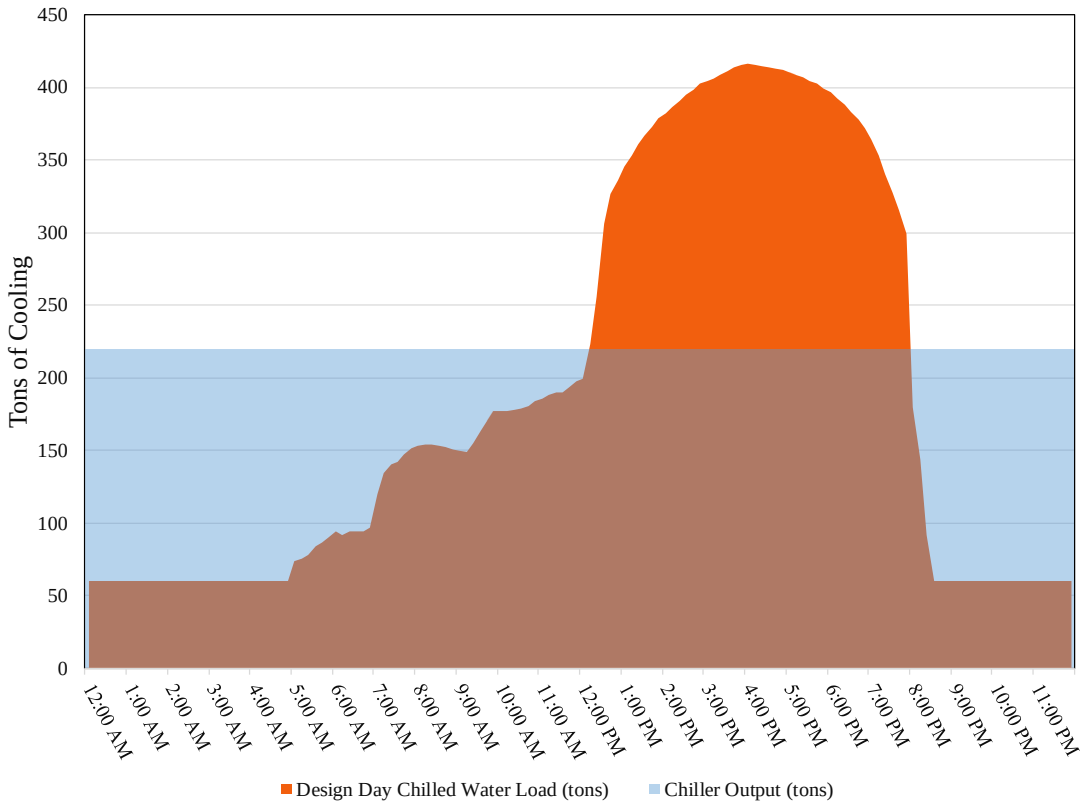

Figure 3-1. Chilled water partial storage strategy on the design day for the Secondary School

The calculations for the ice CTES systems are similar, but the reduced capacity of the chiller when operating at low chilled water set points must be taken into account. During the off-peak hours when the ice CTES system is charging, the chiller leaving glycol set point temperature is reduced in accordance with the performance curves provided in Figure 2-24. To compensate for the reduced chiller capacity at lower leaving glycol temperatures, an increase in rated chiller capacity between ten and twenty percent is required depending on the geographic location.

3.2 Renewable Control Strategies

The *Renewable Control* strategies run the chillers as long as (1) there is sufficient renewable power available and (2) there is a need for the cooling that is produced (either to directly

meet a building load or to charge storage). The varying parameters for these strategies are tabulated in Table 3-1. The first parameter listed in the table, control strategy, is set to *Renewable Control* for these strategies. The minimum storage and chiller capacities are calculated based on the partial storage strategy described in Section 3.1.1. There are two separate control strategies, one for each storage technology.

3.2.1 Chilled Water CTES Renewable Control Strategy

The flow chart in Figure 3-2 details the control decisions made for *Renewable Control* with a stratified chilled water CTES system. This strategy assumes that if sufficient capacity is available in the tank, the diffusers are designed such that any cooling load can be met by storage alone. The time-step used in the simulations in this research is 10 minutes. A short time-step is desired in order to accurately capture the intermittent nature of the wind and solar resources.

The chiller control strategies all operate with a constraint that requires the storage tank to be fully charged once in each 24-hour period. To determine whether or not the chillers should run for the current time-step, the first decision point is to determine whether or not the tank can be charged by the variable defined as “recharge hour” if the chillers were to remain off. This decision requires knowledge of the cooling load for the remainder of the current day. If the chillers must operate to recharge the tank by the beginning of the next day, they will run at full-load capacity regardless of the current level of renewable power available.

If the storage system can be recharged by the beginning of the next day without the chillers operating at full load, the next step is to decide whether the renewable power level available is sufficient to run the chillers. The renewable power available must be sufficient to run the chiller system at the part-load ratio specified by a user-defined parameter. If the available renewable power is sufficient, the next decision point is to evaluate the storage system’s state-of-charge. If

there is available storage tank capacity, the chillers are engaged only up to the system part-load ratio which can be met by current renewable power generation. If there are cooling loads present, the cooling loads are met by the chillers. If the cooling loads are in excess of the available chiller capacity, the CTES system is discharged in parallel with the operating chillers to meet the building loads.

If the tank is already fully charged, there must be building cooling loads for the chiller to operate. If the chillers operate, they are limited to the maximum part-load ratio that can be met by the minimum of the current renewable power generation available or the current building cooling load.

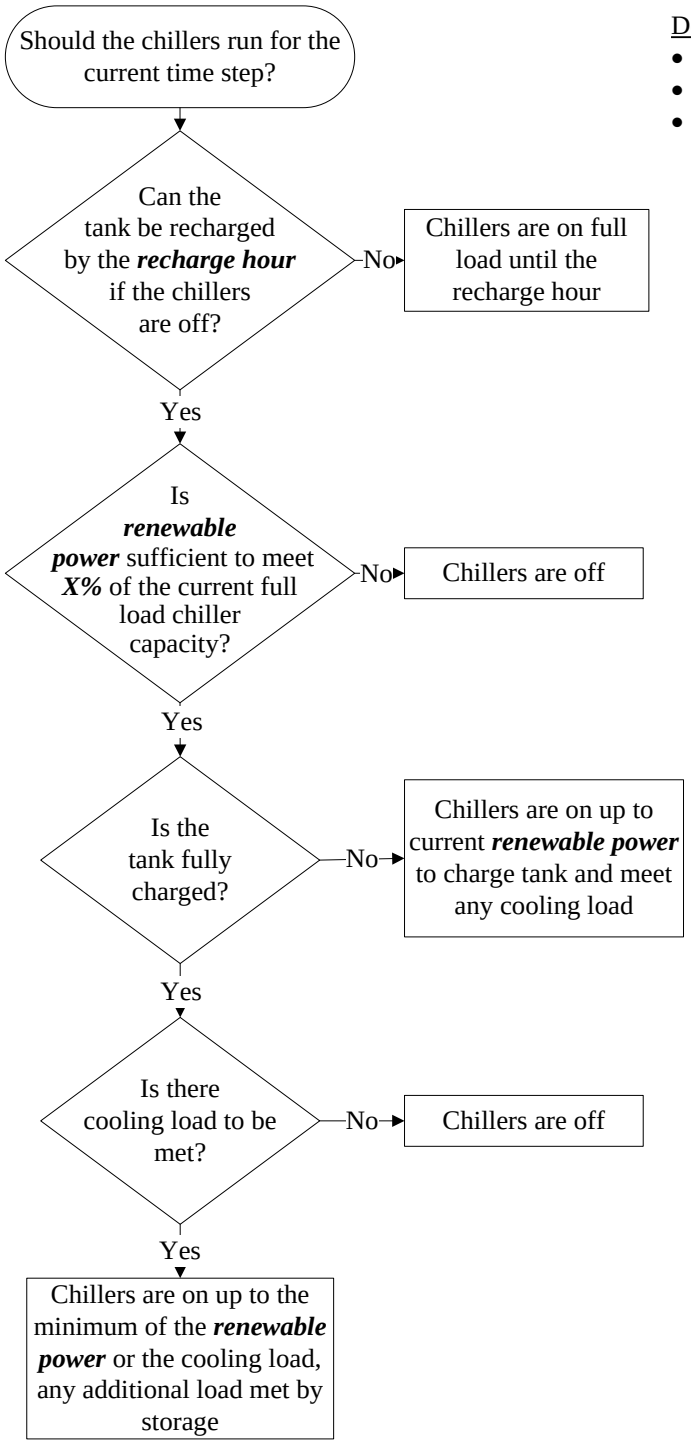

Figure 3-2. Stratified chilled water CTES flow chart for the *Renewable Control* strategy with design parameters highlighted

This control strategy is demonstrated through operation over a three-day period as shown in Figure 3-3. The top plot shows the cooling load for the Secondary School located in Texas on the left y-axis with the storage tank charge on the right axis. The capacity of the partial storage CTES system is 1,500 ton-hr (5,300 kWh). The bottom plot shows the intermittent wind power as well as the chiller power (a function of the *Renewable Control* strategy decisions). Based on sizing for a partial storage strategy and the rated chiller *COP*, the full-load chiller power requires 250 kWe of electricity. The maximum wind output for this example is set at 1,000 kWe. The time of day when storage must be recharged (the storage recharge hour) is 5 a.m. The x-axis on the bottom plot indicates the beginning of each of the three days.

For this particular example three-day period, the integrated daily building cooling load gets progressively greater from the first through the third day while the integrated available wind power shows the opposite trend over these three days. These trends make this particular three-day period ideal for illustrating each aspect of the control system behavior.

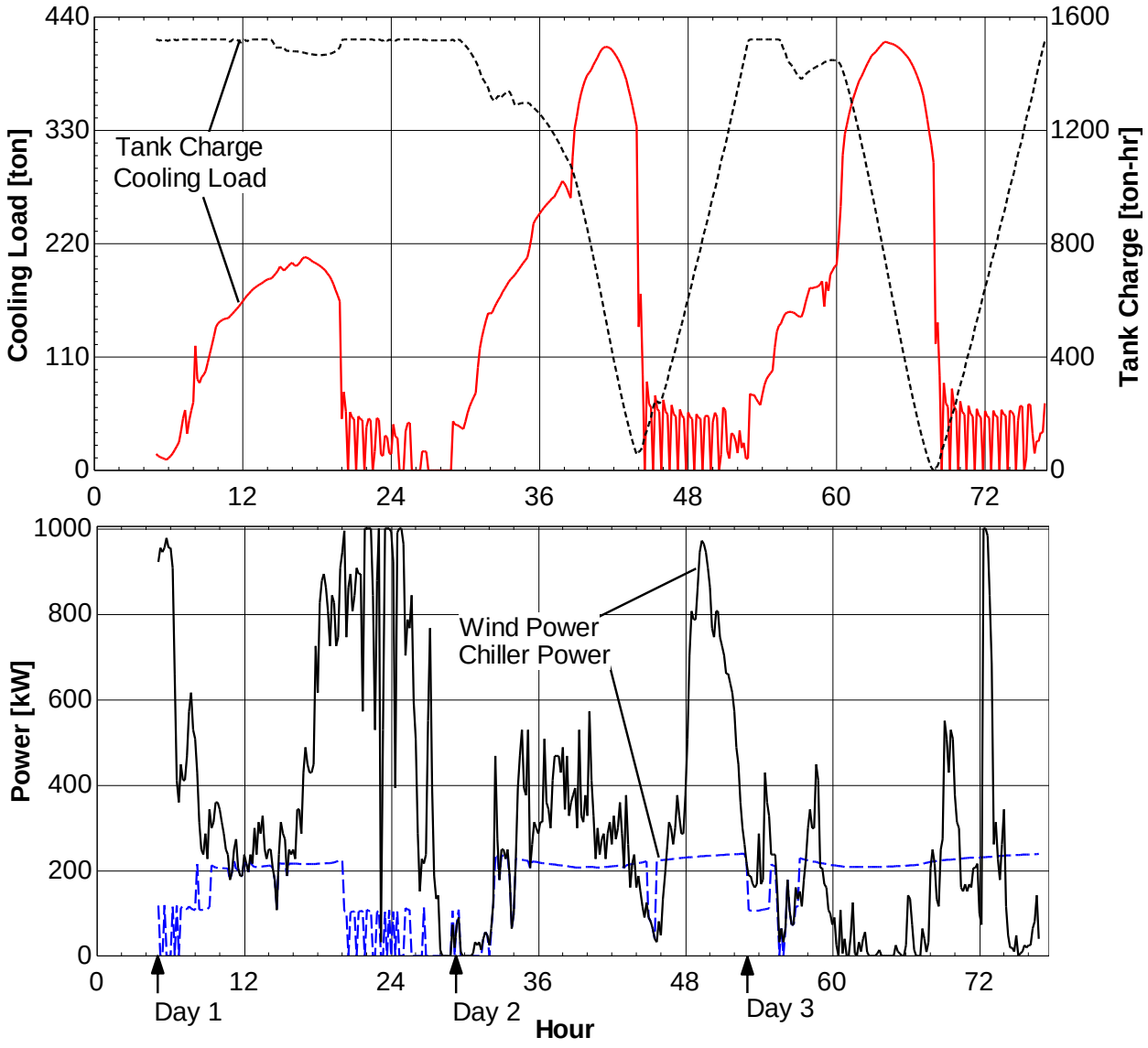

Figure 3-3. *Renewable Control* strategy for the Secondary School cooling load, tank charge (top), wind, and chiller power (bottom)

Figure 3-4 shows a time period during the third day that exhibits the default condition in the *Renewable Control* strategy. This condition dictates that the chillers run at full load regardless of the current level of available renewable power because the storage system must be fully recharged by the beginning of the next day (5 a.m.). Beginning around hour 59, the wind power dips below the chiller's full-load power requirement and the control system compares the remaining cooling load for the day to the available chiller capacity operating at full load. With a

large integrated cooling load remaining, the tank cannot be recharged by the beginning of the next day without running the chillers at full load. Reaching this phase of the control strategy means that there is no need to further evaluate decisions on the control strategy during the time-steps remaining before the beginning of the next cooling day – the chiller must remain on to fully recharge the storage system.

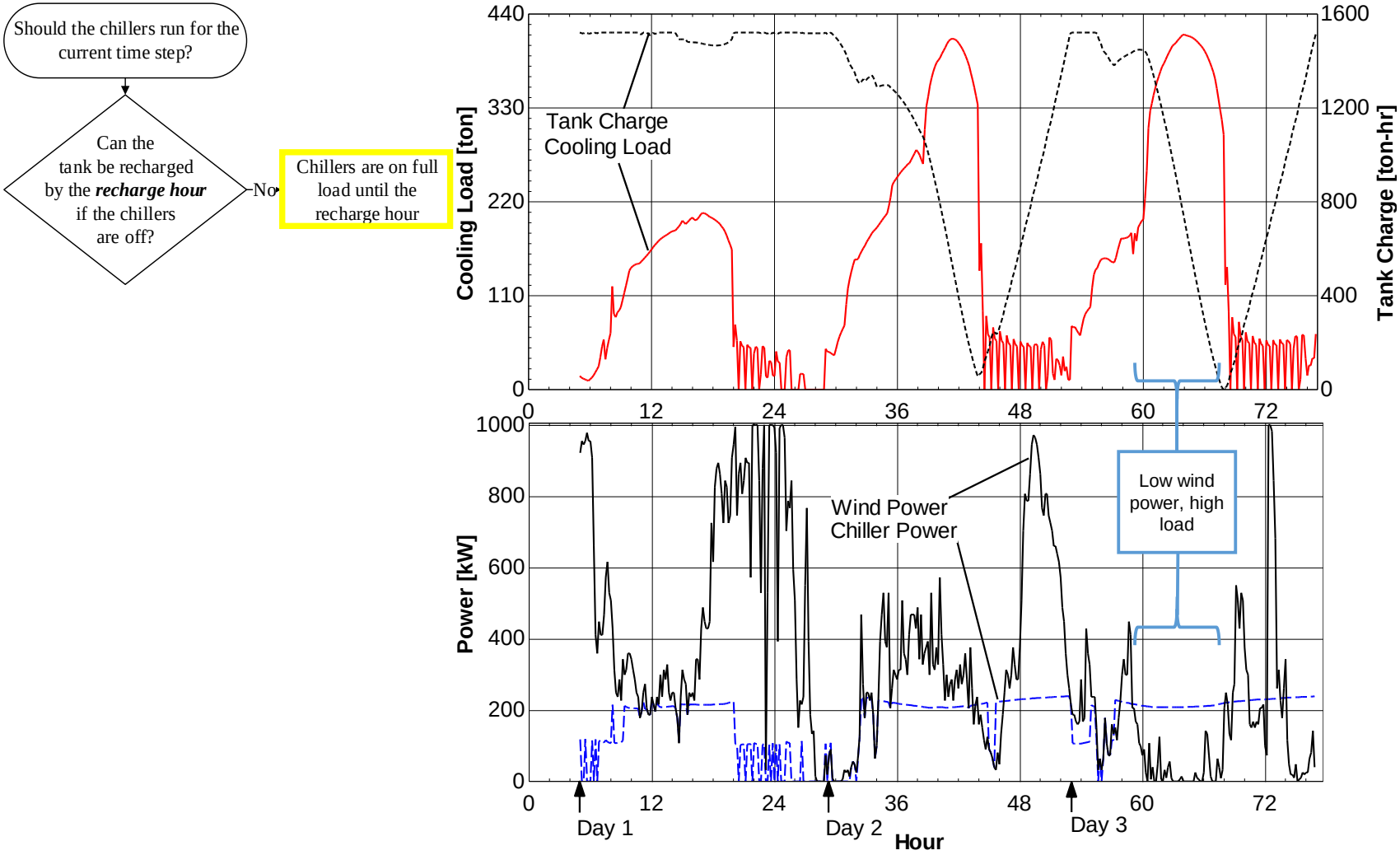

Figure 3-4. *Renewable Control* demonstration of default condition with low renewable resource and high cooling load

At hour 32, during the period of highest cooling load on the second day, the storage system begins to discharge as highlighted in Figure 3-5. At every time-step during this period, the wind power is sufficient to meet the chiller capacity at either full-load or part-load above the minimum chiller system part-load ratio. The next step in the control strategy flow chart is to determine whether the storage tank is fully charged or has available capacity. In the instance shown, the storage system has available capacity since the charge is below the 1,500 ton-hr level which would indicate a full charge. The chillers then operate up to the available wind power and the dip occurring at approximately hour 34 shows that the chiller operates at part load conditions during this time.

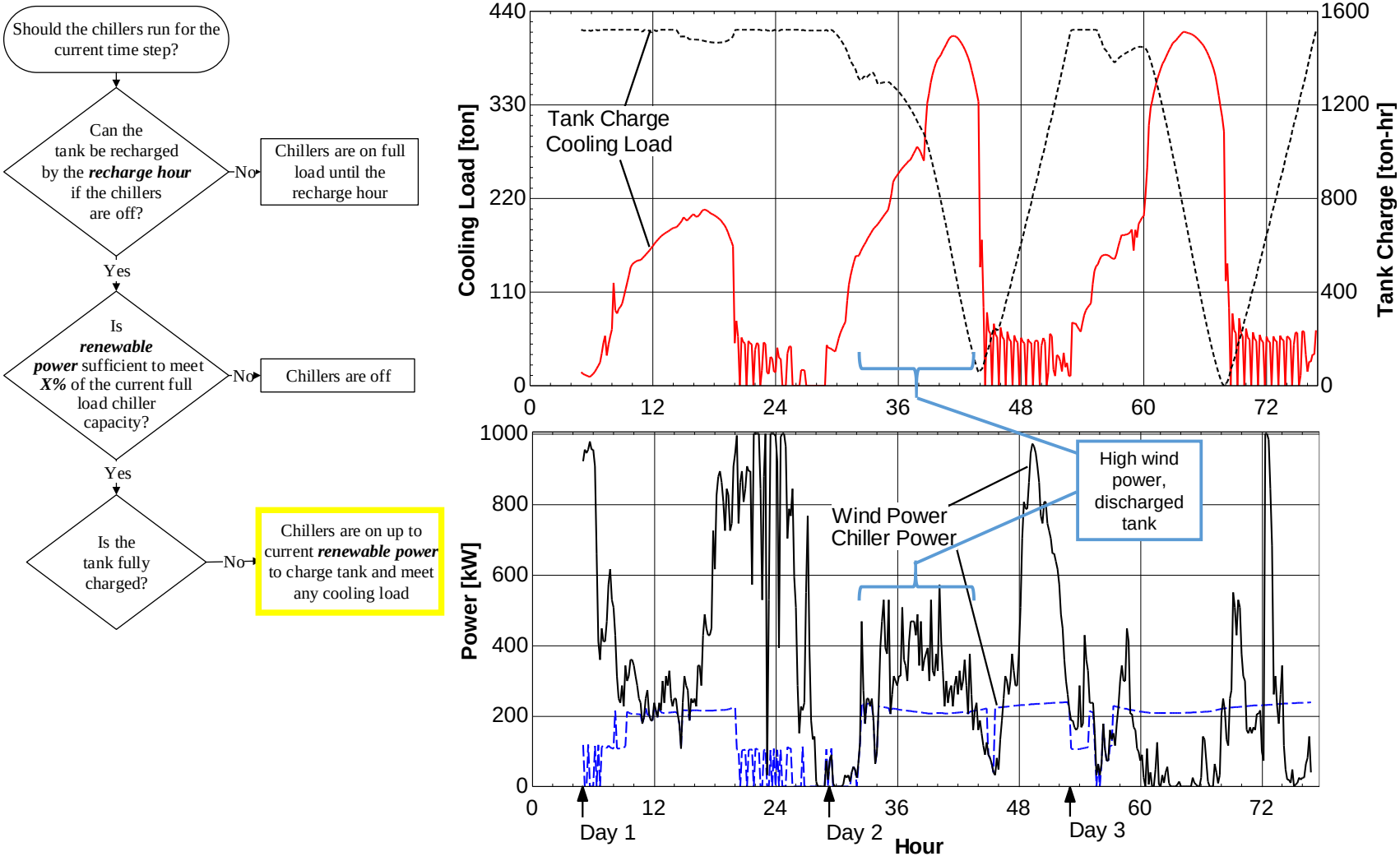

Figure 3-5. *Renewable Control* demonstration of high renewable power with tank capacity available

If wind power is available, but the storage system is already fully charged, the last option for utilizing the resource is to directly meet the cooling load. Figure 3-6 shows a time span where this is the case during the first day of the demonstrated period. At the very beginning of the cooling day, the wind resource is strong, the storage tank is fully charged, and there is a small cooling load to be met. The chillers run to directly meet the cooling load. Once the tank begins discharging at the end of this time period, this portion of the control strategy is no longer in effect.

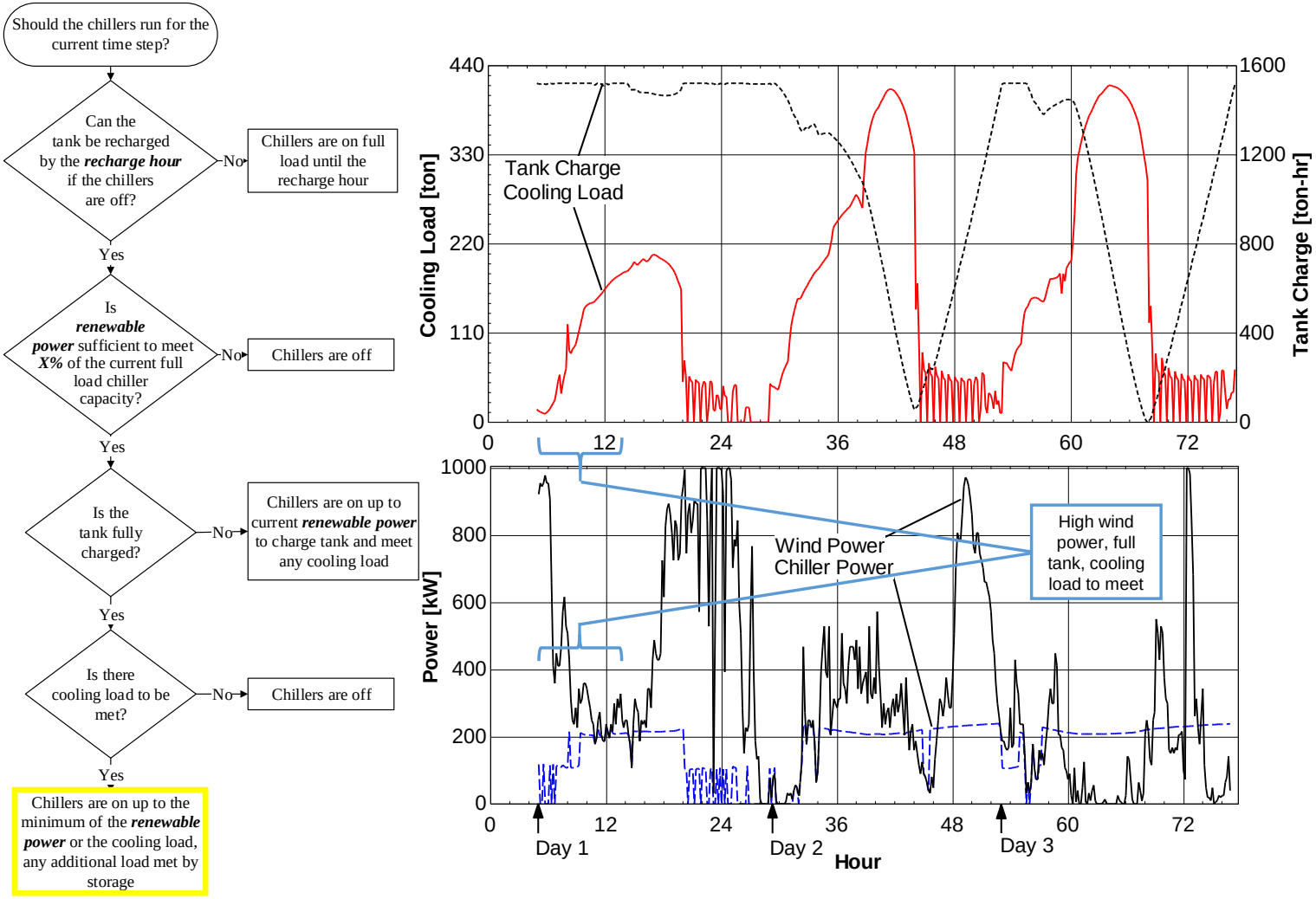

Figure 3-6. *Renewable Control* demonstration of high renewable power with cooling load to be met

3.2.2 Ice CTES Renewable Control Strategy

The *Renewable Control* strategy for ice CTES is similar to that for stratified chilled water, but accounting for the charging and discharging rate characteristics of the storage technology. As noted previously, these charge and discharge rates are a function of the storage state-of-charge. During each time-step where chiller capacity is available to charge storage or meet cooling loads by discharging storage, a second decision is required to evaluate and account for the charge or discharge rate of the CTES system. The control decisions also affect the chiller temperature set point, T_{chws}, whereas this temperature is always constant at 40°F (4.4°C) for chilled water CTES. The control strategy flowchart for *Renewable Control* with ice CTES is shown in Figure 3-7.

The first two control decisions, making sure storage is recharged by the beginning of the day and determining whether there is sufficient renewable power to meet the minimum chiller part-load ratio, are the same as those for the chilled water CTES technology. The next decision is whether or not there is a building cooling load to be met. If the renewable power level is low and there is no building cooling load to be met, the chillers are idled. If there is building cooling load, the storage discharge rate is evaluated. If the storage discharge rate is sufficient to meet the building cooling loads, the chillers are off and the use of non-renewable power is avoided. This operating state is described as the "Ice Only" mode (see Figure 2-17). On the other hand, if the storage discharge rate cannot fully meet the cooling load, then storage is discharged at its maximum rate and the remainder of the cooling load is met by the chillers. This mode is the "Chiller and Ice" mode illustrated in Figure 2-16.

If there is sufficient renewable power to meet the chiller system minimum part-load ratio and no cooling load, the next decision in the third row of the flow chart involves evaluating the storage system's state-of-charge. If storage is fully charged, the chillers are in the "Off" mode (as

described in Section 2.4.3) and the available renewable power goes unconsumed by the chillers. If storage is not fully charged, the operation mode transitions to “Make Ice” as depicted in Figure 2-15. The current storage charge rate is evaluated to determine whether the CTES system can accept the heat transfer rate provided by the chillers. If the maximum charge rate is less than the current chiller capacity at the renewable power level, the chillers run at the storage charge rate. If not, then the chillers run at the current chiller capacity and charge the storage at a rate less than its maximum.

With sufficient renewable power available to meet the chiller system’s part-load ratio as well as cooling load to be met, the magnitude of the cooling load is evaluated in the fourth row of the control flow chart. If the cooling load is not greater than the current chiller capacity, then the storage state of charge is evaluated. If storage is fully charged, the chillers run to meet the building cooling load directly to maximize the utilization of available renewable power. This “Chiller Only” mode is shown in Figure 2-18. If the storage system is not fully charged, the maximum storage charge rate is compared to the difference between the current chiller capacity and the cooling load. This mode is the “Make Ice and Cool” mode illustrated in Figure 2-12. If the charge rate is less than the current chiller capacity minus the cooling load, the chillers run only at the storage rate plus the current cooling load. Some of the available renewable power remains unused by the chillers. If the charge rate is greater than or equal to the current chiller capacity minus the cooling load, the chillers run at that capacity to meet the cooling load and the remaining chiller capacity is used to charge storage.

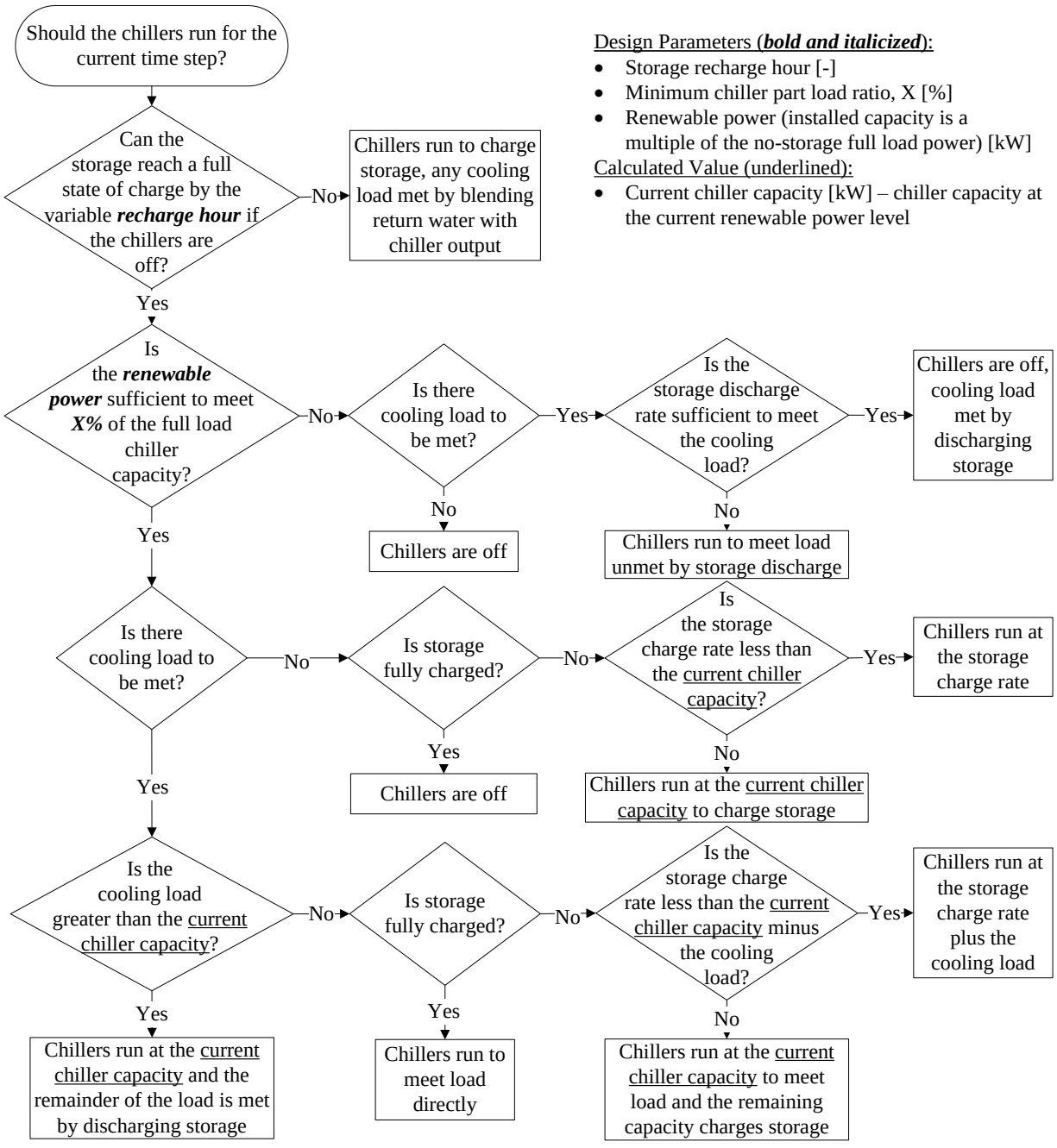

Figure 3-7. Ice CTES flow chart for the *Renewable Control* strategy with design parameters highlighted

3.3 Cost Control Strategies

The *Cost Control* strategies run the chillers as long as the electricity rates are currently off-peak and there is a need for the cooling that is produced (either to directly meet load or to charge storage). These strategies are intended to approximate a typical operating strategy for current CTES systems in the field. The varying parameters for these strategies are tabulated in Table 3-1. Although the level of renewable power is not a factor in decisions for this control strategy, the renewable power level is still varied to provide a point of comparison for renewable utilization among no-storage, *Renewable Control*, and *Cost Control* systems. The first parameter listed in the table, control strategy, is set to *Cost Control* for these strategies. The minimum storage and chiller capacities are calculated based on the partial storage strategy described in Section 3.1.1. As with *Renewable Control*, there are two separate control strategies, one for each storage technology.

3.3.1 Chilled Water CTES Cost Control Strategy

The *Cost Control* strategy flow chart for stratified chilled water CTES is displayed in Figure 3-8. The only design parameter used for making control decisions is the storage recharge hour. The strategy is very similar to the corresponding strategy for *Renewable Control* shown in Figure 3-2 except that the trigger for operating the chillers is off-peak electricity rates rather than available renewable power.

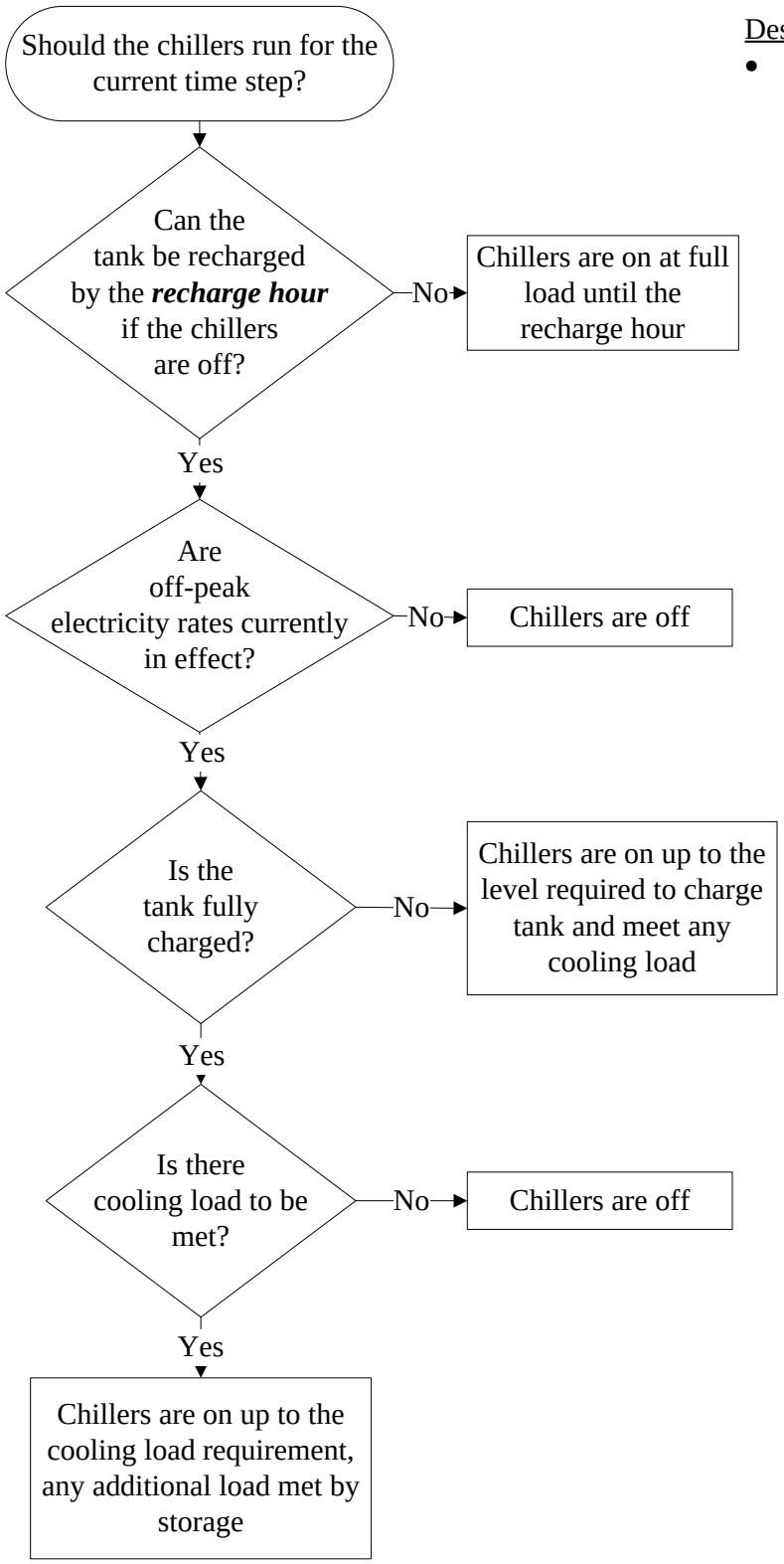

Figure 3-8. Stratified chilled water CTES flow chart for the *Cost Control* strategy with design parameter highlighted

3.3.2 Ice CTES Cost Control Strategy

Figure 3-9 illustrates the *Cost Control* strategy for ice CTES. Once again, the primary difference between this strategy and that for *Renewable Control* is the activation of the chillers through electricity rates rather than the presence of renewable power. Once the off-peak rates are in effect, the chillers are free to run using as much power as is required rather than being limited by the current renewable generation. For this reason, the chillers operate more frequently at full load and only unload when there is not sufficient uncharged storage capacity and/or cooling load to justify running at full load. This is one reason that storage systems in the field are not equipped with variable frequency drives. The improved part load performance gained in a small portion of the operation time does not compare well with the drive losses and does not justify the added cost.

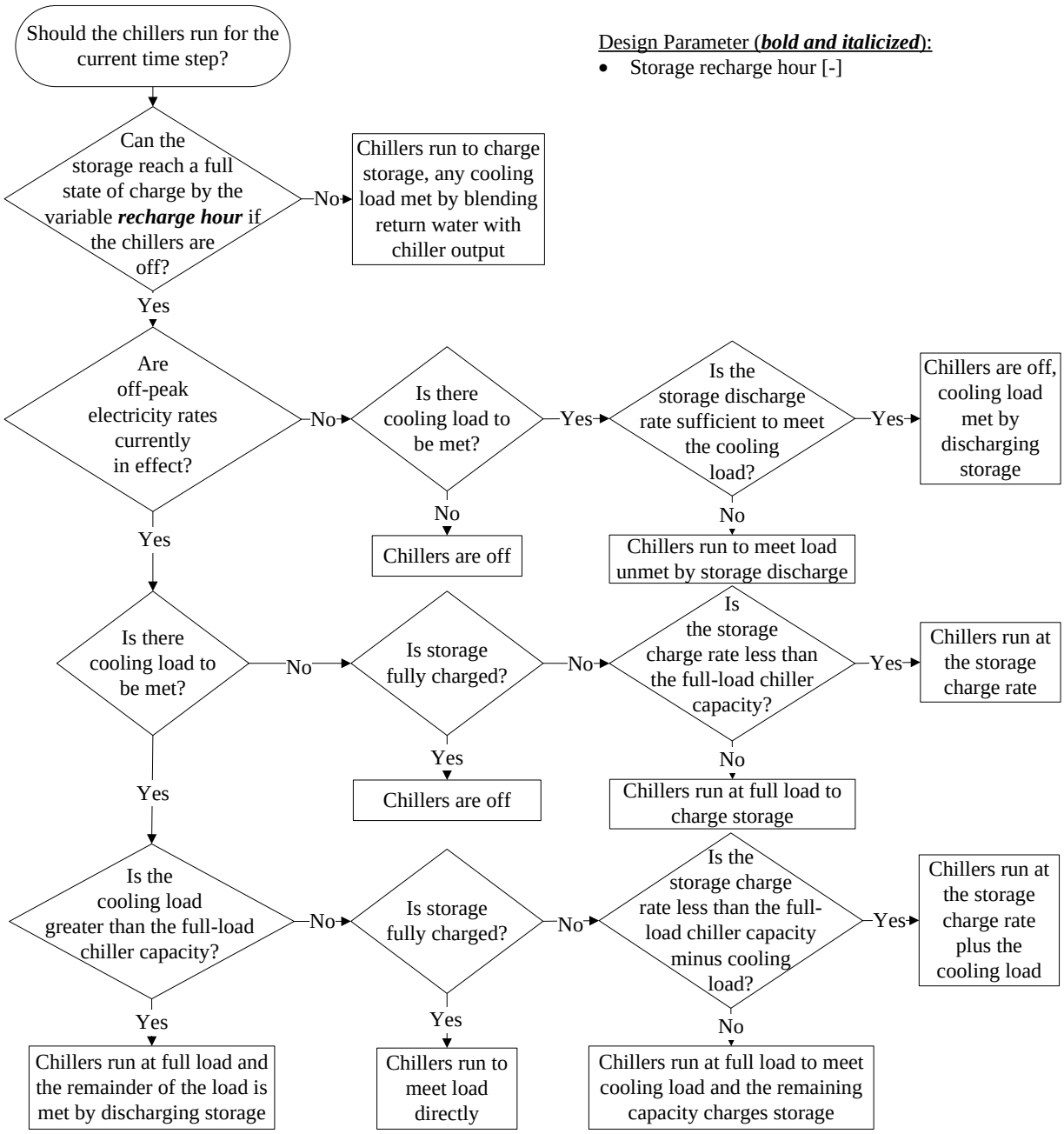

Figure 3-9. Ice CTES flow chart for the *Cost Control* strategy with design parameter highlighted

4 MODEL PREDICTIVE CONTROL STRATEGY

The control strategies presented in the preceding sections seek to maximize the use of renewable electricity or minimize operating cost through control decisions made at each timestep. In order to ensure that the cooling load will be met each day, perfect knowledge of the cooling

load and chiller system capacity for the remainder of the day are assumed. In the *Cost Control* and *Renewable Control* strategies, the knowledge of future cooling loads and chiller system capacity can be used to make key decisions such as whether to default to full-load chiller operation to meet the cooling loads or operate at part-load. Knowledge or forecasts of these and other inputs can also be used to simultaneously make multiple future control decisions determined by optimization algorithms. This method is called model predictive control and is applied here for the chilled water systems with operating cost reduction as the optimization objective.

Model predictive control (MPC) is a computationally-intensive method of process control that involves solving an open-loop control problem at each timestep over a finite horizon (Dai et al. 2012). The current, measured state of the system serves as the initial state for the control problem. An optimization results in a predicted or forecasted optimal control sequence to be implemented over the finite horizon and the first step in the sequence is implemented. The diagram in Figure 4-1 shows the optimal control sequence as the dashed line labeled "Optimal input trajectory (time k)." After the first control step is implemented, a new initial state is measured for use in developing a new optimal control sequence. This new control sequence is shown as the dashed line labeled "Re-optimal input trajectory (time k+1)" in Figure 4-1. Once the new control sequence is adopted, the remainder of the sequence developed during the previous timestep is discarded. This strategy results in shifting control horizons and model predictive control is also known as "receding horizon control" or "moving horizon control."

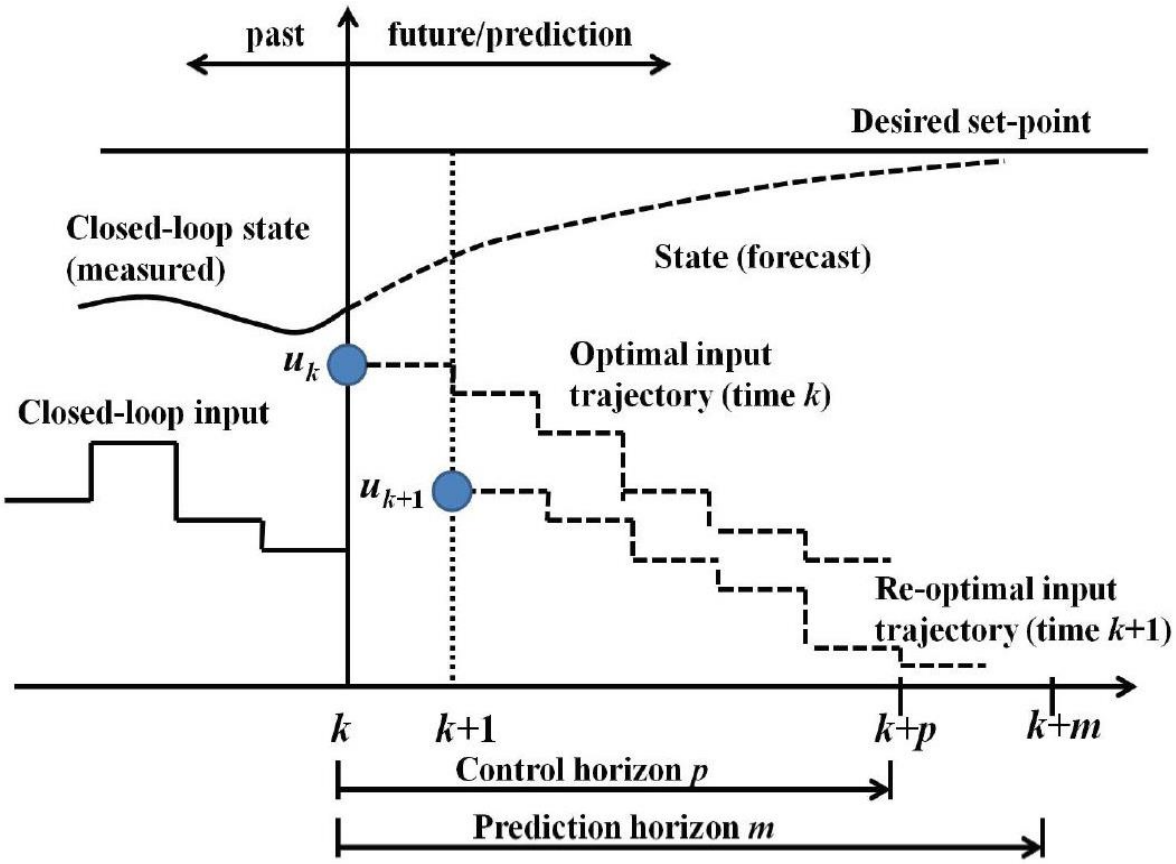

Figure 4-1. Model predictive control diagram (Dai et al. 2012)

4.1 HVAC Model Predictive Control Literature Review

Implementation of cool thermal energy storage systems with MPC strategies has been studied extensively (Wenzel et al. 2014; Wenzel et al. 2016; Kim 2013; Deng et al. 2015; Cole et al. 2012; Ma et al. 2009). Because an optimization is performed at each timestep, either multiple-minute timesteps or significant computational power are required. Early applications of MPC were in chemical processing and oil refining since computational power was limited, but the processes can be successfully controlled with long timesteps. Faster computers and parallel optimization algorithm development have allowed for MPC implementation in systems with faster dynamics such as power and HVAC systems. As long as at least one degree of freedom is provided, MPC and other optimization-based control strategies can be implemented. For a power system,

examples of this degree of freedom could be a pumped hydropower storage system or an array of batteries. For an HVAC system, the degree of freedom could be in the form of a hybrid geothermal and cooling tower heat pump system or cool thermal energy storage.

MPC has been in operation on a large scale at the Stanford University campus since 2015. Wenzel et al. (2014) describe the system and provides estimates of operating cost savings achieved through implementation of their control strategies. In this case, the operating cost is based on natural gas costs, electric energy costs, and electric demand charges. The campus chilling and heating loads are served by heat recovery chillers, conventionally operating chillers with cooling towers, cool thermal energy storage, gas/electric water heaters, and warm thermal energy storage. The finite control horizon used for the MPC algorithm (variable *p* in Figure 4-1) in this case is one week or 168 hours.

By allowing the optimization algorithm to determine the optimum equipment states at each fifteen-minute timestep, the authors found that some equipment states would be switched from off to full load and back to off again in three sequential control decisions. While this sequence provides the theoretical minimum operating cost, the difference in savings between the minimum and the suboptimum cost, which leaves the equipment off or on for all three timesteps, is less than a few dollars. Rather than incorporating models that would address increased equipment maintenance for more frequent cycling as well as the reduced equipment lifetime, the authors implemented an operating cost penalty based on the percentage load change between timesteps as a surrogate to address the negative impacts of more frequent equipment cycling. This penalty encourages more uniform equipment operation as shown by the difference in the profiles of the red, green, and blue curves in the top versus the bottom plots in Figure 4-2. Prior to the application of the load change penalty, the conventional chiller, heat recovery chiller, and cold water storage draw all experienced

drastic state changes over short time periods as shown in the plot on the top. A penalty of one dollar per percent change per hour causes the smoother transitions shown in the bottom plot. The authors note that operating with this penalty adds to the annual operating cost, but they do not specify by how much.

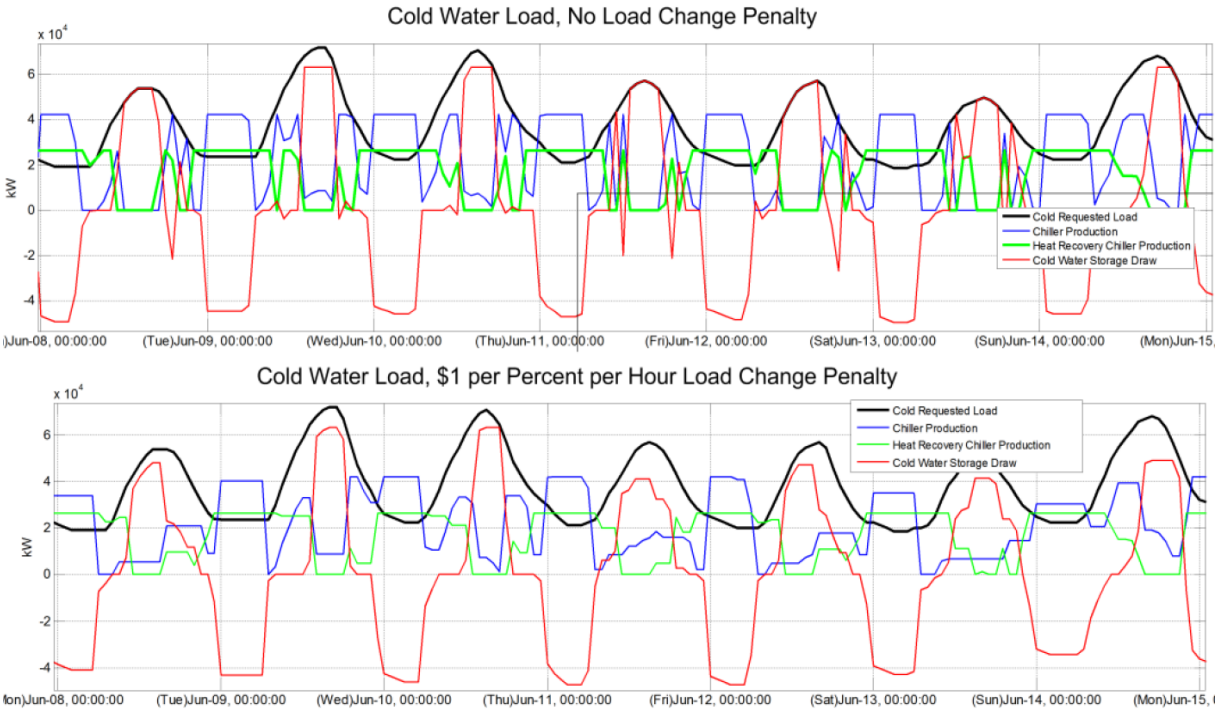

Figure 4-2. Wenzel et al. (2014) simulation impact of load change penalty

After the Stanford University system came online in 2015, Wenzel et al. (2016) provided an update on estimates of the operating cost savings as well as details about operator interaction with the autonomous MPC system. In the first several months of operation, the operating cost savings were over 10% as compared to operating with a set schedule. This savings was realized, in part, because the system was run in autonomous MPC mode over 90% of the time. One major contributor to the cost savings is a reduction in electricity demand charges. Given a fixed set of equipment, electric demand savings can come from two sources. One is that the equipment is routinely being run at part load in which case some equipment pieces may be oversized. The

second potential source of savings is the staging of various equipment types so that they aren't running coincidently.

For the research presented in this dissertation, model predictive control strategies are implemented only on CTES systems and comparisons are drawn between different types of control strategy inputs. Once chiller and CTES capacities are determined for this system, a significant reduction in demand charges is not available. There are not degrees of freedom available for staging the electricity consumption and reducing demand charges. If demand charges were reduced by limiting the chiller system to part-load operation, the chiller system capacity would be reduced to minimize capital costs as well as to increase system efficiency by operating at higher part-load ratios. Demand charges are typically determined by the peak power consumption in the current month or sometimes by the peak consumption over the entire year. During each month the building experiences cooling loads, the chiller operates at full load at some point which establishes the facility demand which serves as the basis for the electricity demand charge.

Cole et al. (2012) modeled a CTES system with MPC in the Austin, Texas climate. One optimization objective in this case is the total electricity cost (including both energy and demand charges) and another is the total system energy usage. As opposed to the Stanford University system, this study considers only the cooling loads to be met and doesn't incorporate heating or hot water loads. The Cole investigation also assumes that all input variables are known perfectly and no disturbances are introduced. This assumption means that the results achieved are an upper limit of what is achievable with actual measured data. The MPC system is compared to two baseline systems, one without any CTES system and another with a CTES system using a storage-priority control strategy. The results for the comparison with a system without any CTES are presented here. When the optimization objective is to minimize overall electricity cost, the MPC

system results in a 41% cost savings and 2% energy savings over a system without storage. When the optimization objective is to reduce annual energy usage, the MPC system results in a 28% cost savings and 4% energy savings over the system without storage. The energy minimization objective results in increased costs (28% savings versus 41% savings) and minimal increases in energy savings (4% savings versus 2% savings).

Verrilli et al. (2016) applied MPC to a district heating system with warm thermal energy storage in Finland. The system is composed of a combined heat and power boiler, a grate boiler and two oil boilers in addition to the warm storage tank. The control strategy timestep is one hour and the control horizon is only twelve hours. The authors state that the short time horizon was chosen due to computation times required for longer time horizons. They also saw a lack of significant performance improvement seen with longer time horizons presumably due to the capacity of the storage system and the length of the daily heating period. The MPC strategy results are compared to a baseline in which operators are manually adjusting boiler operation in what amounts to a "boiler-priority" control. The warm thermal energy storage system is not used efficiently in this manual process. The optimization objective for the MPC strategy is to minimize total fuel cost. Each of the three boiler types has a different efficiency, so the warm thermal energy storage should be utilized to avoid operation of the least efficient boilers. The authors performed a simulation for a 15-day period and drew a cost comparison amongst three different strategies. The baseline strategy described above is referred to as current practice (CP), the baseline MPC (B-MPC) uses perfect input data, and the third strategy utilizes mixed-integer linear programming (MILP) to optimize the MPC strategy using imperfect forecasts (abbreviated as MILP-MPC). The results show total fuel costs which are 7.2% below the current practice with perfect input data and 7.1% below current practice with imperfect forecasts. The minimal difference between the two

strategies using model predictive control demonstrates the robustness to disturbances in the forecasted inputs. The plot in Figure 4-3 shows the warm thermal energy storage state of charge for the three control strategies. From hours 125 to 240 it is clear that the MPC strategies are taking advantage of the storage capacity while the manual boiler-priority control leaves storage with a high state of charge. Focusing on the difference between the blue and black lines, the impact of imperfect forecasted inputs is seen through the high frequency changes in the state of charge for the MILP-MPC strategy.

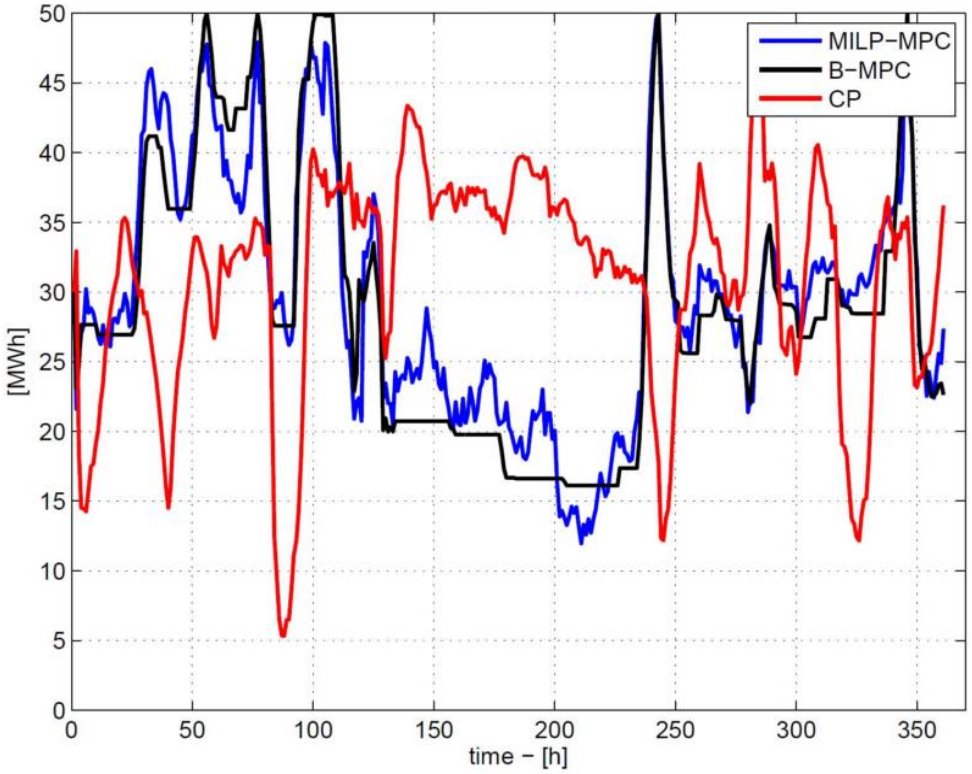

Figure 4-3. Warm thermal storage state of charge for MPC with forecasted inputs (MILP-MPC), MPC with perfect inputs (B-MPC), and manual current practice (CP) (Verrilli et al. 2016)

4.2 Implementation of CTES Model Predictive Control

Model predictive control allows for increased flexibility in CTES operation. A chiller-priority control strategy is one in which the chiller system is preferentially utilized to meet

building cooling loads up until the cooling load exceeds the full-load chiller capacity. A storage-priority control strategy seeks to meet the building cooling load by first discharging the storage system up until either the cooling load exceeds the instantaneous discharge rate of the storage system or the storage has been fully depleted at which time the chiller system comes online to directly meet the load. The *Cost Control* strategy amounts to a chiller-priority control strategy during times with off-peak electricity rates and a storage-priority control strategy when on-peak rates are in effect. The model predictive control strategy does not impose either of these limitations.

The specific MPC strategy detailed here is referred to as *Model Predictive Control* throughout this dissertation. Because *Model Predictive Control* involves optimization at each timestep, perfect knowledge is not required for its implementation. If knowledge of the control inputs is perfect, the optimization need not be repeated at each timestep but only once for each finite time horizon. In the case of these CTES simulations, the horizon is a 24-hour period. *Model Predictive Control* is employed only for stratified chilled water storage systems in this research effort. The optimization problem for each horizon is posed through the following equations with the minimization of electricity cost as the objective:

$$\underset{\boldsymbol{x}}{Min}\ [Cost_{electricity}(\boldsymbol{x})] \tag{22}$$

$$Cost_{electricity} = \sum_{i=1}^{N} Rate_{electricity,i} P_{chiller,i} \Delta t \tag{23}$$

$$\boldsymbol{x} = \begin{Bmatrix} PLR_1 \\ PLR_2 \\ \vdots \\ PLR_N \\ Charge_1 \\ Charge_2 \\ \vdots \\ Charge_N \end{Bmatrix} \tag{24}$$

$$s.t.\ (PLR_i \Delta t) Cap_i + (Charge_{i-1} - Charge_i) = \dot{Q}_{L,i} \Delta t;\ i = 1, 2, ...N \tag{25}$$

$$Cap_1 PLR_1 + Cap_2 PLR_2 + ... + Cap_N PLR_N = \sum_{i=1}^{N} \dot{Q}_{L,i} \tag{26}$$

$$0 \le PLR_i \le 1;\ i = 1, 2, ...N \tag{27}$$

$$0 \le Charge_i \le Cap_{storage};\ i = 1, 2, ...N \tag{28}$$

where the total 24-hour electricity cost is $Cost_{electricity}$ and does not include demand charges for the reasons stated in Section 4.1. N is the number of timesteps in the control horizon and the electricity rate energy charge is $Rate_{electricity}$ in \$/kWh. $P_{chiller}$ is the power consumed by the chillers in kWe and Δt is the length of the simulation timestep. The optimization variables in the vector, $\boldsymbol{x}$, are *PLR*, the chiller system part-load ratio, and *Charge*, the storage charge level (fraction of chilled water at the chiller supply temperature multiplied by the storage capacity) in ton-hours (kWh_t). *Cap* is the thermal capacity of the chiller and $\dot{Q}_L$ is the building cooling load, both in tons (kWt). The constraint specified in Equation (25) is an energy balance that requires that the cooling load is always met whether it is by the chiller system or by the discharging of storage. The constraint in Equation (26) is that over the 24-hour period, the sum of the chiller output must equal the sum of the cooling load. Because the storage system begins with a full state-of-charge, this constraint

ensures that storage is fully charged at the beginning of each 24-hour period. This constraint indicates that heat gains to the CTES system are neglected in these simulations due to their relative insignificance. The daily recharge cycle for the CTES systems along with the moderate delta between the outdoor ambient and chilled water temperatures justify this simplification.

The annual simulations are performed using the MATLAB function for solving linear programs, *linprog* (MathWorks 2018). Use of this function is possible only with the linearized chiller performance curves presented in Section 2.5.5. *Linprog* finds the minimum of a problem specified in the following format:

$$\min_x f^T x \text{ such that } \begin{cases} A \cdot x \le b \\ Aeq \cdot x = beq \\ lb \le x \le ub \end{cases} \tag{29}$$

$$f^T x = f(1)x(1) + f(2)x(2) + ... + f(l)x(l) \tag{30}$$

where $f^T x$ indicates a row vector of constants, *f*, multiplying a column vector of variables, *x*, of length *l* as shown in Equation (30). The *x* vector is the output of interest from the solver. The first constraint, $A \cdot x \le b$, is for linear inequalities where *A* is a *k*-by-*l* matrix where *k* is the number of inequality constraints. $Aeq \cdot x = beq$ is for linear equalities and *Aeq* is an *m*-by-*l* matrix where *m* is the number of equality constraints. Lastly, bound constraints are input into the vectors, *lb* and *ub* for lower and upper bounds, respectively. These vectors are both of length *l* and the variables in *x* must lie between them.

The default linear programming algorithm used by *linprog* is a simplex method algorithm called dual-simplex. The other two available algorithms are different interior point methods. The simplex and interior point methods differ in their approach to the problem in that simplex methods visit the vertices of the feasible region of the problem while interior point methods initially visit

points interior to the feasible region until the optimal vertex is reached. For a linear optimization, unique solutions will be at a vertex. The methods also differ in their number of computational steps to convergence depending on the type of problem being solved. Because the simplex and interior point methods return approximately the same results over annual simulations, the MPC control strategy is implemented using the default, dual-simplex algorithm.

To minimize energy cost for the electricity needed to run CTES system chillers, the chiller power consumption must be minimized. The water-cooled chiller system coefficient of performance is defined as:

$$COP = \frac{Cooling\ Power\ Output}{Electric\ Power\ Input} = \frac{PLR(Cap_{factor} Cap_{rated})}{P_{chiller}} \tag{31}$$

where Cap_{factor} is a value multiplied by the chiller system's rated capacity, Cap_{rated}, to give the capacity at current conditions. Cap_{factor} is given by the chiller performance curves and is function of the ambient conditions and the chiller set point temperature (CEC, 2012). Rearranging Equation (31) to return the chiller power gives:

$$P_{chiller} = \frac{PLR(Cap_{factor} Cap_{rated})}{COP} \tag{32}$$

The first two variables in the numerator and the variable in the denominator are grouped into a chiller power factor, $P_{chiller,factor}$, which is a linear function of the chiller system part-load ratio, the ambient wet-bulb temperature, and the chiller leaving chilled water set point temperature. The set point temperature is constant at 4.4°C (40°F) for the stratified chilled water simulations. The linear function for the $P_{chiller,\,factor}$ comes from a combination of the linearized performance curves plotted in Figure 2-34 and the chiller system capacity at ambient conditions. The chiller power factor is defined as follows:

$$P_{chiller,\,factor} = \frac{PLR(Cap_{factor})}{COP} \tag{33}$$

$$P_{chiller} = P_{chiller,\,factor} Cap_{rated} \tag{34}$$

$$P_{chiller,\,factor} = a + bPLR + cT_{wb} \tag{35}$$

where *a*, *b*, and *c* are constants coming from a linear regression for the chiller power factor.

Inserting Equation (34) into the optimization objective (Equation (23)) gives the following equation:

$$Cost_{electricity} = \sum_{i=1}^{N} Rate_{electricity,i} P_{chiller,\,factor,i} Cap_{rated} \Delta t \tag{36}$$

Optimization objective functions cannot contain constant terms without creating additional variables for these constants and then constraining them to be a constant value. With perfect weather knowledge, both the first and last terms in Equation (35) are constant. Rather than creating additional variables in the optimization, these terms are accounted for in post-processing steps by adding their values to get the actual chiller power. The new optimization objective is thus:

$$Cost_{electricity} = \sum_{i=1}^{N} Rate_{electricity,i} (bPLR) Cap_{rated} \Delta t \tag{37}$$

where the electricity rates considered are described in Section 2.6.3. The only variable to be optimized in Equation (37) is the part-load ratio, *PLR*. These *PLR* values are the first *N* entries in the *x* vector for the *linprog* solver. The corresponding first *N* entries in the *f* vector of constants are the coefficients multiplying *PLR* at each timestep:

$$f_i = Rate_{electricity,i} bCap_{rated} \Delta t;\ i = 1, 2, ..., N \tag{38}$$

The optimization problem also requires N variables for the storage tank charge, *Charge*, because this value must be constrained throughout the optimization so as to avoid the situation where the cooling load is not met as indicated by a negative charge and also the situation where the charge is greater than the physical capacity of the tank. The *f* vector of constants has a value of zero for these N entries because the storage tank charge is not part of the optimization objective. The full *x* vector is given in Equation (24).

The constraints required for this optimization are all defined through equalities and constant bounds, so the inequality constraint type shown in Equation (29) is not required here. The equalities are given in Equations (25) and (26). They ensure that the cooling load is met either by storage or directly by the chiller system and that the storage tank is fully charged each day. In matrix form, these equality constraints are:

$$\underbrace{\left[\begin{array}{cccc|cccc} Cap_1 & Cap_2 & \dots & Cap_N & 0 & 0 & \dots & 0 \\ Cap_1\Delta t & 0 & \dots & 0 & -1 & 0 & \dots & 0 \\ 0 & Cap_2\Delta t & \dots & 0 & 1 & -1 & \dots & 0 \\ 0 & 0 & \ddots & 0 & 0 & \ddots & \ddots & 0 \\ 0 & 0 & \dots & Cap_N\Delta t & 0 & \dots & 1 & -1 \end{array}\right]}_{\boldsymbol{Aeq}} \underbrace{\left\{\begin{array}{c} PLR_1 \\ PLR_2 \\ \vdots \\ PLR_N \\ \hline Charge_1 \\ Charge_2 \\ \vdots \\ Charge_N \end{array}\right\}}_{\boldsymbol{x}} = \underbrace{\left\{\begin{array}{c} \sum_{i=1}^{N} \dot{Q}_{L,i} \\ \dot{Q}_{L,1}\Delta t - Cap_{stor} \\ \dot{Q}_{L,2}\Delta t \\ \vdots \\ \dot{Q}_{L,N}\Delta t \end{array}\right\}}_{\boldsymbol{beq}} \quad \begin{matrix} \\ \\ \\ \\ N+1 \\ \\ \\ \\ \end{matrix}$$

(39)

where *Aeq* is an N+1-by-2N matrix with N+1 equalities for 2N variables. The 2N variables are in the *x* vector and the *beq* vector has N+1 elements, one for each equality. The second element in vector *beq* has an extra term, Cap_{stor}, the capacity of the storage tank. This term accounts for the $Charge_{i-1}$ term in Equation (25). For the first control decision, the charge for the previous timestep

is the capacity of the system since it is constrained to be fully charged at that point. For future control decisions, the charge from the previous timestep is used.

The last set of constraints are constant bounds on the variables which are given in Equations (27) and (28). The first constraint limits the chiller system operation to be between the limits of being idle at a part-load ratio of zero to operating at full load at a part-load ratio of 1. The second constraint limits the storage charge levels to lie between the limits of zero and the physical capacity. The lower bound, *lb*, and upper bound, *ub*, vectors are constructed as follows:

$$lb = \begin{Bmatrix} 0 \\ 0 \\ \vdots \\ 0 \\ 0 \\ 0 \\ \vdots \\ 0 \end{Bmatrix}; \quad ub = \begin{Bmatrix} 1 \\ 1 \\ \vdots \\ 1 \\ Cap_{stor} \\ Cap_{stor} \\ \vdots \\ Cap_{stor} \end{Bmatrix} \tag{40}$$

where each of the vectors has 2*N* elements.

The formulation of the problem shows that the optimization is indifferent to the fact that this is an energy simulation that is stepping through time. The matrices and vectors include variables for each timestep considered, but the algorithm is solved for all of the chiller system part-load ratios and storage charge levels at once. With perfect inputs, the optimization is necessary only once per control horizon or 24 hours in this case. As an example, if the cooling load were a forecast rather than the actual cooling load, the first step would look identical to the only step in the case with perfect knowledge. However, for the second timestep another optimization would be performed using the updated storage charge resulting from the imperfect cooling load prediction and an updated cooling load forecast could also be considered.

Using perfect inputs, optimizations are performed once for each day of the year. The result of each optimization is an *x* vector containing part-load ratio and storage charge values for each timestep of the day. These values are concatenated with the values for the previous days through the final day. The storage charge values are not required for post-processing but could be useful for determining whether or not the storage capacity is over-sized. If the storage tank never approaches a fully depleted state, the storage tank can likely be downsized.

The part-load ratio values are used to determine both the annual chiller electricity consumption as well as the cost for that electricity consumption. To obtain the chiller power from the *PLR* values, Equation (35) is used with *a* equal to 0.0126 kWe, *b* equal to 0.118 kWe, and *c* equal to 0.000511 kWe/°C. These coefficients come from a combination of the linearized chiller system performance model plotted in Figure 2-34 and the chiller system capacity based on ambient conditions. The sum of the chiller power values multiplied by the simulation timestep gives the annual chiller electricity consumption in kWh. Multiplication of the chiller power by the simulation timestep and applicable electricity rate for that time gives the electricity for one timestep. The sum of these values is the annual chiller system electricity cost. The energy consumption and cost are then compared with equivalent results using the *Cost Control* strategy to determine the benefits of *Model Predictive Control*. These results are presented in Section 5.4.

5 RESULTS

5.1 System of Analysis Definition

The results of this research have potential impacts on various stakeholders including building owners (end-users), electric utilities, regional transmission organizations (RTOs), sustainability advocates, and mechanical systems equipment manufacturers. As such, a definition of the system of analysis is important for determination of the benefits and costs to these various stakeholders. The components of the larger "system" include the utility grid (including generation from various sources and transmission), grid-connected wind or solar generation, and the building with an HVAC system (chillers with or without storage). As a simple example, a grid-connected solar PV system, building, and utility grid are illustrated in Figure 5-1. The PV panels produce direct current (DC) that is then converted to alternating current (AC) through an inverter. The AC power is consumed by the building and any excess power is sold to the grid through the electric meter. This process is termed "net metering" and the most common implementation involves the building receiving an offset equal to the retail electricity rate for each unit of renewable power delivered to the grid. This is sometimes referred to as "conventional net metering" because several states have begun to move toward an offset that more closely approaches the wholesale electricity price (National Conference of State Legislatures 2016).

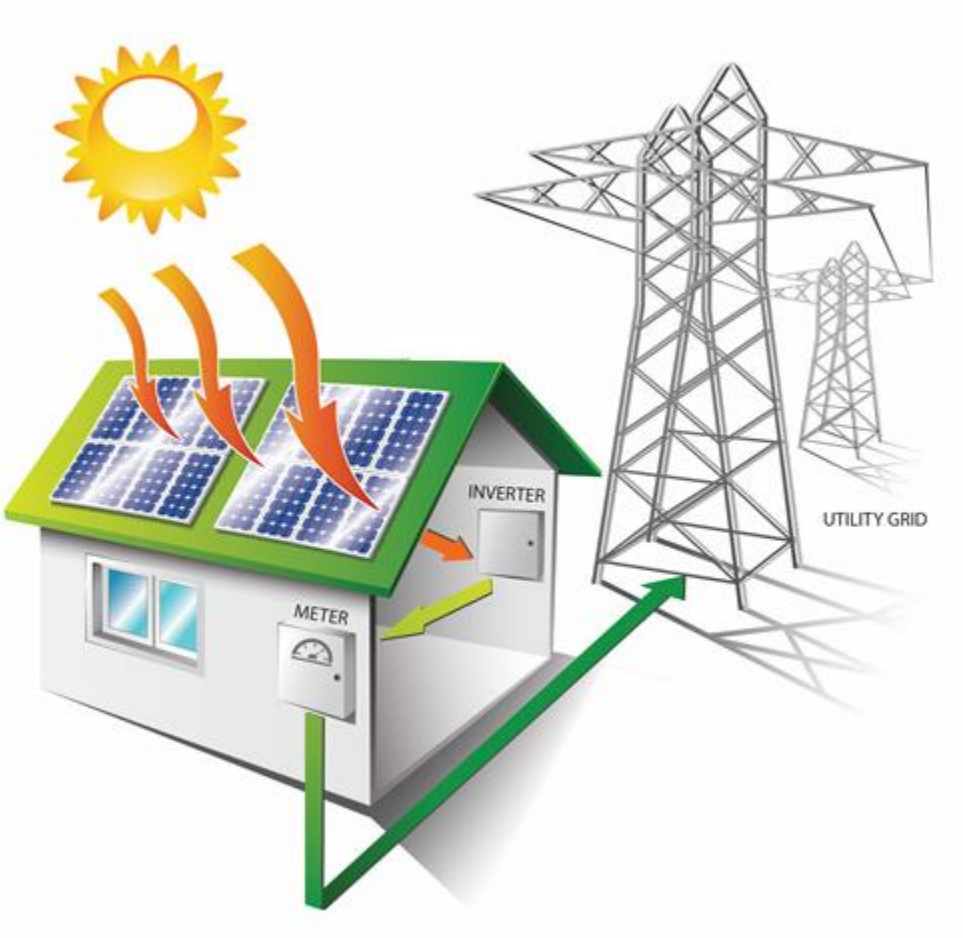

Figure 5-1. Grid-connected PV panel system installed on a small building (Big Dog Solar Energy 2016)

For this research, the boundary of the system of analysis is either the Large Office or Secondary School building. Crossing the system boundary are the electric power lines coming from the renewable generation source to the chillers and the power lines going to and from the utility system. While the renewable power generated could be utilized by the building in many other ways, the focus of this research is the magnitude and timing of the chiller's power profile relative to the demand experienced by the grid and the generation produced by the renewable resource. The approach to the sale of the excess renewable power is the conventional net metering approach whereby the excess power is sold to the grid at the retail electric rate.

5.2 Optimization Target Calculation for Parametric Studies

The optimization targets considered for the parametric studies are directly related to the two types of control strategies detailed in Section 3, *Renewable Control* and *Cost Control*. *Renewable Control* attempts to maximize the use of renewable energy being generated to operate the chillers whenever possible. In this case, the optimization target is the fraction of chiller electrical energy consumption met by renewable energy generation.

$$Chiller\ Energy\ Met\ by\ Renewable\ [-] = \frac{Renewable\ Utilized\ by\ Chiller\ [kWh]}{Total\ Chiller\ Energy\ [kWh]} \tag{41}$$

The *Cost Control* strategy aims to reduce the electricity cost by operating the chillers only when the off-peak electricity rates are in effect. The total 20-year cost is made up of the net present value of the electricity cost over 20 years and the capital costs. The capital costs include installed chiller systems, CTES systems, wind turbines, PV panels, and inverters. The sources and values for these costs are detailed in Section 2.6. While the *Cost Control* strategy aims to reduce the electricity cost, the lowest annual electricity cost does not always correspond with the lowest total 20-year cost. By varying the design parameters shown in Table 3-1, lower electricity costs can be achieved through, for example, larger storage capacities. This is because a larger storage capacity allows the chiller system to remain idle during the on-peak rate period more often since there is more storage available to meet the load. However, the additional storage may cost be more than the electricity cost savings. Selecting a range of parameter values and performing calculations for the total 20-year cost allows for the selection of the design that balances lowest capital cost with lowest operating cost to give the lowest total 20-year cost.

The net annual electricity cost calculation is dependent on the system boundary and net metering definition presented in Section 5.1. By way of example, a 24-hour period is displayed in

the eight plots shown in Figure 5-2. The four plots on the left are for the building with no thermal energy storage (referred to as the no-storage case) and those on the right are for the same building but with storage operating using the *Renewable Control* strategy. The top plot shows the chiller's power consumption as a negative value; note that the discontinuous jumps correspond to the transition between the operation of a single chiller and two chillers in parallel. The second plot shows the solar power output from a PV array rated at 250 kWe. The third, labeled "Net Utility Impact (kWe)," is the sum of the previous two plots and corresponds to the net production (positive) or demand (negative) experienced by the utility. In both the *Renewable Control* and no-storage case, the net impact close to the peak solar generation time of day is near zero. The differences between the two cases are easy to see during the afternoon when the larger size chiller system required for the no-storage case consumes significantly more power in order to directly meet the building's cooling load. The fourth plot shows how the net electricity value is computed by multiplying the time-of-use electricity rate by the net utility impact from the plot in the third row. The shaded area in this plot shows the peak rate portion of the day and the curve features an amplification of the value of the electricity from the third plot during this time period. At 3 p.m. and 8 p.m. (the 15th and 20th hour in the plots), there is a discontinuity in the electricity value due to the utility rate change. The net annual electricity cost is the integration of the net electricity value throughout the entire year.

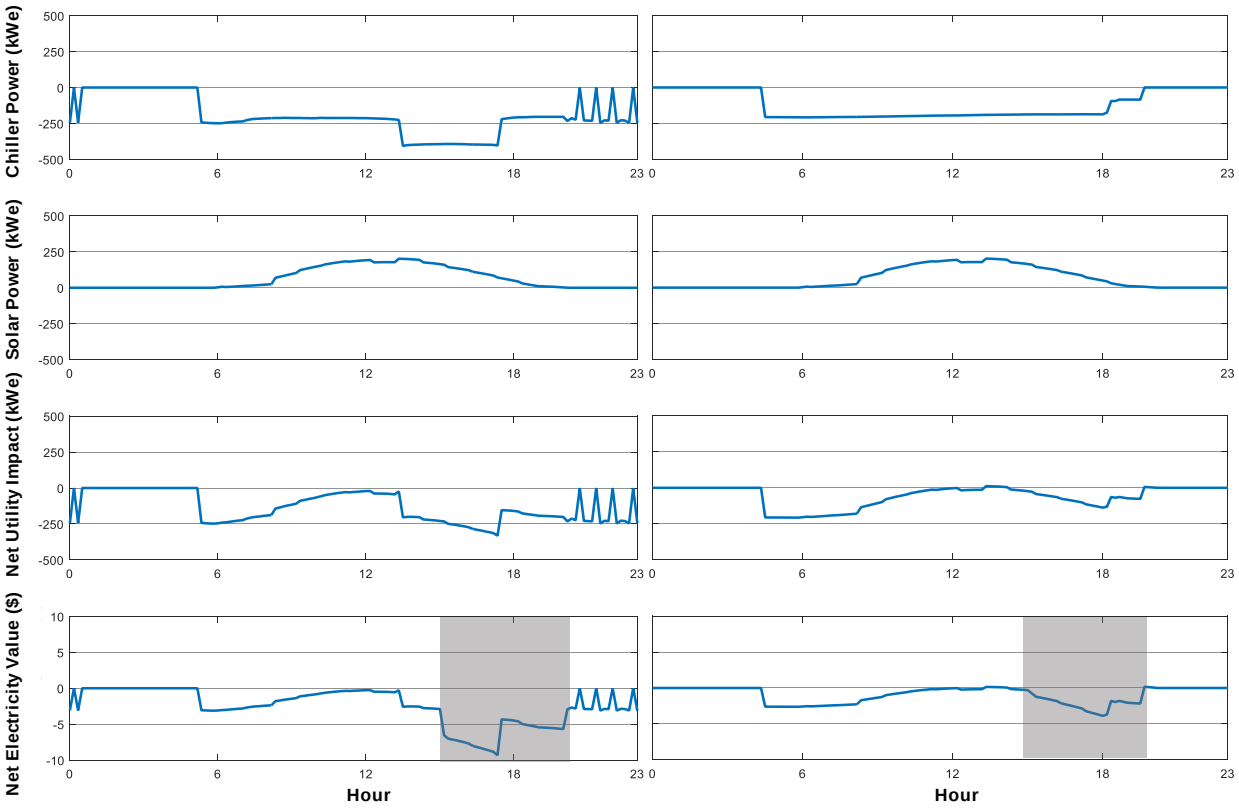

Figure 5-2. Net annual electricity calculation value for 250 kWe of PV capacity for no-storage (left) and with storage operating using *Renewable Control* (right), shaded region shows peak time-of-use rates

5.3 Parametric Study Results

Because there are two targets or objectives being considered in this parametric study, the optimization is multi-objective. A single solution that optimizes both the chiller energy met by renewable and the total 20-year cost does not exist. In addition to being multi-objective, there are many independent parameters (listed in Table 3-1) that can be adjusted in the course of optimization. The multiple objectives and large number of system variables increase the computational intensity of performing a multi-objective optimization. Parametric studies are employed in the multi-objective portion of this research rather than using multi-objective optimization methods. The results of the parametric studies are used to generate Pareto fronts, as

discussed in the subsequent section. Results for model predictive control with a single optimization objective are presented in Section 5.4.

5.3.1 The Pareto Front Concept

A parametric study that varies all of the independent variables shown in Table 3-1 over their range of possible values is carried out. The objective of the parametric study is to identify optimum parameter sets based on the two metrics previously discussed. One method of graphically displaying trade-offs in multi-objective optimizations is by the use of a Pareto front (Stadler 1988). A simple example of the Pareto front concept is shown in Figure 5-3 where many points corresponding to trials in the parametric study are plotted in the two dimensions corresponding to the values of the metrics associated with each point (referred to as Objective 1 and Objective 2). In this example, I am trying to minimize each of these objective functions and therefore better results are closer to the origin. Each of the green points indicates a feasible result for various combinations of values across the parameter space. The yellow point is a result that is infeasible, there is no combination of parameter values that will result in these objective values. The solid red line then maps a series of variable combinations that lie on the edge of what is feasible and infeasible. This line is referred to as a Pareto front and contains the set of solutions that are non-dominated. Non-dominated means that neither of the objective functions can be improved without degrading the other. The Pareto front is useful in that it indicates the set of solutions that should be considered. Barring some other constraint, there is no reason to pick a solution that lies inside the Pareto front as at least one objective function can be improved by moving to the Pareto front.

The plot on the right in Figure 5-3 shows a modification to the general Pareto front concept that is used for this research. The two objectives considered are the total 20-year cost and the fraction of the chiller energy met by renewable. The optimization seeks to minimize the total

life-cycle cost but it seeks to maximize the chiller energy met by renewable and therefore solutions that lie to the left and up are more optimal. The format of the Pareto front has been modified such that the Pareto front lies on the feasible points that maximize the chiller energy met by the renewable resource and minimize the total 20-year cost.

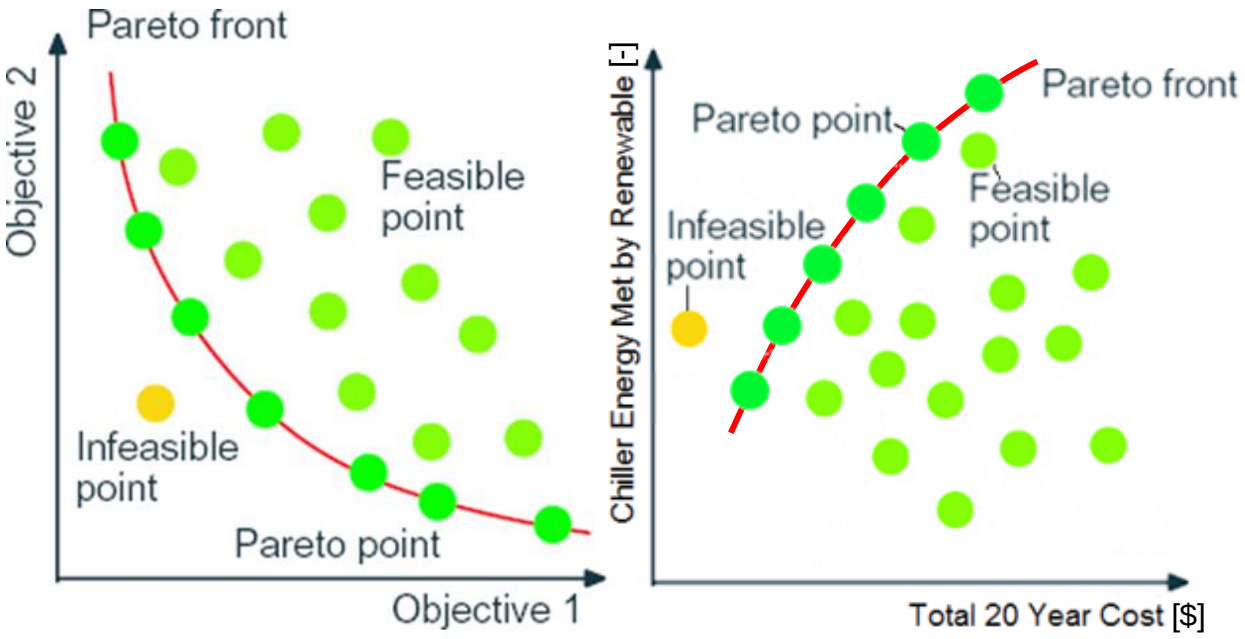

Figure 5-3. General Pareto front concept (left) and Pareto front specific to this research (right)

Figure 5-4 shows an example of the Pareto front developed using simulation results from this research for the Secondary school in California with wind as the installed renewable energy resource and ice as the cool thermal energy storage medium. The ordinate represents the fraction of chiller electrical energy met by renewable energy sources while the abscissa represents the total 20-year cost with storage and renewables normalized to the same cost for the no-storage system without renewables.

Each point on the plot represents a single simulation run using a different set of design parameters in Table 3-1. All of the points consider the wind resource with a generation capacity

that is equal to the no-storage full-load chiller capacity. The specific points that map the Pareto front have the highest chiller electrical energy met by wind generation for a particular cost.

The results with the lowest portion of chiller energy met by wind and the lowest cost, close to point (1), are all associated with operating using the *Cost Control* strategy. Not surprisingly, these lowest-cost systems all have a storage recharge hour around 2 p.m. which is just before the onset of the on-peak electricity rate period. They also have low capital costs and use the minimum possible size storage and chiller systems. The minimum part-load ratio for these systems varies between 0.3 and 0.5 due to the ice CTES charging behavior. Because the thermal storage system charging rate is limited as the ice CTES system approaches a full state-of-charge, allowing the chillers to operate at low part-load ratios means that the storage system will be able to accept the charge more often which results in greater utilization of the renewable power.

The jump from point (1) to (2) occurs as a result of a transition to operating using the *Renewable Control* strategy. The chiller and storage sizes are still at their minimums and the chiller minimum operating part-load ratio is 0.5. Because the wind resource at this location tends to be strong at night, the recharge hour moves towards 8 a.m. which allows for the storage to recharge without any requirement for a building cooling load to be met.

Moving from point (2) to (3), the storage capacity is increasing while all other parameters remain constant. From (3) to (4), the chiller capacity is also increasing. These two segments of the Pareto front show that the effect of increasing equipment size and the associated capital cost provides diminishing returns with respect to the utilization of the renewable resource. At point (4), there is a discontinuity in the Pareto front where the chiller minimum part-load ratio constraint jumps from 0.5 to 1 and both the storage and chiller sizes return to their minimums. This shift occurs when the chiller energy reduction that arises from operating only at full-load outweighs the

gains in the chiller energy met by wind that come from allowing operation at low part-load ratios along with increasing equipment sizes. In the transition from (4) to (5), the storage capacity begins to increase once again which allows the building's chilling system to achieve a greater fraction of chiller system energy met by wind energy but it comes at an increased 20-year cost.

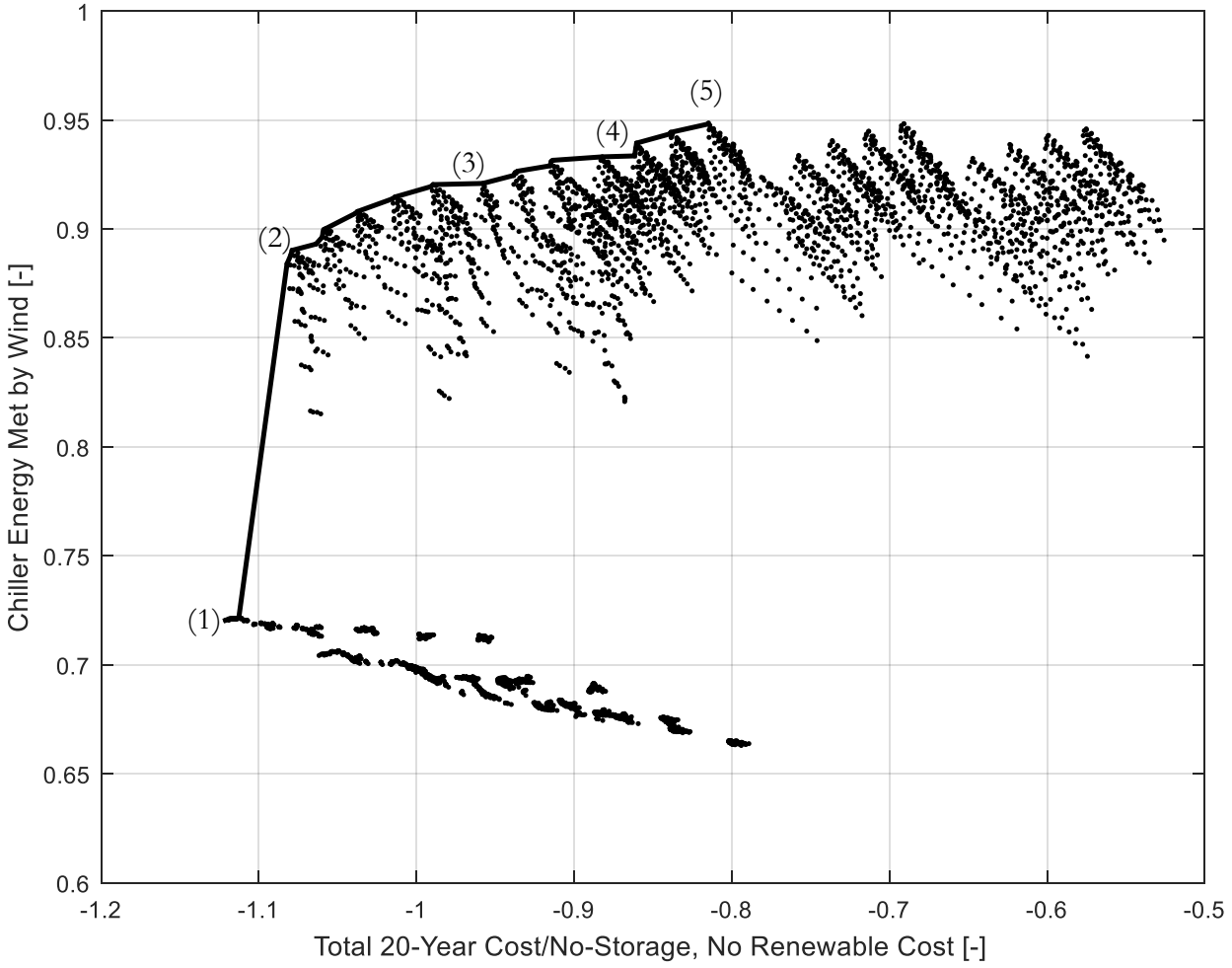

Figure 5-4. Pareto front development example for wind with generation capacity equal to the no-storage full-load chiller power

5.3.2 Results for Direct Chiller Systems without Storage

The 20-year total cost for the no-storage case and the associated chiller energy met by renewable results provide a useful comparison to the *Renewable Control* and *Cost Control* results. The cost result for no-storage without any renewable capacity available is used to normalize all of the other results. The no-storage system results are shown in Table 5-1 for four levels of renewable energy capacity. Each one is a multiple of the no-storage full-load chiller power for that particular location. For the wind resource in particular, the 20-year cost becomes increasingly negative as more renewable capacity is considered. This negative cost is indicative of positive revenue coming from wind generation in excess of the chiller system electric consumption.

Table 5-1. No-storage system results for varying levels of renewable capacity based on the no-storage full-load chiller power

		Wind				**Solar**			
		Secondary School		**Large Office**		**Secondary School**		**Large Office**	
Location	**Renewable Capacity Multiplier**	Total 20-Year Cost [$MM]	Chiller Energy Met by Wind [-]	Total 20-Year Cost [$MM]	Chiller Energy Met by Wind [-]	Total 20-Year Cost [$MM]	Chiller Energy Met by Solar [-]	Total 20-Year Cost [$MM]	Chiller Energy Met by Solar [-]
Texas	0	1.10	-	3.34	-	1.10	-	3.34	-
	1	-1.42	0.66	-1.47	0.58	0.92	0.67	3.00	0.55
	2	-3.94	0.77	-6.29	0.71	0.75	0.77	2.67	0.70
	4	-8.99	0.83	-15.92	0.80	0.40	0.82	2.00	0.77
California	0	1.14	-	4.83	-	1.14	-	4.83	-
	1	-0.76	0.65	-0.44	0.61	1.09	0.70	4.69	0.52
	2	-2.66	0.72	-5.71	0.69	1.04	0.78	4.54	0.64
	4	-6.46	0.76	-16.24	0.75	0.94	0.82	4.26	0.71
Wisconsin	0	0.79	-	2.77	-	0.79	-	2.77	-
	1	-1.14	0.53	-1.89	0.49	1.05	0.59	3.39	0.50
	2	-3.08	0.64	-6.55	0.62	1.31	0.75	4.01	0.67
	4	-6.95	0.72	-15.87	0.72	1.82	0.83	5.25	0.77
New York	0	1.22	-	6.13	-	1.22	-	6.13	-
	1	-1.53	0.60	-0.06	0.60	1.48	0.53	6.73	0.35
	2	-4.28	0.72	-6.26	0.73	1.74	0.66	7.32	0.48
	4	-9.78	0.79	-18.64	0.81	2.27	0.73	8.51	0.57

5.3.3 Results for Secondary School with Chilled Water CTES

Sections 5.3.3 through 5.3.6 provide CTES Pareto front results for all four combinations of building and storage type, Secondary Schools and Large Office buildings with both chilled water and ice CTES. Each set of curves is presented for solar and wind generation capacity at three different levels – one, two and four times the full-load chiller power required for the no-storage chilling system. Additionally, each plot contains individual points for the no-storage case at the various renewable generation levels as points of comparison. In each plot, the total 20-year cost is normalized by the 20-year cost for a direct chiller system without any renewable generation capacity installed. The cost is normalized by a value representative of the peak and integrated cooling load for the particular location so that variations by location are functions of the renewable resource.

Figure 5-5 shows the resulting Pareto fronts for the Secondary School with chilled water CTES and solar as the renewable generation resource. For each Pareto front, the lowest cost points are associated with the *Cost Control* strategy. These points show a marked difference among the locations with greater and lesser solar resource. For Texas and California, installing greater levels of PV capacity decreases the 20-year cost while the opposite is true for Wisconsin and New York. This behavior is due to the relatively low levels of solar irradiance in Wisconsin and New York compared to Texas and California. The single points representing the no-storage case show greater 20-year cost compared to the *Cost Control* values at the same level of solar PV capacity, but they result in a greater fraction of the chiller energy consumption being met by the solar resource when compared to the lowest operating cost cases with storage. This behavior is attributable to some overlap between the solar resource and coincident building cooling loads. The *Cost Control* strategy foregoes operating the chillers during on-peak hours (which start at 3 p.m.) and, during

this period, the solar resource is still significant. Due to the onset of the on-peak hours, the optimum recharge hour for the *Cost Control* strategy is 2 p.m.

Similar to the line between points (1) and (2) in Figure 5-4, each curve displays a near vertical increase in chiller energy met by solar. The point at the top of this sharp increase marks the transition to *Renewable Control* operation. Not surprisingly, each of these points is above the corresponding no-storage point in terms of the chiller energy being met by the solar resource because the *Renewable Control* strategy specifically emphasizes maximizing the utilization of renewable energy generation. Increasing gains in solar utilization are realized with little increase in cost as the minimum chiller plant part-load ratio is reduced. The 20-year cost increases slightly in this case because the cooling load is met by a chiller system that is operating less efficiently on average, but the chiller energy met by solar increases because a lower level of solar irradiance is sufficient to trigger chiller operation. Even though more total electricity is being consumed to meet the same cooling load, a larger fraction of the consumed electricity comes from the solar resource. This trend holds until the minimum chiller plant part-load ratio reaches a low of 0.5 because beyond this point, the increase in 20-year cost outweighs the solar utilization benefit. At this point, the tank recharge hour is approximately 2 p.m. due to a combination of the solar resource being nearly at its peak at that time and a desire to have fully-charged storage going in to the peak cooling loads in the afternoon. Both the tank and chiller capacities are at their minimum size from the partial storage strategy sizing. This particular point can be identified as an inflection point or knee in each Pareto front curve. Each of the Pareto fronts in this and the following sections exhibit a similar behavior and the corresponding knee or inflection point represents the set of operating parameters that enables a significant increase in renewable utilization with only a minor increase in the 20-year cost. The *Renewable Control* points with increasing costs involve increasingly larger

tank and chiller capacities. While the utilization of the solar resource improves, the increased 20-year cost may not justify the oversizing of the equipment.

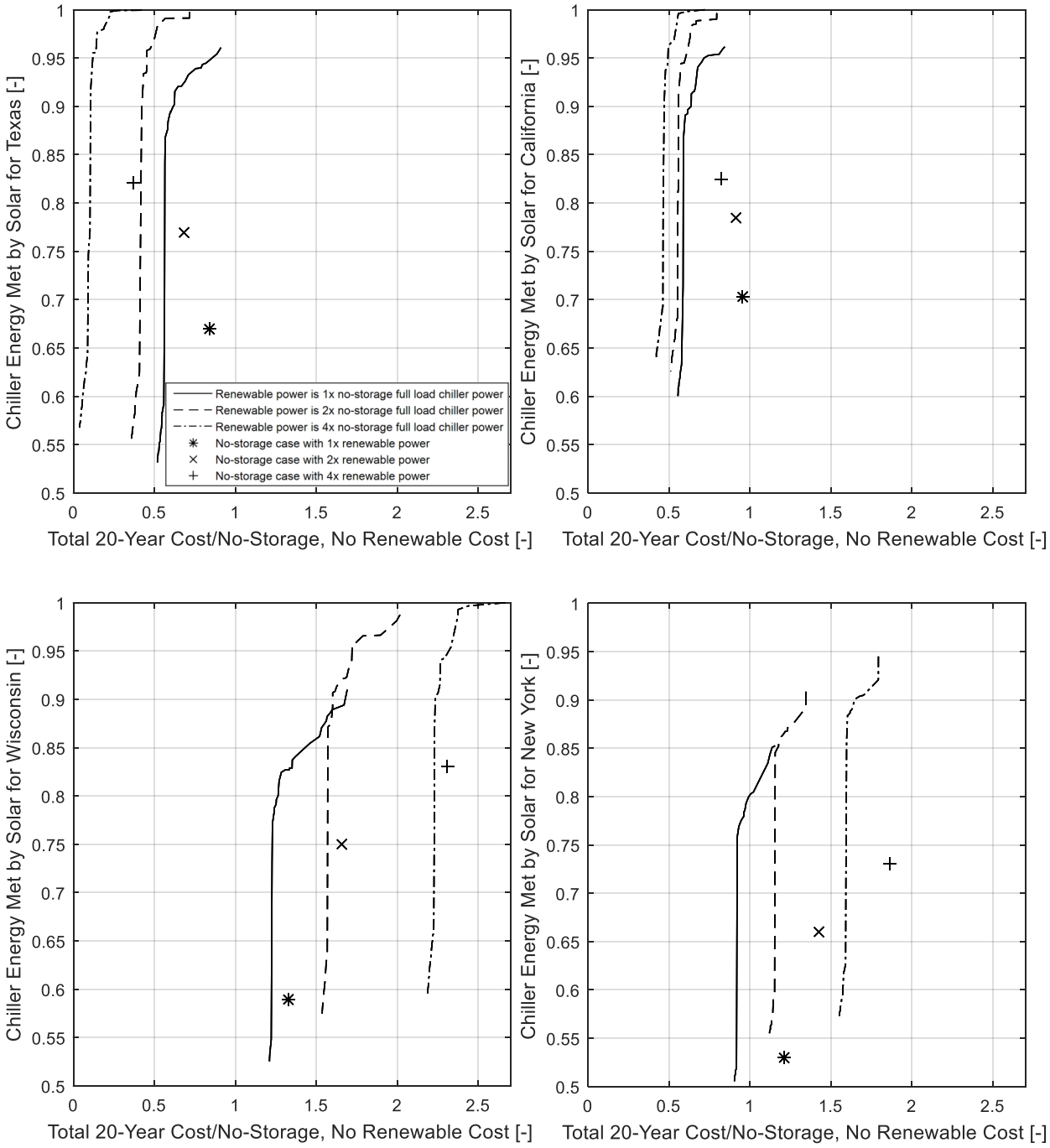

Figure 5-5. Solar resource Pareto fronts for the Secondary School with chilled water CTES for Texas (upper left), California (upper right), Wisconsin (lower left), and New York (lower right)

The Pareto fronts displayed in Figure 5-6 show the results of the parametric study for the Secondary School with stratified chilled water CTES and wind as the renewable resource. One significant distinction between these Pareto fronts and those for the solar resource in Figure 5-5 is that the 20-year costs are negative for each location. The negative cost indicates that revenue is being generated and this is true for all of the storage and no-storage cases. The cost difference between solar and wind is attributed to higher capacity factors for wind compared to solar in all four locations as well as the lower capital costs for wind turbines compared to photovoltaic panels. Another notable difference is that all of the storage strategy points utilize the wind resource more effectively than the no-storage points. Because the wind resource tends to be stronger at night and the *Cost Control* strategy will idle the chillers between 3 p.m. and 8 p.m., this strategy allows a greater fraction of the chiller's energy to be met by wind generation compared to the no-storage case when the chillers use the most energy in the middle of the day. The optimum tank recharge hour for the wind resource is approximately 8 a.m. because the chillers benefit by utilizing the strong nighttime wind resource to charge before the beginning of the cooling day.

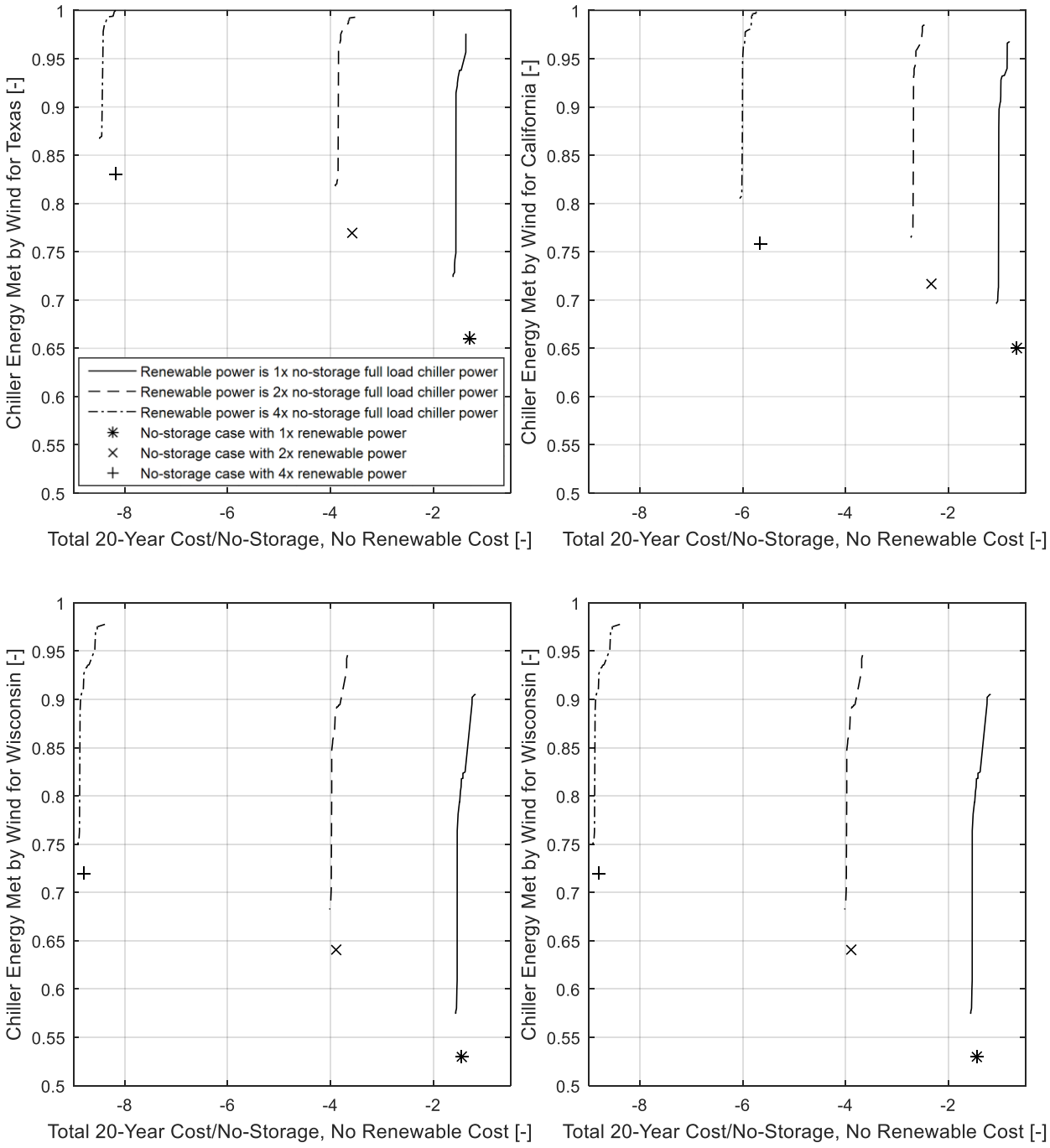

Figure 5-6. Wind resource Pareto fronts for the Secondary School with chilled water CTES for Texas (upper left), California (upper right), Wisconsin (lower left), and New York (lower right)

5.3.4 Results for Large Office Building with Chilled Water CTES

Figure 5-7 and Figure 5-8 show the Pareto fronts for the Large Office building with chilled water CTES for the solar and wind resource, respectively. The patterns seen in these Pareto fronts are very similar to those seen in the Pareto fronts for the Secondary School with stratified chilled water CTES displayed in Section 5.3.3. This indicates that, after normalizing the results by a value that is indicative of the building cooling load as well as the geographic location, the no-storage and no renewable 20-year cost, the results can be applied to different types of buildings. These two buildings have a similar occupancy schedule as shown in Figure 1-9 and the same electricity rate structure for each location. Buildings which vary these two profiles would result in a different set of Pareto fronts. One example of this difference is presented in Section 5.3.7. This example uses a different electricity rate structure that includes demand charges in addition to energy charges.

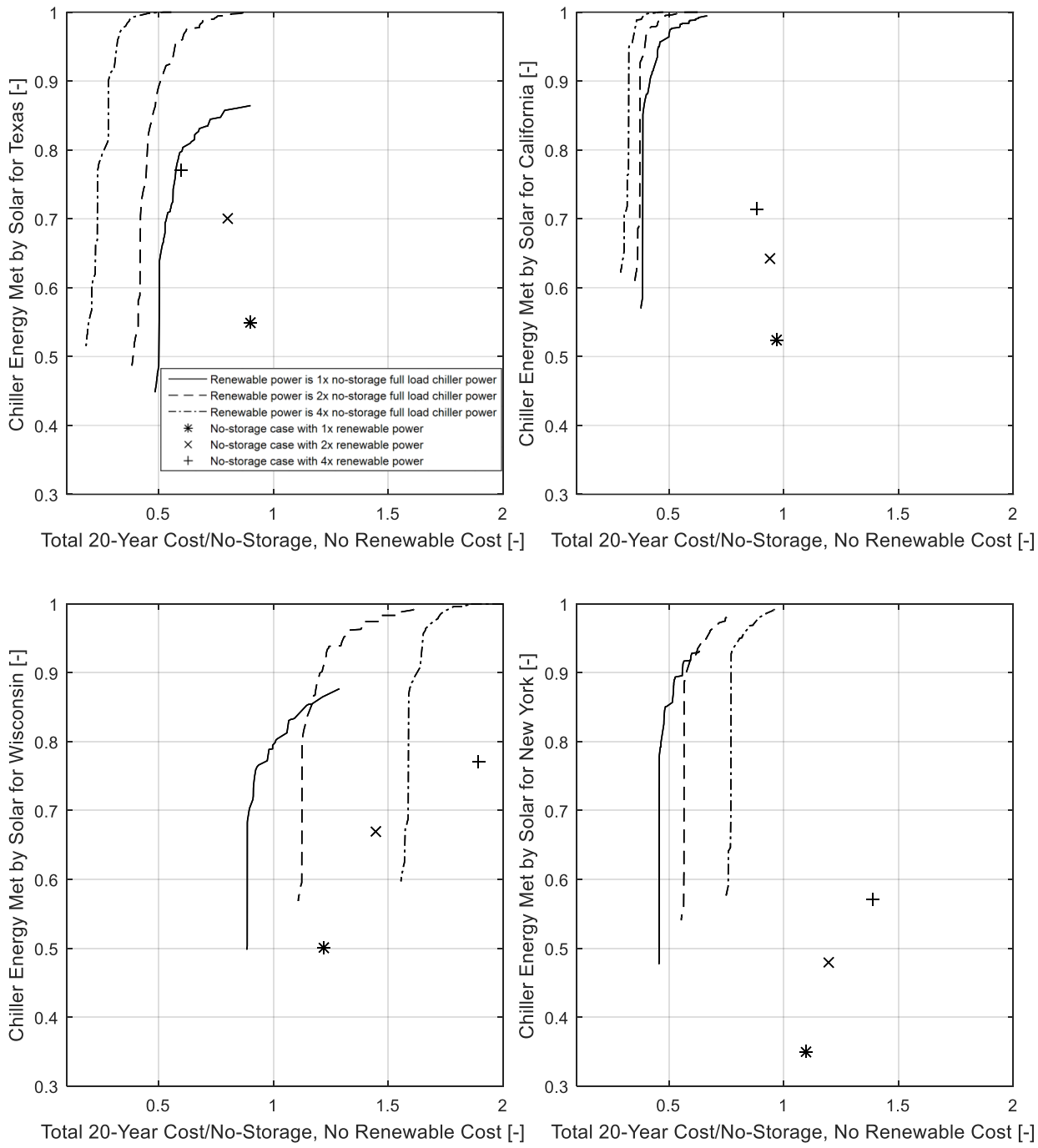

Figure 5-7. Solar resource Pareto fronts for the Large Office with chilled water CTES for Texas (upper left), California (upper right), Wisconsin (lower left), and New York (lower right)

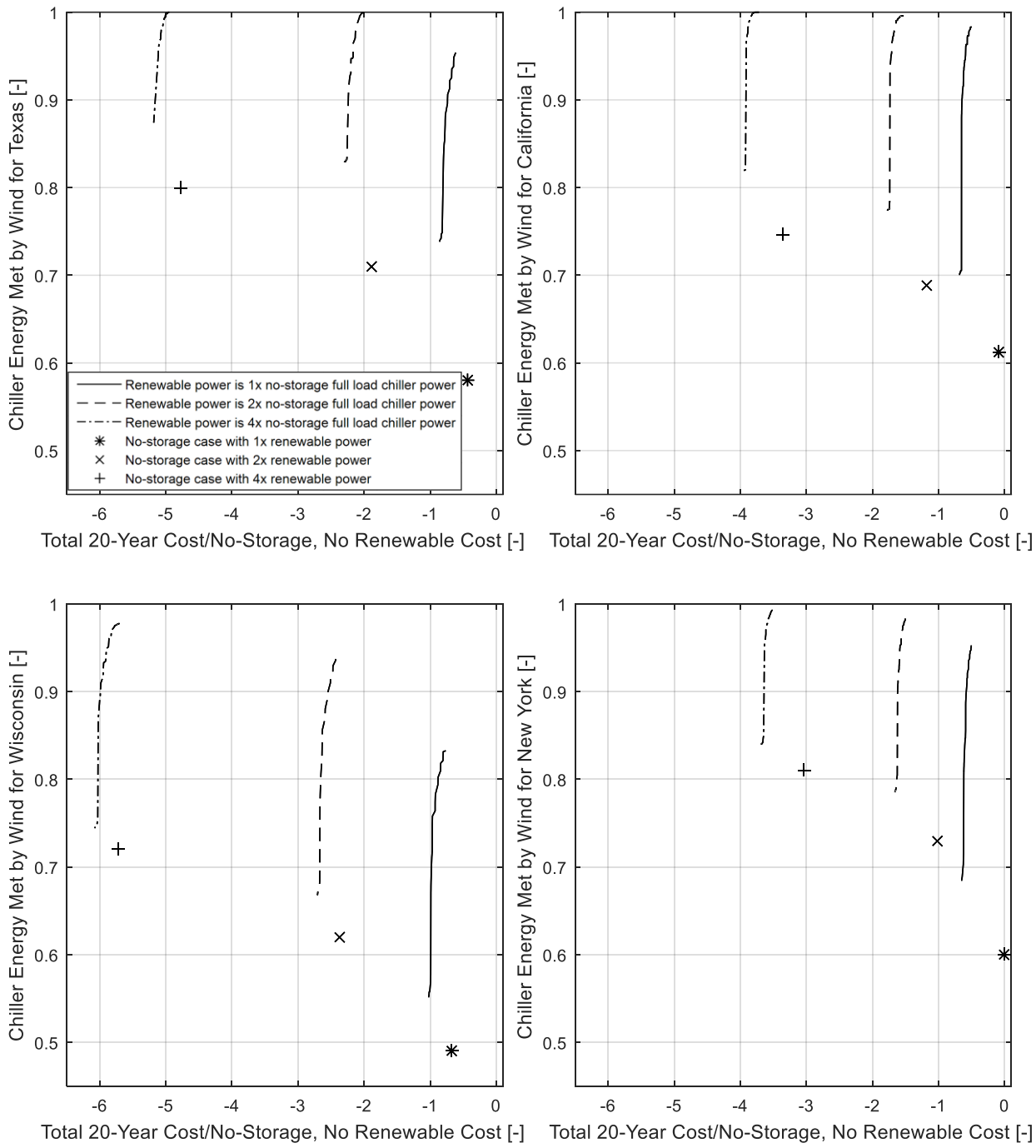

Figure 5-8. Wind resource Pareto fronts for the Large Office with chilled water CTES for Texas (upper left), California (upper right), Wisconsin (lower left), and New York (lower right)

5.3.5 Results for Secondary School with Ice CTES

The Pareto fronts in Figure 5-9 and Figure 5-10 show the results for Secondary Schools with ice CTES systems for the solar and wind resource, respectively. As explained in Section 5.3.1, the minimum chiller system part-load ratio is generally lower along the Pareto front for ice CTES than it is for chilled water CTES. The reason for this difference is due to the fixed glycol temperature set point during charging of the storage system as well as the storage system charge rate characteristics shown in Figure 2-13. When the ice CTES system approaches its full state-of-charge, the charge rate it can accept decreases. If the chillers are able to operate at low part-load ratios, the storage system will be able to accept the charge during more time-steps and a greater fraction of the overall cooling load will be met by renewable power.

Comparing the ice CTES results with the stratified chilled water results in Figure 5-5 and Figure 5-6, there are several similarities and differences. The storage tank recharge hours of approximately 2 p.m. for the solar resource and 8 a.m. for the wind resource are unchanged for the ice CTES case. These recharge hours are primarily a function of the renewable resource profile. While the inflection points or knees of each Pareto front curve occur at similar values of chiller energy met by renewable power, the ice CTES curves do not come as close to meeting 100% of the chiller energy with renewable even as the equipment sizes and renewable generation capacity are increased. This is partially due to the storage system's charging and discharging rate characteristic. When the peak cooling periods occur in the summer and storage begins to discharge, the available storage system discharge rate declines. The chiller system must operate to meet the remaining cooling load if the storage system discharge rate is less than the building cooling load whether renewable power is available or not. Also, the 20-year cost for the ice CTES systems is

slightly lower than for the equivalent stratified chilled water systems. This economic benefit is due, partially, to ice CTES system costs being lower than chilled water systems in this size range.

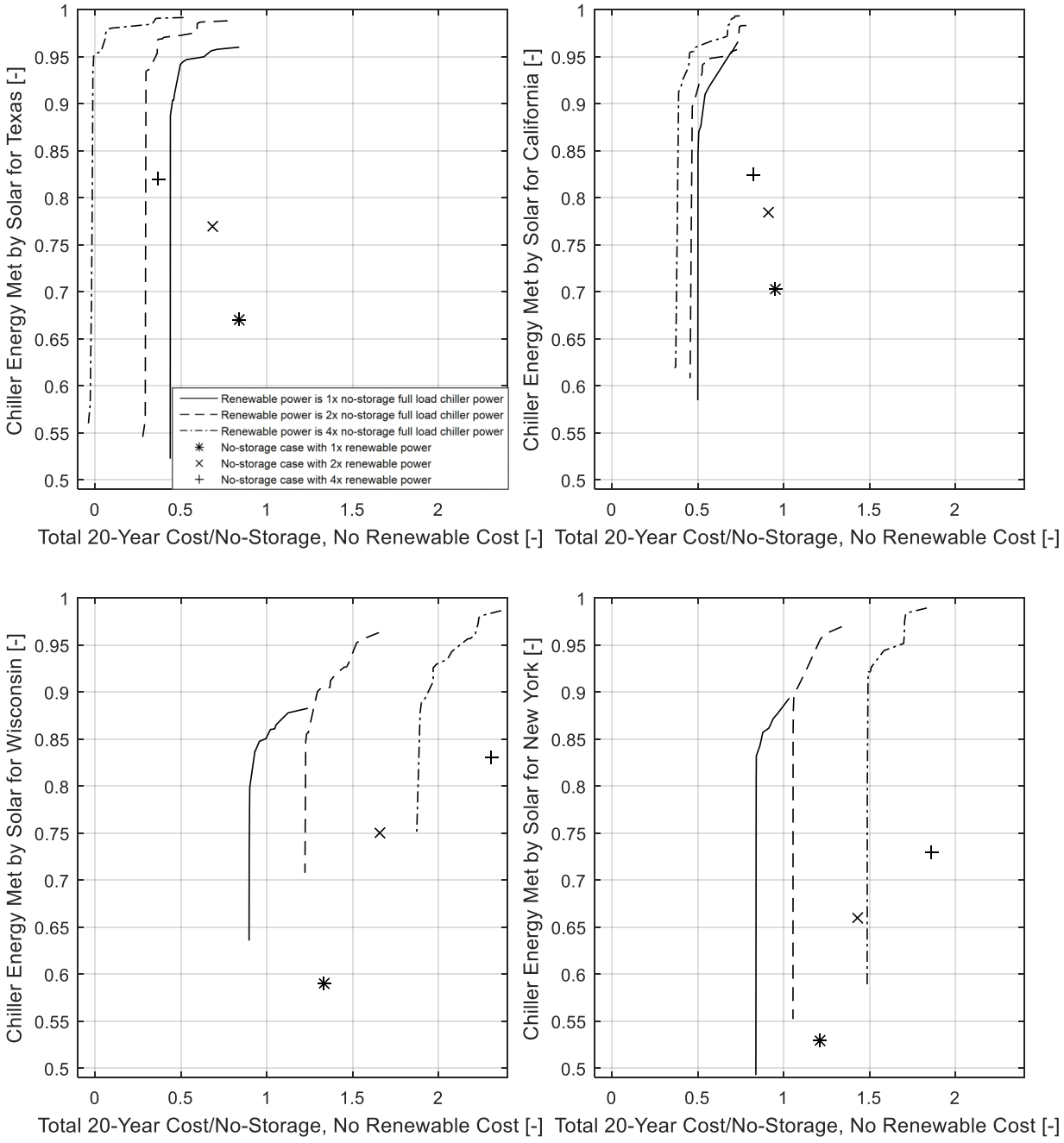

Figure 5-9. Solar resource Pareto fronts for the Secondary School with ice CTES for Texas (upper left), California (upper right), Wisconsin (lower left), and New York (lower right)

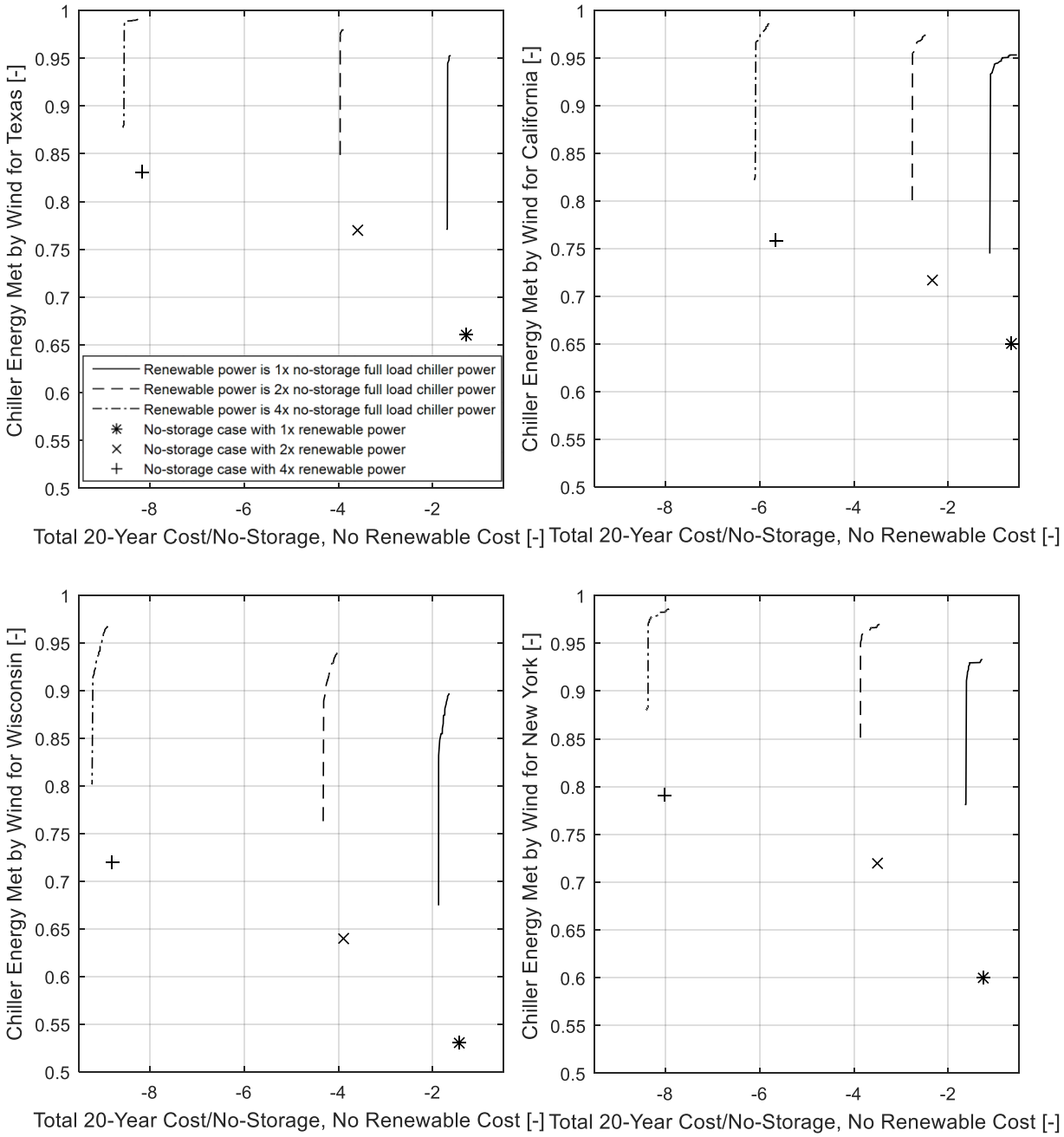

Figure 5-10. Wind resource Pareto fronts for the Secondary School with ice CTES for Texas (upper left), California (upper right), Wisconsin (lower left), and New York (lower right)

5.3.6 Results for Large Office Building with Ice CTES

The Pareto front results for the Large Office building with an ice CTES system are displayed for the solar resource in Figure 5-11 and for the wind resource in Figure 5-12. The differences between these results and those for the Large Office building with stratified chilled water CTES are similar to those between the ice CTES and chilled water CTES cases for the Secondary School. Once again, the minimum chiller system part-load ratio is lower for the ice CTES system than for chilled water. The ice CTES curves are not as close to meeting 100% of the chiller energy with renewable power as the chilled water curves.

One expected difference between the Large Office building and the Secondary School with respect to the variation between the two storage technologies is that the ice CTES system 20-year cost is generally higher than for the chilled water system. Since the Large Office building has over twice as much square footage as the Secondary School, it benefits from the increasing economies of scale associated with the chilled water system.

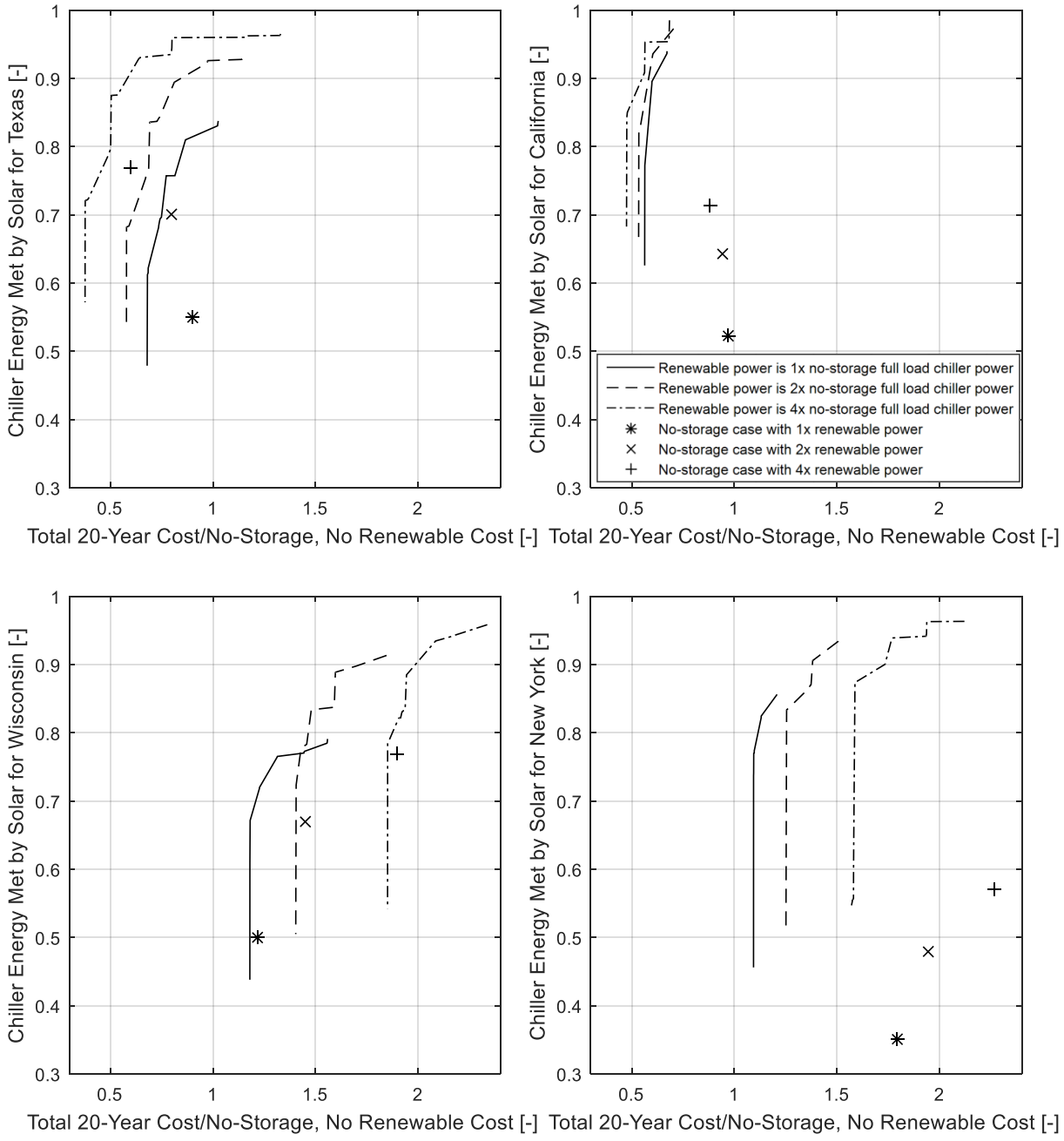

Figure 5-11. Solar resource Pareto fronts for the Large Office with ice CTES for Texas (upper left), California (upper right), Wisconsin (lower left), and New York (lower right)

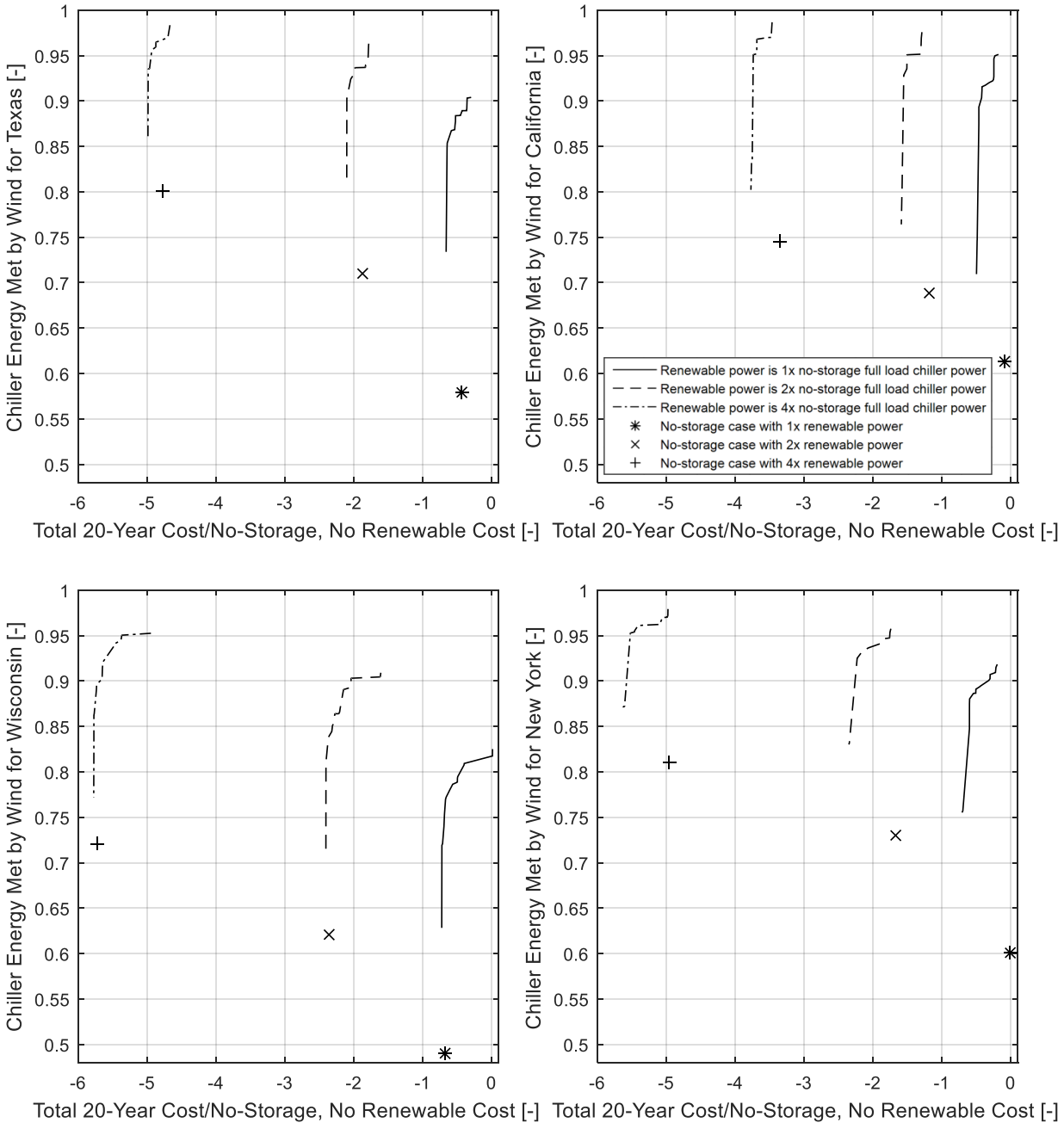

Figure 5-12. Wind resource Pareto fronts for the Large Office with ice CTES for Texas (upper left), California (upper right), Wisconsin (lower left), and New York (lower right)

5.3.7 Results for Large Office Building with Ice CTES and Demand Charges

For comparison purposes, the Large Office building with an ice CTES system is simulated with an additional electricity rate structure. This rate structure was introduced in Section 2.6.2 and it features a time-of-day dependent energy charge and seasonally-varying demand charges. The energy rates are significantly lower than either the on-peak or off-peak rates used in all of the results presented so far. The demand charge analysis is performed only for New York.

For purposes of comparison, the 20-year cost results are not normalized since the two different rate structures result in two different normalizing costs. The Pareto front results for both sets of electricity rate structures are shown in Figure 5-13. The Pareto fronts on the left include energy charges only and are similar to the lower right plots in Figure 5-11 and Figure 5-12 except that the 20-year cost values are not normalized by the no-storage case with no renewable generation. Comparing the two plots in the top row and the two plots in the bottom row with each other, each renewable resource simulated with the two different electricity rates, it is clear that the rate with demand charges produces much higher 20-year costs. The primary reason for this cost difference is the magnitude of the electricity cost difference between a generally applied rate which is close to the US average and a rate that is applicable only to New York City. Another impact is the differing effects of net metering between the two electricity rates. With energy charges only, all renewable energy produced offsets the energy charge alone, but this is not the case with demand charges. Because there is typically at least one time-step in each month where the chiller system is operating at full load, but the renewable power output is close to zero, the renewable offset is not as great when demand charges are considered.

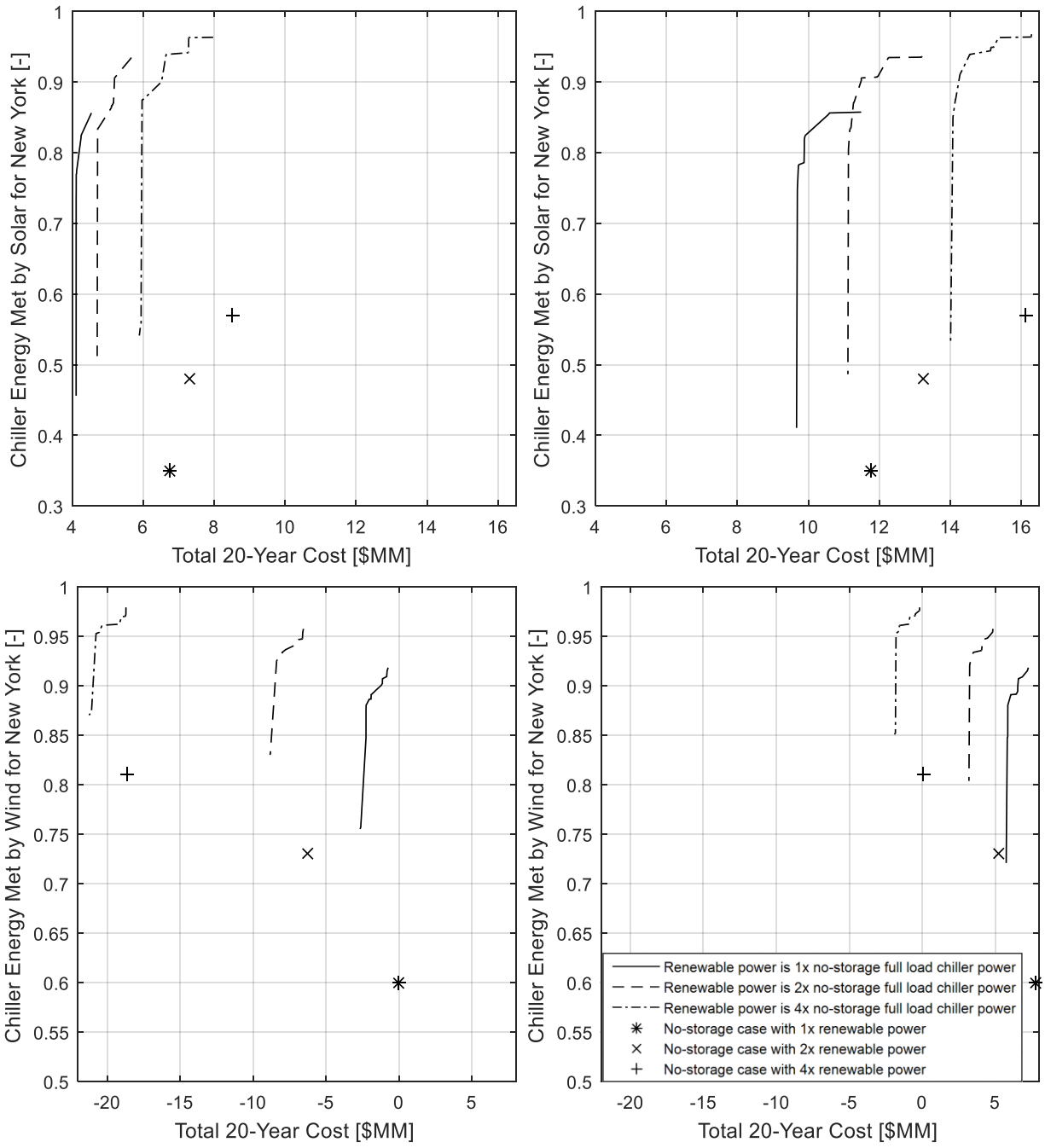

Figure 5-13. Solar (top) and wind (bottom) resource Pareto fronts for New York with energy charges only (left) and energy as well as demand charges (right)

5.3.8 Results for Large Office Building with Wind and Solar in Combination

While this research considers the increasing deployment of renewable energy generation in the forms of solar and wind energy, thus far they have been studied independently of each other. The wind and solar resource profiles are plotted in

Figure 2-1 and Figure 2-5. The solar resource profile obviously peaks close to the middle of the day and is non-existent before sunrise and after sunset. While the wind profile is more variable, for land-based turbines the resource is generally stronger at night than in the middle of the day (Hartman 2017). Since the profiles are approximately time shifted from one another, the addition of the two results in a more uniform renewable generation profile over each day. The more varied profiles used while considering each resource separately represent the extremes of only one resource or the other being utilized. Figure 5-14 shows an example week in the Texas region. The data used are from the month of July and the three scenarios plotted are the power output from 1 MWe of installed wind capacity, 1 MWe of installed solar capacity, and 500 kWe of each. Although the wind power output is incredibly variable, on the first, second, fifth, sixth, and seventh days, the strongest periods of wind power generation are clearly offset from the strongest solar power periods in the middle of the day. The thick, solid line, the profile of the combination of the two resources, still shows considerable variability throughout the week, but it is noticeably more uniform with lower peaks and far fewer periods of zero power output (5% of the time versus 20% for wind alone and 43% for solar alone).

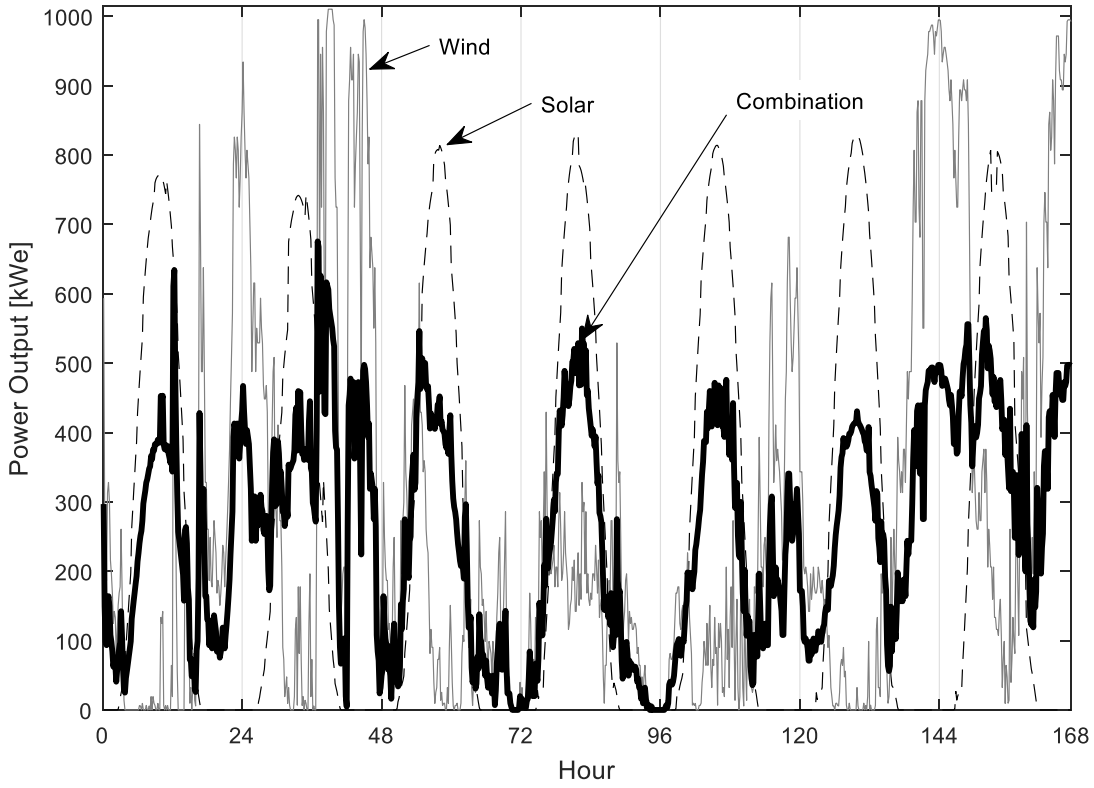

Figure 5-14. Texas week in July showing 1 MWe of installed wind and solar capacity along with a combination of 500 kWe of each

The results in this section focus on the Texas and California regions and the solar and wind combination is based on an even split between the two resources on the basis of installed capacity. The first two sets of plots are duplicates of those in previous sections, but they are presented here on consistent axes for purposes of comparison. Figure 5-15 shows the Pareto fronts for the solar resource, Figure 5-16 shows those for the wind resource, and Figure 5-17 shows the combination of the two resources.

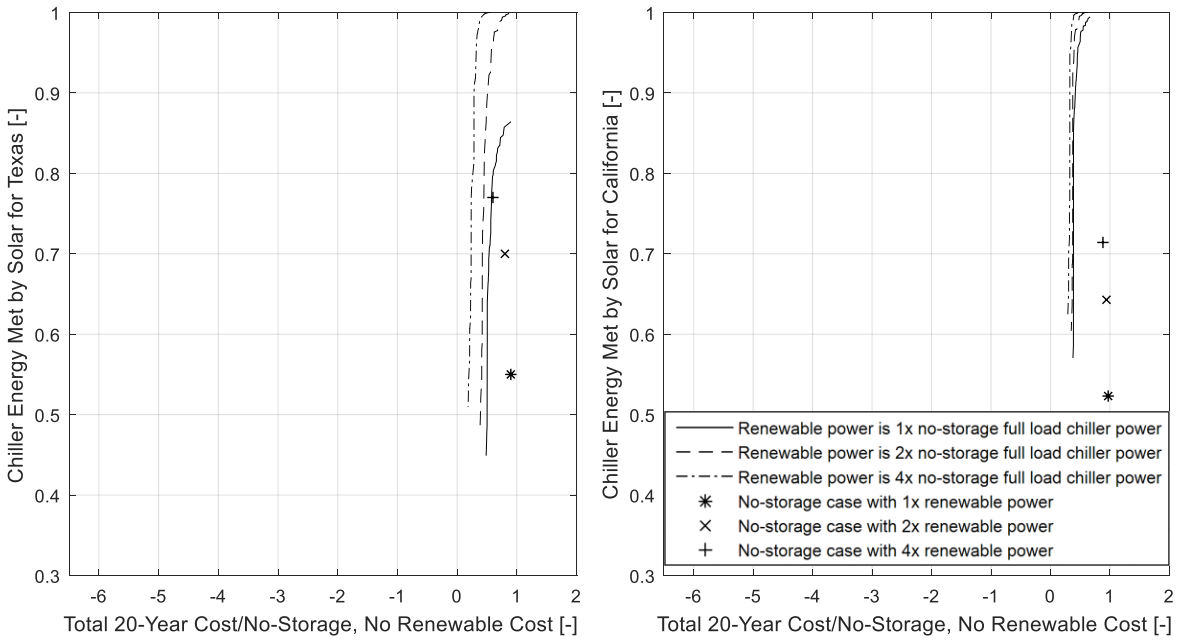

Figure 5-15. Solar resource Pareto fronts for the Large Office with chilled water CTES for Texas (left) and California (right)

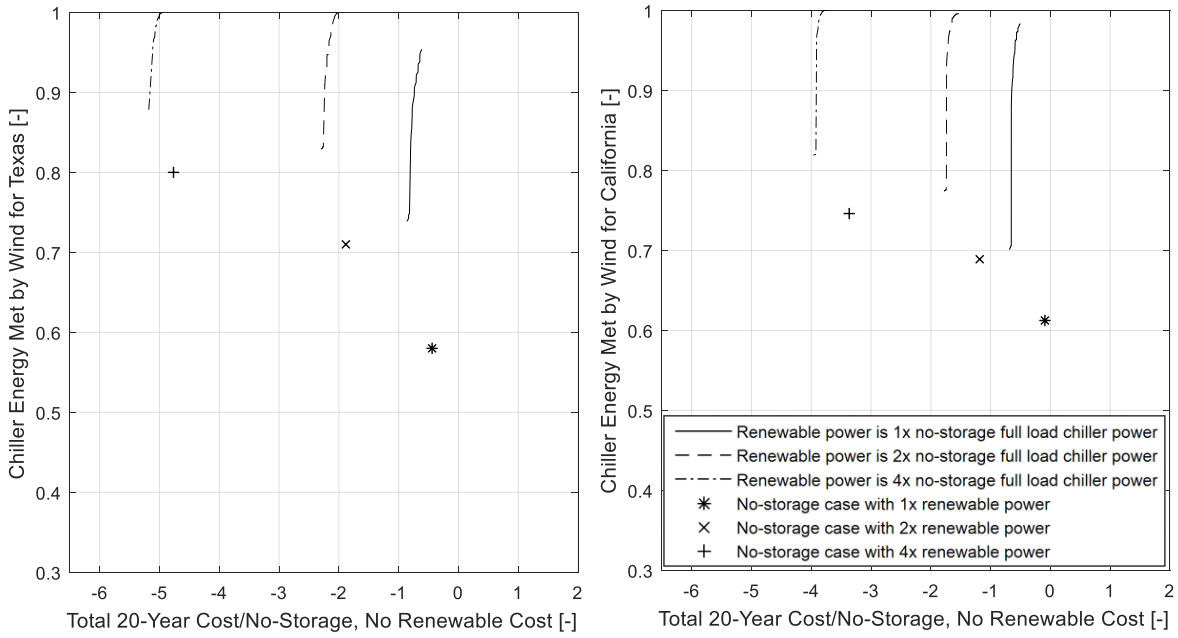

Figure 5-16. Wind resource Pareto fronts for the Large Office with chilled water CTES for Texas (left) and California (right)

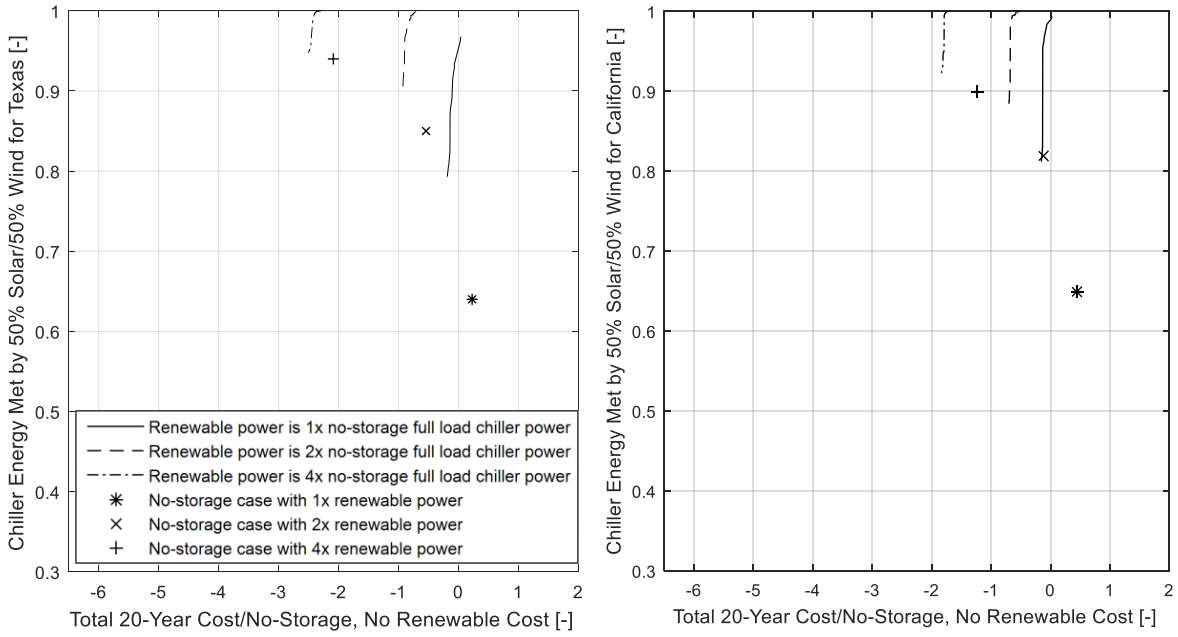

Figure 5-17. Combination solar and wind resource Pareto fronts for the Large Office with chilled water CTES for Texas (left) and California (right)

Looking at the individual plots in comparison to each other, there are some notable differences between the two locations. Note that each figure shows Texas on the left and California on the right. Figure 5-15 shows that a CTES system in California operating in conjunction with the solar resource meets more of the chilling system's energy consumption at a slightly lower life-cycle cost than is possible with the same combination in Texas. This result occurs because the solar resource in California is greater than for Texas. Figure 5-16 shows that the life-cycle cost is lower in Texas than in California when a CTES system is operated in conjunction with the wind resource, which is due to a stronger wind resource in the Texas data set. Finally, the case corresponding to 50% solar generation and 50% wind generation (by installed capacity) in Figure 5-17 shows that a greater portion of the chilling system's energy is met by the renewable resource in the combined no-storage case as compared to the solar or wind no-storage case. This result is due to the approximately inverted profile between the two resources with solar being strong in the

day and wind being generally stronger at night. As expected, the combined profile better matches the building cooling load profile than either profile individually. Still, utilizing a CTES system results in reduced life-cycle costs and increased utilization of renewable energy compared to a no-storage system.

5.4 Model Predictive Control Optimization Results

All of the results presented thus far are drawn from simulations utilizing either the *Renewable Control* or *Cost Control* strategy. When trying to minimize operating cost, the *Cost Control* strategy relies on an individual cut-off rate below which it is desirable to operate the chiller system. This approach is best suited to relatively simple electricity rate structures that have only an on-peak and off-peak rate in a given day. The rate structures presented in Section 2.6.3 fluctuate on an hourly and a single rate cut-off is not ideal for these structures. As the name implies, the hourly day-ahead rates are provided before the day begins and they attempt to predict the rate fluctuations that will occur due to factors such as changing electricity demand, power plant availability, and behind-the-meter distributed generation. While the fluctuations are significant compared to time-of-use rate structures, they typically under-predict the actual fluctuations in the real-time rates as shown in Section 2.6.3. While the results presented in this section use the *Model Predictive Control* strategy only to minimize cost rather than to maximize the utilization of renewables, the comparison of results with different rate structures provides a surrogate for the impact that could be expected with renewable resource profiles. For example, the effect of a varying wind resource profile is best represented by a real-time rate structure that motivates the consumer based on the perceived value of electricity as seen from the utility side. In this way, strategies that minimize cost to the user also maximize the potential utilization of renewable resources.

For these simulations, the assumed Large Office building location is in the vicinity of Central Park in New York City and the operation year is 2016. This location is within the NYISO region covering New York City for which the day-ahead and real-time electricity rates apply. There is no renewable generation capacity installed on-site and the defined beginning of each day, the time by which the storage system must be recharged, is 7 a.m. The *Cost Control* strategy uses the linearized chiller model presented in Section 2.5.5 in order to be more directly comparable to the *Model Predictive Control* strategy. The cooling loads and ambient conditions for chiller operation for both strategies are from 2016 historical weather data rather than TMY data, as described in Section 2.3. Using this historical weather data ensures that weather-related impacts on the day-ahead and real-time electricity rates are reflected in building cooling loads and chiller operating conditions for that time period. The weather data sets and electricity rates are reported on an hourly basis. The weather data is linearly interpolated between hourly observations while the electricity rates are assumed to be constant for the full hour. Weather is only one of many factors affecting rates, but there is a noticeable correlation between dry-bulb temperature and this particular day-ahead rate as shown in Figure 5-18. The rates are generally highest when temperatures are at the low and high extremes. Presumably, the low extreme temperature rates are due to electric heating demand and the high extreme temperature rates are due to cooling demand.

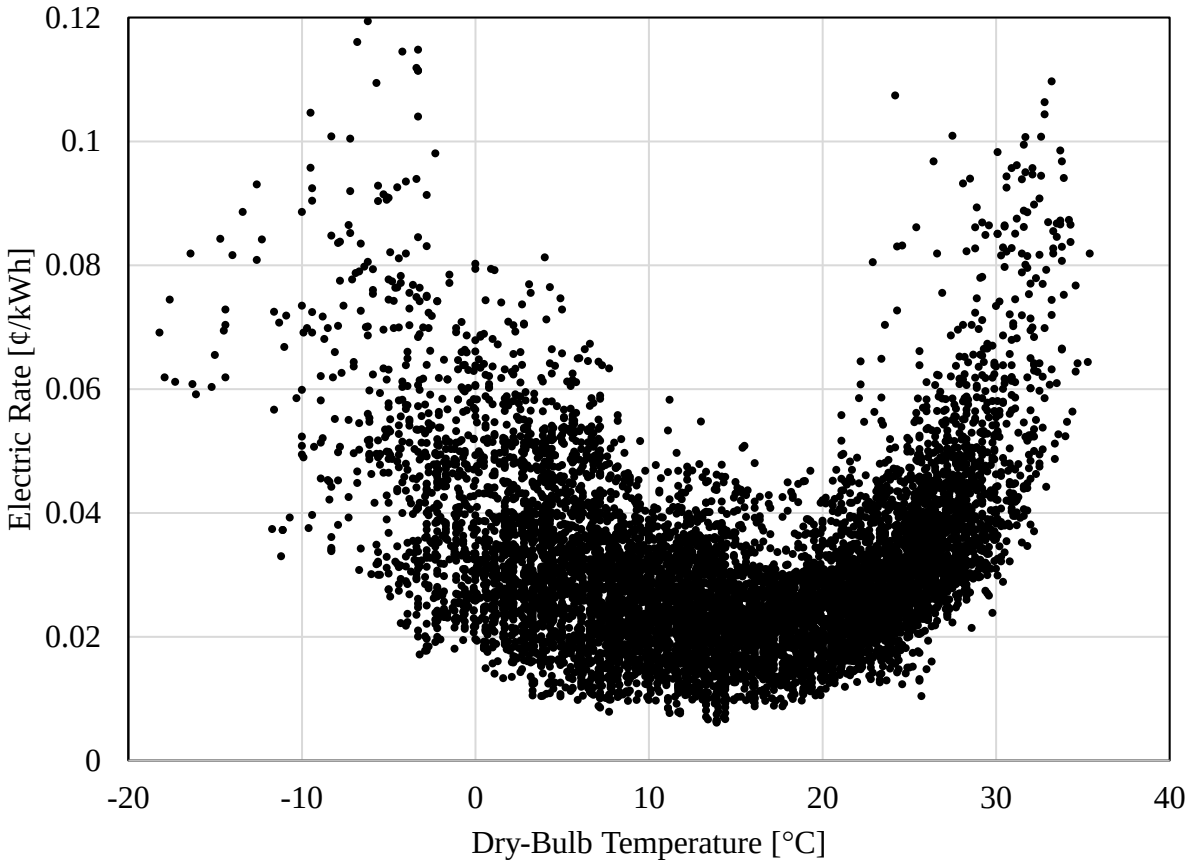

Figure 5-18. Correlation between 2016 NYISO real-time electricity rate and dry-bulb temperature (data from NYISO 2017b; White Box Technologies 2017)

Building cooling loads developed using TMY weather data are sufficient for simulations using simple rate structures that have only on-peak and off-peak rates because those rates have general time windows which reflect the periods that generally see the highest and lowest demands. The utility system is expecting that there will occasionally be high electricity demand during off-peak windows and vice versa. This risk is built in to the rate structure. On the other hand, when the rates are day-ahead or real-time, it matters if there is a heat wave on Monday and Tuesday but the simulation sees one on Wednesday and Thursday. Outside of the weather impact, the effect of building occupancy is significant. The TMY datasets all start on Sunday, January 1st while 2016 started on a Friday. Like most office buildings, the occupancy schedule varies significantly

according to the day of the week. The average occupancy over a 24-hour period for the Large Office building is 42% on weekdays, 15% on Saturdays and 0% on Sundays (USDOE 2011). Other commercial buildings in the utility system are likely to have similar occupancy schedules which results in higher weekday rates. Once again, a shift of a couple of days would make the simulation significantly less realistic.

Since the *Cost Control* and *Model Predictive Control* strategies are operating with the objective of minimizing energy cost, they are compared on the basis of annual energy cost. Along with this comparison metric, the annual chiller system energy consumption is reported. Intuitively, the annual simulations resulting in the lowest annual energy cost should also have the lowest energy consumption, but the inverse relationship reported in this section shows the benefit of *Model Predictive Control*. The optimization algorithm chooses to operate the system in the manner that minimizes cost even if it is at the expense of increased energy consumption.

5.4.1 Day-Ahead Electricity Rate Results

Because the *Cost Control* strategy requires a single electricity rate cut-off value, varying this parameter in a parametric study is expected to yield the optimum value. Selected results of this parametric study are plotted in Figure 5-19 and show that for this particular day-ahead electricity rate, the cut-off that gives the lowest annual energy cost is 1.6 ¢/kWh. Below this value, the annual energy cost begins to rise due to an increase in the frequency of activation of the operating condition where, regardless of the electricity rate and operating conditions, storage charging must occur in order to recharge by the end of the day. This value will vary for other rate structures and even for the same rate structure in a different time period. In the limit that the cut-off rate is adjusted more and more frequently throughout the simulation year it is expected that the cost control strategy will approach a more dynamic strategy like model predictive control. The

results presented here use the constant cut-off rate of 1.6 ¢/kWh for purposes of comparison to the *Model Predictive Control* strategy which considers only the rates in the control horizon when making control decisions.

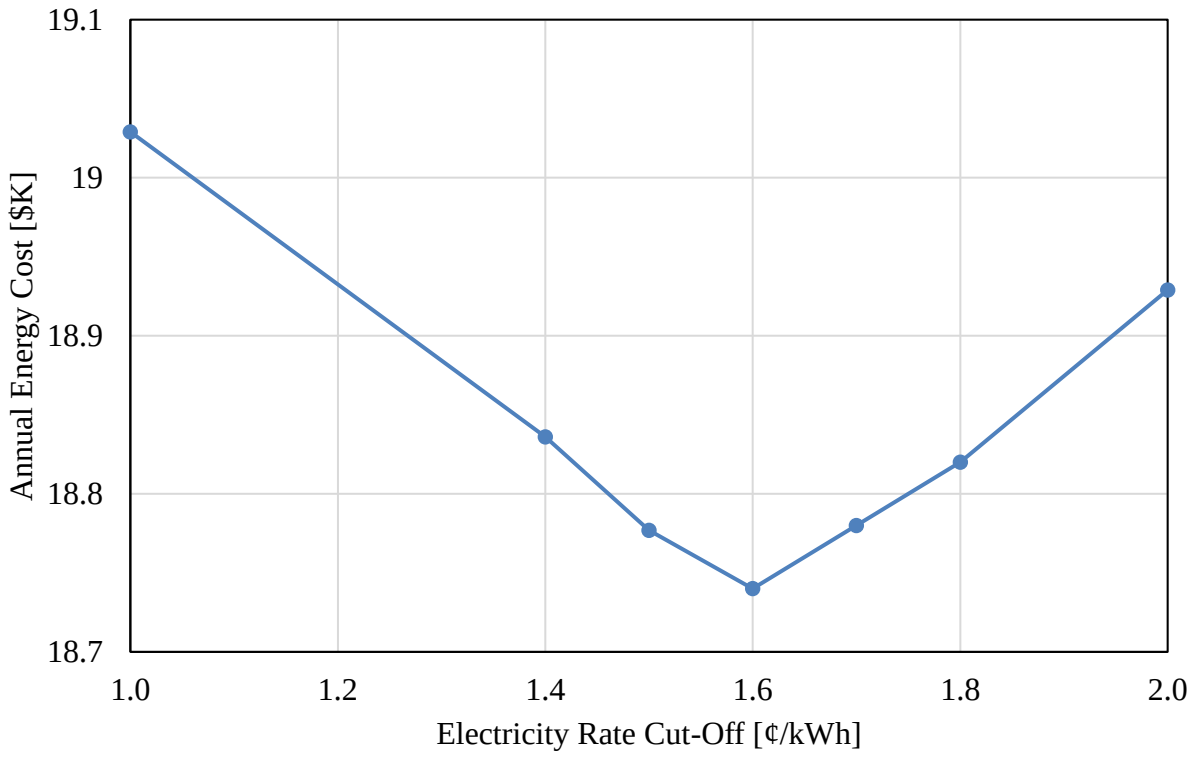

Figure 5-19. Annual energy cost by electricity rate cut-off for day-ahead electricity rate structure

The simulation details and metric calculations are given in Section 4.2. For the day-ahead electricity rate structure, the annual simulations results are given in Table 5-2. The annual energy cost decreases by almost 11% when operating using the *Model Predictive Control* strategy versus *Cost Control*. At the same time, the annual chiller energy consumption increases by 3.6%. The average chiller part-load ratio is nearly identical between the two control strategies, but *Cost Control* operates more frequently at full load or idled. In contrast, the optimization algorithm utilized by *Model Predictive Control* chooses full-load and zero-load operation slightly less frequently in favor of part-load operation. This part-load operation is the primary explanation for

the increased energy consumption since the chiller system operates less efficiently to meet the same cooling load. In Section 5.4.2, an example two-day period for the real-time electricity shows increased part-load operation. The reasoning for the part-load chiller system operation is given in that section.

Table 5-2. Annual simulation results for day-ahead electricity rates

Control Strategy	Rate Structure	Rate Cut-Off [¢/kWh]	Annual Energy Cost [$K]	Annual Chiller Energy Consumption [MWh]
Cost Control	Day-Ahead	1.6	18.7	700
Model Predictive Control	Day-Ahead	N/A	16.7	725

The electricity cost savings shown in Table 5-2 are the aggregated result of more than 50,000 control decisions made over the year-long period. A two-day period at the end of May is used to illustrate the control decisions made by the *Cost Control* and *Model Predictive Control* strategies. For the day-ahead rate structure, the *Cost Control* decisions are plotted in Figure 5-20 and the *Model Predictive Control* decisions are in Figure 5-21. Each 24-hour period begins at 7 a.m. and the storage tank is constrained to be recharged by hour 24 and hour 48. The day-ahead electricity rate is reported on an hourly basis and varies between 0.8 and 2.8 ¢/kWh for this time period although it varies between 0.6 and 15¢/kWh over the year. The building cooling load in red and electricity rates in black are identical in both figures, but the chiller power and the resulting tank charge vary. The electricity rates are generally lower at night and they are higher during the first example day than the second. Because the cooling load is determined using historical weather data that aligns with the electricity rate data, it is also higher on the first day than the second.

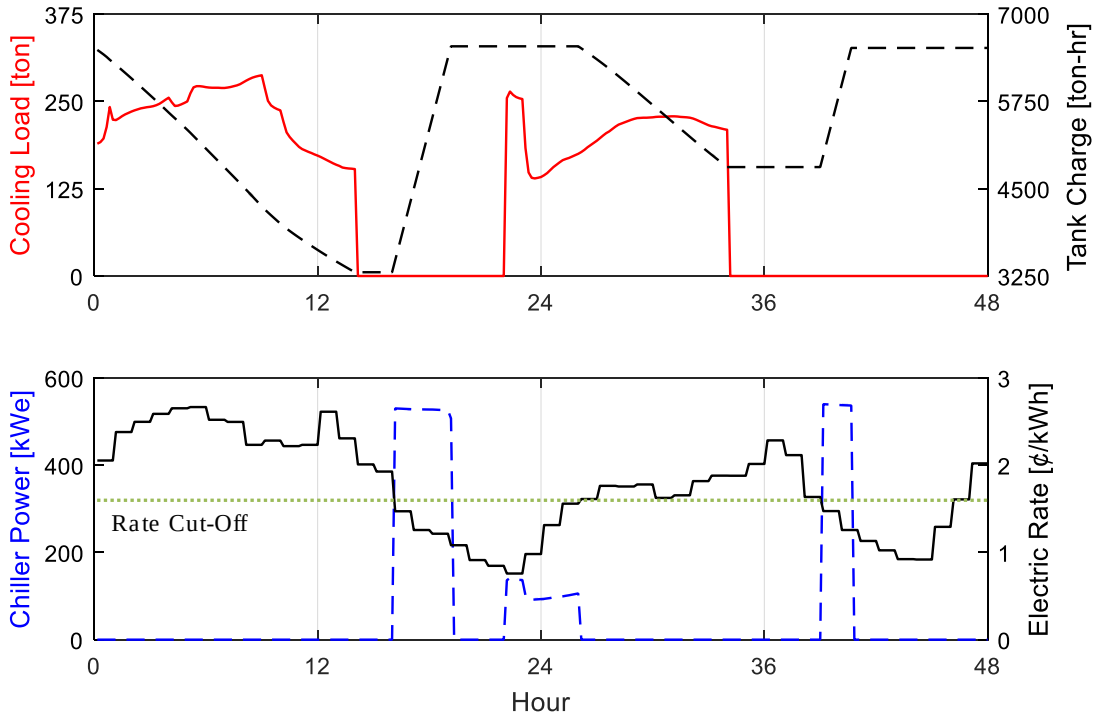

Figure 5-20. *Cost Control* strategy example period using day-ahead electricity rates

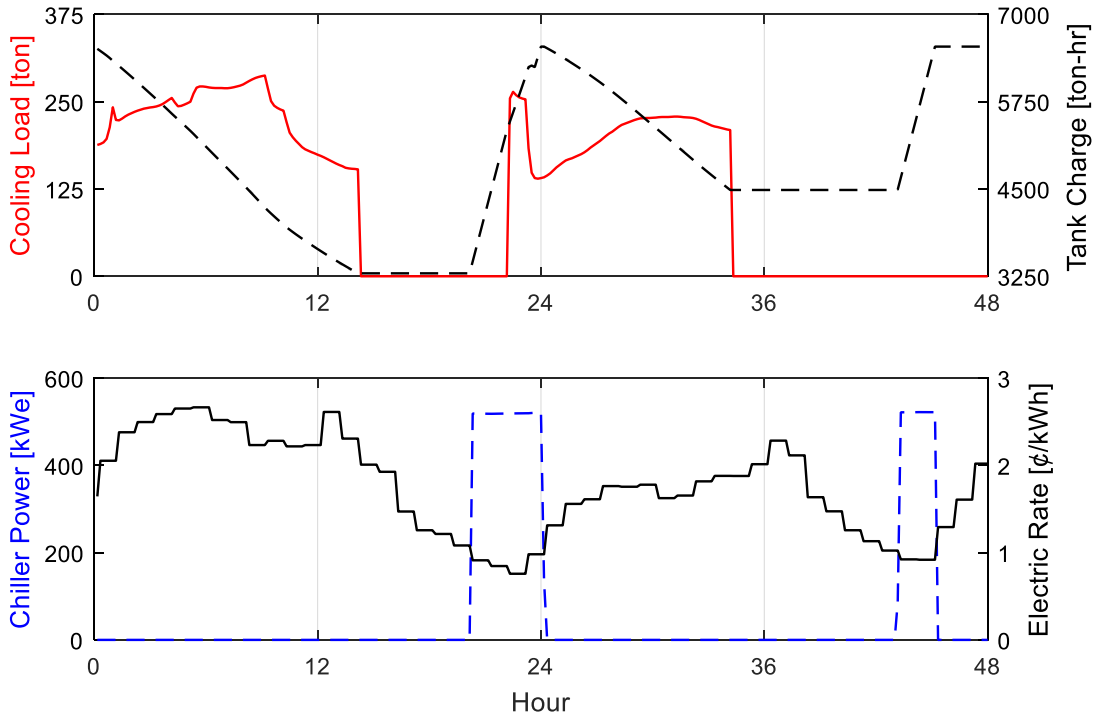

Figure 5-21. *Model Predictive Control* strategy example period using day-ahead electricity rates

On the bottom plot of Figure 5-20, the electricity rate cut-off for the *Cost Control* strategy, 1.6 ¢/kWh is shown as a dotted green line. During this two-day stretch, the chiller is never running when the rate is above this cut-off value as indicated by the time periods encompassed by the dashed blue line. While the *Cost Control* strategy operates the chiller system only during low-electricity-cost periods, the *Model Predictive Control* strategy does better by seeking out the lowest cost periods in the 24-hour control horizon. For example, both strategies manage to recharge the storage tank by hour 48, but the *Cost Control* strategy in Figure 5-20 starts recharging four hours earlier when the rates have not yet reached their minimum. In aggregate, similar behavior throughout the year leads to the significant cost reduction provided by the *Model Predictive Control* strategy.

5.4.2 Real-Time Electricity Rate Results

For the real-time electricity rate structure presented in Section 2.6.3, the optimum cut-off rate for the *Cost Control* strategy is lower than it is for the day-ahead rate structure. Selected simulations are plotted in Figure 5-22 and they show that 1.1 ¢/kWh is the optimum cut-off rate. The results presented in this section for the *Cost Control* strategy use this constant cut-off value.

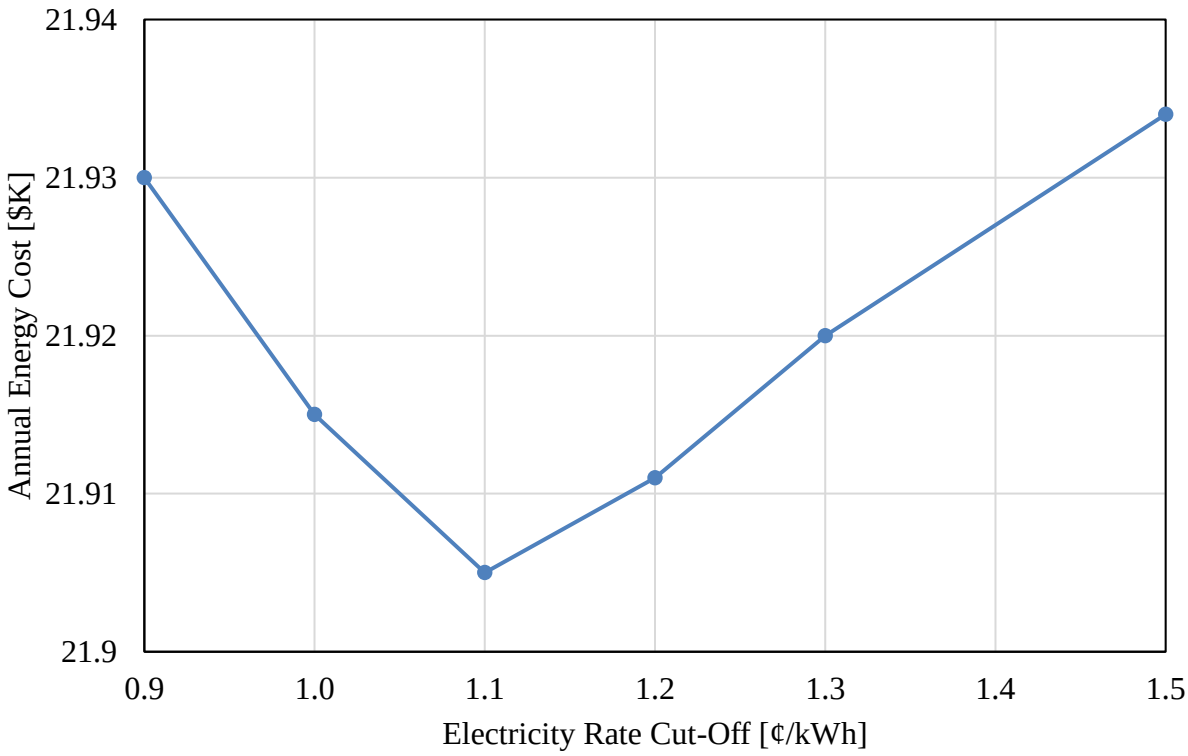

Figure 5-22. Annual energy cost by electricity rate cut-off for real-time electricity rate structure

The results for both control strategies and both electricity rates are given in Table 5-3. They are grouped by control strategy to highlight the impact of the rate structure. Focusing on the first two rows showing the *Cost Control* results, the annual energy cost increases by over 17% when subject to the real-time rate structure instead of the day-ahead one. The annual chiller energy consumption remains approximately constant. In contrast, for the *Model Predictive Control* strategy, the annual energy cost remains approximately constant and the chiller energy consumption decreases slightly. Both rates have the same mean value, but the real-time rate has a standard deviation that is two-and-a-half times as large as that for the day-ahead rate. The median for the real-time rate is also lower than it is for the day-ahead rate. The real-time rate is the more volatile as evidenced by the standard deviation. The day-ahead rate under predicts the peaks and valleys in the eventual real-time rates, but the magnitude of the under-prediction of the peaks is

greater as evidenced by the lower median in the real-time rates. Comparing the two control strategies for the real-time rate, *Model Predictive Control* results in a 24% energy cost reduction from the *Cost Control* strategy. The energy cost reduction for the day-ahead rate structure presented in the previous section is 11%. These results show that the *Model Predictive Control* strategy has a distinct advantage over more traditional control strategies when the inputs have greater variability. Conversely, when inputs are easily predicted and have little variability, the strategy is expected to provide little advantage and may justify the added control system complication.

Table 5-3. Annual simulation results for day-ahead and real-time electricity rates

Control Strategy	Rate Structure	Rate Cut-Off [¢/kWh]	Annual Energy Cost [$K]	Annual Chiller Energy Consumption [MWh]
Cost Control	Day-Ahead	1.6	18.7	700
Cost Control	Real-Time	1.1	21.9	700
Model Predictive Control	Day-Ahead	N/A	16.7	725
Model Predictive Control	Real-Time	N/A	16.7	723

Day-ahead and real-time rates are plotted together in Figure 5-23. For this particular time-period, the two rates follow the same general trend throughout the day, but the real-time rate exhibits greater extremes and hour-to-hour variation. With respect to the *Model Predictive Control* strategy, there are two notable discrepancies between the two rates. The first occurs at hour 25 when the day-ahead rate continues to increase, but the real-time rate drops significantly for an hour. If the strategy is using the day-ahead rate as an input, but the real-time rate is being charged, it is likely that the first portion of this reduced rate period will be missed by the chiller system operation. Because the timestep is only ten minutes long and the rate changes on an hourly basis,

the updated rate can be fed back into the optimization algorithm to be able to take advantage of the rate in subsequent timesteps. The second rate discrepancy occurs at hour 41 when the day-ahead structure predicts a decreasing rate, but the real-time rate behavior is much more drastic. At hour 43, the real-time rate actually goes negative. In this case, the *Model Predictive Control* algorithm is likely planning to activate the chiller system during this time period, so the negative rate will be fully exploited.

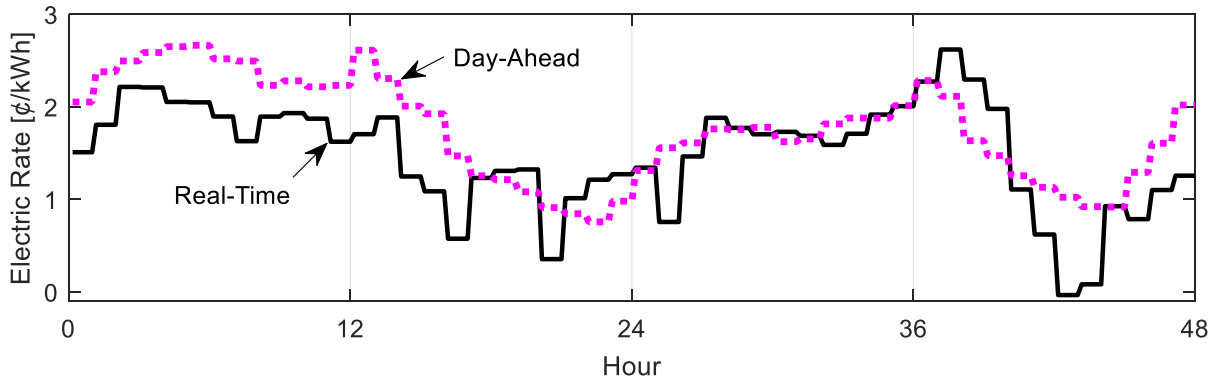

Figure 5-23. Day-ahead and real-time electricity rates for a two-day example period

Control decisions for the same example two-day period used for the day-ahead rate are plotted in Figure 5-24 and Figure 5-25 for the real-time electricity rate. Focusing on the first 24-hour period, both control strategies take advantage of the two lowest rate periods at hours 17 and 21. The *Cost Control* strategy (shown in Figure 5-24) operates the chiller system at full load as soon as the rate drops below the cut-off of 11¢/kWh (shown as a dotted green line) at hour 16. It also idles the system at the end of the second low-rate period because the storage tank has become fully recharged and there are no building cooling loads to be met. Once the cooling loads commence, the chiller system runs at full load for a short time even though the rate is above the cut-off value. This is necessary in order to fully recharge the storage tank by the beginning of the next 24-hour period. In contrast, the *Model Predictive Control* strategy leaves the chillers running

throughout the final hours of the first day. Once the storage tank has been fully recharged, the chiller system is run at a part-load ratio sufficient to just meet the cooling load. This means that during the higher-rate period at the end of the 24-hour period, the chiller system is consuming as little power as possible in order to meet the storage tank recharge constraint in addition to the cooling load. This is a good example scenario to explain the increased annual energy consumption for the *Model Predictive Control* strategy over the *Cost Control* strategy. While both strategies meet the cooling load and recharge the storage tank, *Model Predictive Control* uses 3% more energy to do so due to more frequent part-load operation.

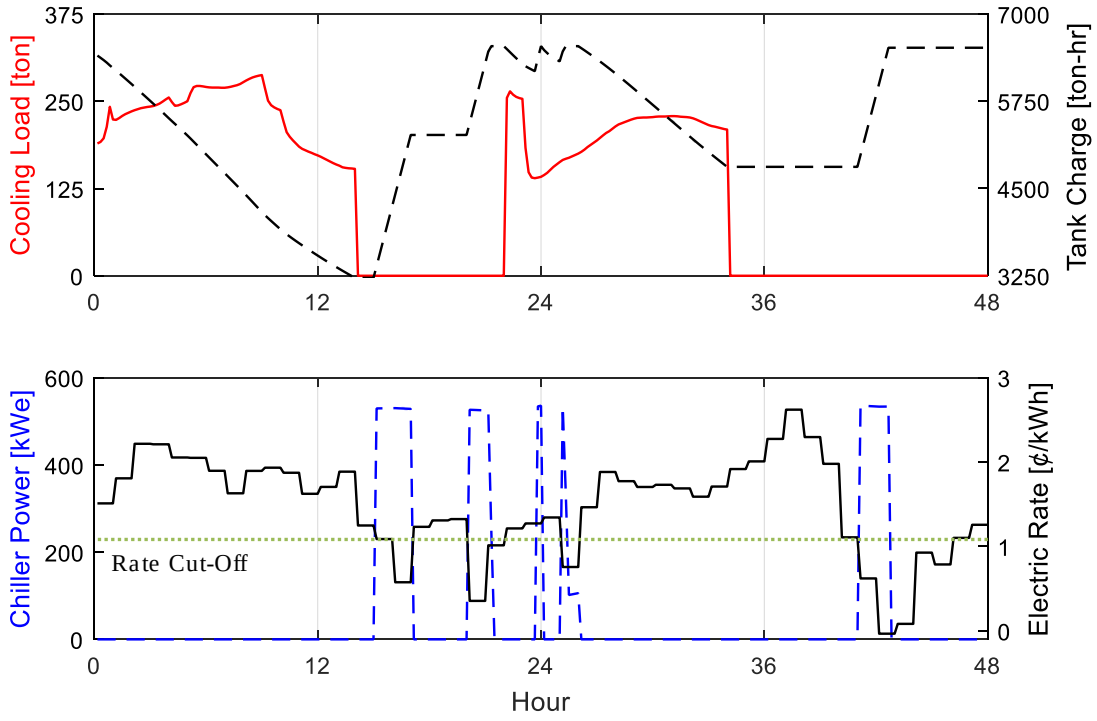

Figure 5-24. *Cost Control* strategy example period using real-time electricity rates

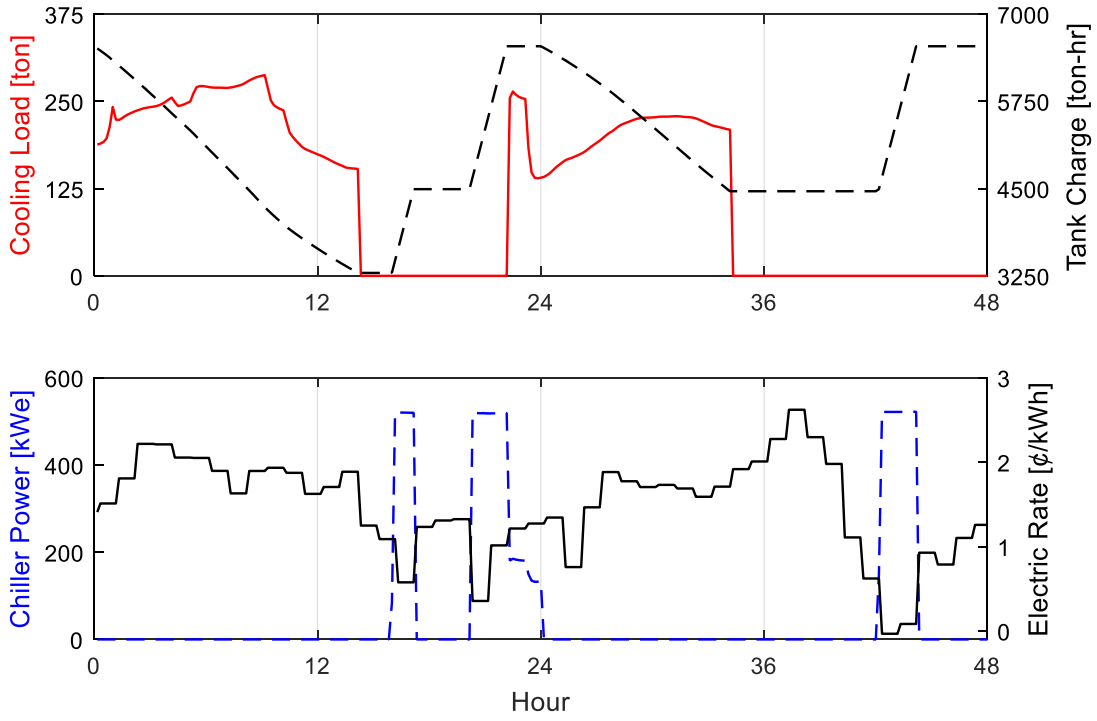

Figure 5-25. *Model Predictive Control* strategy example period using real-time electricity rates

The second 24-hour period in Figure 5-24 and Figure 5-25 demonstrates the advantage of *Model Predictive Control* well. The *Cost Control* strategy activates the chillers when the rate drops below the cut-off in hour 25. The storage tank quickly recharges and the chiller system can only operate at a part-load ratio sufficient to meet the building cooling loads. Toward the end of the second day, when the cooling loads have disappeared, both control strategies take advantage of low-rate periods. The *Model Predictive Control* strategy in Figure 5-25 has the foresight to wait to activate the chillers until the rate has become negative. For this particular day, the electricity cost ends up being ten times greater for the *Cost Control* strategy, a difference of over $26.

The results presented in this section confirm the financial benefits of the *Model Predictive Control* strategy especially when electricity rates vary significantly and on short timescales. While these results only consider minimization of the electricity costs, there is an analog to maximization of the renewable resource utilization. In particular, the wind resource is quite variable and in many locations, there are highly time-resolved wind forecasts which can be used as an input to the *Model Predictive Control* strategy.

5.5 Aggregate *Renewable Control* Impact on Utility Systems

All of the Pareto fronts presented in the parametric study results in Section 5.3 are for a single Secondary School or Large Office building taking advantage of net metering policies with solar or wind power generation equipment installed. The 20-year cost shows the approximate net economic impact on the building owner and the chiller energy met by renewable gives an idea of how a particular CTES or no-storage system would impact the utility system of which the building is a part. In order to forecast how these storage strategies could impact utility systems, the individual parametric study results are aggregated over the population of buildings present in a region.

Each Secondary School and Large Office building in the particular region is assumed to be identical to the Commercial Reference Building modeled. The buildings are modeled both without CTES as well as with a CTES system utilizing *Renewable Control* and the results are multiplied to obtain the aggregate results. Ice CTES is employed for the Secondary School and stratified chilled water for the Large Office building since these options result in the lowest cost systems due to economies of scale for the chilled water tanks. The parameters used for the storage case are consistent with the inflection point of the Pareto front, i.e. the point that has minimal cost difference from the lowest cost point but achieves significantly greater renewable energy utilization. Each of the buildings is assumed to be equipped with solar or wind generation capacity that is equal to the full-load chiller power for the no-storage case.

Table 5-4 shows the parameters used to aggregate the individual facility data. With the exception of Wisconsin, each of the states considered are completely or nearly completely covered by the respective independent system operator (ISO). For Texas this is the Electric Reliability Council of Texas (ERCOT), for California it is the California Independent System Operator (CAISO), and for New York it is the New York Independent System Operator (NYISO). System electric load data is publicly available through the Energy Information Administration (EIA) and each of these three states are approximated as overlapping the ISO region (EIA 2017b). Wisconsin is part of the Midcontinent Independent System Operator (MISO) which covers parts of 16 different states and a Canadian province. Electric load data are publicly available for the MISO region and the portion attributed to Wisconsin is allocated by population.

The number of Secondary Schools in each state is data available through the National Center for Education Statistics (High-Schools.com 2013). The EIA performs an intermittent Commercial Building Energy Consumption Survey and the most recent one was conducted in 2012

(EIA 2012). The data is collected by census region and broken down by principal building activity as well as building square footage. The number of Large Office buildings listed in Table 5-4 comes from an analysis of these data.

The day of the year used for the duck curve, shown previously in Figure 1-3, is March 31st. Using this date highlights the CAISO issue with solar over-generation because the state typically has significant solar resource at this time of year, but cooling loads have not yet reached their peak. To see the aggregate impact of CTES, a day with high peak load can be used to highlight the differences between the no-storage and storage system cases. The chosen days are all within the recent past and listed in the last column of Table 5-4.

Table 5-4. Aggregation parameters for all four geographic locations (data from High-Schools.com 2013, EIA 2012, and EIA 2017b)

Location	ISO	No. of Secondary Schools	No. of Large Office Buildings	Peak Load Date Used
Texas	ERCOT	3,709	651	August 10, 2015
California	CAISO	4,495	756	September 10, 2015
Wisconsin	MISO	885	232	September 1, 2015
New York	NYISO	2,167	1,143	July 19, 2013

The hourly load profile for each ISO on the peak date provides a basis for observing the impact of installing additional solar and wind generation capacity as well as the chiller electricity consumption for buildings with both no-storage and *Renewable Control* storage systems. This load profile is shown as a solid black line in Figure 5-26 for the ERCOT region, Figure 5-27 for the CAISO region, Figure 5-28 for the state of Wisconsin, and Figure 5-29 for the NYISO region. Each figure shows the impact of the solar resource in the top row and the wind resource in the bottom row. The shaded area in the left-most plots shows the net load the utility system must meet after solar or wind generation capacity is installed for every Secondary School and Large Office

building. The capacity installed for each building is equal to the no-storage full-load chiller power. While the impact of the solar energy generation is predictably felt during the middle of the day, the impact of the wind varies and does not necessarily follow the trend stated several times throughout this dissertation that the resource is strongest at night. These plots represent a single day, so the profile and magnitude may not be indicative of the general behavior of the renewable resource.

The shaded area in the middle plot in each row shows the net sum of subtracting the solar or wind generation (as in the left-most plot) and adding back the no-storage chiller power consumption for all of the buildings shown in Table 5-4. The chiller power consumption adds to the peak load as evidenced by the shaded areas above the solid black line. In several cases, there is renewable power generated close to the peak hour and the no-storage chillers consume that renewable generation and more. This is true for the wind resource in CAISO shown in the bottom row of Figure 5-27 as well as the solar resource in NYISO shown in the top row of Figure 5-29. Some of the discontinuities seen in the shaded area profile are due to the intermittent nature of the renewable resource and some are due to the sudden transition in performance when switching between operation of one to two chillers or vice versa.

The right-most plot in each row shows a similar profile to the middle plot, but the buildings now have a *Renewable Control* storage system rather than a no-storage system. In all eight cases, these systems produce a change in the utility net load profile indicating it would be more desirable to the utility system than the one produced by the no-storage case. Without looking at the shape of the profile, each of the storage systems meets the same cooling load with significantly less chiller electricity consumption. Using the wind resource in the bottom row of the ERCOT plots in Figure 5-26 as an example, the wind resource in the left plot is not particularly strong on this day, but the

slight resource present is strongest during the early morning and late evening hours. The middle plot shows that the no-storage case buildings utilizes some of the wind power around 6 a.m., but the primary impact of the no-storage system is to add to the peak load that occurs around 5 p.m. In the right plot showing the impact of the storage system, much of the wind power produced in the early morning is used by the chillers and the overall utility system peak is not increased in the afternoon. While this representation does not provide an annually integrated quantitative measure, it allows for a visual observation of the storage system benefits in a manner that is similar to that used by the duck curve.

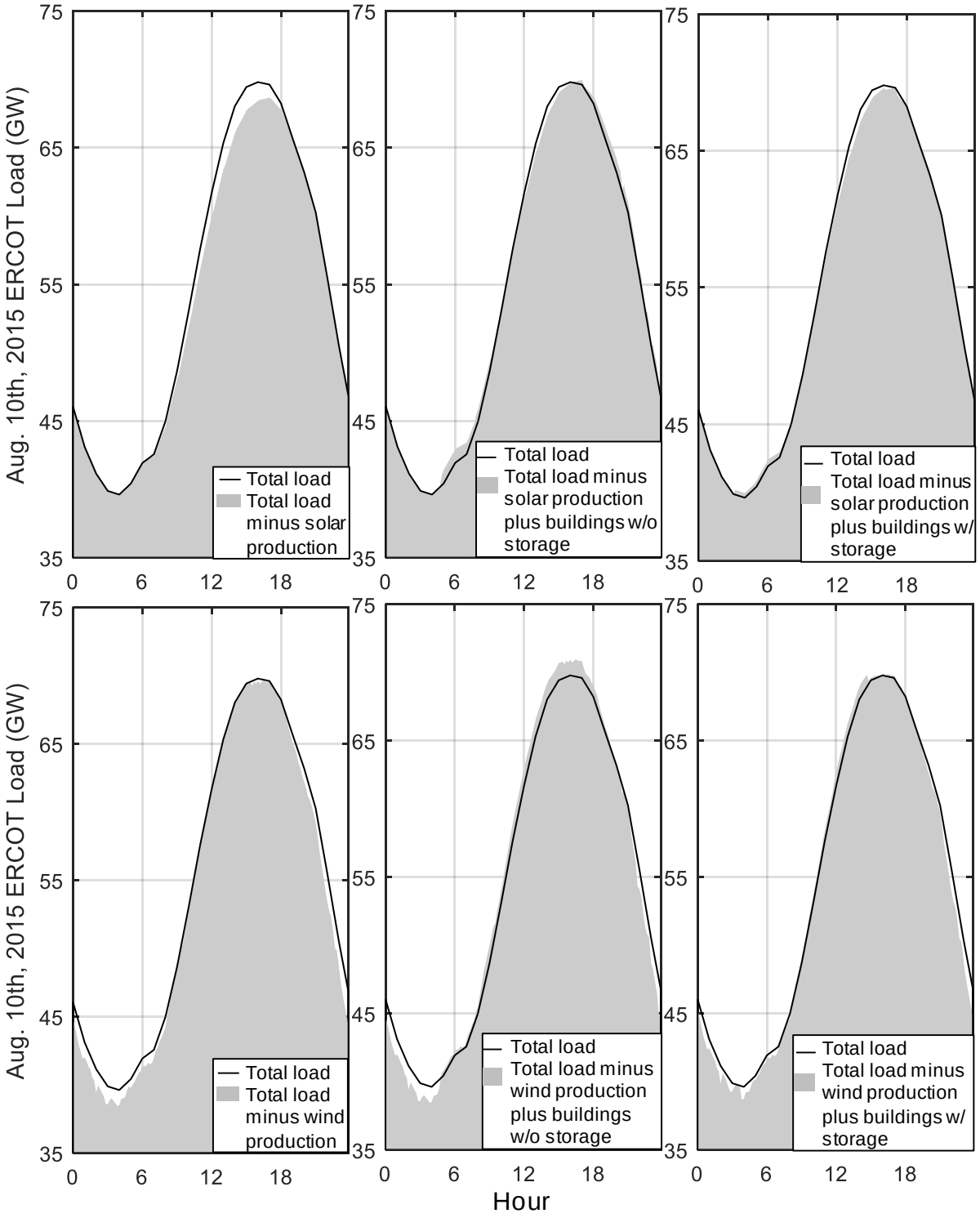

Figure 5-26. Peak ERCOT load minus renewable (left), minus renewable plus no-storage (middle), and minus renewable plus *Renewable Control* CTES for solar (top) and wind (bottom)

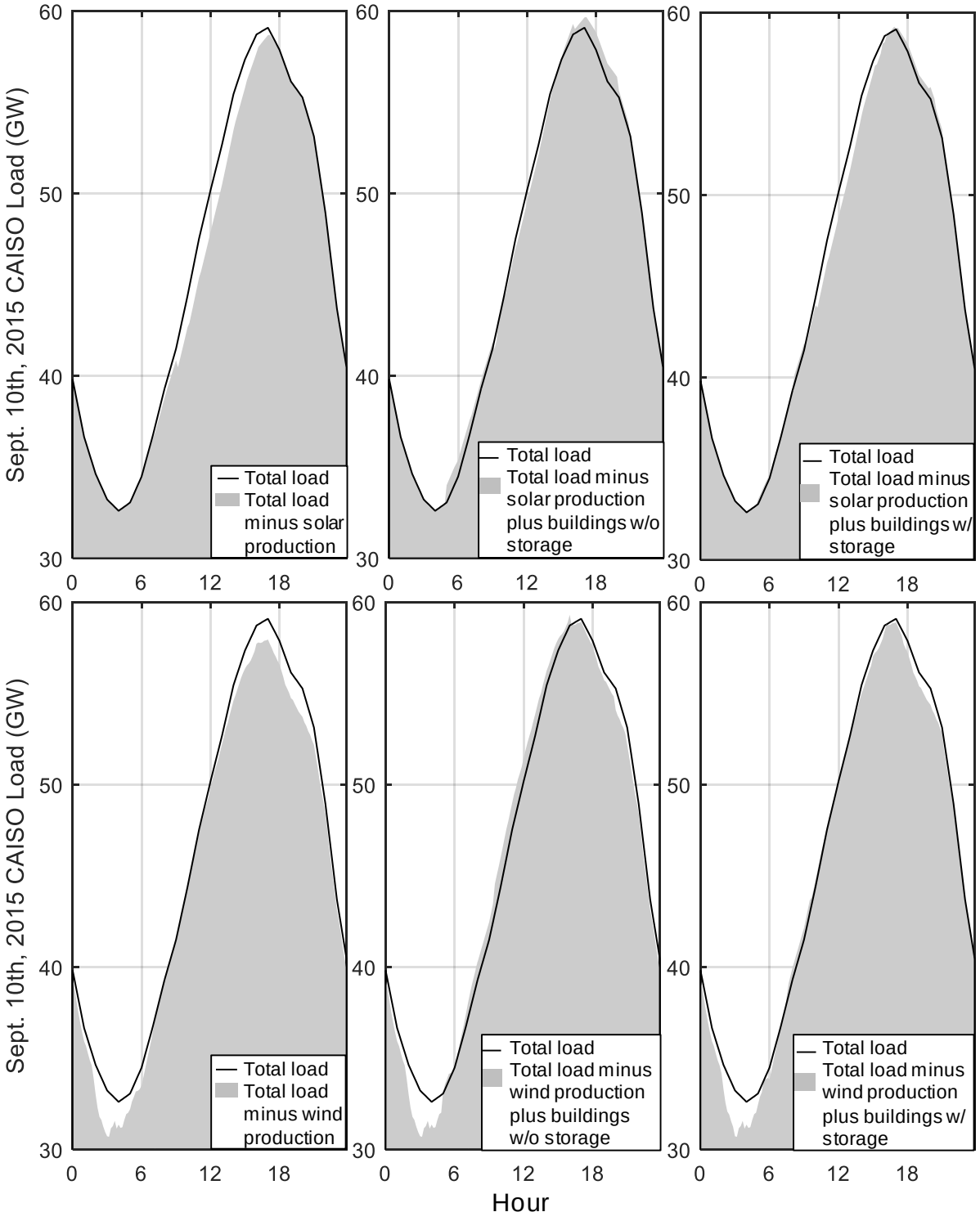

Figure 5-27. Peak CAISO load minus renewable (left), minus renewable plus no-storage (middle), and minus renewable plus *Renewable Control* CTES for solar (top) and wind (bottom)

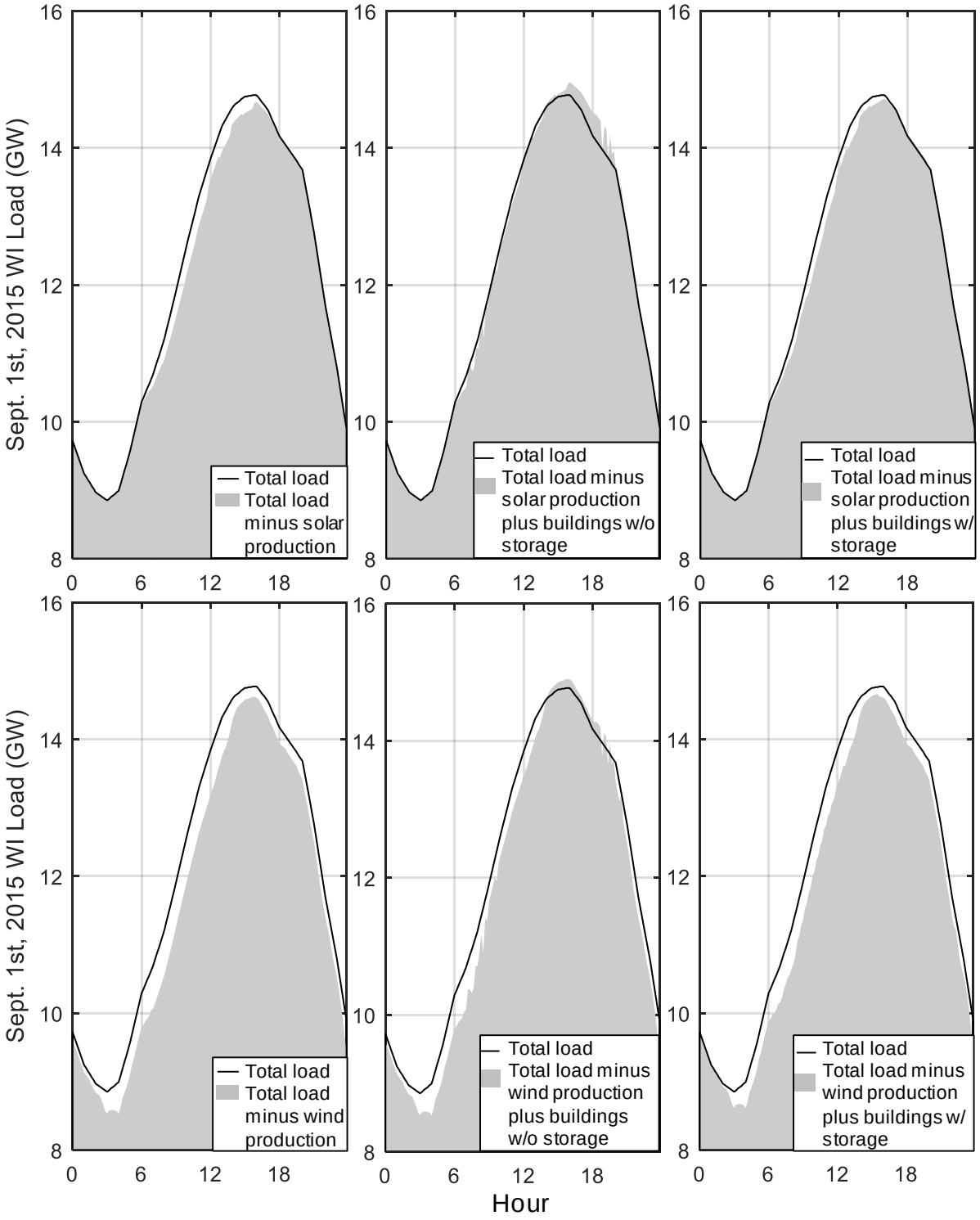

Figure 5-28. Peak WI load minus renewable (left), minus renewable plus no-storage (middle), and minus renewable plus *Renewable Control* CTES for solar (top) and wind (bottom)

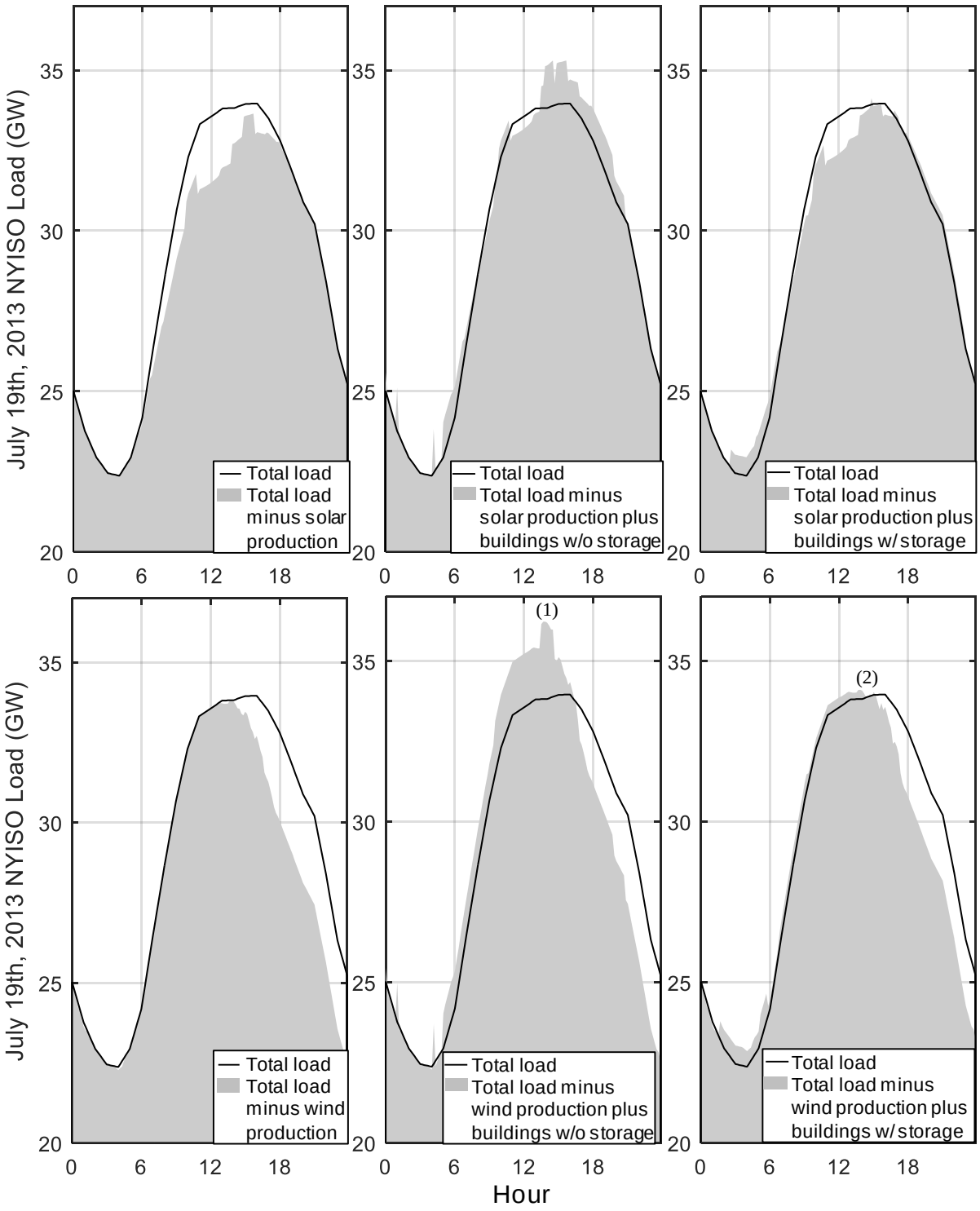

Figure 5-29. Peak NYISO load minus renewable (left), minus renewable plus no-storage (middle), and minus renewable plus *Renewable Control* CTES for solar (top) and wind (bottom)

Comparing points (1) and (2) in the lower right-most plots of Figure 5-29, the storage system reduces the system peak load by approximately 2 GW when applied to each of the secondary schools and large office buildings in the NYISO region. This method of calculating the potential peak load reduction is considered a "bottom-up" approach whereby the total reduction is calculated by summing individual simulation results.

Another method for determining the potential aggregate impact is a "top-down" approach which has been defined in a study by NREL (NREL 2012). The approach involves identifying a summer base load day using historical weather data and comparing it to the system load on the peak summer day. The assumption is that the difference between these two days is primarily due to electricity used for cooling. The cooling load associated with this method includes all cooling – commercial, residential and industrial. Using this approach for the NYISO region in the summer of 2013, the electric demand associated with cooling loads is estimated to be 14 GW or 41% of the peak load as shown in Figure 5-30 (EIA 2017b). This is compared to the 2 GW identified using the bottom-up approach. Results for the top-down approach for the CAISO region in 2016 estimate a total of 20 GW of potential peak demand reduction or 43% of the peak electric demand (CAISO 2017). The ERCOT region in 2016 shows 34 GW of potential peak reduction or a full 48% of the peak demand. The top-down approach plots for CAISO and ERCOT are shown in Figure 5-31 and Figure 5-32, respectively. While not all of this cooling load-associated electric demand has the potential to be shifted using thermal energy storage, the top-down approach provides an upper bound and shows that there is significant potential peak reduction beyond that identified using the bottom-up approach.

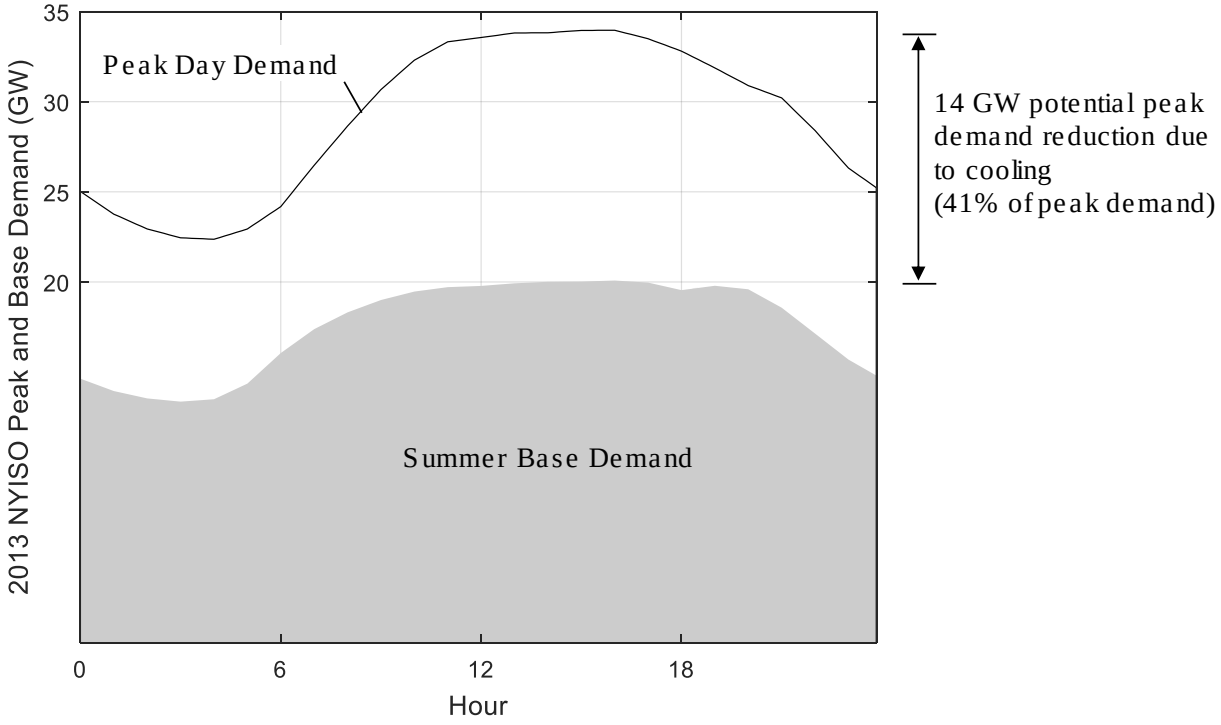

Figure 5-30. NYISO top-down estimate of total cooling load (data from EIA 2017b)

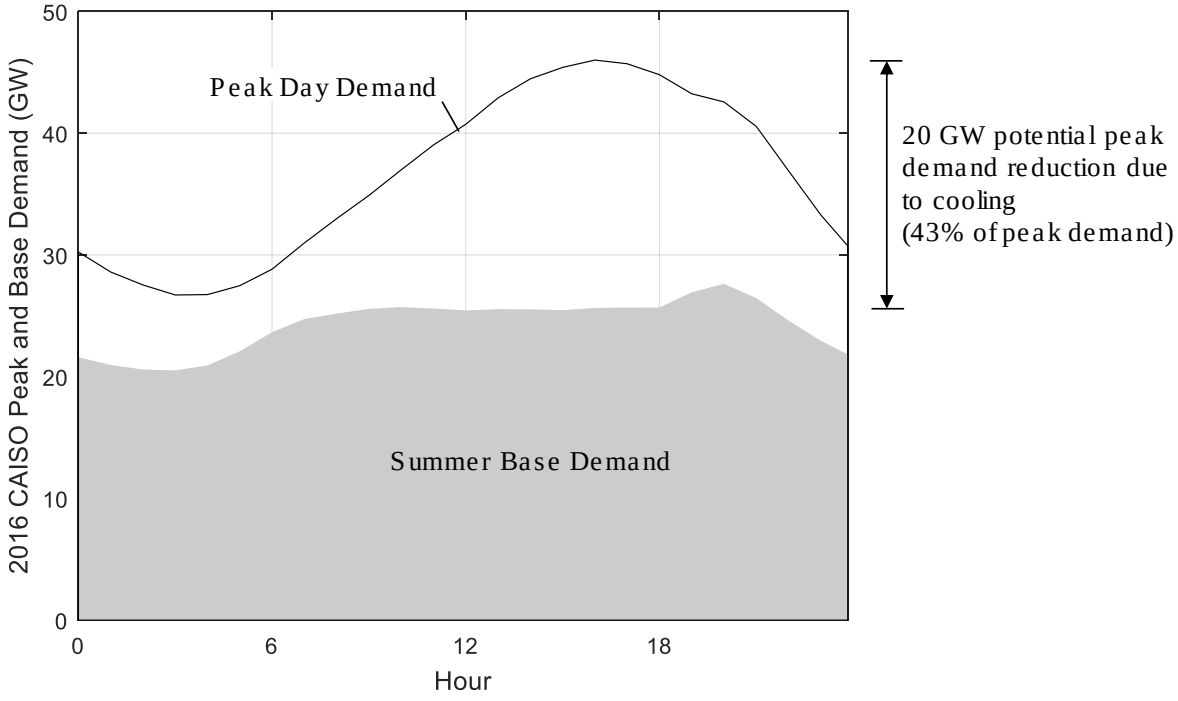

Figure 5-31. CAISO top-down estimate of total cooling load (data from CAISO 2017)

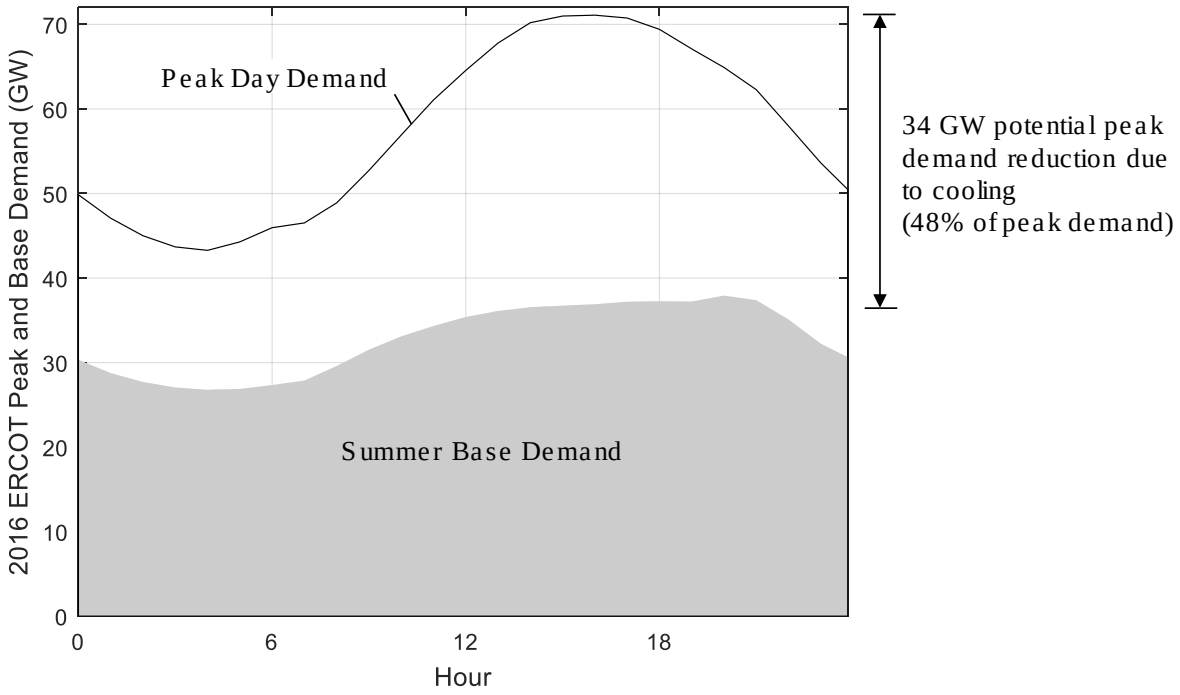

Figure 5-32. ERCOT top-down estimate of total cooling load (data from ERCOT 2017)

5.6 Comparison of Storage Technologies

While Section 5.5 shows graphical representations of the aggregate impact of *Renewable Control* thermal storage systems on the ISOs, it does not address implementation costs and other possible storage technologies. There are currently increasing renewable penetration rates in the electric grid and associated need for various forms of energy storage. The economic value of energy storage to the electricity markets has been addressed in several studies and NREL has compiled a summary of those studies (NREL 2013b). The range of economic value is a function of geographic location, storage technology round-trip efficiency, and duration of the energy storage. The economic values range from $29/kWe up to $115/kWe annually across most of the United States. The range goes up to $240/kWe annually when New York City is included. If the storage system is assumed to have a 20-year lifespan, a simple payback calculation shows that the

storage would be valued at between $500/kWe and $2,300/kWe for most of the country and up to $4,800/kWe in New York City.

Pierpoint performed a review of the capital costs associated with several types of energy storage technology (Pierpoint 2016). The costs are reported on two separate bases: a per power output basis ($/kWe) and a per energy output basis ($/kWh). The power output is the instantaneous charge or discharge rate of the storage technology while the energy output is the total quantity of energy that can be stored regardless of the charge or discharge rate. The results of the study are shown along these two dimensions in Figure 5-33. The most expensive technology considered is lithium-ion battery storage followed by pumped hydroelectric storage. Compressed air and hydrogen energy storage are both relatively inexpensive, but suffer from low roundtrip efficiencies. The information shown in Figure 5-33 for CTES systems is based on the simulations performed for this research. While the capital cost per unit energy output is similar to compressed air and hydrogen energy storage technologies, the cost per unit power output (or reduced power consumption in the case of CTES) is significantly lower than any competing technology.

Each of the non-CTES storage technologies plotted are those which discharge electricity after the systems have been charged. For CTES, the electricity is stored indirectly in the form of thermal energy as it allows the displacement of end-use electricity demand and consumption from one part of the day to another part of the day. The range of CTES capital cost values shown is primarily due to capital cost differences between ice and chilled water. The lower end comes from a chilled water system on the Large Office building and the upper end comes from ice CTES also on the Large Office building. The cost of the CTES system is calculated by subtracting the cost of the no-storage chiller system from the sum of chiller and CTES systems. To calculate the cost per unit power output, the full-load power of the CTES system chiller is subtracted from the same for

the no-storage system. This value is the peak “power output” of the CTES system and the storage system cost is divided by this value to get the capital cost per power output. To calculate the capital cost per energy output ($/kWh), an average coefficient of performance must be assumed. Based on the performance curves presented in Section 2.5, the assumed coefficient of performance is 5.0 for stratified chilled water CTES and 4.0 for ice CTES. The storage system cost is divided by the storage tank thermal capacity in units of kWh. To convert the thermal kWh units to the electric units needed for the comparison, the value is multiplied by the assumed coefficient of performance to give the capital cost per energy output ($/kWh).

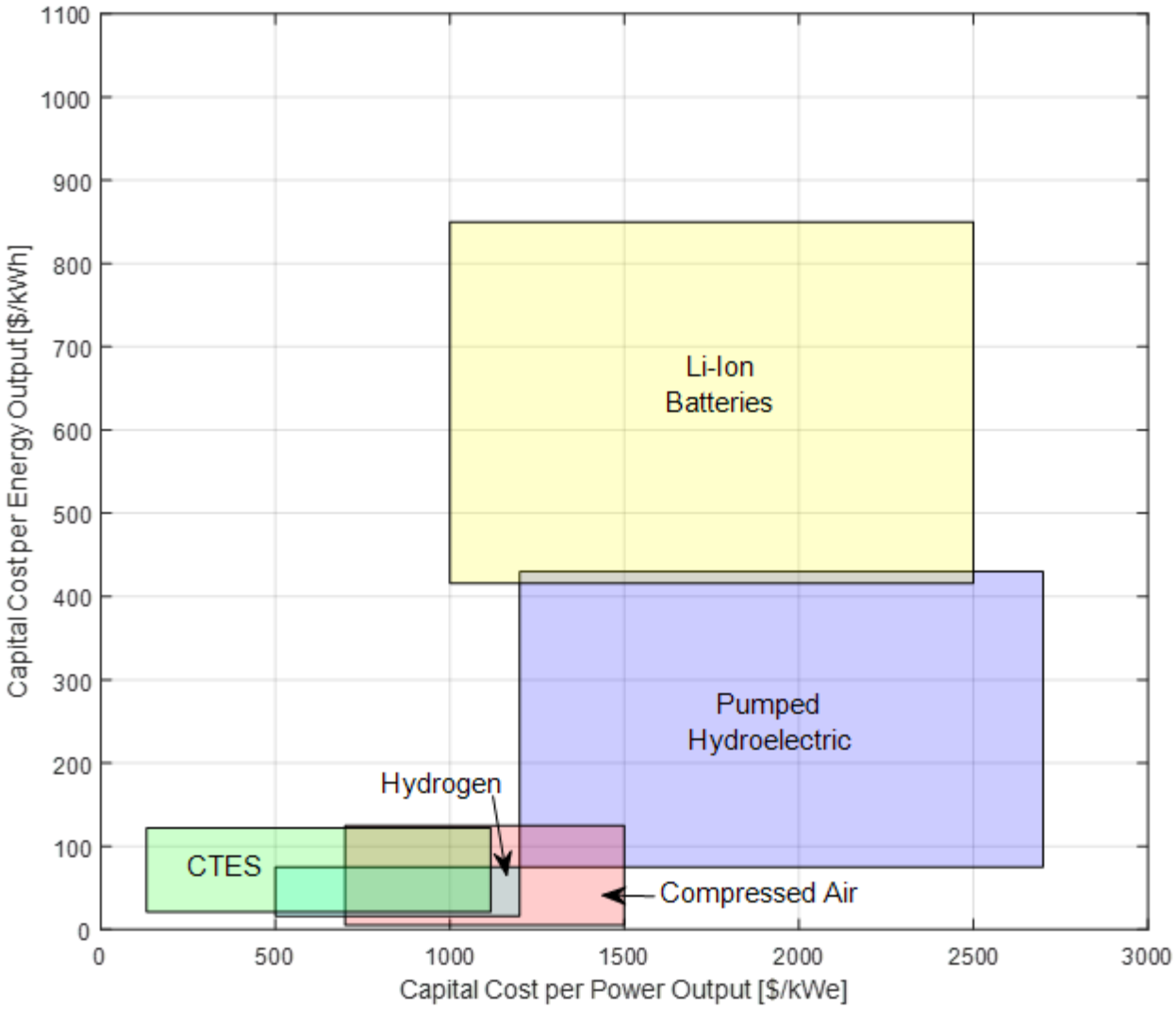

Figure 5-33. Energy storage technology capital cost comparison (data from Pierpoint 2016, Schoenung 2011, Tesla Motors 2016)

In addition to the direct capital cost comparison presented in Figure 5-33, it is important to compare the storage technologies on the basis of roundtrip efficiency, siting considerations, and other advantages and disadvantages. This comparison is shown in Table 5-5.

Table 5-5. Energy storage technology attributes (all but CTES and efficiency data from Gençer & Agrawal 2015; efficiency data from Pierpoint 2016)

Energy Storage Technology	Approximate Roundtrip Efficiency	Siting Considerations	Advantages	Disadvantages
Cool Thermal	≥100%	Requires close proximity to cooling loads and associated cooling equipment	Mature technology, inexpensive, directly counteracts air conditioning loads	De-centralized control of storage systems, less flexible than electricity-based storage, improper operation can result in unmet cooling loads
Pumped Hydroelectric	80%	Requires varied topography	Mature and large economies of scale	Environmental impact of damming rivers and creating reservoirs
Lithium-Ion Battery	80%	Minimal, but reactivity and flammability must be taken into account	Flexible scaling, costs continually declining	14-year lifespan to 80% capacity, end-of-life disposal is an environmental concern, depends on inexpensive supply of materials that are not mined domestically
Compressed Air	50%	Cost-effective installations require specific geologic formations underground	Large-scale, inexpensive	Immature technology, low efficiency, natural gas used emits greenhouse gases
Hydrogen	35%	Cost-effective installations require specific geologic formations underground	Inexpensive, long storage periods without further loss of efficiency	Very low efficiency

The second column indicates the approximate roundtrip efficiency for the storage technology (Gençer & Agrawal 2015). Calculation of the roundtrip efficiency for CTES requires a baseline other than the electrical energy originally stored. The system initially produces and then stores cold water to be circulated when the building experiences cooling loads. The baseline for the efficiency calculation is therefore the chilling system's electric consumption required to meet those cooling loads with a no-storage system. Because chillers exhibit lower performance both when outdoor temperatures are high in the middle of the day as well as when they are operating at less than their full-load capacity, chillers generally consume more electricity when directly meeting cooling loads than they do when operating in conjunction with a CTES system. The systems with CTES allow chillers to operate at their full capacity and during more hours outside of the hottest hours of the day. This means that less electricity is consumed to meet the same cooling loads with a CTES system and while there are thermal losses, they are typically more than offset by the chiller electric savings (Reindl et al. 1995). As a result, chilled water CTES systems are capable of achieving roundtrip efficiencies greater than 100%.

In order to account for the impact of roundtrip efficiency on the life-cycle cost, the capital cost per unit energy values are normalized by the fractional roundtrip efficiencies in Figure 5-34. This plot is similar to that in Figure 5-33 except that all of the capital cost per unit energy values are greater than or equal to those values that don't account for the roundtrip efficiency. Those storage technologies with low roundtrip efficiencies such as hydrogen show a significant increase in the adjusted capital cost per unit energy on the ordinate while CTES, pumped hydroelectric, and lithium-ion battery storage technologies are not affected significantly.

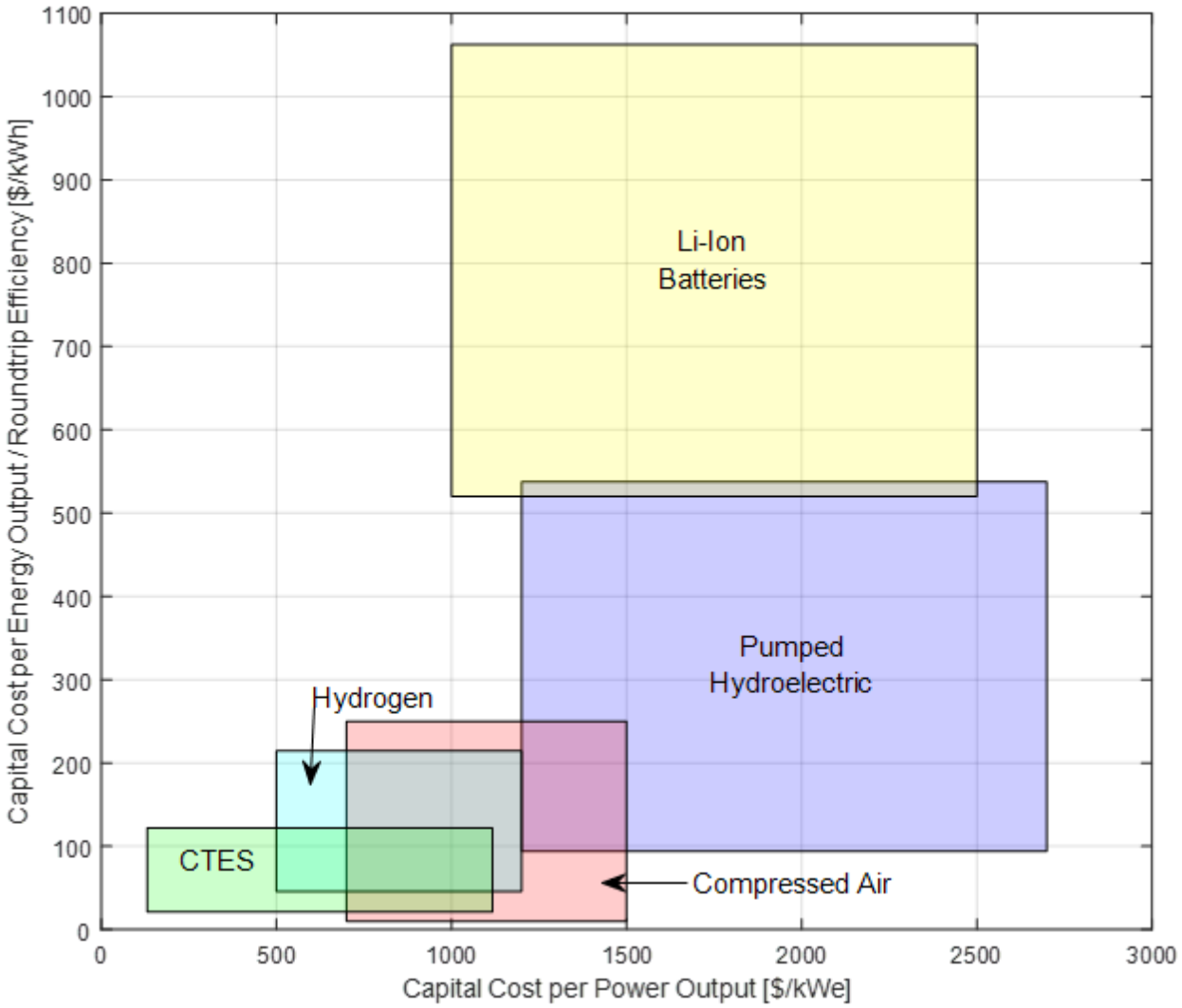

Figure 5-34. Comparison of energy storage technology capital cost normalized by roundtrip efficiency (data from Pierpoint 2016, Schoenung 2011, Tesla Motors 2016)

Siting considerations are a significant factor in selecting storage technologies and the siting flexibility for lithium-ion battery installations is one reason that they have been gaining in popularity (Pierpoint 2016). As seen in Figure 5-33, pumped hydroelectric, compressed air, and hydrogen energy storage are all relatively inexpensive. While compressed air and hydrogen can be stored in above-ground tanks, the most cost-effective and largest scale installations use underground storage features which must be able to withstand cyclic pressure changes over time. For both of these two technologies as well as pumped hydroelectric storage, a specific topography

is required: underground salt formations or aquifers and varied elevation, respectively. These topographical features are not always located adjacent to the largest population centers where energy storage provides the greatest value.

Siting for CTES systems is not as limited as those technologies that require specific topography, but it is also not as flexible as it is for lithium-ion battery systems. Close proximity to buildings with large cooling loads is desirable for the best economies of scale. Fortunately, the ability to shift electric demand is most valuable in close proximity to the large cooling loads associated with high population density and electric demand due to air-conditioning loads. The potential number of sites is limited by the total number of buildings with cooling systems. The upper bound for the amount of electricity that could be shifted for all cooling loads is given in Figure 5-30 through Figure 5-32 for the NYISO, CAISO, and ERCOT regions.

Some advantages and disadvantages of the storage technologies presented are listed in the last two columns of Table 5-5. One of the differentiating advantages relates to system scale. While pumped hydroelectric, compressed air, and hydrogen energy storage are all significantly more cost-effective when implemented on a large scale, CTES is commonly implemented on a small scale for a single school or a larger scale for a campus district system. While there are cost differences between the system capacities, smaller systems can be made up of several modular, standard units which reduces the engineering cost for the system. Lithium-ion batteries are the most flexible in terms of system scale, but larger systems require that more attention be paid to reactivity and flammability hazards.

The disadvantages vary, but three relate to negative externalities associated with the technology. Pumped hydroelectric energy storage projects result in negative environmental impacts on the area flooded by reservoirs. For compressed air energy storage, all designs currently

in use require natural gas in the storage discharge process which results in the emission of greenhouse gases. With daily cycling, lithium-ion batteries last approximately 14 years or 5,000 cycles at which point the storage capacity is estimated to be 80% of the original capacity (International Renewable Energy Agency 2015). While lifespans vary for the other storage technologies, all have longer lifetimes than lithium-ion batteries. CTES and pumped hydroelectric energy storage systems in particular have demonstrated their ability to function for decades with little longitudinal degradation in their performance.

5.7 Value of Energy Storage to the Grid

The capital cost per unit of power output presented for CTES in Section 5.6 is relatively consistent with a published range from the Electric Power Research Institute (EPRI). The range calculated through this research is $130 to $1,120/kWe while the published range is $330 to $1,350/kWe (EPRI 2008). The average annual electricity market value of energy storage is $72/kWe according to a compilation of several studies (NREL 2013b).

As a method of verifying the value of energy storage, there are several utilities providing upfront financial incentives for the installation of CTES systems. The incentives considered here range from $875/kWe for Pacific Gas and Electric and Southern California Edison in California down to $350/kWe for Austin Energy in Texas (PG&E 2015; Austin Energy 2017). Both Florida Power and Light in Florida as well as Consolidated Edison in New York offer $600/kWe (FPL 2015; Con Edison and NYSERDA 2014). These incentives often come with a cap of 50% of the total system cost. To compare these values to the annual $72/kWe value above, a simple payback calculation shows that the utilities recover the incentive cost in approximately 5 to 12 years. This range is well below the expected lifetime of the thermal storage system.

The time period covered by the energy storage value studies extends from 1997 to 2011, so the applicable level of grid penetration by solar and wind power is at most 5% (EIA 2017a). Due to the intermittent nature of these two renewable resources, it is expected that with higher grid penetration levels, the economic value of energy storage would increase. Another study performed by NREL investigates the impact of wind and solar generation on the value of energy storage (NREL 2013a). A case study in Colorado shows that increasing the wind and solar penetration level from 20% to 50% increased the value of energy storage by approximately 35%. While there are many factors that affect the local value, the previous annual estimate of $72/kWe would increase to $97/kWe under these conditions. While a wind and solar penetration level of 50% seems high, both New York and California have codified goals of 50% renewable generation by the year 2030. The NREL study considers a baseline wind and solar penetration level of 20% which is well above the level (5% or lower) at the time of studies done to determine the value of energy storage. While energy storage will generally become increasingly valuable with increasing wind and solar penetration, storage which is capable of directly responding to the local resource profiles will be more valuable to the utility systems.

5.8 Policy Recommendations

While not as widespread as state regulatory mandates to increase renewable energy production, several states have or are currently considering energy storage policies or programs (Maloney 2017). This section focuses specifically on the CAISO and ERCOT regions. These two locations were chosen to demonstrate the impact potential of energy storage as a consequence of the large populations and electric demand coverage as well as their high level of wind and solar resources.

Under Assembly Bill 2514, in 2013 the California Public Utilities Commission (CPUC) established an energy storage procurement target for the state's three investor-owned utilities. By the year 2020, the utilities are mandated to procure a combined total of 1,325 MW of both utility-scale and distributed energy storage (CPUC 2013). The stated reasons for adopting this energy storage goal are to achieve peak demand reduction, improved grid reliability, deferment of transmission and distribution investments, increased renewable energy integration, and reductions in associated greenhouse gas emissions. Additionally, Senate Bill 700 was sent to the California State Assembly after passing in the State Senate and it is scheduled to be debated in 2018 (Andorka 2017). In contrast to Assembly Bill 2514, this energy storage bill would provide rebates to end-use customers who install their own energy storage systems. Because the program is specified to run for ten years, the rebates are intended to drive installation of energy storage to achieve the above-mentioned benefits while also stabilizing energy storage system costs.

The legislative landscape for energy storage in Texas is less ambitious, but some legislation has been passed to improve energy storage economics at the utility scale. In 2011, Texas Senate Bill 943 served to classify energy storage installations as "generation assets" (Texas Legislature 2011). This classification gives the storage assets the right to interconnect, obtain transmission service, and to sell electricity in the wholesale market. The improved economics come from assigning the interconnection costs of the storage systems to the transmission companies as opposed to the power generation companies installing the energy storage facilities (NREL 2014).

One way to meet energy storage procurement targets is to incentivize the installation of energy storage systems. An example of a recently implemented energy storage incentive program is in Orange County, California. Southern California Edison (SCE) has contracted more than 250 MW of various forms of energy storage in order to meet the target established by California Public

Utilities Commission policy (CPUC 2013). Approximately 25 MW of the storage capacity is in the form of cool thermal energy storage (Guess 2017). In this case, the decision was made to deploy a large number of small capacity unitary ice CTES units rather than fewer higher capacity CTES systems that utilize larger-scale ice storage or stratified chilled water storage tanks of the type considered in this research. SCE is purchasing the unitary ice storage systems for installation on the roofs of selected commercial buildings. In exchange for the thermal storage equipment and installation, the end-use customer allows the utility to actually control the storage system, presumably using a control strategy that is similar to the *Renewable Control* strategy. The unitary CTES systems can be controlled so that they charge during the peak solar production period in the middle of the day or, with significant wind power generation, during the off-peak periods at night. They would then be discharged in order to cool the buildings during the peak demand hours that occur in the late afternoon or evening. While operation of the CTES units will allow SCE to level the impact of intermittent renewable generation and reduce its peak electric demand, it will also reduce the end-customers' electricity bills. Energy charges will be reduced since a greater portion of the electricity used to cool the buildings will be consumed outside of the peak hours and any demand charges will be reduced along with the peak chilling system electric demand. One significant challenge for this type of program is the large number of units required and the associated overhead to operate the units in order to achieve meaningful impact. Installing larger ice or chilled water storage systems provides greater storage capacity at each customer site which would maximize the ratio of the storage benefit to the program overhead cost.

Policies that shift the capital expense burden from end-customers to utilities are highly recommended when they reduce or eliminate barriers to entry for new CTES installations. While CTES systems controlled by the utility may be desirable from a utility perspective (as it aims to

coordinate load management associated with intermittent renewable generation sources), the end-customer is saddled with the risk that building cooling loads may not be met. In order for end-customers to adopt CTES technology, they should have the option of controlling their own systems. To encourage control strategies that benefit the utility, hourly day-ahead electricity rate structures should be implemented which greatly penalize the end-customer for chiller electricity consumption during periods of low renewable resource availability and high aggregate electric demand. This type of policy and associated rate structure will provide useful distributed storage capacity to the utility that will be widely adopted due to low upfront costs and the ability to maintain system control by the end-customer.

The increasing need for energy storage systems for both peak shaving and intermittent renewables integration has been acknowledged by both utilities and the market. Market research estimates 2017 energy storage installations at 6 GW and predicts that by 2022 the annual installed capacity will reach more than 40 GW (Energy Storage Association 2017). This is up from just 0.34 GW installed globally in 2013. Lithium-ion battery storage has received significant publicity and the term is sometimes used synonymously with the term “energy storage.” While costs continue to decline, the issues of a relatively short life cycle and end-of-life disposal are significant and may not be fully understood or addressed until they are experienced on a large scale. In addition, increasing demand for lithium-ion batteries in electric and hybrid vehicles will increase demand and, as a result, their costs. Meeting energy storage needs will require implementation of various technologies at all scales. Several energy storage technologies can succeed simultaneously for different applications similar to the example of solar power being generated on a utility scale by concentrating solar power plants and on a smaller scale by photovoltaics.

The only two distributed energy storage technologies considered in Section 5.6 are the two that currently have any significant market presence, lithium-ion batteries and cool thermal energy storage. Considering the system cost and life expectancy advantages that CTES has over lithium-ion batteries, it is logical that policies emphasizing the deployment of CTES should be implemented before lithium-ion battery systems are considered as the primary method to integrate renewables into the electric grid. As states and utilities are developing energy storage policies and incentive programs, explicit inclusion of this technology makes sense from all perspectives.

6 CONCLUSIONS AND RECOMMENDATIONS FOR FUTURE WORK

6.1 Conclusions

Cool thermal energy storage control strategies are presented that have the objective of increasing the penetration of renewable energy resources while minimizing their impact on the grid as well as reducing operating costs. The *Renewable Control* strategy seeks to maximize the proportion of chilling system electricity consumption available from renewable energy resources and the *Cost Control* strategy seeks to minimize the electricity costs associated with chiller operation for building space conditioning. These control strategies were implemented in annual simulations for two different building types covering four geographic regions. Each combination of building type and location were simulated using both stratified chilled water and internal-melt ice CTES systems. As a baseline comparison, simulations were also run for direct chiller systems without storage. The two metrics used to evaluate system performance for these parametric studies are the total 20-year cost and the fraction of the chiller energy met by the renewable resource.

The cost metric is more likely to determine whether the storage systems and the associated control strategies are implemented are not. The results of this research show that reduction of

20-year cost is possible with either type of storage control strategy over a wide range of system parameters compared to equivalent systems without storage. Not surprisingly, there are increased costs associated with a control strategy that has the explicit objective of utilizing the renewable resource (*Renewable Control*) compared to one that aims to reduce operating costs (*Cost Control*). This observation indicates that the time-of-use rate structure applied does not incentivize electricity consumption during periods of high renewable resource availability and vice versa.

Like *Cost Control*, the *Model Predictive Control* strategy aims to minimize electricity costs, but does so more effectively by utilizing optimization algorithms. Simulations run using this strategy showed significant savings are possible through true optimization and these savings are positively correlated with the variability of the control inputs. Real-time and day-ahead pricing structures that more accurately link cost to renewable energy utilization are particularly volatile and this work shows that it is important to use a dynamic optimization technique like *Model Predictive Control* in order to take advantage of this cost structure.

The vast majority of existing chilled water-based building cooling systems do not have any CTES component. Both new facilities and existing facilities can be fitted or retrofitted with CTES systems. In most cases, the life-cycle cost savings associated with the CTES system can provide sufficient financial incentive to install a system and several utility systems supplement this incentive with upfront load-shifting incentives. In order to provide additional incentive to operate with the objective of maximizing renewable resource use, electric utilities should provide further upfront incentives and/or special electricity rate structures to encourage greater penetration of CTES systems utilizing this mode of operation.

The most important outcome of this research is demonstrating that the portion of the chiller energy met by renewable generation can be significantly improved by implementing a control

strategy that aims to better utilize the renewable resource. Further improvements can be realized by implementing *Model Predictive Control* strategies. Buildings equipped with CTES and appropriate chilling system control strategies enabled an increase in renewable energy utilization that ranged from 10% to more than 50% compared to non-storage cases with very little increase in operating cost. Further improvements can be achieved as the chiller system and cool thermal energy storage system capacities are increased beyond their minimums, but this improvement comes at substantial added cost. In practice, the best operation point is one that keeps the equipment sizes at close to a minimum, but aims to utilize the renewable resource using system parameters that accommodate the renewable resource profile and the storage technology. This point provides benefits to the utility system in terms of utilizing the renewable resource, but at little added 20-year cost.

To demonstrate this point with an example, consider the California region with the solar resource that is the primary driver for the duck curve. Table 6-1 shows the chiller system utilization of the solar and wind resources as well as comparisons between a system without storage and one operating using the *Renewable Control* strategy. From this comparison, a simple payback time period has been calculated. Each system has a solar PV or wind turbine system installed with a rating equal to the full load chiller power without storage. This example shows little variation in system fixed costs along with annual operating cost savings with a storage system, so the simple payback time period is very short. Additionally, the renewable resource has been utilized to meet a greater fraction of the chiller energy. This is just one example, but the benefits are similar across locations, building types, and CTES technologies.

Table 6-1. Example *Renewable Control* results for California

Renew-able Resource	Building Type	Storage Type	Chiller Energy Met by Solar [-]		First Cost [$MM]		Annual Operating Cost [$MM]		Simple Payback [months]
			No-Storage	Storage	No-Storage	Storage	No-Storage	Storage	
Solar	School	Ice	0.70	0.87	1.13	1.14	0.088	-0.026	< 2
	Large Office	Chilled Water	0.52	0.85	3.35	3.72	0.40	-0.079	9
Wind	School	Ice	0.65	0.93	0.90	0.91	0.026	-0.089	1
	Large Office	Chilled Water	0.61	0.88	2.72	3.08	0.22	-0.42	7

6.2 Recommendations for Future Work

The control strategies considered in this research assume that the cooling load profile is known for the remainder of the current day and that equipment is capable of responding quickly to changes in the renewable power level. These assumptions represent the limit of the practically achievable benefit that can be realized with the CTES systems. Implementing simulations with less-than-perfect knowledge of the cooling load and chiller ambient conditions would be more realistic for implementation in actual facilities. For the *Model Predictive Control* strategy, imperfect inputs require a significant increase in computational power. The simulations run for this research are performed with full knowledge of the daily input data and the system is effectively reset every 24 hours by requiring that the storage system be full at a particular time of day. As a result, the control strategy runs the optimization algorithm only once per twenty-four-hour period. Using forecasted data, the optimization should be updated in each timestep requiring increased computational power and time. With sub-hour timestep lengths, it is important that the optimization be completed well within that timeframe so that the next control decision can be

implemented. With complicated combinations of equipment in campus district systems, linearized models like the chiller model detailed in Section 2.5.5 are necessary. Longer timesteps along with more accurate system models could be implemented, but there would be a trade-off in the *Model Predictive Control* savings. There may also be an occupant comfort penalty if cooling loads are not met throughout the duration of the longer timestep.

The *Model Predictive Control* strategy employed in this research considers only a cost minimization objective. While increasingly variable electricity rate structures were applied in order to identify the added value of dynamic control with more variable inputs, simulations should be performed which explicitly aim to increase the utilization wind and solar resources. For many locations, wind and solar power forecasts are produced continually for the purpose of integrating this power into the grid (Hodge 2016). These power forecasts can be used as inputs to the *Model Predictive Control* strategy along with weather and cooling load forecasts. Particularly for wind power, the expected benefits of dynamic control over traditional control methods are significant.

The *Model Predictive Control* simulations presented in this dissertation consider electricity rates with energy charges only. Demand charges should be considered and they should be incorporated along with an expansion of the system definition. The current simulations consider only the chiller plant electric consumption and treat other electrical loads such as lighting and plug loads as outside of the scope. Because these loads are also simulated in the Commfercial Reference Building simulations, they can be input into the *Model Predictive Control* strategy with an objective to minimize the total electricity cost including demand charges.

The *Cost Control* and *Renewable Control* strategies in this research utilize a constant set of control parameters throughout the simulation year. Because the locations analyzed have three cooling seasons – spring, summer, and fall, improved performance may result from using more

than one set of parameters. This could be in the form of a separate set of parameters for each of the three cooling seasons or just two, one for the spring and fall and another set for the summer. One example of a potential benefit is allowing the chiller system to operate at lower part-load ratios during the summer months when wind plant capacity factors are generally at their lowest as shown in Figure 6-1. If the chiller is constrained to operate only at full load in the spring when the wind resource is generally strong, the annual simulation may be able to meet a greater portion of its chiller energy consumption by wind power if the chiller system is allowed to operate with part-load ratios of less than one. Varying control parameters would also be useful for time-of-use electricity rate structures that vary significantly by season.

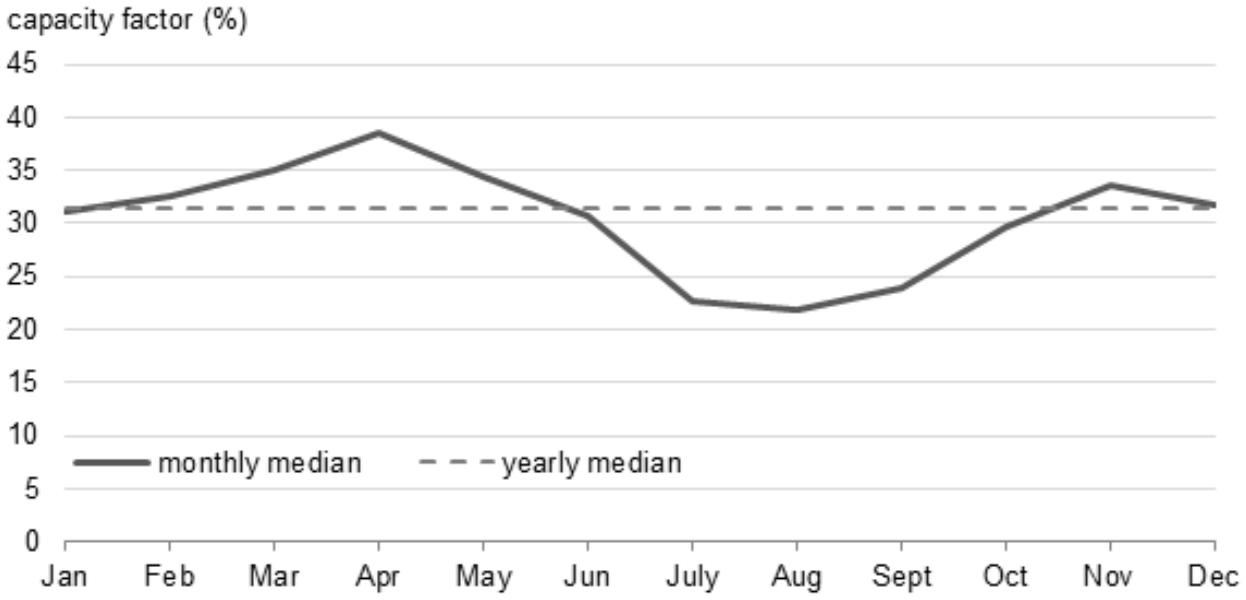

Figure 6-1. U.S. monthly median wind plant capacity factors for 2001-2013 (EIA 2015)

Another recommendation regarding the control parameters is related to the constraint that the CTES system be fully recharged at least once in each twenty-four-hour period. This constraint has been adopted in this research in acknowledgement of practical considerations of CTES system operation. Traditionally, because future cooling loads are always uncertain and tiered electricity

rate structures reset on a daily basis, storage systems are recharged each day. In consideration of the system operation objective of maximizing renewable energy utilization in addition to the cost minimization objective, relaxation of this constraint should be considered. For example, with the *Model Predictive Control* strategy, the recharging constraint could be fully relaxed with sufficient computational power and oversized storage and chiller system capacities. If the control time horizon is extended to several days and the optimization is performed for that period regardless of the current time, the CTES system state-of-charge could be continuously optimized. In this case, the CTES system would not explicitly require a full recharge although full recharges would be necessary to meet the cooling loads during periods when they are significant. With forecasted input data, there should be constraints in place to ensure that an under-predicted cooling load doesn't result in future cooling loads being unmet.

None of the control strategies implemented in this research take into account the cost of added maintenance due to repeated idling and activation of the chiller system in successive ten-minute timesteps. They also do not consider the time required to initiate a startup (and shut down) sequence for chillers. Ideally, the simulations should restrict individual chiller from switching on and off more than a few times per day. For the *Model Predictive Control* strategy, this limitation can be achieved by adding an artificial cost penalty that is a function of the frequency of the equipment start-up and shut-down. This penalty forces the optimization algorithm to favor control trajectories that switch chiller system operation infrequently. The appropriate function and magnitude for the penalty must be determined carefully so that it does not end up selecting an overly conservative trajectory at the expense of the optimization objective. It also must serve its purpose of representing the added cost associated with frequent chiller system idling and re-activation.

All simulations performed for this research utilize standardized Commercial Reference Building cooling loads, standard chiller system performance curves, and most use Typical Meteorological Year weather data. While these resources are ideal for this type of research due to their standardized format and public availability, actual buildings should be used for simulation and eventual implementation. An existing building that has a chiller system installed, has available cooling load data, and is in need of a retrofit would be ideal. This building would have a more accurate baseline for the energy consumption (as a function of weather, day of the week, and building occupancy) in the no-storage system case and a CTES system could be designed and installed to run with any of the three proposed control strategies. This would also provide experimental data regarding the influence of losses not considered in the simulations.

7 REFERENCES

Air-Conditioning Heating and Refrigeration Institute (AHRI), 2011. *Standard for Performance Rating Of Water-Chilling and Heat Pump Water-Heating Packages Using the Vapor Compression Cycle*,

Alternative Energy Institute (AEI), 2012. Wind Data: White Deer, TX. Available at: http://www.windenergy.org/datasites/ [Accessed June 1, 2015].

American Society of Heating Refrigerating and Air-Conditioning Engineers (ASHRAE), 2013. Standard 90.1-2013- Energy Standard for Buildings Except Low-Rise Residential Buildings.

Andorka, F., 2017. California pushes forward with storage support. *PV Magazine*. Available at: https://pv-magazine-usa.com/2017/06/02/california-pushes-forward-with-storage-support-read-the-bill-here/ [Accessed June 14, 2017].

Austin Energy, 2017. Austin Energy Commercial Rebate Offerings. Available at: http://powersaver.austinenergy.com/wps/wcm/connect/aebd1c3a-f26a-4a72-acbf-533c59e9c4ee/FINAL_DSMCOMRebateList2928_0217.pdf?MOD=AJPERES&CONVERT_TO=url&CACHEID=aebd1c3a-f26a-4a72-acbf-533c59e9c4ee [Accessed February 23, 2017].

Big Dog Solar Energy, 2016. Grid-Tie Solar Power Systems. Available at: http://www.bigdogsolar.com/grid-tie-solar-systems/ [Accessed January 3, 2017].

Bowker, D., 2016. Douglas Bowker Motion Graphics. Available at: https://www.douglasbowker-motiongraphics.com/ [Accessed December 21, 2016].

Braun, J.E., Klein, S.A. & Mitchell, J.W., 1989. Effectiveness Models for Cooling Towers and Cooling Coils. *ASHRAE Transactions*, 95(2), pp.164–174.

California Energy Commission (CEC), 2016. California Renewables Portfolio Standard. Available at: http://www.energy.ca.gov/portfolio/ [Accessed November 21, 2016].

California Energy Commission (CEC), 2012. Nonresidential Alternative Calculation Method Reference Manual. Available at: http://www.energy.ca.gov/title24/2013standards/implementation/documents/2013_nonres_ACM_reference/2012-10-26_2013_Nonres_ACM_Refernce_manual.pdf.

California Independent System Operator (CAISO), 2017. California ISO - Historical hourly load data from EMS. Available at: http://www.caiso.com/planning/Pages/ReliabilityRequirements/Default.aspx#Historical [Accessed June 1, 2017].

California Independent System Operator (CAISO), 2013. What the duck curve tells us about managing a green grid. , CommPR/HS/.

California Public Utilities Commission (CPUC), 2013. CPUC Sets Energy Storage Goals for Utilities. , (Docket #: R.10-12-007). Available at: http://docs.cpuc.ca.gov/PublishedDocs/Published/G000/M079/K171/79171502.PDF [Accessed June 8, 2017].

Chinneck, J.W., 2015. *Practical Optimization: a Gentle Introduction*, Available at: http://www.sce.carleton.ca/faculty/chinneck/po.html [Accessed February 19, 2018].

Coin News, 2015. Historical Inflation Rates: 1914-2016. Available at: http://www.usinflationcalculator.com/inflation/historical-inflation-rates/ [Accessed January 15, 2017].

Cole, W., Edgar, T. & Novoselac, A., 2012. Use of model predictive control to enhance the flexibility of thermal energy storage cooling systems. *American Control*, pp.2788–2793.

Con Edison and NYSERDA, 2014. Enhanced Load Reduction Program. Available at: https://www.ny-best.org/sites/default/files/type-page/31348/attachments/ConEdison.pdf [Accessed February 23, 2017].

Consolidated Edison Company of New York Inc. (Con Edison), 2017a. conEdison Market Supply Charge Calculator. Available at: https://apps.coned.com/CEMyAccount/csol/MSCcc.aspx [Accessed February 23, 2017].

Consolidated Edison Company of New York Inc. (Con Edison), 2017b. Schedule for Electricity Service. , p.449. Available at: https://www.coned.com/_external/cerates/documents/elecPSC10/SCs.pdf [Accessed February 23, 2017].

Consolidated Edison Company of New York Inc. (Con Edison), 2017c. Schedule for Electricity Service - General Rules. Available at: https://www.coned.com/_external/cerates/documents/elecPSC10/GR25-Forms.pdf [Accessed March 18, 2018].

Consolidated Edison Company of New York Inc. (Con Edison), 2018. Schedule for Electricity Service - Riders. Available at: https://www.coned.com/_external/cerates/documents/elecPSC10/GR24.pdf [Accessed March 19, 2018].

CoServ, 2015. CoServ Electric Rates And Tariff - Time-Of-Use. Available at: http://www.coserv.com/Customer-Service/Electric-Rates-And-Tariff/Time-Of-Use [Accessed June 20, 2015].

Dai, L. et al., 2012. Discrete-Time Model Predictive Control. In *Advances in Discrete Time Systems*. InTech. Available at: http://www.intechopen.com/books/advances-in-discrete-time-systems/discrete-time-model-predictive-control [Accessed March 21, 2017].

Deng, K. et al., 2015. Model Predictive Control of Central Chiller Plant With Thermal Energy Storage Via Dynamic Programming and Mixed-Integer Linear Programming. *IEEE Transactions on Control Systems Technology*, 12(2), pp.565–579.

Duffie, J.A. & Beckman, W.A., 2013. *Solar Engineering of Thermal Processes* 4th ed., Hoboken, New Jersey: Wiley.

Electric Power Research Institute (EPRI), 2008. Thermal energy storage. *Technology Brief - Thermal Energy Storage*, (November).

Electric Reliability Council of Texas (ERCOT), 2017. ERCOT Hourly Load Data Archives. Available at: http://www.ercot.com/gridinfo/load/load_hist [Accessed June 1, 2017].

Energy Information Administration (EIA), 2005. 2003 Commercial Buildings Energy Consumption Survey. Available at: http://www.eia.gov/consumption/commercial/data/2003/ [Accessed May 10, 2015].

Energy Information Administration (EIA), 2017a. Annual Electric Power Industry Report (EIA-861 data file). Available at: https://www.eia.gov/electricity/data/eia861/ [Accessed March 19, 2018].

Energy Information Administration (EIA), 2012. Commercial Buildings Energy Consumption Survey (CBECS) 2012 Data. Available at: http://www.eia.gov/consumption/commercial/data/2012/#b11-b14 [Accessed December 29, 2016].

Energy Information Administration (EIA), 2017b. Electricity data browser - Net generation for all sectors. Available at: http://www.eia.gov/electricity/data/browser/ [Accessed February 23, 2017].

Energy Information Administration (EIA), 2015. Today in Energy Wind generation seasonal patterns vary across the United States. *Today in Energy*. Available at: https://www.eia.gov/todayinenergy/detail.php?id=20112 [Accessed March 16, 2018].

Energy Information Administration (EIA), 2017c. U.S. Electric System Operating Data. Available at: http://www.eia.gov/beta/realtime_grid/?src=l2#/summary/demand?end=20160725&start=20160625 [Accessed January 12, 2017].

Energy Storage Association, 2017. Facts & Figures. Available at: http://energystorage.org/energy-storage/facts-figures [Accessed June 20, 2017].

Federal Energy Regulatory Commission (FERC), 2015. Regional Transmission Organizations (RTO)/Independent System Operators (ISO). Available at: https://www.ferc.gov/industries/electric/indus-act/rto.asp [Accessed June 15, 2015].

Federal Reserve Bank of St. Louis, 2016. 10-Year Treasury Constant Maturity Rate. *Federal Reserve Economic Data*. Available at: https://fred.stlouisfed.org/series/DGS10 [Accessed January 15, 2017].

Florida Power & Light Company (FPL), 2015. Business HVAC Program Tables. Available at: https://www.fpl.com/business/pdf/SMB-tables.pdf [Accessed February 23, 2017].

Gençer, E. & Agrawal, R., 2015. A commentary on the US policies for efficient large scale renewable energy storage systems: Focus on carbon storage cycles. *Energy Policy*, 88, pp.477–484.

Guess, M., 2017. California utility augments 1,800 air conditioning units with "ice battery." *Ars Technica*. Available at: https://arstechnica.com/business/2017/05/ice-batteries-commissioned-by-utility-will-cool-california-businesses/.

Hamon Group, 2016. Induced draft cooling towers. Available at: http://www.hamon.com/en/cooling-systems/wet-cooling-systems/mechanical-draft-cooling-towers/induced-draft-cooling-towers/ [Accessed January 9, 2017].

Hartman, L., 2017. Top 10 Things You Didn't Know About Offshore Wind Energy. *Wind Energy Technologies Office*. Available at: https://www.energy.gov/eere/wind/articles/top-10-things-you-didn-t-know-about-offshore-wind-energy [Accessed April 2, 2018].

High-Schools.com, 2013. High Schools Data. Available at: http://high-schools.com/ [Accessed January 12, 2017].

Hodge, B.-M., 2016. An Introduction to Wind and Solar Power Forecasting. *Greening the Grid*. Available at: http://greeningthegrid.org/trainings-1/presentation-an-introduction-to-wind-and-solar-power-forecasting-1 [Accessed March 19, 2018].

International Renewable Energy Agency, 2015. *Battery Storage for Renewables: Market Status and Technology Outlook*, Available at: http://www.irena.org/documentdownloads/publications/irena_battery_storage_report_2015.pdf [Accessed July 6, 2017].

Iterson, V., 2009. Process Cooling. Available at: http://web.stanford.edu/group/narratives/classes/08-09/CEE215/ReferenceLibrary/CoolingTowers/Cooling Tower Analysis.doc [Accessed July 12, 2016].

Kim, S.H., 2013. Building demand-side control using thermal energy storage under uncertainty: An adaptive Multiple Model-based Predictive Control (MMPC) approach. *Building and Environment*, 67, pp.111–128. Available at: http://ac.els-cdn.com.ezproxy.library.wisc.edu/S0360132313001443/1-s2.0-S0360132313001443-

main.pdf?_tid=b2f371b0-0ff8-11e7-8f7f-00000aacb360&acdnat=1490294828_06e43ca1b6ee9eb957293d3aca43da7d [Accessed March 23, 2017].

Ma, Y. et al., 2009. Model Predictive Control of Thermal Energy Storage in Building Cooling Systems. *48th IEEE Conference on Decision and Control and 28th Chinese Control Conference, Shanghai, P.R.China, Dec. 16-18*, pp.392–397.

Maloney, P., 2017. Maryland, Hawaii turn to storage incentives as state markets gain momentum. *Utility Dive*. Available at: http://www.utilitydive.com/news/maryland-hawaii-turn-to-storage-incentives-as-state-markets-gain-momentum/444261/.

MathWorks, 2018. Solve linear programming problems - MATLAB linprog. Available at: https://www.mathworks.com/help/optim/ug/linprog.html?s_tid=gn_loc_drop [Accessed February 26, 2018].

Midcontinent Independent System Operator (MISO), 2016. MISO Market Reports. Available at: https://www.misoenergy.org/Library/MarketReports/Pages/MarketReports.aspx [Accessed June 14, 2016].

Myers, K.S., Klein, S.A. & Reindl, D.T., 2010. Assessment of high penetration of solar photovoltaics in Wisconsin. *Energy Policy*, 38(11), pp.7338–7345.

National Conference of State Legislatures, 2016. State Net Metering Policies. Available at: http://www.ncsl.org/research/energy/net-metering-policy-overview-and-state-legislative-updates.aspx [Accessed January 3, 2017].

National Renewable Energy Laboratory (NREL), 2014. A Survey of State Policies to Support Utility-Scale and Distributed-Energy Storage. , (NREL/BR-7A40-62726). Available at: http://www.nrel.gov/docs/fy14osti/62726.pdf [Accessed June 6, 2017].

National Renewable Energy Laboratory (NREL), 2010. Eastern and Western Wind Integration Data Sets. Available at: http://www.nrel.gov/grid/eastern-western-wind-data.html [Accessed November 21, 2016].

National Renewable Energy Laboratory (NREL), 2011. NREL: Dynamic Maps, GIS Data, and Analysis Tools - Maps. Available at: http://www.nrel.gov/gis/maps.html [Accessed May 20, 2015].

National Renewable Energy Laboratory (NREL), 2015. System Advisor Model. Available at: https://sam.nrel.gov/download.

National Renewable Energy Laboratory (NREL), 2013a. The Impact of Wind and Solar on the Value of Energy Storage. Available at: http://www.nrel.gov/docs/fy14osti/60568.pdf [Accessed February 23, 2017].

National Renewable Energy Laboratory (NREL), 2013b. The Value of Energy Storage for Grid Applications. , (NREL/TP-6A20-58465). Available at: http://www.nrel.gov/docs/fy13osti/58465.pdf [Accessed December 10, 2016].

National Renewable Energy Laboratory (NREL), 2008. *Users Manual for TMY3 Data Sets*, Available at: http://www.nrel.gov/docs/fy08osti/43156.pdf [Accessed November 20, 2016].

National Renewable Energy Laboratory (NREL), 2012. Using Utility Load Data to Estimate Demand for Space Cooling and Potential for Shiftable Loads. Available at: http://www.nrel.gov/docs/fy12osti/54509.pdf.

New York Independent System Operator (NYISO), 2017a. NYISO Installed Capacity Strip Auction Summary. Available at: http://icap.nyiso.com/ucap/public/auc_view_strip_detail.do [Accessed February 25, 2017].

New York Independent System Operator (NYISO), 2017b. NYISO Markets & Operations -

Market Data - Pricing Data. Available at: http://www.nyiso.com/public/markets_operations/market_data/pricing_data/index.jsp [Accessed December 14, 2017].

Oak Ridge National Laboratory, 1997. Energy and Global Warming Impacts of HFC Refrigerants and Emerging Technologies.

Pacific Gas and Electric Company (PG&E), 2015. Thermal Energy Storage Program. Available at: http://www.pge.com/includes/docs/pdfs/mybusiness/energysavingsrebates/demandresponse/pls/TESFactsheet.pdf [Accessed February 26, 2017].

Pierpoint, L.M., 2016. Harnessing electricity storage for systems with intermittent sources of power: Policy and R&D needs. *Energy Policy*, 96, pp.751–757.

Reindl, D.T., Beckman, W.A. & Duffie, J.A., 1990. Evaluation of Hourly Tilted Surface Radiation Models. *Solar Energy*, 45(1), pp.9–17.

Reindl, D.T., Knebel, D.E. & Gansler, R.A., 1995. Characterizing the Marginal Basis Source Energy and Emissions Associated with Comfort Cooling Systems. *ASHRAE Transactions*, 101(1), pp.1353–1363.

RSMeans, 2015. *RSMeans 2016 Mechanical Cost Data*, Rockland, MA: RSMeans Construction Publishers.

Sandia National Laboratories, 2016. DOE Global Energy Storage Database. Available at: https://www.energystorageexchange.org/projects/data_visualization [Accessed May 31, 2017].

Schoenung, S., 2011. *Economic Analysis of Large-Scale Hydrogen Storage for Renewable Utility Applications*, Available at: http://prod.sandia.gov/techlib/access-control.cgi/2011/114845.pdf [Accessed June 15, 2017].

Simpson, W.M. & Sherwood, T.K., 1946. Performance of Small Mechanical Draft Cooling Towers. *Journal of the ASRE*, 52(6), pp.535-543-576.

Spiller, B., 2015. All Electricity is Not Priced Equally: Time-Variant Pricing 101. Available at: http://blogs.edf.org/energyexchange/2015/01/27/all-electricity-is-not-priced-equally-time-variant-pricing-101/ [Accessed March 19, 2018].

Stadler, W., 1988. *Multicriteria Optimization in Engineering and in the Sciences*, New York: Springer.

Tesla Motors, 2016. Build Your Powerpack Energy Storage Solution. Available at: https://www.tesla.com/powerpack/design#/ [Accessed October 19, 2016].

Texas Legislature, 2011. Senate Bill 943 Summary. Available at: http://www.capitol.state.tx.us/billlookup/BillSummary.aspx?LegSess=82R&Bill=SB943 [Accessed June 30, 2017].

Thermal Energy System Specialists LLC (TESS), 2016. TRNSYS: Transient System Simulation Software.

Trane, 1990. How Much Ice? , 19(1), pp.1–3. Available at: https://www.trane.com/content/dam/Trane/Commercial/global/products-systems/education-training/engineers-newsletters/waterside-design/enews19_1.pdf.

Trane, 2016. Series R Helical RTAC. Available at: http://www.trane.com/commercial/north-america/us/en/products-systems/equipment/chillers/air-cooled-chillers/seriesr-rtac.html [Accessed December 29, 2016].

United States Department of Energy (USDOE), 2016. 2015 Wind Technologies Market Report. Available at: https://energy.gov/sites/prod/files/2016/08/f33/2015-Wind-Technologies-

Market-Report-08162016.pdf [Accessed December 22, 2016].

United States Department of Energy (USDOE), 2012. Commercial Reference Buildings. Available at: http://energy.gov/eere/buildings/commercial-reference-buildings [Accessed June 20, 2015].

United States Department of Energy (USDOE), 2010. EnergyPlus Engineering Reference: The Reference to EnergyPlus Calculations. Available at: https://energyplus.net/sites/default/files/pdfs_v8.3.0/EngineeringReference.pdf.

United States Department of Energy (USDOE), 2015. Photovoltaic System Pricing Trends: Historical, Recent, and Near-Term Projections. , NREL/PR-6A. Available at: https://emp.lbl.gov/sites/all/files/pv_system_pricing_trends_presentation_0.pdf.

United States Department of Energy (USDOE), 2011. *U.S. Department of Energy Commercial Reference Building Models of the National Building Stock*, Available at: http://www.nrel.gov/docs/fy11osti/46861.pdf [Accessed November 22, 2015].

Verrilli, F. et al., 2016. Model Predictive Control-Based Optimal Operations of District Heating System With Thermal Energy Storage and Flexible Loads. , pp.1–11.

Wenzel, M.J. et al., 2016. Autonomous Optimization and Control for Central Plants with Energy Storage. In *International High Performance Buildings Conference*. Available at: http://docs.lib.purdue.edu/cgi/viewcontent.cgi?article=1213&context=ihpbc [Accessed April 10, 2017].

Wenzel, M.J. et al., 2014. Model Predictive Control for Central Plant Optimization with Thermal Energy Storage. In *International High Performance Buildings Conference*. Available at: http://docs.lib.purdue.edu/cgi/viewcontent.cgi?article=1121&context=ihpbc [Accessed April 10, 2017].

White Box Technologies, 2017. Weather Data for Energy Calculations - Historical Files. Available at: http://weather.whiteboxtechnologies.com/map-hist?k=uscan [Accessed March 2, 2018].

8 APPENDIX: MATLAB THERMAL STORAGE SIMULATION PROGRAM CODE

The MATLAB program code used for annual simulations and the associated functions are provided here.

```
function [TotalCost,ChillerMetbyRenewable] = ThermalStorage(x)
%This function performs an annual simulation of a thermal storage system and
%includes Renewable Control and Cost Control Strategies for Cool Thermal
%Energy Storage

%Input x is a cell and should be surrounded by { }
ControlStrategy=x{1};               % 'Renewable' Control or 'Cost' Control
RenewableFactor=x{2};               % [-] Multiplier of no-storage full-load chiller power
MinLoading=x{3};                    % Chiller minimum unloading ratio (thermal)
Hour=x{4};                          % Time of day by which tank must be recharged (0 to 23)
TankFactor=x{5};                    % Multiplier of partial storage sized tanks
ChillerFactor=x{6};                 % Multiplier of partial storage sized chillers
Resource=x{7};                      % 'Solar' or 'Wind' resource
ChillerType=x{8};                   % 'Water'-cooled (office) or 'Air'-cooled (school)
Location=x{9};                      % 'TX' 'LA' 'MSN' 'NY' (Amarillo, Los Angeles, Madison, New York)
StorageType=x{10};                  % 'CHW' or 'Ice'

%Constant Parameters
MinTemp=15.56;                      % [C] min Tdb for air-cooled performance advantage
N=6;                                % Number of timesteps per Hour
n=20;                               % Timespan for economic analysis (years)
Tset=4.44;                          % [C] chilled water chiller set point
c_gly=3.76;                         % [kJ/kg-K] specific heat capacity of 25% ethylene glycol
Tfr=0;                              % [C] freezing temperature of water for ice storage
Tice=-6.67;                         % [C] set ice-making temperature
Tload=6.67;                         % [C] ice storage load-meeting temperature
mice_each=3.9;                      % [kg/s] rated ice storage mass flow rate per tank (60 GPM)
Ice_Cap=570;                        % [kWh] rated ice storage tank capacity (162 ton-hrs)
Treturn=13.33;                      % [C] ice storage load return temperature

%Normalize renewable energy by full load chiller power for no storage case
if strcmp('Water',ChillerType)==1   % Office building
    if strcmp('TX',Location)==1
```

```
        FullLoadChillerPower=0.955; % 955 kW Chiller power for TX
    elseif strcmp('LA',Location)==1
        FullLoadChillerPower=1.061; % 1,061 kW for LA
    elseif strcmp('MSN',Location)==1
        FullLoadChillerPower=1.101; % 1,101 kW for MSN
    elseif strcmp('NY',Location)==1
        FullLoadChillerPower=1.313; % 1,313 kW for NY
    end
elseif strcmp('Air',ChillerType)==1 % Secondary School
    if strcmp('TX',Location)==1
        FullLoadChillerPower=0.500; % 500 kW for TX
    elseif strcmp('LA',Location)==1
        FullLoadChillerPower=0.383; % 383 kW for LA
    elseif strcmp('MSN',Location)==1
        FullLoadChillerPower=0.457; % 457 kW for MSN
    elseif strcmp('NY',Location)==1
        FullLoadChillerPower=0.583; % 583 kW for NY
    end
end

%Load all of the pre-calculated variables
%Texas
if strcmp('TX',Location)==1
    if strcmp('Air',ChillerType)==1                %Secondary School
        if strcmp('CHW',StorageType)==1            %Stratified chilled water storage
            Tank_Cap=5500*TankFactor;              %[kWh] oversized by TankFactor
            Chiller_Rated=640*ChillerFactor;       %[kW] thermal chiller capacity oversized by ChillerFactor
        elseif strcmp('Ice',StorageType)==1        %Ice storage
            Tank_Cap=3000*TankFactor;
            Chiller_Rated=740*ChillerFactor;
        end
        V2='CoolingLoadTX';CoolingLoad=load('CoolingLoadTX.mat',V2);CoolingLoad=CoolingLoad.(V2);
    elseif strcmp('Water',ChillerType)==1          %Large Office building
        if strcmp('CHW',StorageType)==1
            Tank_Cap=18500*TankFactor;
            Chiller_Rated=2050*ChillerFactor;
        elseif strcmp('Ice',StorageType)==1
            Tank_Cap=27000*TankFactor;
            Chiller_Rated=2350*ChillerFactor;
```

```
        end
        V2='CoolingLoadOfficeTX';
        CoolingLoad=load('CoolingLoadOfficeTX.mat',V2);CoolingLoad=CoolingLoad.(V2);
    end
    if strcmp('Solar',Resource)==1
        V1='SolarPowerTX';
        RenewablePower1=load('SolarPowerTX.mat',V1);RenewablePower1=RenewablePower1.(V1);
        RenewablePower=RenewablePower1.*RenewableFactor.*FullLoadChillerPower;
        %Solar power sized as a multiple of the no-storage full-load chiller power
    elseif strcmp('Wind',Resource)==1
        V1='WindPowerTX';
        RenewablePower1=load('WindPowerTX.mat',V1);RenewablePower1=RenewablePower1.(V1);
        RenewablePower=RenewablePower1.*RenewableFactor.*FullLoadChillerPower;
        %Wind power sized as a multiple of the no-storage full-load chiller power
    end
    V3='TempTX';                                    %Dry-bulb temperature
    Temp=load('TempTX.mat',V3);Temp=Temp.(V3);
    V8='WBTempTX';                                  %Wet-bulb temperature
    Twb=load('WBTempTX.mat',V8);Twb=Twb.(V8);

%Los Angeles
elseif strcmp('LA',Location)==1
    if strcmp('Air',ChillerType)==1
        if strcmp('CHW',StorageType)==1
            Tank_Cap=4490*TankFactor;
            Chiller_Rated=469*ChillerFactor;
        elseif strcmp('Ice',StorageType)==1
            Tank_Cap=3050*TankFactor;
            Chiller_Rated=570*ChillerFactor;
        end
        V2='CoolingLoadLA';
        CoolingLoad=load('CoolingLoadLA.mat',V2);CoolingLoad=CoolingLoad.(V2);
    elseif strcmp('Water',ChillerType)==1
        if strcmp('CHW',StorageType)==1
            Tank_Cap=19200*TankFactor;
            Chiller_Rated=2250*ChillerFactor;
        elseif strcmp('Ice',StorageType)==1
            Tank_Cap=28000*TankFactor;
            Chiller_Rated=2550*ChillerFactor;
```

```
        end
        V2='CoolingLoadOfficeLA';
        CoolingLoad=load('CoolingLoadOfficeLA.mat',V2);CoolingLoad=CoolingLoad.(V2);
    end
    if strcmp('Solar',Resource)==1
        V1='SolarPowerLA';
        RenewablePower1=load('SolarPowerLA.mat',V1);RenewablePower1=RenewablePower1.(V1);
        RenewablePower=RenewablePower1.*RenewableFactor.*FullLoadChillerPower;
    elseif strcmp('Wind',Resource)==1
        V1='WindPowerLA';
        RenewablePower1=load('WindPowerLA.mat',V1);RenewablePower1=RenewablePower1.(V1);
        RenewablePower=RenewablePower1.*RenewableFactor.*FullLoadChillerPower;
    end
    V3='TempLA';
    Temp=load('TempLA.mat',V3);Temp=Temp.(V3);
    V8='WBTempLA';
    Twb=load('WBTempLA.mat',V8);Twb=Twb.(V8);

%Madison
elseif strcmp('MSN',Location)==1
    if strcmp('Air',ChillerType)==1
        if strcmp('CHW',StorageType)==1
            Tank_Cap=5000*TankFactor;
            Chiller_Rated=595*ChillerFactor;
        elseif strcmp('Ice',StorageType)==1
            Tank_Cap=2100*TankFactor;
            Chiller_Rated=650*ChillerFactor;
        end
        V2='CoolingLoadMSN';
        CoolingLoad=load('CoolingLoadMSN.mat',V2);CoolingLoad=CoolingLoad.(V2);
    elseif strcmp('Water',ChillerType)==1
        if strcmp('CHW',StorageType)==1
            Tank_Cap=18900*TankFactor;
            Chiller_Rated=2500*ChillerFactor;
        elseif strcmp('Ice',StorageType)==1
            Tank_Cap=30000*TankFactor;
            Chiller_Rated=2750*ChillerFactor;
        end
        V2='CoolingLoadOfficeMSN';
```

```
        CoolingLoad=load('CoolingLoadOfficeMSN.mat',V2);CoolingLoad=CoolingLoad.(V2);
    end
    if strcmp('Solar',Resource)==1
        V1='SolarPowerMSN';
        RenewablePower1=load('SolarPowerMSN.mat',V1);RenewablePower1=RenewablePower1.(V1);
        RenewablePower=RenewablePower1.*RenewableFactor.*FullLoadChillerPower;
    elseif strcmp('Wind',Resource)==1
        V1='WindPowerMSN';
        RenewablePower1=load('WindPowerMSN.mat',V1);RenewablePower1=RenewablePower1.(V1);
        RenewablePower=RenewablePower1.*RenewableFactor.*FullLoadChillerPower;
    end
    V3='TempMSN';
    Temp=load('TempMSN.mat',V3);Temp=Temp.(V3);
    V8='WBTempMSN';
    Twb=load('WBTempMSN.mat',V8);Twb=Twb.(V8);

%New York
elseif strcmp('NY',Location)==1
    if strcmp('Air',ChillerType)==1
        if strcmp('CHW',StorageType)==1
            Tank_Cap=6300*TankFactor;
            Chiller_Rated=718*ChillerFactor;
        elseif strcmp('Ice',StorageType)==1
            Tank_Cap=2500*TankFactor;
            Chiller_Rated=800*ChillerFactor;
        end
        V2='CoolingLoadNY';
        CoolingLoad=load('CoolingLoadNY.mat',V2);CoolingLoad=CoolingLoad.(V2);
    elseif strcmp('Water',ChillerType)==1
        if strcmp('CHW',StorageType)==1
            Tank_Cap=22000*TankFactor;
            Chiller_Rated=2850*ChillerFactor;
        elseif strcmp('Ice',StorageType)==1
            Tank_Cap=33500*TankFactor;
            Chiller_Rated=3100*ChillerFactor;
        end
        V2='CoolingLoadOfficeNY';
        CoolingLoad=load('CoolingLoadOfficeNY.mat',V2);CoolingLoad=CoolingLoad.(V2);
    end
```

```
    if strcmp('Solar',Resource)==1
        V1='SolarPowerNY';
        RenewablePower1=load('SolarPowerNY.mat',V1);RenewablePower1=RenewablePower1.(V1);
        RenewablePower=RenewablePower1.*RenewableFactor.*FullLoadChillerPower;
    elseif strcmp('Wind',Resource)==1
        V1='WindPowerNY';
        RenewablePower1=load('WindPowerNY.mat',V1);RenewablePower1=RenewablePower1.(V1);
        RenewablePower=RenewablePower1.*RenewableFactor.*FullLoadChillerPower;
    end
    V3='TempNY';
    Temp=load('TempNY.mat',V3);Temp=Temp.(V3);
    V8='WBTempNY';
    Twb=load('WBTempNY.mat',V8);Twb=Twb.(V8);
end

% Energy charges only
% V4='ElectricRate';
% ElectricRate=load('ElectricRate.mat',V4);ElectricRate=ElectricRate.(V4);
% Demand charges
V4='ElectricRateDemand';
ElectricRate=load('ElectricRateDemand.mat',V4);ElectricRate=ElectricRate.(V4);

%Initialize all vectors for computational efficiency
PLR=zeros(8760*N+1,1);COP=zeros(8760*N+1,1);ChillerAdded=zeros(8760*N+1,1);TankCharge=zeros(8760*N+1,1);
PowerUsed=zeros(8760*N+1,1);COP_Calc=zeros(8760*N+1,1);RenewablePowerUsed=zeros(8760*N+1,1);
OperatingCost=zeros(8760*N+1,1);OperationCode=zeros(8760*N+1,1);Qice=zeros(8760*N+1,1);
Qchiller=zeros(8760*N+1,1);Qicemax=zeros(8760*N+1,1);Tin=-6.67.*ones(8760*N+1,1);
PLR_Int=zeros(8760*N+1,1);ChillerCap=zeros(8760*N+1,1);ChillerCapLoad=zeros(8760*N+1,1);
FullLoadEffIce=zeros(8760*N+1,1);PLRIntLoad=zeros(8760*N+1,1);FullLoadEff=zeros(8760*N+1,1);
mice=zeros(8760*N+1,1);Tout=zeros(8760*N+1,1);Tchwi=zeros(8760*N+1,1);UA=zeros(8760*N+1,1);
TimeUntilHour=zeros(8760*N+1,1);ChargeTimeReqd=zeros(8760*N+1,1);

%Calculate chiller capacity and full load power at each timestep
k=1:(8760*N+1);
if strcmp('Ice',StorageType)==1
    %Default chiller capacity for ice storage is at Tice
    if strcmp('Air',ChillerType)==1
        ChillerCap=ChillerCapacity(Temp(k),Tice,Chiller_Rated);ChillerCap(1)=0;
    elseif strcmp('Water',ChillerType)==1
```

```
        ChillerCap=ChillerCapacityWater(Twb(k),Tice,Chiller_Rated);ChillerCap(1)=0;
    end
end
if strcmp('CHW',StorageType)==1
    if strcmp('Air',ChillerType)==1
        ChillerCap=ChillerCapacity(Temp(k),Tset,Chiller_Rated);ChillerCap(1)=0;
    elseif strcmp('Water',ChillerType)==1
        ChillerCap=ChillerCapacityWater(Twb(k),Tset,Chiller_Rated);ChillerCap(1)=0;
    end
end

%Calculate Load, Chiller Capacity remaining in the day for CHW
CapRemaining=ChillerCapacityRemaining(N,Hour,ChillerCap);
LoadRemaining=CoolingLoadRemaining(N,Hour,CoolingLoad);

%Calculate the intermediate PLR when renewable power isn't sufficient for full-load operation
if strcmp('Renewable',ControlStrategy)==1
    for k=1:(8760*N+1)
        if strcmp('CHW',StorageType)==1
            if strcmp('Air',ChillerType)==1
                PLR_Int(k)=PLRIntermediate(RenewablePower(k),Temp(k),Tset,ChillerCap(k));
            elseif strcmp('Water',ChillerType)==1
                PLR_Int(k)=PLRIntermediateWater(RenewablePower(k),Twb(k),Tset,ChillerCap(k));
            end
        elseif strcmp('Ice',StorageType)==1
            %Default chiller set point temperature is Tice for ice storage
            if strcmp('Air',ChillerType)==1
                PLR_Int(k)=PLRIntermediate(RenewablePower(k),Temp(k),Tice,ChillerCap(k));
            elseif strcmp('Water',ChillerType)==1
                PLR_Int(k)=PLRIntermediateWater(RenewablePower(k),Twb(k),Tice,ChillerCap(k));
            end
        end
    end
end

%Run one of the four control strategies, renewable or cost with ice or chilled water
for j=2:(8760*N+1)
    if strcmp('CHW',StorageType)==1              %Chilled water storage
        if strcmp('Air',ChillerType)==1          %Calculate full-load chiller efficiency
```

```
        FullLoadEff(j)=Efficiency2Chiller(1,Temp(j),Tset);
    elseif strcmp('Water',ChillerType)==1
        FullLoadEff(j)=Efficiency2ChillerWater(1,Twb(j),Tset);
    end
    if strcmp('Renewable',ControlStrategy)==1 %Renewable Control
        TankCharge(1)=Tank_Cap/TankFactor;    %Tank is initially charged to meet one day's load
        if CapRemaining(j)<=(LoadRemaining(j)+(Tank_Cap/TankFactor-TankCharge(j-1)))
            %For fully charging the tank by the end of each day
            PLR(j)=1;
            OperationCode(j)=4;               %For determining the flow chart branch
        elseif RenewablePower(j)<MinLoading*ChillerCap(j)/FullLoadEff(j)
            %Renewable power is not sufficient to meet minimum PLR
            PLR(j)=0;
            OperationCode(j)=1;
        elseif (((Tank_Cap-TankCharge(j-1))*N+CoolingLoad(j))/...
                ChillerCap(j))<MinLoading
            %Not enough cooling load and/or tank capacity to meet minimum PLR
            PLR(j)=0;
            OperationCode(j)=2;
        elseif RenewablePower(j)<=ChillerCap(j)*FullLoadEff(j)
            %Operating PLR if renewable power isn't sufficient for full-load operation
            PLR(j)=max(MinLoading,min([((Tank_Cap-TankCharge(j-1))*N+...
                CoolingLoad(j))/ChillerCap(j),PLR_Int(j),1]));
            OperationCode(j)=3;
        else
            %Operates at minimum of full load or the available storage capacity plus cooling load
            PLR(j)=max(MinLoading,min(((Tank_Cap-TankCharge(j-1))*N+CoolingLoad(j))/...
                ChillerCap(j),1));
            OperationCode(j)=3;
        end
        % COP for Chillers based on 2013 CA Building Energy
        % Efficiency Standards ACM as a function of ambient dry bulb and PLR
        if strcmp('Air',ChillerType)==1
            COP(j)=max(0,Efficiency2Chiller(PLR(j),Temp(j),Tset));
        elseif strcmp('Water',ChillerType)==1
            COP(j)=max(0,Efficiency2ChillerWater(PLR(j),Twb(j),Tset));
        end
        %Calculation for tank charge at the current time step
        ChillerAdded(j)=PLR(j)*ChillerCap(j)/N;
```

```
            TankCharge(j)=min(Tank_Cap,TankCharge(j-1)-CoolingLoad(j)/N+ChillerAdded(j));
            %Power consumed at each timestep
            if PLR(j)==0
                PowerUsed(j)=0;
            else
                PowerUsed(j)=((TankCharge(j)-TankCharge(j-1))*N+CoolingLoad(j))/COP(j);
            end
            %Renewable Power Used
            if PowerUsed(j)>=RenewablePower(j)
                RenewablePowerUsed(j)=RenewablePower(j);
            else
                RenewablePowerUsed(j)=PowerUsed(j);
            end
        elseif strcmp('Cost',ControlStrategy)==1
            TankCharge(1)=Tank_Cap/TankFactor;
            %Tank is initially charged to meet one day's load
            if TankCharge(j-1)<Min_Tank_Charge*(Tank_Cap/TankFactor)
                PLR(j)=1;
                OperationCode(j)=4;
            elseif CapRemaining(j)<=(LoadRemaining(j)+(Tank_Cap/TankFactor-TankCharge(j-1)))
                %For fully charging the tank each day
                PLR(j)=1;
                OperationCode(j)=4;
            elseif ElectricRate(j)>0.10
                %On-peak rates, chillers off
                PLR(j)=0;
                OperationCode(j)=1;
            elseif (((Tank_Cap-TankCharge(j-1))*N+CoolingLoad(j))/...
                    ChillerCap(j))<MinLoading
                %Not enough storage capacity or cooling load to run at minimum PLR
                PLR(j)=0;
                OperationCode(j)=2;
            elseif (Tank_Cap-TankCharge(j-1))>0
                %Tank capacity available, run chillers
                PLR(j)=max(MinLoading,min(((Tank_Cap-TankCharge(j-1))*N+CoolingLoad(j))/...
                    ChillerCap(j),1));
                OperationCode(j)=3;
            end
            % COP for chillers
```

```
            if strcmp('Air',ChillerType)==1
                COP(j)=max(0,Efficiency2Chiller(PLR(j),Temp(j),Tset));
            elseif strcmp('Water',ChillerType)==1
                COP(j)=max(0,Efficiency2ChillerWater(PLR(j),Twb(j),Tset));
            end
            %Calculation for tank charge at the current time step
            ChillerAdded(j)=PLR(j)*ChillerCap(j)/N;
            TankCharge(j)=min(Tank_Cap,TankCharge(j-1)-CoolingLoad(j)/N+ChillerAdded(j));
            %Power Used
            if PLR(j)==0
                PowerUsed(j)=0;
            else
                PowerUsed(j)=((TankCharge(j)-TankCharge(j-1))*N+CoolingLoad(j))/COP(j);
            end
            %Renewable Power Used
            if PowerUsed(j)>=RenewablePower(j)
                RenewablePowerUsed(j)=RenewablePower(j);
            else
                RenewablePowerUsed(j)=PowerUsed(j);
            end
        end
    elseif strcmp('Ice',StorageType)==1           %Ice storage
        if strcmp('Renewable',ControlStrategy)==1 %Renewable Control
            if strcmp('Air',ChillerType)==1
                %Chiller capacity at Tload, full-load efficiency at Tice, and PLR intermediate at Tload
                ChillerCapLoad(j)=ChillerCapacity(Temp(j),Tload,Chiller_Rated);
                FullLoadEffIce(j)=Efficiency2Chiller(1,Temp(j),Tice);
            elseif strcmp('Water',ChillerType)==1
                ChillerCapLoad(j)=ChillerCapacityWater(Twb(j),Tload,Chiller_Rated);
                FullLoadEffIce(j)=Efficiency2ChillerWater(1,Twb(j),Tice);
            end
            %Calculate the current hour of the day and time until the recharge hour
            CurrentHour=((j-2)-24*N*floor((j-2)/(24*N)))/N;
            if (24-CurrentHour)+Hour>24
                TimeUntilHour(j)=Hour-CurrentHour;
            else
                TimeUntilHour(j)=(24-CurrentHour)+Hour;
            end
            %Control Strategy to Determine PLR for Current Timestep
```

```
            TankCharge(1)=0.9*Tank_Cap/TankFactor;
            ChargeTimeReqd(j)=(8.76115124E+00-4.41084737E+00*(TankCharge(j-1)/(0.9*Tank_Cap))-...
                    1.66356667E+01*(TankCharge(j-1)/(0.9*Tank_Cap))^2+...
                    6.65651816E+01*(TankCharge(j-1)/(0.9*Tank_Cap))^3-...
                    1.39814032E+02*(TankCharge(j-1)/(0.9*Tank_Cap))^4+...
                    1.37814193E+02*(TankCharge(j-1)/(0.9*Tank_Cap))^5-...
                    5.21558688E+01*(TankCharge(j-1)/(0.9*Tank_Cap))^6);
            %Tank is initially charged to meet one day's load
            if CapRemaining(j)<=(LoadRemaining(j)+(0.9*Tank_Cap/TankFactor-TankCharge(j-1)))||...
                    TimeUntilHour(j)<=ChargeTimeReqd(j)||TankCharge(j-1)<0.2*(Tank_Cap/TankFactor)
                %For fully charging the tank by the end of each day
                %Uses the remaining chiller capacity versus the remaining load
                %and the time needed to fully recharge the tank based on the current state of charge
                PLR(j)=1;
                Tin(j)=Tice;
                Qchiller(j)=ChillerCap(j);
                if CoolingLoad(j)==0 && TankCharge(j-1)>=0.90*Tank_Cap              %Off
                    OperationCode(j)=5;
                    PLR(j)=0;
                    TankCharge(j)=TankCharge(j-1);
                elseif CoolingLoad(j)==0 && TankCharge(j-1)<0.90*Tank_Cap           %Make Ice
                    OperationCode(j)=1;
                    [UA(j),~,~]=IceModel(TankCharge(j-1)/Tank_Cap,1,1,Tank_Cap,1);
                    C=min(-UA(j)*Tank_Cap*Tin(j)/(PLR(j)*ChillerCap(j)*Ice_Cap),6);
                    Tout(j)=Tin(j)*(4.43460676E+00-6.13886419E+00.*C+3.63956353E+00.*C.^2-...
                        1.14819817E+00.*C.^3+2.00374524E-01.*C.^4-1.82304475E-02.*C.^5+...6.74396219E-
04.*C.^6);
                    mice(j)=PLR(j).*ChillerCap(j)/(c_gly*(Tout(j)-Tin(j)));
                    [~,Qice(j),~]=IceModel(TankCharge(j-1)/Tank_Cap,Tin(j),1,Tank_Cap,mice(j));
                    if Qice(j)>=Qchiller(j)
                        Qice(j)=Qchiller(j);
                    elseif Qice(j)<Qchiller(j)
                        PLR(j)=max(MinLoading,Qice(j)/ChillerCap(j));
                    end
                    TankCharge(j)=TankCharge(j-1)+Qice(j)/N;
                elseif CoolingLoad(j)~=0 && CoolingLoad(j)<=0.8*ChillerCap(j)...
                        && TankCharge(j-1)<0.90*Tank_Cap                            %Make Ice and Cool
                    OperationCode(j)=2;
                    mload=CoolingLoad(j)/(c_gly*(Treturn-Tload));
```

```
                    [UA(j),~,~]=IceModel(TankCharge(j-1)/Tank_Cap,1,1,Tank_Cap,1);
                    UA(j)=min(UA(j),35);
                    [Tin(j),mice(j),Tout(j),Tchwi(j)]=...
                        MakeIceandCool(PLR(j),UA(j),CoolingLoad(j),Chiller_Rated,Tank_Cap);
                    Qice(j)=mice(j)*c_gly*(Tout(j)-Tin(j));
                    Qchiller(j)=mice(j)*c_gly*(Tchwi(j)-Tin(j));
                    TankCharge(j)=TankCharge(j-1)+Qice(j)/N;
                elseif CoolingLoad(j)~=0 && CoolingLoad(j)<=ChillerCapLoad(j)       %Chiller Only
                    OperationCode(j)=3;
                    Tin(j)=Tload;
                    Qchiller(j)=CoolingLoad(j);
                    ChillerCap(j)=ChillerCapLoad(j);
                    PLR(j)=max(MinLoading,Qchiller(j)/ChillerCap(j));
                    TankCharge(j)=TankCharge(j-1);
                elseif CoolingLoad(j)~=0 && CoolingLoad(j)>ChillerCapLoad(j)        %Chiller and Ice
                    OperationCode(j)=4;
                    ChillerCap(j)=ChillerCapLoad(j);
                    mload=CoolingLoad(j)/(c_gly*(Treturn-Tload));
                    Tin(j)=Treturn-PLR(j)*ChillerCap(j)/(mload*c_gly);
                    [UA(j),~,~]=IceModel(TankCharge(j-1)/Tank_Cap,1,2,Tank_Cap,1);
                    C=min(-UA(j)*Tank_Cap/((Tload/Tin(j)-1)*mload*c_gly*Ice_Cap),6);
                    Tout(j)=Tin(j)*(4.43460676E+00-6.13886419E+00.*C+3.63956353E+00.*C.^2-...
                        1.14819817E+00.*C.^3+2.00374524E-01.*C.^4-1.82304475E-02.*C.^5+6.74396219E-
04.*C.^6);
                    Qchiller(j)=mice(j)*c_gly*(Treturn-Tin(j));
                    mice(j)=mload*((Tload/Tin(j))-1)/((Tout(j)/Tin(j))-1);
                    Qice(j)=mice(j)*c_gly*(Tin(j)-Tout(j));
                    TankCharge(j)=TankCharge(j-1)-Qice(j)/N;
                end
            elseif RenewablePower(j)<MinLoading*ChillerCap(j)/FullLoadEffIce(j)
                if CoolingLoad(j)==0                                                %Off
                    OperationCode(j)=5;
                    PLR(j)=0;
                    TankCharge(j)=TankCharge(j-1);
                elseif CoolingLoad(j)~=0
                    Tin(j)=Treturn;
                    mload=CoolingLoad(j)/(c_gly*(Treturn-Tload));
                    Qice(j)=IceModel(TankCharge(j-1)/Tank_Cap,Tin(j),2,Tank_Cap,mload);
                    if Qice(j)>=CoolingLoad(j)                                      %Ice Only
```

```
                    OperationCode(j)=6;
                    PLR(j)=0;
                    [UA(j),~,~]=IceModel(TankCharge(j-1)/Tank_Cap,1,2,Tank_Cap,1);
                    C=min(-UA(j)*Tank_Cap/((Tload/Treturn-1)*mload*c_gly*Ice_Cap),6);
                    Tout(j)=Tin(j)*(4.43460676E+00-6.13886419E+00.*C+3.63956353E+00.*C.^2-...
                        1.14819817E+00.*C.^3+2.00374524E-01.*C.^4-1.82304475E-02.*C.^5+...
                        6.74396219E-04.*C.^6);
                    mice(j)=mload*((Tload/Treturn)-1)/((Tout(j)/Treturn)-1);
                    Qice(j)=mice(j)*c_gly*(Tin(j)-Tout(j));
                elseif Qice(j)<CoolingLoad(j);                                  %Chiller and Ice
                    OperationCode(j)=4;
                    Tin(j)=10;
                    if strcmp('Air',ChillerType)==1
                        ChillerCap(j)=ChillerCapacity(Temp(j),Tin(j),Chiller_Rated);
                    elseif strcmp('Water',ChillerType)==1
                        ChillerCap(j)=ChillerCapacityWater(Twb(j),Tin(j),Chiller_Rated);
                    end
                    mload=CoolingLoad(j)/(c_gly*(Treturn-Tload));
                    [UA(j),~,~]=IceModel(TankCharge(j-1)/Tank_Cap,1,2,Tank_Cap,1);
                    C=min(-UA(j)*Tank_Cap/((Tload/Tin(j)-1)*mload*c_gly*Ice_Cap),6);
                    Tout(j)=Tin(j)*(4.43460676E+00-6.13886419E+00.*C+3.63956353E+00.*C.^2-...
                        1.14819817E+00.*C.^3+2.00374524E-01.*C.^4-1.82304475E-02.*C.^5+...
                        6.74396219E-04.*C.^6);
                    Qchiller(j)=mice(j)*c_gly*(Treturn-Tin(j));
                    mice(j)=mload*((Tload/Tin(j))-1)/((Tout(j)/Tin(j))-1);
                    Qice(j)=mice(j)*c_gly*(Tin(j)-Tout(j));
                    TankCharge(j)=TankCharge(j-1)-Qice(j)/N;
                    PLR(j)=max(MinLoading,Qchiller(j)/ChillerCap(j));
                end
                TankCharge(j)=TankCharge(j-1)-Qice(j)/N;
            end
        elseif RenewablePower(j)>=MinLoading*ChillerCap(j)/FullLoadEffIce(j)
            if CoolingLoad(j)==0 && TankCharge(j-1)<0.90*Tank_Cap
                OperationCode(j)=1;                                             %Make Ice
                Tin(j)=Tice;
                [UA(j),~,~]=IceModel(TankCharge(j-1)/Tank_Cap,1,1,Tank_Cap,1);
                C=min(-UA(j)*Tank_Cap*Tin(j)/(PLR(j)*ChillerCap(j)*Ice_Cap),6);
                Tout(j)=Tin(j)*(4.43460676E+00-6.13886419E+00.*C+3.63956353E+00.*C.^2-...
                    1.14819817E+00.*C.^3+2.00374524E-01.*C.^4-1.82304475E-02.*C.^5+6.74396219E-
```

```
04.*C.^6);
                    PLR(j)=max(MinLoading,min([((Tank_Cap-TankCharge(j-1))*N+...
                        CoolingLoad(j))/ChillerCap(j),PLR_Int(j),1]));
                    mice(j)=PLR(j).*ChillerCap(j)/(c_gly*(Tout(j)-Tin(j)));
                    [~,Qice(j),~]=IceModel(TankCharge(j-1)/Tank_Cap,Tin(j),1,Tank_Cap,mice(j));
                    Qchiller(j)=mice(j)*c_gly*(Tout(j)-Tin(j));
                    if Qice(j)>=Qchiller(j)
                        Qice(j)=Qchiller(j);
                    elseif Qice(j)<Qchiller(j)
                        PLR(j)=max(MinLoading,Qice(j)/ChillerCap(j));
                    end
                    TankCharge(j)=TankCharge(j-1)+Qice(j)/N;
                elseif CoolingLoad(j)==0 && TankCharge(j-1)>=0.90*Tank_Cap          %Off
                    OperationCode(j)=5;
                    PLR(j)=0;
                    TankCharge(j)=TankCharge(j-1);
                elseif CoolingLoad(j)~=0
                    PLR(j)=max(MinLoading,min([((Tank_Cap-TankCharge(j-1))*N+...
                        CoolingLoad(j))/ChillerCap(j),PLR_Int(j),1]));
                    if CoolingLoad(j)<=ChillerCapLoad(j)
                        if TankCharge(j-1)<0.90*Tank_Cap && CoolingLoad(j)<=0.8*ChillerCap(j)
                            OperationCode(j)=2;                                    %Make Ice and Cool
                            Tin(j)=Tice;
                            mload=CoolingLoad(j)/(c_gly*(Treturn-Tload));
                            [UA(j),~,~]=IceModel(TankCharge(j-1)/Tank_Cap,1,1,Tank_Cap,1);
                            UA(j)=min(UA(j),35);
                            [Tin(j),mice(j),Tout(j),Tchwi(j)]=...
                                MakeIceandCool(PLR(j),UA(j),CoolingLoad(j),Chiller_Rated,Tank_Cap);
                            Qice(j)=mice(j)*c_gly*(Tout(j)-Tin(j));
                            Qchiller(j)=mice(j)*c_gly*(Tchwi(j)-Tin(j));
                            TankCharge(j)=TankCharge(j-1)+Qice(j)/N;
                        else                                                       %Chiller Only
                            OperationCode(j)=3;
                            Tin(j)=Tload;
                            ChillerCap(j)=ChillerCapLoad(j);
                            if strcmp('Air',ChillerType)==1
                                PLR_Int(j)=PLRIntermediate(RenewablePower(j),Temp(j),Tload,ChillerCap(j));
                            elseif strcmp('Water',ChillerType)==1
                                PLR_Int(j)=PLRIntermediate(RenewablePower(j),Twb(j),Tload,ChillerCap(j));
```

```
                    end
                    PLR(j)=max(MinLoading,min(PLR_Int(j),CoolingLoad(j)/ChillerCap(j)));
                    Qchiller(j)=ChillerCap(j)*PLR(j);
                    TankCharge(j)=TankCharge(j-1);
                end
            elseif CoolingLoad(j)>ChillerCapLoad(j)                         %Chiller and Ice
                OperationCode(j)=4;
                ChillerCap(j)=ChillerCapLoad(j);
                mload=CoolingLoad(j)/(c_gly*(Treturn-Tload));
                Tin(j)=Treturn-PLR(j)*ChillerCap(j)/(mload*c_gly);
                [UA(j),~,~]=IceModel(TankCharge(j-1)/Tank_Cap,1,2,Tank_Cap,1);
                C=min(-UA(j)*Tank_Cap/((Tload/Tin(j)-1)*mload*c_gly*Ice_Cap),6);
                Tout(j)=Tin(j)*(4.43460676E+00-6.13886419E+00.*C+3.63956353E+00.*C.^2-...
                    1.14819817E+00.*C.^3+2.00374524E-01.*C.^4-1.82304475E-02.*C.^5+...
                    6.74396219E-04.*C.^6);
                Qchiller(j)=mice(j)*c_gly*(Treturn-Tin(j));
                mice(j)=mload*((Tload/Tin(j))-1)/((Tout(j)/Tin(j))-1);
                Qice(j)=mice(j)*c_gly*(Tin(j)-Tout(j));
                TankCharge(j)=TankCharge(j-1)-Qice(j)/N;
            end
        end
    end
    % COP for chillers
    if strcmp('Air',ChillerType)==1
        COP(j)=max(0,Efficiency2Chiller(PLR(j),Temp(j),Tin(j)));
    elseif strcmp('Water',ChillerType)==1
        COP(j)=max(0,Efficiency2ChillerWater(PLR(j),Twb(j),Tin(j)));
    end
    %Power/Energy Used
    if PLR(j)==0
        PowerUsed(j)=0;
    else
        PowerUsed(j)=Qchiller(j)/COP(j);
    end
    %Renewable Power Used
    if PowerUsed(j)>=RenewablePower(j)
        RenewablePowerUsed(j)=RenewablePower(j);
    else
        RenewablePowerUsed(j)=PowerUsed(j);
```

```
        end
    elseif strcmp('Cost',ControlStrategy)==1  %Cost Control
        if strcmp('Air',ChillerType)==1
            %Chiller capacity at Tload, full-load efficiency at Tice, and PLR intermediate at Tload
            ChillerCapLoad(j)=ChillerCapacity(Temp(j),Tload,Chiller_Rated);
            FullLoadEffIce(j)=Efficiency2Chiller(1,Temp(j),Tice);
        elseif strcmp('Water',ChillerType)==1
            ChillerCapLoad(j)=ChillerCapacityWater(Twb(j),Tload,Chiller_Rated);
            FullLoadEffIce(j)=Efficiency2ChillerWater(1,Twb(j),Tice);
        end
        CurrentHour(j)=((j-2)-24*N*floor((j-2)/(24*N)))/N;
        if (24-CurrentHour(j))+Hour>24
            TimeUntilHour(j)=Hour-CurrentHour(j);
        else
            TimeUntilHour(j)=(24-CurrentHour(j))+Hour;
        end
        TankCharge(1)=0.9*Tank_Cap/TankFactor;
        ChargeTimeReqd(j)=(8.76115124E+00-4.41084737E+00*(TankCharge(j-1)/(0.9*Tank_Cap))-...
                1.66356667E+01*(TankCharge(j-1)/(0.9*Tank_Cap))^2+...
                6.65651816E+01*(TankCharge(j-1)/(0.9*Tank_Cap))^3-...
                1.39814032E+02*(TankCharge(j-1)/(0.9*Tank_Cap))^4+...
                1.37814193E+02*(TankCharge(j-1)/(0.9*Tank_Cap))^5-...
                5.21558688E+01*(TankCharge(j-1)/(0.9*Tank_Cap))^6);
        %Tank is initially charged to meet one day's load
        if CapRemaining(j)<=(LoadRemaining(j)+(0.9*Tank_Cap/TankFactor-TankCharge(j-1)))||...
                TimeUntilHour(j)<=ChargeTimeReqd(j)||TankCharge(j-1)<0.2*(Tank_Cap/TankFactor)
            %For fully charging the tank by the end of each day
            %Uses the remaining chiller capacity versus the remaining load
            %and the time needed to fully recharge the tank based on the current state of charge)
            PLR(j)=1;
            Tin(j)=Tice;
            Qchiller(j)=ChillerCap(j);
            if CoolingLoad(j)==0 && TankCharge(j-1)>=0.90*Tank_Cap              %Off
                OperationCode(j)=5;
                PLR(j)=0;
                TankCharge(j)=TankCharge(j-1);
            elseif CoolingLoad(j)==0 && TankCharge(j-1)<0.90*Tank_Cap           %Make Ice
                OperationCode(j)=1;
                [UA(j),~,~]=IceModel(TankCharge(j-1)/Tank_Cap,1,1,Tank_Cap,1);
```

```
                    C=min(-UA(j)*Tank_Cap*Tin(j)/(PLR(j)*ChillerCap(j)*Ice_Cap),6);
                    Tout(j)=Tin(j)*(4.43460676E+00-6.13886419E+00.*C+3.63956353E+00.*C.^2-...
                        1.14819817E+00.*C.^3+2.00374524E-01.*C.^4-1.82304475E-02.*C.^5+6.74396219E-
04.*C.^6);
                    mice(j)=PLR(j).*ChillerCap(j)/(c_gly*(Tout(j)-Tin(j)));
                    [~,Qice(j),~]=IceModel(TankCharge(j-1)/Tank_Cap,Tin(j),1,Tank_Cap,mice(j));
                    if Qice(j)>=Qchiller(j)
                        Qice(j)=Qchiller(j);
                    elseif Qice(j)<Qchiller(j)
                        PLR(j)=max(MinLoading,Qice(j)/ChillerCap(j));
                    end
                    TankCharge(j)=TankCharge(j-1)+Qice(j)/N;
                elseif CoolingLoad(j)~=0 && CoolingLoad(j)<=0.8*ChillerCap(j)...
                        && TankCharge(j-1)<0.90*Tank_Cap                              %Make Ice and Cool
                    OperationCode(j)=2;
                    mload=CoolingLoad(j)/(c_gly*(Treturn-Tload));
                    [UA(j),~,~]=IceModel(TankCharge(j-1)/Tank_Cap,1,1,Tank_Cap,1);
                    UA(j)=min(UA(j),35);
                    [Tin(j),mice(j),Tout(j),Tchwi(j)]=...
                        MakeIceandCool(PLR(j),UA(j),CoolingLoad(j),Chiller_Rated,Tank_Cap);
                    Qice(j)=mice(j)*c_gly*(Tout(j)-Tin(j));
                    Qchiller(j)=mice(j)*c_gly*(Tchwi(j)-Tin(j));
                    TankCharge(j)=TankCharge(j-1)+Qice(j)/N;
                elseif CoolingLoad(j)~=0 && CoolingLoad(j)<=ChillerCapLoad(j)       %Chiller Only
                    OperationCode(j)=3;
                    Tin(j)=Tload;
                    Qchiller(j)=CoolingLoad(j);
                    ChillerCap(j)=ChillerCapLoad(j);
                    PLR(j)=max(MinLoading,Qchiller(j)/ChillerCap(j));
                    TankCharge(j)=TankCharge(j-1);
                elseif CoolingLoad(j)~=0 && CoolingLoad(j)>ChillerCapLoad(j)        %Chiller and Ice
                    OperationCode(j)=4;
                    ChillerCap(j)=ChillerCapLoad(j);
                    mload=CoolingLoad(j)/(c_gly*(Treturn-Tload));
                    Tin(j)=Treturn-PLR(j)*ChillerCap(j)/(mload*c_gly);
                    [UA(j),~,~]=IceModel(TankCharge(j-1)/Tank_Cap,1,2,Tank_Cap,1);
                    C=min(-UA(j)*Tank_Cap/((Tload/Tin(j)-1)*mload*c_gly*Ice_Cap),6);
                    Tout(j)=Tin(j)*(4.43460676E+00-6.13886419E+00.*C+3.63956353E+00.*C.^2-...
                        1.14819817E+00.*C.^3+2.00374524E-01.*C.^4-1.82304475E-02.*C.^5+6.74396219E-
```

```
04.*C.^6);
                    Qchiller(j)=mice(j)*c_gly*(Treturn-Tin(j));
                    mice(j)=mload*((Tload/Tin(j))-1)/((Tout(j)/Tin(j))-1);
                    Qice(j)=mice(j)*c_gly*(Tin(j)-Tout(j));
                    TankCharge(j)=TankCharge(j-1)-Qice(j)/N;
                end
%           elseif ElectricRate(j)>0.10                                     %On-peak rates
            elseif ElectricRate(j)>0.052                                    %Demand charge rate
                if CoolingLoad(j)==0                                        %Off
                    OperationCode(j)=5;
                    PLR(j)=0;
                    TankCharge(j)=TankCharge(j-1);
                elseif CoolingLoad(j)~=0
                    Tin(j)=Treturn;
                    mload=CoolingLoad(j)/(c_gly*(Treturn-Tload));
                    Qice(j)=IceModel(TankCharge(j-1)/Tank_Cap,Tin(j),2,Tank_Cap,mload);
                    if Qice(j)>=CoolingLoad(j)                              %Ice Only
                        OperationCode(j)=6;
                        PLR(j)=0;
                        [UA(j),~,~]=IceModel(TankCharge(j-1)/Tank_Cap,1,2,Tank_Cap,1);
                        C=min(-UA(j)*Tank_Cap/((Tload/Treturn-1)*mload*c_gly*Ice_Cap),6);
                        Tout(j)=Tin(j)*(4.43460676E+00-6.13886419E+00.*C+3.63956353E+00.*C.^2-...
                            1.14819817E+00.*C.^3+2.00374524E-01.*C.^4-1.82304475E-02.*C.^5+...
                            6.74396219E-04.*C.^6);
                        mice(j)=mload*((Tload/Treturn)-1)/((Tout(j)/Treturn)-1);
                        Qice(j)=mice(j)*c_gly*(Tin(j)-Tout(j));
                    elseif Qice(j)<CoolingLoad(j);                          %Chiller and Ice
                        OperationCode(j)=4;
                        Tin(j)=10;
                        if strcmp('Air',ChillerType)==1
                            ChillerCap(j)=ChillerCapacity(Temp(j),Tin(j),Chiller_Rated);
                        elseif strcmp('Water',ChillerType)==1
                            ChillerCap(j)=ChillerCapacityWater(Twb(j),Tin(j),Chiller_Rated);
                        end
                        mload=CoolingLoad(j)/(c_gly*(Treturn-Tload));
                        [UA(j),~,~]=IceModel(TankCharge(j-1)/Tank_Cap,1,2,Tank_Cap,1);
                        C=min(-UA(j)*Tank_Cap/((Tload/Tin(j)-1)*mload*c_gly*Ice_Cap),6);
                        Tout(j)=Tin(j)*(4.43460676E+00-6.13886419E+00.*C+3.63956353E+00.*C.^2-...
                            1.14819817E+00.*C.^3+2.00374524E-01.*C.^4-1.82304475E-02.*C.^5+...
```

```
                        6.74396219E-04.*C.^6);
                    Qchiller(j)=mice(j)*c_gly*(Treturn-Tin(j));
                    mice(j)=mload*((Tload/Tin(j))-1)/((Tout(j)/Tin(j))-1);
                    Qice(j)=mice(j)*c_gly*(Tin(j)-Tout(j));
                    TankCharge(j)=TankCharge(j-1)-Qice(j)/N;
                    PLR(j)=max(MinLoading,Qchiller(j)/ChillerCap(j));
                end
                TankCharge(j)=TankCharge(j-1)-Qice(j)/N;
            end
%           elseif ElectricRate(j)<0.10                                     %Off-peak rates
            elseif ElectricRate(j)<0.052                                    %Demand charge rate
                if CoolingLoad(j)==0 && TankCharge(j-1)<0.90*Tank_Cap
                    OperationCode(j)=1;                                     %Make Ice
                    Tin(j)=Tice;
                    [UA(j),~,~]=IceModel(TankCharge(j-1)/Tank_Cap,1,1,Tank_Cap,1);
                    C=min(-UA(j)*Tank_Cap*Tin(j)/(PLR(j)*ChillerCap(j)*Ice_Cap),6);
                    Tout(j)=Tin(j)*(4.43460676E+00-6.13886419E+00.*C+3.63956353E+00.*C.^2-...
                        1.14819817E+00.*C.^3+2.00374524E-01.*C.^4-1.82304475E-02.*C.^5+6.74396219E-
04.*C.^6);
                    PLR(j)=max(MinLoading,min([((Tank_Cap-TankCharge(j-1))*N+...
                        CoolingLoad(j))/ChillerCap(j),1]));
                    mice(j)=PLR(j).*ChillerCap(j)/(c_gly*(Tout(j)-Tin(j)));
                    [~,Qice(j),~]=IceModel(TankCharge(j-1)/Tank_Cap,Tin(j),1,Tank_Cap,mice(j));
                    Qchiller(j)=mice(j)*c_gly*(Tout(j)-Tin(j));
                    if Qice(j)>=Qchiller(j)
                        Qice(j)=Qchiller(j);
                    elseif Qice(j)<Qchiller(j)
                        PLR(j)=max(MinLoading,Qice(j)/ChillerCap(j));
                    end
                    TankCharge(j)=TankCharge(j-1)+Qice(j)/N;
                elseif CoolingLoad(j)==0 && TankCharge(j-1)>=0.90*Tank_Cap          %Off
                    OperationCode(j)=5;
                    PLR(j)=0;
                    TankCharge(j)=TankCharge(j-1);
                elseif CoolingLoad(j)~=0
                    PLR(j)=max(MinLoading,min([((Tank_Cap-TankCharge(j-1))*N+...
                        CoolingLoad(j))/ChillerCap(j),1]));
                    if CoolingLoad(j)<=ChillerCapLoad(j)
                        if TankCharge(j-1)<0.90*Tank_Cap && CoolingLoad(j)<=0.8*ChillerCap(j)
```

```
                            OperationCode(j)=2;                                     %Make Ice and Cool
                            Tin(j)=Tice;
                            mload=CoolingLoad(j)/(c_gly*(Treturn-Tload));
                            [UA(j),~,~]=IceModel(TankCharge(j-1)/Tank_Cap,1,1,Tank_Cap,1);
                            UA(j)=min(UA(j),35);
                            [Tin(j),mice(j),Tout(j),Tchwi(j)]=...
                                MakeIceandCool(PLR(j),UA(j),CoolingLoad(j),Chiller_Rated,Tank_Cap);
                            Qice(j)=mice(j)*c_gly*(Tout(j)-Tin(j));
                            Qchiller(j)=mice(j)*c_gly*(Tchwi(j)-Tin(j));
                            TankCharge(j)=TankCharge(j-1)+Qice(j)/N;
                        else                                                        %Chiller Only
                            OperationCode(j)=3;
                            Tin(j)=Tload;
                            ChillerCap(j)=ChillerCapLoad(j);
                            PLR(j)=max(MinLoading,CoolingLoad(j)/ChillerCap(j));
                            Qchiller(j)=ChillerCap(j)*PLR(j);
                            TankCharge(j)=TankCharge(j-1);
                        end
                    elseif CoolingLoad(j)>ChillerCapLoad(j)                         %Chiller and Ice
                        OperationCode(j)=4;
                        ChillerCap(j)=ChillerCapLoad(j);
                        mload=CoolingLoad(j)/(c_gly*(Treturn-Tload));
                        Tin(j)=Treturn-PLR(j)*ChillerCap(j)/(mload*c_gly);
                        [UA(j),~,~]=IceModel(TankCharge(j-1)/Tank_Cap,1,2,Tank_Cap,1);
                        C=min(-UA(j)*Tank_Cap/((Tload/Tin(j)-1)*mload*c_gly*Ice_Cap),6);
                        Tout(j)=Tin(j)*(4.43460676E+00-6.13886419E+00.*C+3.63956353E+00.*C.^2-...
                            1.14819817E+00.*C.^3+2.00374524E-01.*C.^4-1.82304475E-02.*C.^5+6.74396219E-
04.*C.^6);
                        Qchiller(j)=mice(j)*c_gly*(Treturn-Tin(j));
                        mice(j)=mload*((Tload/Tin(j))-1)/((Tout(j)/Tin(j))-1);
                        Qice(j)=mice(j)*c_gly*(Tin(j)-Tout(j));
                        TankCharge(j)=TankCharge(j-1)-Qice(j)/N;
                    end
                end
            end
            % COP for chillers
            if strcmp('Air',ChillerType)==1
                COP(j)=max(0,Efficiency2Chiller(PLR(j),Temp(j),Tin(j))); %2 chillers in parallel
            elseif strcmp('Water',ChillerType)==1
```

```
                COP(j)=max(0,Efficiency2ChillerWater(PLR(j),Twb(j),Tin(j)));
            end
            %Power/Energy Used
            if PLR(j)==0
                PowerUsed(j)=0;
            else
                PowerUsed(j)=Qchiller(j)/COP(j);
            end
            %Renewable Power Used
            if PowerUsed(j)>=RenewablePower(j)
                RenewablePowerUsed(j)=RenewablePower(j);
            else
                RenewablePowerUsed(j)=PowerUsed(j);
            end
        end
    end
end

%Total Renewable Power Used by Chiller
ChillerEnergyUsed=sum(PowerUsed./N);
RenewableEnergyUsed=sum(RenewablePowerUsed./N);
ChillerMetbyRenewable=RenewableEnergyUsed/ChillerEnergyUsed;                    %Metric

%Electricity Cost
% ElecCostStorage=sum((PowerUsed-RenewablePower).*ElectricRate)/N;               %Energy charges only
                                                                                %With demand charges
ElecCostStorage=(sum((PowerUsed-RenewablePower).*ElectricRate)/N)+max(PowerUsed)*(3.5*6+10.99*6)+...
    max(PowerUsed(2:4466))*16.44+...
    max(PowerUsed(4467:8498))*16.44+max(PowerUsed(8499:12962))*16.44+max(PowerUsed(12963:17282))*16.44+...

max(PowerUsed(17283:21746))*16.44+max(PowerUsed(21747:26066))*39.64+max(PowerUsed(26067:30530))*39.64+...

max(PowerUsed(30531:34994))*39.64+max(PowerUsed(34995:39314))*39.64+max(PowerUsed(39315:43778))*16.44+...
    max(PowerUsed(43779:48098))*16.44+max(PowerUsed(48099:52561))*16.44;

%Capital Cost
%Chillers
if strcmp('Air',ChillerType)==1
    ChillerCost=2*((-0.0716*(Chiller_Rated/2)+258.53)*(Chiller_Rated/2)); %[$] from RS Means 2010
```

```
elseif strcmp('Water',ChillerType)==1
    ChillerCost=2*(119.2*Chiller_Rated/2+28205)+2*(34.121*(1.16*Chiller_Rated/2)+3838.9);
    %[$] from RS Means 2010 includes cooling tower
    %1.16 Cooling tower factor is 1/Rated_COP to get from Qc to Qh
end
%Storage tanks
if strcmp('CHW',StorageType)==1
    TankCost=(Tank_Cap*20.68)*(1.5087*(Tank_Cap*20.68/10^6)^-0.366);
    %Andrepoint Correspondence, 20.68 converts kWh to Mgal
elseif strcmp('Ice',StorageType)==1
    TankCost=Tank_Cap*140*0.2843;
    %MacCracken correspondence, $140/ton-hr, 0.2843 converts kWh to ton-hr
end
%Renewable capacity
if strcmp('Solar',Resource)==1
    ResourceCost=2310000*RenewableFactor*FullLoadChillerPower;
    %Renewable resource cost from SunShot report 2015 (commercial), includes $0.14/W for inverter
replacement
elseif strcmp('Wind',Resource)==1
    ResourceCost=1710000*RenewableFactor*FullLoadChillerPower;
    %from DOE Wind Technologies Market Report 2015, includes $0.14/W for inverter replacement
end

%Total Cost Calculation
DiscountRate=0.08;                              %Discount rate used
InflationRate=0.05;                             %Inflation rate used
PresentWorthFactor=(1/(DiscountRate-InflationRate))*(1-((1+InflationRate)/(1+DiscountRate))^n);
%from Duffie and Beckman Solar Engineering of Thermal Processes
OperatingCostTotal=PresentWorthFactor*ElecCostStorage;
TotalCost=(ChillerCost+TankCost+ResourceCost+OperatingCostTotal)/10^6;              %[$MM]
end
```

```
function [ChillerCap] = ChillerCapacity(Temp,Tset,Chiller_Rated)
%Returns full load capacity for an air cooled chiller with a set point of
%Tset based on 2013 CA Building Energy
%Efficiency Standards ACM as a function of ambient dry bulb
MinTemp=65; %[F]
%Minimum Tdb for a capacity advantage
ChillerCap=Chiller_Rated.*(-0.09464899+0.03834070.*(Tset*9/5+32)+...
    -0.00009205.*(Tset*9/5+32).^2+0.00378007*max(MinTemp,Temp*9/5+32)+...
    -0.00001375.*max(MinTemp,Temp*9/5+32).^2+...
    -0.00015464.*(Tset*9/5+32).*max(MinTemp,Temp*9/5+32));     %[kW]
end
```

```
function [ChillerCap] = ChillerCapacityWater(Twb,Tset,Chiller_Rated)
%Returns full load capacity for water cooled chiller with a set point of
%Tset based on 2013 CA Building Energy
%Efficiency Standards as a function of entering condenser water temperature
MinTemp=65; %[F]
%Minimum Tecw for a capacity advantage
%Minimum
Temp=(Twb.*9./5+32)+7; %[F] 7 degree approach temperature used, Temp is Tecw
%Twb is in [C] and needs to be converted to [F]
ChillerCap=Chiller_Rated.*(-0.29861976+...
    0.02996076.*(Tset*9/5+32)+...
    -0.00080125.*(Tset*9/5+32).^2+...
    0.01736268*max(MinTemp,Temp)-...
    0.00032606.*max(MinTemp,Temp).^2+...
    0.00063139.*(Tset*9/5+32).*max(MinTemp,Temp));
end
```

```
function [PLR_Int] = PLRIntermediate(RenewablePower,Temp,Tset,ChillerCap)
%Returns air-cooled intermediate PLR value when renewable power isn't sufficient to meet full-load power
%Gives the intersection of the ChillerCap/Power ratio and the COP curves to get the intermediate PLR
if RenewablePower>0
    if (ChillerCap/RenewablePower)<(-0.1039*Temp+6.5573)    %Solution for part-load ratios above 0.5
        PLR_Int_high=3.58357177E+01+4.82523637E-02*Tset+3.34311354E-03*Tset^2-8.48062324E-01*Temp+...
            5.23087048E-03*Temp^2-1.01921108E+01*(ChillerCap/RenewablePower)+...
            7.49241960E-01*(ChillerCap/RenewablePower)^2+1.01768078E-03*Tset*Temp-...
            1.45202420E-02*Tset*(ChillerCap/RenewablePower)+1.13113410E-01*Temp*(ChillerCap/RenewablePower);
        PLR_Int_low=0;
    elseif (ChillerCap/RenewablePower)>-0.1702*Temp+11.906 %Solution for part-load ratios below 0.5
        PLR_Int_low=1.86897425E+01+6.81135131E-02*Tset+1.52137313E-03*Tset^2-4.57107205E-01*Temp+...
            2.92416151E-03*Temp^2-2.55813103E+00*(ChillerCap/RenewablePower)+...
            8.89464142E-02*(ChillerCap/RenewablePower)^2-2.48210163E-04*Tset*Temp-...
            6.62532446E-03*Tset*(ChillerCap/RenewablePower)+2.94548715E-02*Temp*(ChillerCap/RenewablePower);
        PLR_Int_high=0;
    else                                                    %Solution in between is 0.5
        PLR_Int_high=0.5;
        PLR_Int_low=0.5;
    end
else                                                        %If no renewable power, the PLR is zero
    PLR_Int_high=0;
    PLR_Int_low=0;
end
if PLR_Int_low>0.5                                          %Make sure solutions are on the correct PLR side
    PLR_Int_low=0;
end
if PLR_Int_high<0.5
    PLR_Int_high=0;
end
PLR_Int=max(PLR_Int_low,PLR_Int_high);                      %Use the maximum calculated PLR
if PLR_Int>1                                                %limit solutions to physically possible range
    PLR_Int=0;
end
if PLR_Int<0.075
    PLR_Int=0;
end
end
```

```
function [PLR_Int] = PLRIntermediateWater(RenewablePower,Twb,Tset,ChillerCap)
 %Returns intermediate PLR values
%Solve for the intersection of the ChillerCap/Power ratio and the
%COP curves to get the intermediate PLR
%Solution is piecewise for different chiller set points, Tset
MinTwb=14.44; %[C] lowest Tecw for water cooled chiller based on 7F approach temperature
if Tset==4.44
    if RenewablePower>0
        %Solve for the intersection of the ChillerCap/Power ratio and the
        %COP curves to get the intermediate PLR
        a=-7.42449047E-01; b=1.56517946E+01; c=2.21856960E+01; d=-2.32515285E+01; e=2.15128994E-02; f=-
8.43395688E-05;
        g=-1.51354274E-06; h=-4.00210936E-01; j=2.77731546E-03; k=-1.40854145E-01; m=1.89357829E-03;
        vector_low=[d,...
            c+k*max(Twb,MinTwb)+m*max(Twb,MinTwb)^2,...
            -ChillerCap/RenewablePower+b+h*max(Twb,MinTwb)+j*max(Twb,MinTwb)^2,...
            a+e*max(Twb,MinTwb)+f*max(Twb,MinTwb)^2+g*max(Twb,MinTwb)^3];
        PLR_Int_low=max(roots(vector_low));                %Solve for curve intersection for PLR<0.5
        a=-2.57868782E+00; b=1.36523428E+01; c=1.65525811E+00; d=-4.36764334E+00; e=1.26505695E-01; f=-
1.22346019E-03;
        g=-5.67475075E-07; h=-5.44510909E-01; j=4.99322469E-03; k=2.54456936E-01; m=-2.59114209E-03;
        vector_high=[d,...
            c+k*max(Twb,MinTwb)+m*max(Twb,MinTwb)^2,...
            -ChillerCap/RenewablePower+b+h*max(Twb,MinTwb)+j*max(Twb,MinTwb)^2,...
            a+e*max(Twb,MinTwb)+f*max(Twb,MinTwb)^2+g*max(Twb,MinTwb)^3];
        PLR_Int_high=max(roots(vector_high));               %Solve for curve intersection for PLR>=0.5
    else
        PLR_Int_low=0;
        PLR_Int_high=0;
    end
    if PLR_Int_low>0.5
        PLR_Int_low=0;
    end
    if imag(PLR_Int_low)~=0                                %Check for imaginary solutions
        PLR_Int_low=0;
    end
    if PLR_Int_high<=0.5
        PLR_Int_high=0;
```

```
    end
    if imag(PLR_Int_high)~=0
        PLR_Int_high=0;
    end
    PLR_Int=max(PLR_Int_low,PLR_Int_high);                  %Use the maximum PLR
    if PLR_Int>1                                            %Don't use an intersection that isn't physical
        PLR_Int=1;
    end
    if ChillerCap/RenewablePower>Efficiency2ChillerWater(1,Twb,Tset) &&...
            ChillerCap/RenewablePower<(2*Efficiency2ChillerWater(0.5,Twb,Tset)) &&...
            PLR_Int<=0.00001                                %Throttle back to one chiller if solution is
                                                            %above 0.5 PLR, but below two chillers
        PLR_Int=0.5;
    end
elseif Tset==6.67
    if RenewablePower>0
        a=-7.93519489E-01; b=1.62977109E+01; c=2.42075800E+01; d=-2.50145136E+01; e=2.45371098E-02; f=-
1.69920825E-04;
        g=-3.53194913E-07; h=-4.16124034E-01; j=2.79785692E-03; k=-1.63323236E-01; m=2.16486634E-03;
        vector_low=[d,...
            c+k*max(Twb,MinTwb)+m*max(Twb,MinTwb)^2,...
            -ChillerCap/RenewablePower+b+h*max(Twb,MinTwb)+j*max(Twb,MinTwb)^2,...
            a+e*max(Twb,MinTwb)+f*max(Twb,MinTwb)^2+g*max(Twb,MinTwb)^3];
        PLR_Int_low=max(roots(vector_low));
        a=-2.79814026E+00; b=1.44807368E+01; c=1.88273626E+00; d=-4.80504740E+00; e=1.40591452E-01; f=-
1.45940189E-03;
        g=1.12542903E-06; h=-5.87148329E-01; j=5.37881648E-03; k=2.78718968E-01; m=-2.84217960E-03;
        vector_high=[d,...
            c+k*max(Twb,MinTwb)+m*max(Twb,MinTwb)^2,...
            -ChillerCap/RenewablePower+b+h*max(Twb,MinTwb)+j*max(Twb,MinTwb)^2,...
            a+e*max(Twb,MinTwb)+f*max(Twb,MinTwb)^2+g*max(Twb,MinTwb)^3];
        PLR_Int_high=max(roots(vector_high));
    else
        PLR_Int_low=0;
        PLR_Int_high=0;
    end
    if PLR_Int_low>0.5
        PLR_Int_low=0;
    end
```

```
    if imag(PLR_Int_low)~=0
        PLR_Int_low=0;
    end
    if PLR_Int_high<=0.5
        PLR_Int_high=0;
    end
    if imag(PLR_Int_high)~=0
        PLR_Int_high=0;
    end
    PLR_Int=max(PLR_Int_low,PLR_Int_high);
    if PLR_Int>1
        PLR_Int=1;
    end
    if ChillerCap/RenewablePower>Efficiency2ChillerWater(1,Twb,Tset) &&...
            ChillerCap/RenewablePower<(2*Efficiency2ChillerWater(0.5,Twb,Tset)) &&...
            PLR_Int<=0.00001
        PLR_Int=0.5;
    end
elseif Tset==-6.67
    if RenewablePower>0
        a=-5.54210667E-01; b=1.28848159E+01; c=1.51660734E+01; d=-1.68929963E+01; e=1.19178367E-02; f=1.43839497E-04;
        g=-4.37196646E-06; h=-3.28559330E-01; j=2.51409588E-03; k=-6.91108362E-02; m=1.00295136E-03;
        vector_low=[d,...
            c+k*max(Twb,MinTwb)+m*max(Twb,MinTwb)^2,...
            -ChillerCap/RenewablePower+b+h*max(Twb,MinTwb)+j*max(Twb,MinTwb)^2,...
            a+e*max(Twb,MinTwb)+f*max(Twb,MinTwb)^2+g*max(Twb,MinTwb)^3];
        PLR_Int_low=max(roots(vector_low));
        a=-1.76382674E+00; b=1.04068352E+01; c=9.30878415E-01; d=-2.83553612E+00; e=7.74792815E-02; f=-5.17397776E-04;
        g=-5.14081018E-06; h=-3.85075217E-01; j=3.63177421E-03; k=1.67168214E-01; m=-1.74892158E-03;
        vector_high=[d,...
            c+k*max(Twb,MinTwb)+m*max(Twb,MinTwb)^2,...
            -ChillerCap/RenewablePower+b+h*max(Twb,MinTwb)+j*max(Twb,MinTwb)^2,...
            a+e*max(Twb,MinTwb)+f*max(Twb,MinTwb)^2+g*max(Twb,MinTwb)^3];
        PLR_Int_high=max(roots(vector_high));
    else
        PLR_Int_low=0;
        PLR_Int_high=0;
    end
    if PLR_Int_low>0.5
        PLR_Int_low=0;
```

```
    end
    if imag(PLR_Int_low)~=0
        PLR_Int_low=0;
    end
    if PLR_Int_high<=0.5
        PLR_Int_high=0;
    end
    if imag(PLR_Int_high)~=0
        PLR_Int_high=0;
    end
    PLR_Int=max(PLR_Int_low,PLR_Int_high);
    if PLR_Int>1
        PLR_Int=1;
    end
    if ChillerCap/RenewablePower>Efficiency2ChillerWater(1,Twb,Tset) &&...
            ChillerCap/RenewablePower<(2*Efficiency2ChillerWater(0.5,Twb,Tset)) &&...
            PLR_Int<=0.00001
        PLR_Int=0.5;
    end
end
end
```

```
function [CapRemaining] = ChillerCapacityRemaining(N,hour,ChillerCap)
%Returns chiller capacity remaining for the remainder of a day (for the whole year)
hour=round(hour);
CapRemaining=zeros(1+8760*N,1);                                    %Initialize the vector
for j=2:(hour*N+1)                                                 %Chiller cap remaining for the first day
    CapRemaining(j)=sum(ChillerCap(j:hour*N+1))/N;
end
for k=2:365                                                        %for the rest of the year
    for j=hour*N+2+(24*N*(k-2)):hour*N+1+(24*N*(k-1))
        CapRemaining(j)=sum(ChillerCap(j:hour*N+1+24*N*(k-1)))/N;
    end
end
%capacity wraps around to the beginning of the year
for j=2+8760*N-(24-hour)*N:1+8760*N
    CapRemaining(j)=sum(ChillerCap(j:(8760*N+1)))/N+CapRemaining(2);
end
end
```

```
function [LoadRemaining] = CoolingLoadRemaining(N,hour,CoolingLoad)
%Returns cooling load remaining for the remainder of a day (for the whole year)
hour=round(hour);
LoadRemaining=zeros(1+8760*N,1);                                   %initialize the vector
for j=2:(hour*N+1)                                                 %Load remaining for the first day
    LoadRemaining(j)=sum(CoolingLoad(j:hour*N+1))/N;
end
for k=2:365                                                        %for the rest of the year
    for j=hour*N+2+(24*N*(k-2)):hour*N+1+(24*N*(k-1))
        LoadRemaining(j)=sum(CoolingLoad(j:hour*N+1+24*N*(k-1)))/N;
    end
end
%load wraps around to the beginning of the year
for j=2+8760*N-(24-hour)*N:1+8760*N
    LoadRemaining(j)=sum(CoolingLoad(j:(8760*N+1)))/N+LoadRemaining(2);
end
end
```

```
function [COP] = Efficiency2Chiller(PLR,Temp,Tset)
%Returns COP for two parallel screw air-cooled chillers with a specified set point
%Based on 2013 CA Building Energy
%Efficiency Standards Alternative Calculation Method as a function of Tdb,PLR and Tset
MinTemp=15.56; %[C]
%Minimum Tdb for a performance advantage
if PLR<=0.5                                                 %One chiller operation
    a=2.36021747E-01;
    b=1.35877978E+01;
    c=-3.16493822E+00;
    d=-2.20834773E-02;
    e=1.22756001E-03;
    f=-2.69765360E-02;
    g=4.31575561E-04;
    h=3.11886270E-02;
    i=-1.72786099E-01;
    j=7.59350700E-04;
    COP=a+b.*PLR+c.*PLR.^2+d.*Tset+e.*Tset.^2+f.*max(Temp,MinTemp)+g.*max(Temp,MinTemp).^2+h.*PLR.*Tset+...
        i.*PLR.*max(Temp,MinTemp)+j.*Tset.*max(Temp,MinTemp);
else                                                        %Two chillers in parallel
    a=5.76141843E-01;
    b=6.47704975E+00;
    c=-7.37168474E-01;
    d=-2.94603441E-02;
    e=1.69563586E-03;
    f=-4.30449443E-02;
    g=5.96137862E-04;
    h=1.41613159E-02;
    i=-7.84541920E-02;
    j=1.04889559E-03;
    COP=a+b.*PLR+c.*PLR.^2+d.*Tset+e.*Tset.^2+f.*max(Temp,MinTemp)+g.*max(Temp,MinTemp).^2+h.*PLR.*Tset+...
        i.*PLR.*max(Temp,MinTemp)+j.*Tset.*max(Temp,MinTemp);
end
end
```

```
function [COP] = Efficiency2ChillerWater(PLR,Twb,Tset)
%Returns COP for two optimized water cooled chillers with a variable set point
%based on 2013 CA Building Energy
%Efficiency Standards ACM as a function of ambient wet bulb, PLR, and Tset
%Also accounts for cooling tower fan and pumping power
MinTemp=4.44; %[C] minimum Twb
if PLR<=0.5                                 %One chiller operation
    if Twb>=14.44
        a=-4.29666828E-01;
        b=1.88108834E+01;
        c=-1.08678764E+00;
        d=2.57188808E-02;
        e=-3.74748986E-03;
        f=-1.92316518E-02;
        g=7.73710465E-04;
        h=2.54387190E-01;
        i=-2.79691124E-01;
        j=-1.62880334E-03;
COP=a+b.*PLR+c.*PLR.^2+d.*Tset+e.*Tset.^2+f.*max(Twb,MinTemp)+g.*max(Twb,MinTemp).^2+h.*PLR.*Tset+...
            i.*PLR.*max(Twb,MinTemp)+j.*Tset.*max(Twb,MinTemp);
    elseif Twb<14.44
        a=-1.09062674E-01;
        b=6.92733733E+00;
        c=3.41753030E-01;
        d=-4.07600377E-02;
        e=1.24429103E-03;
        f=-8.65892215E-02;
        g=2.79639598E-03;
        h=2.70451143E-01;
        i=5.70327738E-01;
        j=2.93929115E-03;

COP=a+b.*PLR+c.*PLR.^2+d.*Tset+e.*Tset.^2+f.*max(Twb,MinTemp)+g.*max(Twb,MinTemp).^2+h.*PLR.*Tset+...
            i.*PLR.*max(Twb,MinTemp)+j.*Tset.*max(Twb,MinTemp);
    end
elseif PLR>0.5
   if Twb>=14.44
        a=-1.10955651E+00;
        b=1.24875522E+01;
```

```
        c=-3.56681278E+00;
        d=6.23535681E-02;
        e=-1.50369890E-03;
        f=-5.28947498E-02;
        g=9.76716377E-04;
        h=8.44533720E-02;
        i=-9.74080099E-02;
        j=-2.02315661E-03;

COP=a+b.*PLR+c.*PLR.^2+d.*Tset+e.*Tset.^2+f.*max(Twb,MinTemp)+g.*max(Twb,MinTemp).^2+h.*PLR.*Tset+...
            i.*PLR.*max(Twb,MinTemp)+j.*Tset.*max(Twb,MinTemp);
   elseif Twb<14.44
        a=-1.59628492E+00;
        b=7.31774789E+00;
        c=-2.28084584E+00;
        d=-3.85480843E-02;
        e=1.76810916E-03;
        f=-2.10927976E-02;
        g=2.05195556E-03;
        h=1.19134097E-01;
        i=1.91646782E-01;
        j=3.74421585E-03;

COP=a+b.*PLR+c.*PLR.^2+d.*Tset+e.*Tset.^2+f.*max(Twb,MinTemp)+g.*max(Twb,MinTemp).^2+h.*PLR.*Tset+...
            i.*PLR.*max(Twb,MinTemp)+j.*Tset.*max(Twb,MinTemp);
   end
end
```

```
function [UA,Qice,Tout] = IceModel(Fc,Tin,Mode,Tank_Cap,mice)
%function [Qice] = IceModel(Fc,Tin,Mode,Tank_Cap)
%EnergyPlus "Simple" Ice Storage Model
%Fc: Fraction of tank charged
%Tin: ice tank inlet temperature
%Mode: 1: Charging 2: Discharging
%Tank_Cap: Ice tank capacity [kWh]

Tank_Cap_kJ=Tank_Cap*3600;              %Convert units from kWh to kJ
delta_t=3600;                           %[s] to get UA into instantaneous units
delta_T_nom=10;                         %[C] assumed temperature difference in model
Tfr=0;                                  %[C] freezing point of water
%mice=3.9;                              %rated 3.9 kg/s for each 570 kWh tank at 60 GPM
c_gly=3.76;                             %[kJ/kg-K] for 25% ethylene glycol mixture
Ice_Cap=570*3600;                       %[kJ] 162 ton-hrs per tank

if Mode==1                              %Charging
    UAIceCh=(1.3879-7.6333*(Fc)+26.3423*(Fc)^2-47.6084*(Fc)^3+41.8498*(Fc)^4-14.2948*(Fc)^5)*...
        Ice_Cap/(delta_t*delta_T_nom);
    Tout=Tin*exp(-UAIceCh/((mice*Ice_Cap/Tank_Cap)*c_gly)); %Energy balance on the tank
    LMTD=(Tout-Tin)/log((Tfr-Tin)/(Tfr-Tout));
    Qice=UAIceCh*LMTD;                  %[kW]
    UA=UAIceCh;
elseif Mode==2                              %Discharging
    UAIceDisCh=(1.3879-7.6333*(1-Fc)+26.3423*(1-Fc)^2-47.6084*(1-Fc)^3+41.8498*(1-Fc)^4-14.2948*(1-Fc)^5)*...
        Ice_Cap/(delta_t*delta_T_nom);
    Tout=Tin*exp(-UAIceDisCh/((mice*Ice_Cap/Tank_Cap)*c_gly));%Energy balance on the tank
    LMTD=(Tin-Tout)/log((Tin-Tfr)/(Tout-Tfr));
    Qice=UAIceDisCh*LMTD;               %[kW]
    UA=UAIceDisCh;
end
end
```

```
% CTES Model Predictive Control Strategy
clear all; close all; clc;

% System inputs
N=144;                                                  % Number of 10-minute timesteps optimized
ChillerRated=3830;                                      % Rated chiller capacity [kWt]
CapStorage=23000;                                       % Thermal storage capacity [kWh]

%Load cooling load and Twb variables
V1='CoolingLoadOfficeNY20167AM';                        % 2016 NY cooling load
CoolingLoad=load('CoolingLoadOfficeNY20167AM.mat',V1);
CoolingLoad=CoolingLoad.(V1);
CoolingLoad=CoolingLoad(2:52561);
V2='WBTempNY20167AM';                                   % 2016 NY wet-bulb temperature
Twb=load('WBTempNY20167AM.mat',V2);
Twb=Twb.(V2);
Twb=Twb(2:52561);
V3='ElectricRateNYISORT7AM';                            % 2016 NYISO electricity rates
Rate_e=load('ElectricRateNYISORT7AM.mat',V3);
Rate_e=Rate_e.(V3);
Rate_e=Rate_e(2:52561);
ChillerPower=zeros(52560,1);                            % Initialize chiller power vector
Results=zeros(52560,2);                                 % Initialize vector of results
Timestep=1/6;                                           % Ten-minute timesteps (one-sixth of an hour)

for i=1:365                                             % Step through 365 days of the year
FirstTimestep=(i-1)*144+1;                              % First timestep at the beginning of each day

% Objective function
Coeff(1:N)=Timestep.*ChillerRated.*Rate_e(FirstTimestep:(FirstTimestep+N-1)).*0.1176;
f=zeros(2*N,1);                                         % Objective function has 2*timesteps elements
f(1:N)=Coeff;                                           % All of the PLR values

% Pre-calculations
CapCh=ChillerCapacityWater(Twb,1.11,ChillerRated);      % Uses chiller capacity function

% Bounded constraints
lb=-Inf(size(f));                                       % Initialize lower bound
lb(1:N)=0;                                              % PLR lower bound
```

```
lb(N+1:2*N)=0;                                          % Tank charge lower bound
ub=Inf(size(f));                                        % Initialize upper bound
ub(1:N)=1;                                              % PLR upper bound
ub(N+1:2*N)=CapStorage*1.0;                             % Tank charge upper bound

% Equality constraints
Aeq=zeros(N+1,2*N);                                     % Initialize equality matrix
beq=zeros(N+1,1);                                       % Initialize equality vector

% Tank recharged by the end of the time period
beq(1,1)=sum(CoolingLoad(FirstTimestep:(FirstTimestep+N-1)));
for j=1:N
    Aeq(1,j)=CapCh(FirstTimestep+j-1);
end

% Tank charge within physical capacity
% For first timestep
beq(2,1)=CoolingLoad(FirstTimestep)*Timestep-CapStorage;
Aeq(2,1)=CapCh(FirstTimestep)*Timestep;
Aeq(2,N+1)=-1;
for j=1:(N-1)                                           % Subsequent timesteps
    beq(j+2,1)=CoolingLoad(FirstTimestep+j)*Timestep;   % Cooling load
    Aeq(j+2,j+1)=CapCh(FirstTimestep+j)*Timestep;       % Added by chiller
    Aeq(j+2,N+j)=1;                                     % Previous tank charge
    Aeq(j+2,N+j+1)=-1;                                  % Current tank charge
end

% Solve
% Options to use the dual-simplex algorithm and suppress display each day
options = optimoptions('linprog','Algorithm','dual-simplex','Display','none');

% No inequality constraints
[x,fval,exitflag,output] = linprog(f,[],[],Aeq,beq,lb,ub,options);

% Post-processing - concatenate PLR and TankCharge values
PLR(FirstTimestep:(FirstTimestep+143),1)=x(1:144);
TankCharge(FirstTimestep:(FirstTimestep+143),1)=x(145:288);
end
```

```
for j=1:52560
    if PLR(j)>0.01
        % Calculate chiller power using linearized performance curves
        ChillerPower(j)=(0.01258+0.1176.*PLR(j)+0.0005105.*Twb(j)).*ChillerRated;
    end
end

TimestepCost=ChillerPower.*Rate_e;                    % Cost for each timestep
EnergyCost=sum(TimestepCost)*Timestep;                % Total energy cost
EnergyUsed=sum(ChillerPower)*Timestep;                % Total energy consumed
AvgPowerUsed=mean(ChillerPower);                      % Average power consumed
```